Bosonization of
Nonequilibrium Quantum Wire Networks

Zur Erlangung des akademischen Grades eines

DOKTORS DER NATURWISSENSCHAFTEN

von der Fakultät für Physik
des Karlsruher Instituts für Technologie

genehmigte

DISSERTATION

von

Dipl.-Phys. Stéphane Ngo Dinh
aus Goslar

To the companions of my present and past. Thank you for the gift of my future.

Contents

1

Introduction

Significant technological advances in nanolithography and cryogenics since the 1960s have facilitated the fabrication of novel, mesoscopic, structures in which quantum effects are prevalent and give rise to remarkable phenomena[1]. While conventional macroscopic systems exceed in size by far the inelastic mean free path and phase breaking length, i.e. the length scales at which their carries (such as electrons) scatter inelastically and lose their quantum mechanical phase information, dimensions of the mesoscopic devices are of comparable order of magnitude. Consequently, both relaxation into thermal equilibrium and decoherence can be significantly suppressed.

The quantum coherent movement of carriers comes along with non-local correlations, interference and Aharonov-Bohm oscillations which become manifest in phenomena such as universal conductance fluctuations, conductance quantization, and weak localization. At the same time mesoscopic devices often are large enough to feature the onset of decoherence and thus represent an ideal laboratory to study the crossover between quantum mechanical and classical behavior.

While most traditional experimental systems, such as bulk magnets and superconductors, can hardly be driven significantly away from equilibrium, mesoscopic devices, metallic and superconducting, have proven to be appropriate to establish and maintain nonequilibrium conditions and expose specifically nonequilibrium phenomena. Particularly the interplay with strong Coulomb interaction can lead to sizable changes of the systems' behavior, e.g. in the context of the Kondo[2–5] and Fermi-edge singularity[6, 7] problem. And not least, nonequilibrium enlarges the phase space for inelastic scattering and thus is a prime source of dephasing.

The conceptually simplest device to expose decoherence is the interferometer. Different electronic variants can be realized in mesoscopic systems. Of these the clearest interference patterns were obtained in interferometers which are constructed with edge states in quantum Hall systems, e.g.[9]. The quantum Hall effect arises in two-dimensional electron gases when a strong perpendicular magnetic field is applied. The bulk conductance vanishes and dissipationless currents flow along the edges of the sample. In quantum point contacts (QPCs) edges which are usually separated by large distances are brought into close proximity e.g. by applying negative voltages on suitably shaped electrodes. They allow for tunneling between different edges and thus serve as beamsplitters. By an appropriate arrangement of such QPCs (see Fig. 1.1) electrons traveling from source to drain reservoirs along the edges can be offered several different paths. Quantum mechanics tells us that the total current is given by the interference of all possible paths and thus is an oscillatory function of the relative phase of these trajectories. Due to the Aharonov-Bohm (AB) effect[10] the latter can be tuned via the magnetic field. Indeed, in experiments device conductances show clear AB oscillations. The visibility of these
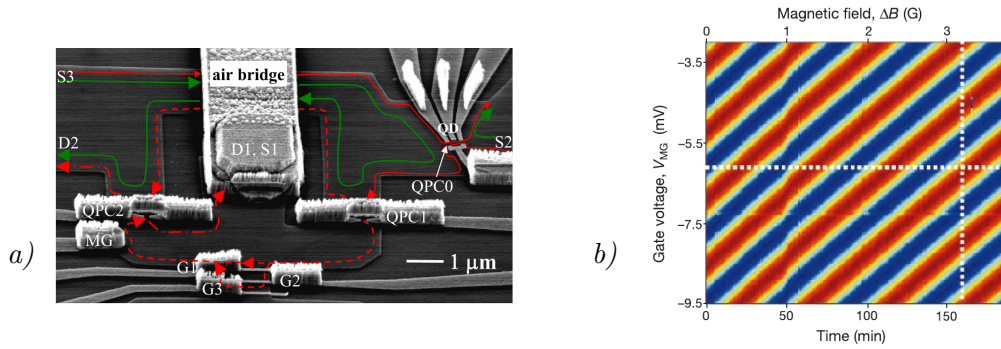
Figure 1.1: *a) Micrograph of a Mach-Zehnder interferometer realized in a quantum Hall system[8]. In analogy to optical interferometers edge states, indicated by arrows, play the role of light beams while quantum point contacts (QPCs) serve as beam-splitters. b) Two-dimensional colour plot of current in a quantum Hall interferometer[9]. Oscillations arise upon varying magnetic field and gate voltages. Gate electrodes are used to manipulate the potential landscape for the electron gas and thus its geometric shape. Changing the size of the interference loop, varies the accumulated Aharonov-Bohm phase.*

interference patterns is suppressed upon increasing the source-drain voltage and hence the energy of the injected electrons. While this is obviously a sign of nonequilibrium-induced decoherence and as such little surprising, later measurements on similar samples have revealed quite unexpectedly additional oscillatory features in the visibility, leading even to its complete vanishing at certain values of the voltage (Fig. 1.2). It became quickly clear that this "lobe" structure is caused by Coulomb interaction and considerable theoretical effort is being made to account for it.
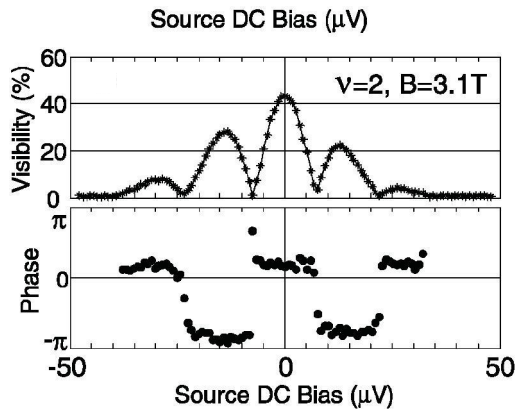
Figure 1.2: *Visibility and phase of Aharonov-Bohm conductance oscillations in the quantum Hall Mach-Zehnder interferometer[8].*

The quantum Hall edge currents are commonly viewed as being carried by one-dimensional fermions. While this is an effective quantum mechanical description of drifting/skipping cyclotron orbits, arising

from the interplay of strong magnetic field and a confining potential at the sample boundaries, a more typical example of one-dimensional fermions is found in very thin nanostructures. Their small lateral extent leads to a strong finite size quantization of the transverse propagation modes of the carriers. At low temperature all modes, but the lowest, are frozen out and the carrier motion is effectively one-dimensional. Examples for such quantum wires are semiconducting and metallic nanowires and carbon nanotubes.

In one dimension the restricted phase space drastically enhances the effect of Coulomb interaction, and the conventional Fermi liquid picture of weakly interacting fermionic quasiparticles breaks down. For screened, short-range interaction its place is usually taken by the *Luttinger liquid* which exhibits bosonic collective density modes (plasmons) and shows critical behavior with nonuniversal power-law correlations. They are experimentally accessible e.g. via the algebraic suppression of tunneling density of states (zero bias anomaly) and tunnel barrier transmission. The latter result was first found in the seminal paper Ref. [11] which considered a Luttinger liquid with a single impurity. Since then this system is subject of extensive ongoing research.

The quantum Hall interferometers considered above and quantum wires with single impurities are in fact very similar when considered as networks of tunnel-coupled one-dimensional fermionic channels. While in the quantum Hall interferometers QPCs couple unidirectional (chiral) channels at different edges, backscattering at the impurities is a tunneling process beween right- and left-moving states.
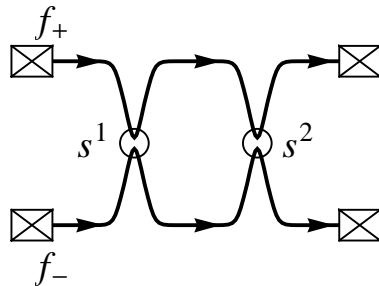
Figure 1.3: *Network model of the electronic Mach-Zehnder interferometer: Chiral wires (solid lines), each connected to reservoirs (white boxes), are tunnel-coupled by two point scatterers (white circles).*

Fig. 1.3 shows a quantum wire network which corresponds to the electronic Mach-Zehnder interferometer. Chiral fermionic channels (the edge states) are coupled by two point scatterers (the QPCs) with scattering matrices s^1, s^2. The channels are connected to reservoirs via incoming and outgoing leads, which are usually assumed to be noninteracting. The reservoirs may be hold at different chemical potentials and temperatures or in generic nonequilibrium states. Population of the wires is determined by the incoming leads through which electrons with given distribution functions f_+ and f_- are injected.

One of the main goals of this thesis is the development of a theoretical framework to treat such nonequilibrium interacting quantum wire networks.

A powerful and elegant theoretical approach to one-dimensional interacting systems is bosonization [12]. In its standard operator formulation all operators such as fermionic fields, the Hamiltonian and thus the equilibrium density operator are expressed in terms of bosonic fields. In a clean metallic wire the low energy physics is determined by free bosonic excitations. Out of equilibrium, however, the

density operator is not as straightforwardly bosonized.

Recently, a nonequilibrium generalization of the bosonization framework was formulated[13, 14] in the functional integral language, within which instead of direct bosonization of the density operator, the nonequilibrium many-body state is encoded in the "Keldysh action". Its specific structure in the case of clean wires allows for an exact evaluation of many-body averages.

The key requirement of the technique is that the electronic nonequilibrium states is established in the noninteracting reservoirs and injected into the interacting wire. In this sense our interest lies in a more complicated situation when tunneling/backscattering occurs in the interacting region, and the state of the system is a nonequilibrium bath of plasmons populated through inelastic tunneling processes of electrons. Such coupling terms represent in general a very serious complication for the full bosonization approach. We choose instead an alternative route based on the functional bosonization formalism[15] that retains both fermionic and bosonic degrees of freedom, and was used in the Keldysh formulation by Ref. [16] to reconsider the problem of Luttinger liquid with impurity.

We find that under specific assumptions the problem of a network with two scatterers (the quantum Hall Mach-Zehnder interferometer) can be solved exactly. In general, however, this is not the case and we develop a saddle-point (real-time instanton) approximation scheme, which applies for weak interchannel tunneling but goes beyond pure perturbation theory. This approach will enable us to describe decoherence effects due to the noise induced by the nonequilibrium plasmon bath, which having Poissonian, rather than Gaussian (like external or thermal noise) correlations cannot be captured satisfactorily in usual perturbative treatments.

The structure of this thesis is as follows: In Chapter 2 we give a short overview over different bosonization techniques, including the functional bosonization method for clean wires. Chapter 3 presents its generalization to quantum wire networks and the real-time instanton approximation scheme. This method is illustrated in Chapter 4 where the tunneling density of states of a nonequilibrium Luttinger liquid containing a single impurity is calculated. The subsequent two chapters are devoted to the study of interaction effects in quantum Hall interferometers: dephasing and oscillatory features of the visibility. The Fabry-Pérot geometry is considered in Chapter 5. The Mach-Zehnder geometry, treated in Chapter 6, is a notable example of quantum wire network which can be dealt with exactly. Chapter 7 is devoted to the time evolution of a clean nonequilibrium Luttinger liquid after an interaction quench.

2 Chapter 2
Nonequilibrium Bosonization

Due to the constrained phase space in one-dimensional systems interaction leads to drastic effects. Already for weak interaction and in close proximity to the Fermi energy the spectral function has no sharp peaks, and Landau's Fermi liquid picture of weakly interacting fermionic quasiparticles, which proves so successful in describing higher-dimensional fermion systems, breaks down. The key step on the route to an alternative description is the observation that for free fermions with linear spectrum particle-hole pair excitations have a well-defined energy-momentum relation, and that the excitations of the Fermi gas can be mapped onto excitations of a free boson gas. Hence, while a brute force fermionic treatment is still possible, an alternative and very powerful approach is bosonization, in which the theory is formulated in terms of bosonic degrees of freedom.

In this chapter we will quickly review the basic ideas. We adress the standard, operator bosonization method (Sect. 2.1) and its nonequilibrium extension (Sect. 2.3). We will turn our attention to the functional bosonization technique, which is more convenient when dealing with one-dimensional systems in the presence of scatterers such as impurities or quantum point contacts. In fact, the generalization of the functional bosonization approach to quantum wire networks is one of the main goals of this work, and Chapter 3 will be devoted to this problem.

2.1 Standard Bosonization

We outline the standard bosonization technique for which a host of reviews and pedagogical introductions exists (e.g. [12]).

Usually bandwidth Λ and Fermi energy E_F exceed by far the energy scales set by temperature and voltage. The interest therefore lies in a model which captures the low energy physics and takes into account excitations of electrons from states close to E_F to other close states. In striking contrast to their higher-dimensional counterparts, in 1D systems the Fermi surface is a disconnected set of points which are separated by large momenta. When sufficiently long-range interaction or disorder scattering is considered, transitions between these Fermi points are negligible. One can thus treat them separately, pretending that states close to different Fermi points belong to different fermion species η. One then forgets that species η was defined by the proximity of its momentum states p to a specific Fermi point, and assumes that it has an unbounded range of momenta $p \in (-\infty, \infty)$ at its disposal. The gain of adding artificaly these infinitely many states – which do not affect the low-energy physics – is that they allow for an exact bosonization of the theory.

Our prime example are single-channel spinless electron, say with dispersion $E_p = p^2/(2m)$. The

Fermi energy E_F defines 2 Fermi points $\pm p_F = \pm\sqrt{2mE_F}$ with velocities $v_\pm = \pm v_F = \pm p_F/m$. One linearizes the spectrum around $\pm p_F$ and introduces two fermion species $\eta = \pm$, commonly dubbed "right- and left-movers". Their dispersion is $E - E_F = v_\eta k$ where the momentum $k = p - \eta p_F$ is measured relative to the respective Fermi momentum ηp_F. In systems of finite size L momenta are discretized, $k = \frac{2\pi}{L} n_k$, $n_k \in \mathbb{Z}$ when periodic boundary conditions are assumed.

We introduce fermionic creation and annihilation operators for the corresponding single-particle states which satisfy the canonical anticommutation relation $\left\{ c_{k\eta}, c^\dagger_{k'\eta'} \right\} = \delta_{kk'} \delta_{\eta\eta'}$. Fourier transformation yields the field operators $\psi_\eta(x) = \frac{1}{\sqrt{L}} \sum_k e^{ikx} c_{k\eta}$.

The noninteracting ground state $|0\rangle$ is the Fermi sea with all negative-energy states filled. It is annihilated by $c_{k,+}$, $c_{-k,-}$ for $k > 0$ and $c^\dagger_{k,+}$, $c^\dagger_{-k,-}$ for $k \leq 0$. The existence of infinitely many negative-energy single-particle states of which always infinitely many are occupied, or for short the lack of a lower band edge, leads to ultraviolet (UV) divergencies. The simplest example is the total kinetic energy

$$\tilde{H}_0 = \sum_\eta \sum_k v_\eta k \, c^\dagger_{k\eta} c_{k\eta} = \sum_\eta \int_{-L/2}^{L/2} \mathrm{d}x \, \psi^\dagger_\eta(x)(-iv_\eta\partial_x)\psi_\eta(x) \tag{2.1}$$

the ground state expectation value of which is, of course, negative infinity. One way to deal with these divergencies is normal-ordering. Normal-ordering of products of operators means interchanging factor operators such that those which annihilate $|0\rangle$ stand right from all the others. Interchange of two fermionic operators is to be accompanied by a global sign switch. Physically, one is interested in observables such as energies and momenta relative to their groundstate values, and an equivalent representation of normal-ordering is

$$: ABC\ldots :\equiv ABC\ldots - \langle 0| \, ABC\ldots |0\rangle \, .$$

The normal-ordered density operators $\varrho_\eta(x) =: \psi^\dagger_\eta(x)\psi_\eta(x):$ measures density fluctuations on top of the homogeneous ground state $|0\rangle$. Fourier transformation yields $\varrho^\dagger_\eta(p) =: \sum_k c^\dagger_{k+p,\eta} c_{k\eta}:$ which, for $p \neq 0$, create particle-hole pairs with momentum p or, for $p = 0$, measure the relative total particle number $\hat{N}_\eta \equiv \varrho^\dagger_\eta(p = 0)$. Let us consider their commutation relations. For different species $\eta \neq \eta'$ the operators ϱ_η, $\varrho_{\eta'}$ obviously commute, in the other case ($p \neq 0 \neq p'$)

$$\left[\varrho^\dagger_\eta(p), \varrho^\dagger_\eta(-p')\right] = \sum_k \left(c^\dagger_{k+p,\eta} c_{k+p',\eta} - c^\dagger_{k+p-p',\eta} c_{k,\eta} \right).$$

For $p \neq p'$ the expression can be split into a difference of two infinite sums each of which acts on physical states (with arbitrary but finite numbers of particle and hole excitations) in a well-defined way. By performing the index shift $k \mapsto k + p'$ the second sum can be made manifestly equal to the first one and the commutator vanishes. For $p = p'$ more care is needed since sums $\sum_k c^\dagger_{k+p,\eta} c_{k+p,\eta}$ are infinite and may only be treated separately after normal-ordering. After the split the above index shift yields a vanishing difference and one is left with

$$\left[\varrho^\dagger_\eta(p), \varrho^\dagger_\eta(-p)\right] = \sum_k \left(: c^\dagger_{k+p,\eta} c_{k+p,\eta} : - : c^\dagger_{k\eta} c_{k\eta} : + \langle 0| c^\dagger_{k+p,\eta} c_{k+p,\eta} |0\rangle - \langle 0| c^\dagger_{k\eta} c_{k\eta} |0\rangle \right)$$

$$= \sum_k \left(\langle 0| c^\dagger_{k+p,\eta} c_{k+p,\eta} |0\rangle - \langle 0| c^\dagger_{k\eta} c_{k\eta} |0\rangle \right)$$

$$= -\eta n_p = -\eta \frac{L}{2\pi} p. \tag{2.2}$$

The appearance of this nonvanishing commutator is intimately related to the UV divergence and usually referred to as "Schwinger anomaly". Under the assumption of unbounded discrete momenta, up to normalization the density operators satisfy bosonic commutations relation. This leads us to define for $p > 0$ the bosonic creation and annihilation operators

$$b_p^\dagger = \frac{1}{\sqrt{n_p}} \varrho_+^\dagger(p), \qquad\qquad b_{-p}^\dagger = \frac{1}{\sqrt{n_p}} \varrho_-^\dagger(-p),$$

$$b_p = \frac{1}{\sqrt{n_p}} \varrho_+(p), \qquad\qquad b_{-p} = \frac{1}{\sqrt{n_p}} \varrho_-(-p)$$

which indeed satisfy the bosonic commutation relations $[b_p, b_q^\dagger] = \delta_{pq}$ and $b_p |0\rangle = 0 = b_{-p} |0\rangle$. The operators $b_p^\dagger$ generate particle-hole pairs and do not change the overall particle number. For the latter purpose "ladder operators", the Klein factors F_η, can be constructed such that they commute with all bosonic operators b_p, are unitary, $F_\eta^{-1} = F_\eta^\dagger$, and satisfy

$$\left[\hat{N}_\eta, F_{\eta'}^\dagger\right] = \delta_{\eta\eta'} F_\eta^\dagger, \qquad\qquad \left[\hat{N}_\eta, F_{\eta'}\right] = -\delta_{\eta\eta'} F_\eta,$$

$$\left\{F_\eta^\dagger, F_{\eta'}\right\} = 2\delta_{\eta\eta'}, \qquad\quad \left\{F_\eta^\dagger, F_{\eta'}^\dagger\right\} = 0 = \left\{F_\eta, F_{\eta'}\right\} \quad \text{for } \eta \neq \eta'.$$

By careful counting of states, it can be proven that bosonic operators $b_q^\dagger$ together with Klein factors generate a complete basis of the many-electron Hilbert space. Fig. 2.1 illustrates how the action of a fermionic creation operator can be mimicked by a Klein factor and a bosonic creation operator.
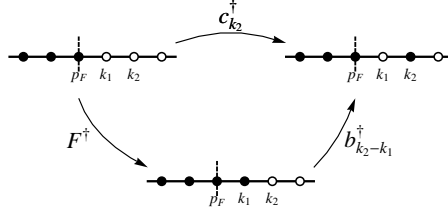
Figure 2.1: *Adding an electron in momentum state k_2 can be accomplished by first increasing the total ground state electron number by 1 (via $F^\dagger$) and subsequently creating an electron hole pair (via $b_{k_2-k_1}^\dagger$)*

This implies that any reasonable operator can be expressed in terms of these bosonic operators as well. For the normal-ordered free Hamiltonian $H_0 =: \tilde{H}_0 :$, cf. (2.1), which has the commutators $\left[H_0, b_p^\dagger\right] = v_F p b_p^\dagger$ one can show

$$H_0 = \sum_q v_F |q| b_q^\dagger b_q + v_F \frac{2\pi}{L} \frac{1}{2} \sum_\eta \hat{N}_\eta \left(\hat{N}_\eta + 1\right).$$

Formally, one has mapped the original free fermion Hamiltonian with linear dispersion (which is bilinear in fermionic operators) onto a free boson Hamiltonian which is bilinear in density operators (and thus biquadratic in fermionic operators). Bosonization of H_0 merely makes explicit that thanks to the linear fermion dispersion, electron-hole pairs are stable excitations with well-defined linear energy-momentum relation. Indeed by promoting, say, a right-moving electron from state p to $p + q > p$, i.e. creating

an electron-hole pair with momentum $q > 0$ one creates an excitation of energy $v_F q$, regardless of the initial electron momentum p. The situation changes when a finite curvature of the electronic band structure is taken into account. Then for given momentum q corresponding electron-hole states cover a continuous range of energies; H_0 contains higher-order-in-b_q terms, i.e. interaction of bosonic modes.

Similarly the field operators which satisfy e.g.

$$\left[\psi_+(x), b_p^\dagger\right] = \frac{1}{\sqrt{n_p}}\, e^{ipx}\, \psi_+(x), \quad \left[\psi_-(x), b_{-p}^\dagger\right] = \frac{1}{\sqrt{n_p}}\, e^{-ipx}\, \psi_-(x)$$

(for $p > 0$) can be expressed in terms of bosonic operators. To this end we define the fields

$$\varphi_+(x) = -i \sum_{q>0} \frac{1}{\sqrt{n_q}} e^{-\alpha q/2} e^{iqx} b_q, \quad \varphi_-(x) = -i \sum_{q>0} \frac{1}{\sqrt{n_q}} e^{-\alpha q/2} e^{-iqx} b_{-q}.$$

The "effective band-width" α^{-1} is necessary to regularize ultraviolet divergent momentum sums which appear in certain non-normal-ordered expressions. The fermionic operators are then

$$\psi_\eta(x) = \frac{1}{\sqrt{L}}\, F_\eta e^{i\frac{2\pi}{L}\hat{N}_\eta x}\, e^{i\varphi_\eta^\dagger(x)} e^{i\varphi_\eta(x)}.$$

A more instructive representation works with the field

$$\phi_\eta(x) \equiv \varphi_\eta(x) + \varphi_\eta^\dagger(x)$$

which is related to density via

$$\varrho_\eta(x) = \frac{\eta}{2\pi}\partial_x \phi_\eta(x) + \frac{1}{L}\hat{N}_\eta$$

and has the anomalous commutator

$$\left[\phi_\eta(x), \phi_{\eta'}(x')\right] = i\pi\eta\delta_{\eta\eta'}\,\mathrm{sign}\,(x - x').$$

These unusual commutator relations — referred to as Kac-Moody algebra — imply

$$\left[\frac{\eta}{2\pi}\partial_x \phi_\eta, \phi_{\eta'}(x')\right] = i\delta(x - x'),$$

i.e. the field conjugate to ϕ_η is the derivative of ϕ_η itself, or more precisely the density $\varrho_\eta - \hat{N}_\eta/L$. A very common representation of the above bosonization identity is

$$\psi_\eta(x) = \frac{1}{\sqrt{2\pi\alpha}}\, F_\eta e^{i\frac{2\pi}{L}\hat{N}_\eta x} e^{i\phi_\eta(x)}. \tag{2.3}$$

It is not normal-ordered and therefore necessarily contains the cutoff α explicitly.

A representation of the bosonic fields which is also commonly found in the literature is

$$\vartheta = \frac{1}{2}\left(\phi_+ + \phi_-\right), \quad \phi = -\frac{1}{2}\left(\phi_+ - \phi_-\right).$$

The latter is a phonon-like displacement field, satisfying $\varrho = \varrho_+ + \varrho_- = -\partial_x\phi/\pi$, while the former is related to current via $j = \varrho_+ - \varrho_- = \partial_x\vartheta/\pi$. These fields have the commutator

$$\left[\phi(x), \vartheta(x')\right] = i\frac{\pi}{2}\mathrm{sign}\left(x - x'\right)$$

which makes $P_\phi \equiv \partial_x\vartheta/\pi$ the momentum field conjugate to ϕ. With that we can understand the phase operator in the bosonization identity (2.3) in the following way:

$$e^{i\phi_\eta(x)} = e^{-i\eta\phi(x)}e^{i\vartheta(x)} \hat{=} e^{i\eta\pi\int_{-\infty}^x \mathrm{d}x'\,\varrho(x')}e^{i\pi\int_{-\infty}^x \mathrm{d}x'\,P_\phi(x')}.$$

The second factor acts as a translation operator for ϕ and produces a π-kink, $\phi(x') \mapsto \phi(x') - \pi\theta(x-x')$ (here, θ denotes the Heaviside step function), which amounts to the charge dip, $\varrho(x') \mapsto \varrho(x') - \delta(x-x')$. This charge extraction is exactly what one would expect from the field operator $\psi(x)$. At the same time it is a fermionic operator. Fermi statistics is endowed by the first factor, the "Jordan-Wigner string", which counts the number of electrons left from the position x, weighing each electron with the phase π, i.e. a sign switch.

In terms of these bosonic fields the free Hamiltonian reads

$$\begin{aligned} H_0 &= \frac{v}{2}\sum_\eta\left\{\frac{1}{2\pi}\int\mathrm{d}x\,:\left(\partial_x\phi_\eta\right)^2: +\frac{2\pi}{L}\hat{N}_\eta\left(\hat{N}_\eta + 1\right)\right\} \\ &= \frac{v_F}{2\pi}\int\mathrm{d}x\,:\left(\partial_x\phi\right)^2 + \left(\partial_x\vartheta\right)^2: +\frac{v_F\pi}{L}\sum_\eta\hat{N}_\eta\left(\hat{N}_\eta + 1\right). \end{aligned} \tag{2.4}$$

In the following we focus on the thermodynamic limit $L \to \infty$ and neglect the charging terms $\hat{N}_\eta$.

Once the free Hamiltonian is cast into bosonized form, adding interaction does not represent a major technical difficulty. Since interaction couples densities, the respective Hamiltonian is already bosonized, and, further, also quadratic in bosonic fields. The free boson model, thus, stays free.

Let us consider a spinless Lutinger model with short-range interaction. The induced scattering processes can involve either electrons of the same ("g_4-processes") or of different species ("g_2-processes"). The interaction Hamiltonian reads

$$\begin{aligned} H_{\mathrm{int}} &= \frac{g_4}{2}\int\mathrm{d}x\,:\varrho_+(x)^2 + \varrho_-(x)^2: +g_2\int\mathrm{d}x\,:\varrho_+(x)\varrho_-(x): \\ &= \frac{g_4}{(2\pi)^2}\int\mathrm{d}x\,:\left(\partial_x\phi\right)^2 + \left(\partial_x\vartheta\right)^2: +\frac{g_2}{(2\pi)^2}\int\mathrm{d}x\,:\left(\partial_x\phi\right)^2 - \left(\partial_x\vartheta\right)^2:. \end{aligned}$$

Obviously the g_4-processes only renormalize the Fermi velocity $v_F \mapsto v_F\left(1 + \frac{g_4}{2\pi v_F}\right)$. Adding all terms gives the full Hamiltonian

$$H = H_0 + H_{\mathrm{int}} = \frac{u}{2\pi}\int\mathrm{d}x\,:\left[K^{-1}\left(\partial_x\phi\right)^2 + K\left(\partial_x\vartheta\right)^2\right]: \tag{2.5}$$

with plasmon velocity and Luttinger constant

$$u = v_F\sqrt{\left(1 + \frac{g_4}{2\pi v_F}\right)^2 - \left(\frac{g_2}{2\pi v_F}\right)^2}, \quad K = \sqrt{\frac{2\pi v_F + g_4 - g_2}{2\pi v_F + g_4 + g_2}}. \tag{2.6}$$

By rescaling the fields $\phi \mapsto \sqrt{K}\phi$, $\vartheta \mapsto \vartheta/\sqrt{K}$ the full Hamiltonian can be mapped to the free one (2.4) with velocity v_F replaced by u. That shows that interaction gives rise to new free bosonic modes, plasmons, with a linear dispersion and velocity u.

Another way to see this and to construct the plasmonic creation and annihilation operators $\tilde{b}_q$ explicitly is to diagonalize

$$H = \sum_{q>0} v_F q \left(b_q, b_{-q}^\dagger \right) \begin{pmatrix} 1 + g_4/(2\pi v_F) & g_2/(2\pi v_F) \\ g_2/(2\pi v_F) & 1 + g_4/(2\pi v_F) \end{pmatrix} \begin{pmatrix} b_q^\dagger \\ b_{-q}^\dagger \end{pmatrix} = \sum_q u|q| \tilde{b}_q^\dagger \tilde{b}_q$$

by the Bogoliubov transformation

$$\begin{pmatrix} b_q^\dagger \\ b_{-q} \end{pmatrix} = \begin{pmatrix} \cosh \zeta & \sinh \zeta \\ \sinh \zeta & \cosh \zeta \end{pmatrix} \begin{pmatrix} \tilde{b}_q^\dagger \\ \tilde{b}_{-q} \end{pmatrix} \quad \text{with } \cosh \zeta = \frac{1+K}{2\sqrt{K}}, \ \sinh \zeta = -\frac{1-K}{2\sqrt{K}}. \tag{2.7}$$

Having expressed the Hamiltonian completely in terms of bosonic fields we are also immediately able to bosonize the equilibrium density operator $\varrho = \mathcal{Z}^{-1} e^{-\beta H}$ with $\beta = 1/T$. Important quantities from which various observables such as charge density, density of states, response functions etc. can be derived are correlation functions such as the single-particle Green's functions

$$iG_\eta^>(t_1, x_1, t_2, x_2) = \left\langle \psi_\eta(t_1, x_1) \psi_\eta^\dagger(t_2, x_2) \right\rangle, \quad iG_\eta^<(t_1, x_1, t_2, x_2) = - \left\langle \psi_\eta^\dagger(t_2, x_2) \psi_\eta(t_1, x_1) \right\rangle.$$

The time-dependence is to be understood in the sense of the usual Heisenberg representation $\psi_\eta(t, x) = e^{iHt} \psi_\eta(x) e^{-iHt}$, such that in equilibrium

$$G_\eta^<(t_1, x_1, t_2, x_2) = \mathcal{Z}^{-1} \frac{i}{2\pi\alpha} \operatorname{Tr} \left[e^{-\beta H} e^{iHt_2} e^{-i\phi_\eta(x_2)} e^{-iH(t_2 - t_1)} e^{i\phi_\eta(x_1)} e^{-iHt_1} \right]$$

All operators in the exponentials are quadratic in bosonic fields and the many-body trace amounts to a Gaussian average. To tackle such problems a large effective toolbox exists in which important tools are e.g. Wick's theorem and the cumulant expansion method, and which is treated extensively in a large range of textbooks. One finds

$$G_\eta^{\gtrless}(t = t_1 - t_2, x = x_1 - x_2) = \frac{\mp i}{2\pi v_F a} \left[\frac{\mp i a \pi T}{\sinh \pi T(t - \eta x/u \mp ia)} \right]^{1+\gamma} \left[\frac{\mp i a \pi T}{\sinh \pi T(t + \eta x/u \mp ia)} \right]^\gamma \tag{2.8}$$

with $\gamma = \sinh^2 \zeta = (1-K)^2/(4K)$. For future reference we chose to use a short-*time* cutoff $a \sim \alpha/v_F \sim \alpha/u$ rather than the short-*distance* cutoff α. It corresponds to a high-energy cutoff $\Lambda \sim a^{-1}$.

It may appear that the considered formalism is restricted to thermal equilibrium situations where the density operator is a simple function of the Hamiltonian. In arbitrary nonequilibrium situations the density operator cannot be as straightforwardly bosonized, and in fact a generalization to such cases within the Keldysh formulation[17, 18] was developed very recently. This will be the subject of Sect. 2.3. Let us consider an alternative approach first, also based on the Keldysh technique, which is fully equivalent to standard bosonization when considering clean one-dimensional systems in equilibrium, but is more convenient when dealing with more complicated situations, e.g. in the presence of scatterers.

2.2 Functional Bosonization

The functional bosonization method[15] derives its name from the fact that it relies very heavily on the functional integral formulation, where many-body traces are performed in the coherent-state basis, and simple properties of functional (Gaussian) integrals.Its main conceptual difference from the standard bosonization approaches is that it retains both fermionic and bosonic degrees of freedom.

Let us start by reviewing shortly the Keldysh technique: Arbitrary (nonequilibrium) many-body states are dealt with by extending the real-time contour to the Keldysh contour $\mathcal{C}$ which consists of a forward and a backward branch. Equivalently, this amounts to doubling the field degrees of freedom φ by distinguishing between "forward" and "backward" components φ^f and φ^b respectively (which reside on the corresponding branches of $\mathcal{C}$). Correspondingly, Green's functions obtain an additional 2×2-matrix structure:

$$G(x_1, t_1; x_2, t_2) = -i \left\langle T_{\mathcal{C}} \begin{pmatrix} \varphi_1^f \varphi_2^{f\dagger} & \varphi_1^f \varphi_2^{b\dagger} \\ \varphi_1^b \varphi_2^{f\dagger} & \varphi_1^b \varphi_2^{b\dagger} \end{pmatrix} \right\rangle = -i \left\langle \begin{pmatrix} T\varphi_1 \varphi_2^\dagger & \pm \varphi_2^\dagger \varphi_1 \\ \varphi_1 \varphi_2^\dagger & \tilde{T} \varphi_1 \varphi_2^\dagger \end{pmatrix} \right\rangle$$

$$\equiv \begin{pmatrix} G^T(\xi_1; \xi_2) & G^>(\xi_1; \xi_2) \\ G^<(\xi_1; \xi_2) & G^{\tilde{T}}(\xi_1; \xi_2) \end{pmatrix}$$

where we wrote $\xi_j = (t_j, x_j)$, $\varphi_j = \varphi(\xi_j)$. T and $\tilde{T}$ denote time-ordering and anti-time ordering along the real time axis, $T_{\mathcal{C}}$ denotes time-ordering along the Keldysh contour. Operators with later times are to the left of those with earlier times. Interchanging fermionic operators induces a sign switch (the signs "$\pm$" in the above equation hold for bosonic/fermionic fields φ). Backward times are later than forward times. This implies

$$G^{T(\tilde{T})}(\xi_1; \xi_2) = \theta(t_1 - t_2) G^{>(<)}(\xi_1; \xi_2) + \theta(t_2 - t_1) G^{<(>)}(\xi_1; \xi_2).$$

An alternative representation is obtained by the rotation

$$\varphi^c(\xi) = \frac{1}{2} \left(\varphi^f(\xi) + \varphi^b(\xi) \right), \quad \varphi^q(\xi) = \frac{1}{2} \left(\varphi^f(\xi) - \varphi^b(\xi) \right)$$

in Keldysh space which yields the corresponding Green's functions

$$G^r(\xi_1, \xi_2) = -i \left\langle \varphi^c(\xi_1) \varphi^{q\dagger}(\xi_2) \right\rangle = \frac{1}{2} \left(G^T - G^{\tilde{T}} + G^> - G^< \right)(\xi_1, \xi_2),$$

$$G^a(\xi_1, \xi_2) = -i \left\langle \varphi^q(\xi_1) \varphi^{c\dagger}(\xi_2) \right\rangle = \frac{1}{2} \left(G^T - G^{\tilde{T}} - G^> + G^< \right)(\xi_1, \xi_2),$$

$$G^k(\xi_1, \xi_2) = -i \left\langle \varphi^c(\xi_1) \varphi^{c\dagger}(\xi_2) \right\rangle = \frac{1}{2} \left(G^T + G^{\tilde{T}} + G^> + G^< \right)(\xi_1, \xi_2),$$

which we refer to as retarded, advanced, and Keldysh components.

As our key example we consider free 1D chiral fermions ψ_η with Hamiltonian (2.1) at temperatures T_η and chemical potentials eV_η, and hence distribution function $f_\eta(\epsilon) = \left[e^{-(\epsilon - eV_\eta)/(k_B T)} + 1 \right]^{-1}$. The Keldysh action of such electrons is

$$\mathcal{A}_0[\psi, \bar{\psi}] = \sum_\eta \int_{\mathcal{C}} \mathrm{d}t \, \mathrm{d}x \, \bar{\psi}_\eta (i\partial_t + iv_\eta \partial_x) \psi_\eta. \tag{2.9}$$

where integration along $\mathcal{C}$ is generally understood as the real-time integration

$$\int_{\mathcal{C}} \mathrm{d}t'\, A(t') = \int_{-\infty}^{\infty} \mathrm{d}t' \left[A^f(t') - A^b(t') \right].$$

The free Green's functions are

$$G_{0\eta}^{\gtrless}(x,t) = -\frac{1}{2\pi|v_\eta|} \frac{\pi T e^{-ieV(t - x/v_\eta)}}{\sinh \pi T(t \mp ia - x/v_\eta)},$$

with short-time cutoff a.

Now let us include interaction, encoded in the action

$$\mathcal{A}_{\mathrm{int}}[\psi, \bar{\psi}] = -\frac{1}{2} \sum_{\eta\nu} \int_{\mathcal{C}} \mathrm{d}t\, \mathrm{d}x\, \mathrm{d}x'\, U_{\eta\nu}(x, x') \varrho_\eta(t, x) \varrho_\nu(t'x') \tag{2.10}$$

with regularized density $\varrho_\eta(x) \equiv \bar{\psi}_\eta(x + 0)\psi_\eta(x)$. We consider the thermodynamic limit and neglect $1/L$-terms. Here we encounter yet another UV regularization procedure, "point-splitting", which can be shown to be equivalent to the normal-ordering regularization of the previous section.

In this work different interaction models $U_{\eta\nu}$ will be considered. In the spinless Luttinger model with right- and left-moving fermions $\eta = \pm$, which we concentrate on in this introduction,

$$U_{+-}(x, x') = U_{-+}(x, x') = g_2(x)\delta(x - x'), \quad U_{++}(x, x') = U_{--}(x, x') = g_4(x)\delta(x - x'). \tag{2.11}$$

What makes interaction, in general, nontrivial is the fact that the corresponding action $\mathcal{A}_{\mathrm{int}}$ is not quadratic, but biquadratic in the fermionic fields. The key idea of functional bosonization is the observation that this quartic terms can be decoupled at the expense of introducing a new bosonic field φ. Physically very transparently, it can be viewed as the mediator of the interaction (comparable to the photon field which mediates electromagnetic interaction). The process of two electrons interacting with each other is split into two subprocesses each of which involves only one electron and the boson. Firstly, one of the electrons generates a "potential" φ (or "emits a φ-quantum"), which, secondly, acts on the other electron (the latter "absorbs a φ-quantum").

Formally, the "Hubbard-Stratonovich" decoupling is based on the simple integral identity

$$1 = \int \mathcal{D}\varphi\, e^{i\mathcal{A}_{\mathrm{int}}[\varphi]} = \int \mathcal{D}\varphi \exp\left[i\mathcal{A}_{\mathrm{int}}[\varphi] - i\sum_\eta \int_{\mathcal{C}} \mathrm{d}t \mathrm{d}x\, \varphi_\eta(x)\varrho_\eta(x) - i\mathcal{A}_{\mathrm{int}}[\psi, \bar{\psi}] \right]$$

$$\text{with } \mathcal{A}_{\mathrm{int}}[\varphi] \equiv \frac{1}{2} \sum_{\eta\nu} \int_{\mathcal{C}} \mathrm{d}t\, \mathrm{d}x\, \mathrm{d}x'\, U_{\eta\nu}^{-1}(x, x')\varphi_\eta(t, x)\varphi_\nu(t, x'). \tag{2.12}$$

The first equality is based on the fact that time-evolution along the full Keldysh contour is trivial in the absence of non-classical external fields and that the Keldysh partition sum is, thus, unity. The second equality results from the shift

$$\varphi_\mu(x') \mapsto \varphi_\mu(x') - \sum_\eta \int \mathrm{d}x''\, U_{\mu\eta}(x', x'')\varphi_\eta(x'')$$

of the integration variable. Making use of this "fat unity", many-body averages can be written

$$\langle \mathcal{O} \rangle \equiv \int \mathcal{D}\psi \mathcal{D}\bar{\psi}\, e^{i\mathcal{A}_0[\psi, \bar{\psi}]} \mathcal{O}[\psi, \bar{\psi}] = \int \mathcal{D}\psi \mathcal{D}\bar{\psi} \mathcal{D}\varphi\, e^{i\mathcal{A}_0[\psi, \bar{\psi}, \varphi]} \mathcal{O}[\psi, \bar{\psi}] \tag{2.13}$$

with the new Keldysh action

$$\mathcal{A}[\psi, \bar{\psi}, \varphi] = \mathcal{A}_{\text{int}}[\varphi] + \sum_{\eta} \int_{\mathcal{C}} \mathrm{d}t \, \mathrm{d}x \, \bar{\psi}_{\eta}(i\partial_t + iv_{\eta}\partial_x - \varphi_{\eta})\psi_{\eta}. \tag{2.14}$$

The applicability of the Hubbard-Stratonovich decoupling is not restricted to one dimension or fermionic systems. However, 1D allows for a further decoupling by the gauge transformation

$$\psi_{\eta}^{f/b}(t, x) \mapsto e^{i\Theta_{\eta}^{f/b}(t,x)} \psi_{\eta}^{f/b}(t, x), \quad \bar{\psi}_{\eta}^{f/b}(t, x) \mapsto \bar{\psi}_{\eta}^{f/b}(t, x) \, e^{-i\Theta_{\eta}^{f/b}(t,x)}$$

$$\text{with the condition} \quad (\partial_t + v_{\eta}\partial_x)\Theta_{\eta}^{f/b}(t, x) = -\varphi_{\eta}^{f/b}(t, x). \tag{2.15}$$

One has to resolve this gauge condition properly taking the Keldysh structure into account, which yields

$$\begin{pmatrix} \Theta_{\mu}^f \\ \Theta_{\mu}^b \end{pmatrix}_{\xi} = - \int \mathrm{d}\xi' \begin{pmatrix} D_{0\mu}^T & D_{0\mu}^< \\ D_{0\mu}^> & D_{0\mu}^{\tilde{T}} \end{pmatrix}_{\xi - \xi'} \begin{pmatrix} \varphi_{\mu}^f \\ -\varphi_{\mu}^b \end{pmatrix}_{\xi'}, \tag{2.16}$$

with $\xi = (x, t)$ and real time t, or symbolically $\Theta_{\mu} = -D_{0\mu}\varphi_{\mu}$. Here the blocks of the particle-hole propagator $D_{0\mu}$ satisfy the relations

$$\begin{aligned} (\partial_t + v_{\eta}\partial_x)D_{0\eta}^{T/\tilde{T}}(\xi, \xi') &= \pm\delta(\xi - \xi'), \\ (\partial_t + v_{\eta}\partial_x)D_{0\eta}^{\gtrless}(\xi, \xi') &= 0. \end{aligned} \tag{2.17}$$

In the frequency-momentum representation the retarded/advanced bare particle-hole propagator $D_{0\eta}$ in channel η is given by

$$D_{0\eta}^{r/a}(\omega, q) = \frac{i}{\omega_{\pm} - v_{\eta}q}, \quad \omega_{\pm} = \omega \pm i0, \tag{2.18}$$

$$D_{0\eta}^k(\omega, q) = \left(1 + 2N_{\eta}(\omega)\right) \left[D_{0\eta}^r(\omega, q) - D_{0\eta}^a(\omega, q)\right] \tag{2.19}$$

with the particle-hole pair distribution function

$$N_{\eta}(\omega) = \int \frac{\mathrm{d}\epsilon}{\omega} f_{\eta}(\epsilon) \left(1 - f_{\eta}(\epsilon - \omega)\right) = \left[e^{\epsilon/(k_B T_{\eta})} - 1\right]^{-1}. \tag{2.20}$$

The Eq. (2.19) which relates the Keldysh component $D_{0\eta}^k$ to the particle-hole pair spectral weight $D_{0\eta}^r - D_{0\eta}^a$ and their distribution function N_{η} is another example of the fluctuation-dissipation theorem.

In many-body averages (2.13) the decoupling amounts to replacing $\mathcal{A}[\psi, \bar{\psi}, \varphi]$ simply by $\mathcal{A}_0[\psi, \bar{\psi}]$. In addition, being a (linear) transformation of the functional integration variables ψ, $\bar{\psi}$ the gauge transformation gives rise to a ($\psi, \bar{\psi}$-independent) Jacobian $\mathcal{Z}[\varphi]$,

$$\langle \mathcal{O} \rangle = \int \mathcal{D}\varphi \, e^{i\mathcal{A}_{\text{int}}[\varphi]} \mathcal{Z}[\varphi] \int \mathcal{D}\psi \mathcal{D}\bar{\psi} \, e^{i\mathcal{A}_0[\psi, \bar{\psi}]} \, \mathcal{O}\left[e^{i\Theta}\psi, \bar{\psi}e^{-i\Theta}\right].$$

That Jacobian,

$$\mathcal{Z}[\varphi] \equiv \frac{\int \mathcal{D}\psi \mathcal{D}\bar{\psi} \, e^{i\mathcal{A}_0[\psi, \bar{\psi}, \varphi]}}{\int \mathcal{D}\psi \mathcal{D}\bar{\psi} \, e^{i\mathcal{A}_0[\psi, \bar{\psi}] + i\mathcal{A}_{\text{int}}[\varphi]}} = e^{\sum_{\eta} \text{Tr Ln}[1 - iG_{0\eta}\varphi_{\eta}]} = \exp\left[-\sum_{\eta} \sum_{n=1}^{\infty} \frac{i}{n} \text{Tr}\left[G_{0\eta}\varphi_{\eta}\right]^n\right], \tag{2.21}$$

is the sum over vacuum loops with external lines corresponding to the φs. Logarithms "Ln" and traces "Tr" are to be taken with respect to Keldysh times and space coordinates, $G_{0\eta}$ are the free Keldysh Green's functions. For the partial equilibrium situation we described in the beginning of this section, all loops with $n > 3$ vanish [16, 19]. The $n = 1$-term is the mean-field (Hartree) contribution. The $n = 2$-term is nontrivial because of the Schwinger anomaly which we encountered already in the previous section where it gave rise to the non-vanishing commutator (2.2) of density operators. We obtain the Jacobian

$$\mathcal{Z}[\varphi] = \exp\left[-i\sum_\eta \varrho_{0\eta} \int_\mathcal{C} \mathrm{d}\xi\, \varphi_\eta(\xi) - i\frac{1}{2}\sum_\eta \int_\mathcal{C} \mathrm{d}\xi\mathrm{d}\xi'\, \varphi_\eta(\xi)\Pi_\eta(\xi,\xi')\varphi_\eta(\xi')\right] \tag{2.22}$$

with mean charge density $\varrho_{0\eta} = \frac{eV_\eta}{2\pi|v_\eta|}$ and polarization operator $\Pi_\eta^{\alpha\beta}(\xi) = -iG_{0\eta}^{\alpha\beta}(\xi)G_{0\eta}^{\beta\alpha}(-\xi)$, $\alpha,\beta = f, b$. After rotation in Keldysh space and transformation into frequency-momentum representation one obtains

$$\Pi_\eta^{r/a}(\omega,q) = \frac{1}{2\pi|v_\eta|}\frac{v_\eta q}{\omega_\pm - v_\eta q}, \tag{2.23}$$

$$\Pi_\eta^k(\omega,q) = \left(1 + 2N_\eta(\omega)\right)\left[\Pi_\eta^r(\omega,q) - \Pi_\eta^a(\omega,q)\right] \tag{2.24}$$

with bosonic distribution functions (2.20).

With that the fermionic and bosonic fields ψ, $\bar\psi$ and φ are effectively decoupled with actions $\mathcal{A}_0[\psi,\bar\psi]$ and $\mathcal{A}[\varphi] = \mathcal{A}_{\mathrm{RPA}}[\varphi] + \mathcal{A}_{\mathrm{MF}}[\varphi]$ with

$$\mathcal{A}_{\mathrm{RPA}}[\varphi] = \frac{1}{2}\sum_{\eta\nu} \int_\mathcal{C} \mathrm{d}\xi\mathrm{d}\xi'\, \varphi_\eta(\xi)V_{\eta\nu}^{-1}(\xi,\xi')\varphi_\nu(\xi'), \quad \mathcal{A}_{\mathrm{MF}}[\varphi] = -\sum_\eta \int_\mathcal{C} \mathrm{d}\xi\, \varrho_{0\eta}\, \varphi_\eta(\xi) \tag{2.25}$$

and effective interaction $V_{\eta\nu}^{-1} = U_{\eta\nu}^{-1} - \delta_{\eta\nu}\Pi_\eta$. Thus only the mean density $\varrho_{0\eta}$ and the polarizability $\propto \Pi_\eta$ of the electronic system remain perceptible to the Hubbard-Stratonovich field φ.

Before concluding this section, let us illustrate the equivalence between the two bosonization techniques outlined here and in the previous section. To this end we recompute the fermionic Green's functions

$$iG_\eta^{\gtrless}(\xi_1,\xi_2) = \left\langle \psi_\eta^{b/f}(\xi_1)\bar\psi_\eta^{f/b}(\xi_2)\right\rangle = \int \mathcal{D}\varphi\, e^{i\mathcal{A}[\varphi]}\, e^{i\Theta_\eta^{b/f}(\xi_1) - i\Theta_\eta^{f/b}(\xi_2)} \int \mathcal{D}\psi\mathcal{D}\bar\psi\, e^{i\mathcal{A}_0[\psi,\bar\psi]}\, \psi_\eta^{f/b}(\xi_1)\bar\psi_\eta^{b/f}(\xi_2)$$

in functional bosonization. For simplicity we focus on the zero temperature limit and $eV_\eta = 0$.

Since $\mathcal{A}[\varphi]$ is Gaussian, the respective average value $\left\langle \varphi_\mu(\xi)\right\rangle_0$ and the correlator of the fluctuations $\delta\varphi_\mu(\xi) \equiv \varphi_\mu(\xi) - \left\langle \varphi(\xi)\right\rangle_0$ are simply given by $\left\langle \varphi_\mu(\xi)\right\rangle_0 = \sum_\nu \int_\mathcal{C} \mathrm{d}\xi'\, V_{\mu\nu}(\xi,\xi')\varrho_{0\nu}(\xi') = 0$ and $\left\langle \delta\varphi_\mu(\xi)\delta\varphi_\nu(\xi')\right\rangle_0 = iV_{\mu\nu}(\xi,\xi')$. Further, Gaussian cumulant expansion shows $\left\langle e^{i\Phi[\varphi]}\right\rangle_0 = e^{\left\langle i\Phi[\varphi] - \frac{1}{2}\delta\Phi[\varphi]^2\right\rangle_0}$ for linear functions $\Phi[\varphi]$ of φ and, thus,

$$iG_\eta^{\gtrless}(\xi_1,\xi_2) = \exp\left\{-\frac{1}{2}\left\langle \left[\delta\Theta_\eta^{b/f}(\xi_1) - \delta\Theta_\eta^{f/b}(\xi_2)\right]^2\right\rangle_0\right\}\, iG_{0\eta}^{\gtrless}(\xi_1,\xi_2),$$

i.e. we are left with evaluating the phase correlators $iD_{\Theta,\mu\nu}(\xi,\xi') = \left\langle \delta\Theta_\mu(\xi)\delta\Theta_\nu(\xi') \right\rangle$. From (2.16), or symbolically $\Theta_\mu = -D_{0\mu}\varphi_\mu$, one obtains the relation

$$D_{\Theta,\mu\nu} = -D_{0\mu}V_{\mu\nu}D_{0\nu}. \tag{2.26}$$

Within the Luttinger model (2.11) the retarded and advanced components of the effective interaction read in frequency-momentum representation

$$V_{\eta\eta}^{r/a}(\omega,q) = g_4 \frac{\left[\omega + \eta v_F(1+\kappa)q\right]\left[\omega - \eta v_F q\right]}{\omega_\pm^2 - u^2 q^2}, \quad \kappa \equiv \frac{1}{2\pi v_F}\frac{g_4^2 - g_2^2}{g_4},$$

$$V_{+-}^{r/a}(\omega,q) = V_{-+}^{r/a}(\omega,q) = g_2 \frac{\omega^2 - v_F^2 q^2}{\omega_\pm^2 - u^2 q^2}$$

with $\omega_\pm = \omega \pm i0$. Plasmon velocity u and Luttinger parameter K were defined in (2.6).The relation (2.26), combined with the bare particle-hole propagator (2.18), gives then the phase correlators

$$D_{\Theta,\eta\eta}^{r/a}(\omega,q) = -\,\eta \frac{g_4}{2u\omega}\frac{\omega + \eta v_F(1+\kappa)q}{\omega}\left[\frac{u}{u-v_F}\frac{1}{q-\eta\omega_\pm/u} - \frac{u}{u+v_F}\frac{1}{q+\eta\omega_\pm/u}\right. \tag{2.27}$$

$$\left. -\frac{2uv_F}{u^2 - v_F^2}\frac{1}{q-\eta\omega_\pm/v_F}\right], \tag{2.28}$$

$$D_{\Theta,-\eta\eta}^{r/a}(\omega,q) = -\frac{g_2}{2u\omega}\left[\frac{1}{q-\omega_\pm/u} - \frac{1}{q+\omega_\pm/u}\right]. \tag{2.29}$$

Transforming the above relations into the mixed space-frequency representation one obtains

$$D_{\Theta,\eta\nu}^{r/a}(\omega,x) = \mp\frac{2\pi i}{\omega}\left\{\theta(\pm\eta x)\left[c_{\eta\nu}^+ \, e^{i\eta\omega x/u} - \delta_{\eta\nu} \, e^{i\eta\omega/v_F}\right] + \theta(\mp\eta x) \, c_{\eta\nu}^- \, e^{-i\eta\omega x/u}\right\} \tag{2.30}$$

$$\text{with } c_{\eta\eta}^\pm = (1\pm K)^2/(4K), \quad c_{\eta,-\eta}^\pm = (1-K^2)/(4K). \tag{2.31}$$

Note that the prefactors are intimately linked to the Bogoliubov transformation (2.7): $c_{\eta\eta}^+ = \cosh^2\zeta$, $c_{-\eta\eta}^- = \sinh^2\zeta$, and $c_{\eta,-\eta}^\pm = -\sinh\zeta\cosh\zeta$. The Keldysh component of the phase correlator is given by the fluctuation-dissipation theorem

$$D_{\Theta,\eta\nu}^k(\omega,x) = \left(1 + 2N(\omega)\right)\left(D_{\Theta,\eta\nu}^r(\omega,x) - D_{\Theta,\eta\nu}^a(\omega,x)\right) \tag{2.32}$$

with bosonic distribution function $N(\omega)$, see (2.20). For simplicity we concentrate on zero temperature where $1 + 2N(\omega) = \text{sign}\,\omega$. Keldysh rotation then yields

$$D_{\Theta,\eta\nu}^{\gtrless}(\omega,x) = \pm\,\theta(\pm\omega)\left(D_{\Theta,\eta\nu}^r(\omega,x) - D_{\Theta,\eta\nu}^a(\omega,x)\right),$$
$$D_{\Theta,\eta\nu}^{T/\tilde{T}}(\omega,x) = \pm\,\theta(\pm\omega)D_{\Theta,\eta\nu}^r(\omega,x) \pm \theta(\mp\omega)D_{\Theta,\eta\nu}^a(\omega,x) \tag{2.33}$$

In the real-time representation (x,t) these phase-phase correlation functions can be decomposed into plasmon (moving with velocity u) and bare particle-hole pair (having velocity v_F) contributions

$$iD_{\Theta,\eta\nu}^{\alpha\beta}(t,x) = c_{\eta\nu}^+ \, \mathcal{L}_{\eta u}^{\alpha\beta}(t,x) - c_{\eta\nu}^- \, \mathcal{L}_{-\eta u}^{\alpha\beta}(t,x) - \delta_{\eta\nu} \, \mathcal{L}_{\eta v_F}^{\alpha\beta}(t,x) \tag{2.34}$$

where for given velocity v the functions $\mathcal{L}_v^{\alpha\beta}(t,x)$ satisfy the equations

$$\partial_t \mathcal{L}_v^{\gtrless}(t,x) = -(t \mp ia - x/v)^{-1}, \quad \partial_t \mathcal{L}_v^{T/\tilde{T}}(t,x) = -(t \mp ia \operatorname{sign} x/v - x/v)^{-1}.$$

This follows from Eq. (2.33) and Fourier transformation from ω to t, taking into account the high-energy cutoff $\Lambda \sim a^{-1}$. We choose the solutions

$$\mathcal{L}_v^{\gtrless}(t,x) = \ln \frac{\mp ia}{t \mp ia - x/v}, \quad \mathcal{L}_v^{T/\tilde{T}}(t,x) = \ln \frac{\mp ia \operatorname{sign} x/v}{t \mp ia \operatorname{sign} x/v - x/v}. \tag{2.35}$$

It is worth mentioning that the appearance of both plasmon and bare particle-hole pair "light-cone" singularities in our phase-phase correlation function is a characteristic feature of the functional bosonization approach. Here, the latter exactly cancels the free electron singularity from the noninteracting Green's function, yielding

$$iG_\eta^{\gtrless}(\xi = \xi_1 - \xi_2) = \frac{\mp i}{2\pi v_F a} \left(\frac{\mp ia}{t - \eta x/u \mp ia} \right)^{1+\gamma} \left(\frac{\mp ia}{t + \eta x/u \mp ia} \right)^{\gamma}, \tag{2.36}$$

which is indeed the zero temperature limit of Eq. (2.8). Before turning to the generalization of the presented approach to quantum wire networks in Chapter 3, we conclude the present chapter with the nonequilibrium extension of the operator bosonization technique.

2.3 Nonequilibrium Bosonization

The conventional bosonization approach of Section 2.1 was extended within the Keldysh framework in Refs. [13, 14] to arbitrary nonequilibrium situations in the absence of scattering between different fermion species. The bosonization identities for field operators (2.3) and the Hamiltonian (2.5) are exact operator identities and do not depend on the many-body state of the system, which is encoded in the density operator $\hat{\rho}$. In general nonequilibrium situations where it is not a simple function of the Hamiltonian bosonization of $\hat{\rho}$ is far from straightforward. Even a *free* nonequilibrium fermionic system is in general not garanteed to be mapped to a *Gaussian* bosonic theory as we will see in this section.

Rather than bosonizing the density operator explicity, one derives the bosonic Keldysh action which likewise encodes the full many-body state. Knowing that the mapping to bosonic degrees of freedoms (density ϱ) is exact one finds the bosonic action by

$$e^{i\mathcal{A}[\varrho]} = \int \mathcal{D}\psi \mathcal{D}\bar{\psi}\, e^{i\mathcal{A}[\psi,\bar{\psi}]} \delta[\bar{\psi}\psi - \varrho]$$

$$= \int \mathcal{D}V \int \mathcal{D}\psi \mathcal{D}\bar{\psi}\, e^{i\mathcal{A}[\psi,\bar{\psi}] - iV\left(\bar{\psi}\psi - \varrho\right)}.$$

We resort here on a formal notation where e.g. $V\varrho \equiv \int_\mathcal{C} \mathrm{d}\xi\, V(\xi)\varrho(\xi)$. Note that in the thermodynamic limit and in the absence of scattering between different fermion species, Klein factors in the action are negligible. Bosonization is completed, once $\psi, \bar{\psi}$-fields are integrated out. This is straightforwardly achieved if interaction is absent, whence the action is Gaussian in fermionic fields. In the presence of

interaction one can decouple quartic terms by a Hubbard-Stratonovich transformation as described in the previous section. Let us consider this general situation:

$$
\begin{aligned}
e^{i\mathcal{A}[\varrho]} &= \int \mathcal{D}V \int \mathcal{D}\psi \mathcal{D}\bar{\psi}\mathcal{D}\varphi \, e^{i\mathcal{A}_0[\psi,\bar{\psi}]+i\mathcal{A}_{\mathrm{int}}[\varphi]-i(V+\varphi)\bar{\psi}\psi+iV\varrho} \\
&= \int \mathcal{D}V\mathcal{D}\varphi \left(\int \mathcal{D}\psi \mathcal{D}\bar{\psi} \, e^{i\mathcal{A}_0[\psi,\bar{\psi}]-iV\bar{\psi}\psi} \right) e^{i\mathcal{A}_{\mathrm{int}}[\varphi]+i(V-\varphi)\varrho} \\
&= \int \mathcal{D}V\mathcal{D}\varphi \, \mathcal{Z}[V] \, e^{i(V-\varphi)\varrho} \, e^{i\mathcal{A}_{\mathrm{int}}[\varphi]} \\
&= \int \mathcal{D}V \, \mathcal{Z}[V] \, e^{iV\varrho} e^{i\mathcal{A}_{\mathrm{int}}[\varrho]}
\end{aligned}
\tag{2.37}
$$

where $\mathcal{A}_{\mathrm{int}}[\varphi]$ is defined in (2.12) and

$$
\mathcal{A}_{\mathrm{int}}[\varrho] = -2\sum_{\eta\nu} \int \mathrm{d}\xi\mathrm{d}\xi' \, \varrho_\eta^c(\xi) U_{\eta\nu}(\xi,\xi')\varrho_\nu^q(\xi').
$$

Of course, $\mathcal{A}[\varrho]$ is the bosonized version of $\mathcal{A}_{\mathrm{int}}[\psi,\bar{\psi}]$. For what follows it is convenient to work in the rotated Keldysh representation $\varrho_\eta^{c/q}$; time integration, $\int \mathrm{d}\xi = \int \mathrm{d}t\mathrm{d}x$ is to be performed along the real axis.

The partition sum $\mathcal{Z}[V]$ quite obviously coincides with the Jacobian $\mathcal{Z}[\varphi]$ of the gauge transformation in the previous section (with HS field φ replaced by the "source field" V) ,(2.22), and is the sum of vacuum loops with external field V. In the general nonequilibrium situation the Dzyaloshinskii-Larkin theorem does not apply and higher-order loops contribute. It is then more convenient to represent $\mathcal{Z}[V]$ in a different form which exposes the dependence on the Keldysh field components of φ more explicitly. To this end one makes use of an identity derived by [20] which relates many-body traces to single-particle determinants. Since we will derive these results in a more general setup in Chapter 3 we skip the details here. The partition sum reads

$$
\mathcal{Z}[V] = \prod_\eta e^{-2iV_\eta^c \Pi_\eta^a V_\eta^q} \, \tilde{\mathcal{Z}}[V_\eta^q], \quad \tilde{\mathcal{Z}}[V_\eta^q] = \mathrm{Det}\left[\mathbb{1} + \left(e^{i\delta_\eta} - \mathbb{1} \right) f_\eta \right]
$$

with the time-dependent phase

$$
\delta_\eta(t) = -2|v_\eta|^{-1} \int_{-\infty}^{\infty} \mathrm{d}x \, V_\eta^q(x,t+x/v_\eta)
\tag{2.38}
$$

and the distribution functions $f_\eta(\epsilon)$ of fermion species η.

Remarkably, summing up all vacuum loops is thus equivalent to evaluating a 1D functional determinant which purely depends on the quantum component V_η^q. Solely the Schwinger anomalous contributions to the 2nd-order loop which couple to V_η^c are not captured by the determinant. With V_η^c appearing only linearly in the exponent, the V-integral (2.37) can be exactly calculated:

$$
e^{i\mathcal{A}_0[\varrho]} = e^{i\mathcal{A}_{\mathrm{int}}[\varrho]} \prod_\eta e^{2i\varrho_\eta^c \Pi_\eta^{a-1}\varrho_\eta^q} \, \mathrm{Det}\left[\mathbb{1} + \left(e^{i\delta_\eta} - \mathbb{1} \right) f_\eta \right]\Bigg|_{V_\eta^q = \Pi_\eta^{a-1}\varrho_\eta^q}.
$$

For a given density configuration ϱ_η^q the counting phases δ_η are related via (2.38) to the source fields

$$V_\eta^q(x,t) = -2\pi|v_\eta| \left[\varrho_\eta^q(x,t) + \int_{t_0}^{x/v_\eta} dt' \, \dot\varrho_\eta^q(v_\eta t', t) \right] \tag{2.39}$$

where t_0 is an arbitrary integration constant, that will turn out to be unimportant. This completes the bosonization of the Keldysh action. Very conveniently it has an especially simple dependence on ϱ_η^c that will enable us to perform ϱ-integration exactly.

To illustrate this we consider the fermionic Green's function $G_\eta^{\gtrless}$. Using that the relation $\varrho_\eta^c = \frac{\eta}{2\pi}\partial_x\phi_\eta^c$ implies a linear dependence of ϕ_η^c on ϱ_η^c, say,

$$\phi_\eta^c(x,t) = 2\pi\eta \sum_\nu \int dt' dx' \, \delta(t-t')\theta(x-x')\delta_{\eta\nu}\varrho_\nu^c(x',t')$$

$$\equiv \sum_\nu \int dt' dx' \, J_{\eta,x,t}(x',t',\nu)\varrho_\nu^c(x',t'), \quad \text{with} \quad \frac{\eta}{2\pi}\partial_{x'}J_{\eta,x,t}(x',t',\nu) = -\delta_{\eta\nu}\delta(t-t')\delta(x-x')$$

the Green's function can be written

$$G_\eta^{\gtrless}(\xi_1,\xi_2) = -\frac{i}{2\pi a} \left\langle e^{i\phi_\eta^{b/f}(\xi_1)} e^{-i\phi_\eta^{f/b}(\xi_2)} \right\rangle$$

$$= -\frac{i}{2\pi a} \, e^{\pm i(J_{\eta\xi_1}+J_{\eta\xi_2})\varrho^q} \prod_\mu \mathrm{Det}\left[\mathbb{1} + \left(e^{i\delta_\mu} - \mathbb{1}\right) f_\mu \right] \Bigg|_{(U-\Pi^{a-1})\varrho^q = \frac{1}{2}(J_{\eta\xi_1}-J_{\eta\xi_2})} \tag{2.40}$$

with counting phases δ_η related by (2.38) and (2.39) to the *advanced* solution ϱ_μ^q of

$$\left(\partial_t + v_\mu\partial_x\right)\varrho_\mu^q(\xi) + \sum_\nu \int dx' \, \frac{\mu}{2\pi}\partial_x U_{\mu\nu}(x,x')\varrho_\nu^q(x',t) = \frac{1}{2}\delta_{\mu\eta}\left[\delta(\xi_2-\xi) - \delta(\xi_1-\xi)\right].$$

Advancedness of the quantum density configuration, $\varrho^q(x,t) = 0$ for $t \to +\infty$ (in the above example specifically $t > t_1, t_2$), is a general feature of the theory. Taking this into account (2.38), (2.39) can be combined to

$$\delta_\eta(t) = 4\pi|v_\eta| \lim_{\tilde t \to -\infty} \int_{\tilde t - t}^{t_0} d\tau \, \varrho_\eta^q(v_\eta\tau, \tilde t). \tag{2.41}$$

The phase is thus sensitive to the asymptotic behavior of the charge density in the *incoming* leads.

The 1D fermionic field theories presented in this chapter are based on single-particle spectra without lower band edges. While the infinitely many artificial negative-energy states do not contribute to the low-energy physics, they lead to UV divergent Fredholm determinants in (2.40). A possible regularization scheme is discretization of the time coordinate t in steps $\Delta t = \pi/\Lambda$ which amounts to the introduction of the "hard" UV cutoff Λ and a restriction of energies to the range $(-\Lambda, \Lambda]$. The discretization turns operators $g(t,t')$ into (possibly infinite) matrices $\left(g_{jk}\right)$. The resulting observables, in our example $G_\eta^>(\xi_1,\xi_2)$, will have a slow dependence on positions and times ξ_j and other low-energy parameters like temperatures and voltages which is independent of the regularization scheme. Fast oscillations, set by the energy scale Λ, in contrast, are nonuniversal and sensitive to the regularization

scheme, and usually not of interest. To be consistent with the previous sections where the equilibrium Green's functions $G_{0\eta}^{>}$ were obtained with a "smooth" cutoff procedure, one can write

$$G_{\eta}^{\gtrless}(\xi_1, \xi_2) = G_{0\eta}^{\gtrless}(\xi_1, \xi_2) \prod_{\mu} \bar{\Delta}_{\mu}. \tag{2.42}$$

Here, the determinant is normalized with respect to equilibrium (with distribution function f_0),

$$\bar{\Delta}_{\mu} \equiv \frac{\mathrm{Det}\left[\mathbb{1} + \left(e^{i\delta_{\mu}} - \mathbb{1}\right) f_{\mu}\right]}{\mathrm{Det}\left[\mathbb{1} + \left(e^{i\delta_{\mu}} - \mathbb{1}\right) f_0\right]}. \tag{2.43}$$

Being UV convergent the ratio is insensitive to the regularization scheme. We will later apply the "hard" cutoff regularization (time discretization) outlined above.

To be specific, let us turn to the spinless Luttinger model with $U_{+-}(x, x') = U_{-+}(x, x') = g_2(x)\delta(x - x')$, $U_{++}(x, x') = U_{--}(x, x') = g_4(x)\delta(x - x')$ and $\eta = +$. The equations of motion for the density then read

$$\left[\partial_t + v_F \partial_x \left(1 + \frac{g_4(x)}{2\pi v_F}\right)\right] \varrho_+^q(x, t) + v_F \partial_x \frac{g_2(x)}{2\pi v_F} \varrho_-^q(x, t) = \frac{1}{2} \left[\delta(\xi_2 - \xi) - \delta(\xi_1 - \xi)\right]$$

$$\left[\partial_t - v_F \partial_x \left(1 + \frac{g_4(x)}{2\pi v_F}\right)\right] \varrho_-^q(x, t) - v_F \partial_x \frac{g_2(x)}{2\pi v_F} \varrho_+^q(x, t) = 0. \tag{2.44}$$

In principle, the interaction parameters g_2, g_4 may have arbitrary time and position dependences. In Ref. [14] e.g. the effect of sharp boundaries between the interacting wire and the noninteracting leads was studied, at which plasmons are partially reflected. Let us focus here on a simpler situation. The main purpose of this introductory treatment is to relate the presented approach to the previously shown bosonization techniques with which we computed the Green's functions of an infinitely long wire. To this end we assume the wire to be adiabatically connected to the leads, such that $\partial_x g_j(x) = 0$ are negligible, the equations of motion can be decoupled by the Bogoliubov transformation (compare with (2.7))

$$\begin{pmatrix} \varrho_+^q \\ \varrho_-^q \end{pmatrix} = \begin{pmatrix} \cosh\zeta & \sinh\zeta \\ \sinh\zeta & \cosh\zeta \end{pmatrix} \begin{pmatrix} \tilde{\varrho}_+^q \\ \tilde{\varrho}_-^q \end{pmatrix}, \quad \text{with } \cosh\zeta(x) = \frac{1 + K(x)}{2\sqrt{K(x)}}, \quad \sinh\zeta(x) = -\frac{1 - K(x)}{2\sqrt{K(x)}},$$

which yields the equations for the right- and left-moving plasmonic modes

$$\left(\partial_t + \partial_x u(x)\right) \tilde{\varrho}_+^q(\xi) = \frac{1}{2} c \left[\delta(\xi_2 - \xi) - \delta(\xi_1 - \xi)\right], \quad c \equiv \cosh\zeta,$$

$$\left(\partial_t - \partial_x u(x)\right) \tilde{\varrho}_-^q(\xi) = -\frac{1}{2} s \left[\delta(\xi_2 - \xi) - \delta(\xi_1 - \xi)\right], \quad s \equiv \sinh\zeta. \tag{2.45}$$

Luttinger parameter and plasmon velocity are related to the coupling strengths via (2.6). The Green's function $G_+(\xi_1, \xi_2)$ measures the response of the interacting system to the injection of a right-moving electron at ξ_1 and its later extraction at ξ_2. In the presence of interaction the corresponding charge

excitation splits into a right-moving and a left-moving plasmonic excitation $\tilde{\varrho}_+$ and $\tilde{\varrho}_-$ with relative weights $(1 + K)/2$ and $(1 - K)/2$, respectively.

Let us consider exemplarily the charge response to a single source,

$$\left(\partial_t \pm \partial_x u(x)\right) \tilde{\varrho}_\pm = \frac{Q}{2} \delta(t - \bar{t}) \delta(x - \bar{x}).$$

The advanced solution, which vanishes for $t > \bar{t}$, is

$$\tilde{\varrho}_\pm(x, t) = -\frac{Q}{2} \frac{v_F}{u(x)} \, \delta\left[\int_{\bar{x}}^{x} dx' \, \frac{v_F}{u(x')} \mp v_F(t - \bar{t})\right] \theta(\bar{t} - t).$$

We are interested in the asymptotic behavior of $\tilde{\varrho}_\pm$ for $t \to -\infty$, i.e. in the incoming leads, $\pm x \to -\infty$, where interaction is assumed to be absent and $u(x \to \pm\infty) = v_F$. Let $u(x)$ interpolate adiabatically between the free and the full value v_F and $\bar{u} = u(\bar{x})$, respectively, such that in a broad region which contains $x = \bar{x}$ (and all possibly relevant sources) and, say, $x = 0$, the function $u(x)$ takes on the constant value $\bar{u}$, and for very negative or positive coordinates, say, $x \leq x_-$ and $x \geq x_+$, it is constantly $u(x) = v_F$ (see Fig. 2.2). For $\pm x \to -\infty$ it is

$$\tilde{\varrho}_\pm(x, t) = -\frac{Q}{2} \theta(\bar{t} - t) \delta\left[x - \tilde{x}_\pm - \frac{v_F}{\bar{u}} \bar{x} \mp v_F(t - \bar{t})\right] \quad \text{with } \tilde{x}_\pm \equiv x_\mp - \int_0^{x_\mp} dx' \, \frac{v_F}{u(x')}.$$
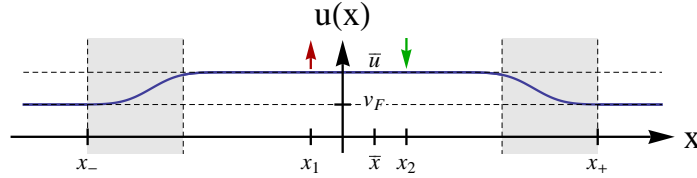

Figure 2.2: *Sketch of local plasmon velocity $u(x)$ in a Luttinger liquid, adiabatically connected to noninteracting leads. Regions where $u(x)$ interpolates between $\bar{u}$ and v_F are gray shaded*

The corresponding counting phase (2.41) is

$$\tilde{\delta}_\pm(t) = -2\pi Q \, \theta(t - \bar{t} \pm \bar{x}/\bar{u} \pm \tilde{x}_\pm/v_F).$$

In our example of the Luttinger liquid model (2.44), (2.45) the phases read

$$\begin{aligned}
\delta_+(t) &= -2\pi\bar{c} \, \left[\theta(t - t_2 + x_2/\bar{u} + \tilde{x}_+/v_F) - \theta(t - t_1 + x_1/\bar{u} + \tilde{x}_+/v_F)\right], \\
\delta_-(t) &= 2\pi\bar{s} \, \left[\theta(t - t_2 - x_2/\bar{u} - \tilde{x}_-/v_F) - \theta(t - t_1 - x_1/\bar{u} - \tilde{x}_-/v_F)\right]
\end{aligned} \tag{2.46}$$

with $\bar{c} = \cosh\bar{\zeta}$, $\bar{s} = \sinh\bar{\zeta}$, and $\bar{\zeta} = \zeta(x_1) = \zeta(x_2)$. Fig. 2.3 shows the corresponding density trajectories $\varrho_\pm^q$ in response to the sources at ξ_2 and ξ_1, and depicts pictorially how the phase (2.41) "counts" the charge in the incoming leads.
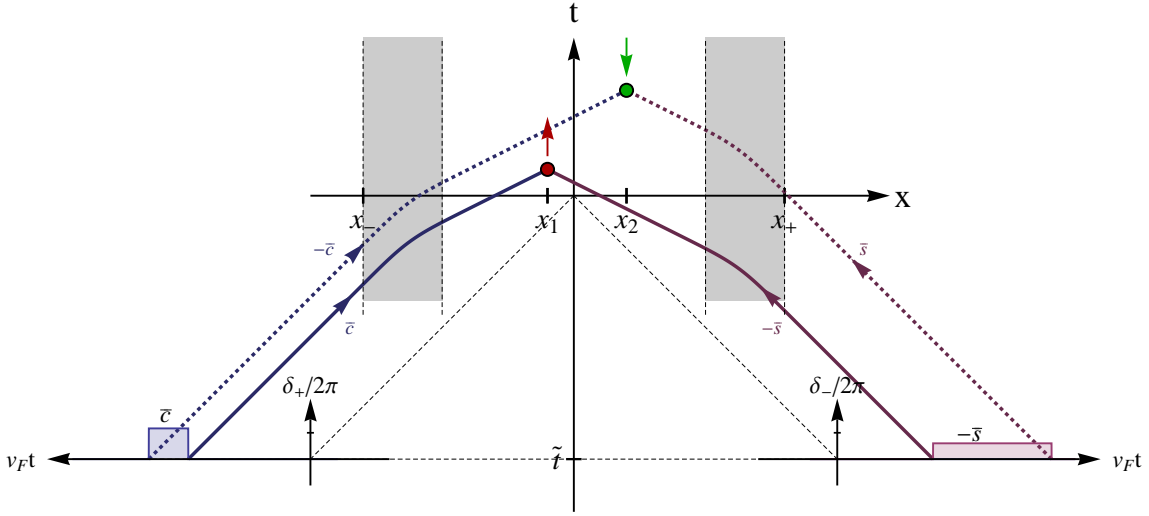
Figure 2.3: *Sketch of the density trajectories $\varrho_\pm^q$. Right-moving densities are depicted* blue, *left-moving ones* purple. *Lines correspond to traces of peaks with different weights $\bar{c}$, $-\bar{s}$. Solid lines correspond to positive, dashed ones to negative weights. In the gray shaded region $u(x)$ interpolates between $\bar{u}$ and v_F such that trajectories bend.*

Evaluation of the Fredholm determinant

In the Luttinger liquid and some other interaction models, the phases $\delta_\mu(t)$ are, quite generically, piecewise constant functions. In the example of the Luttinger liquid Green's function, which we consider, they are constant on some interval $I_\mu = [\bar{t}, \bar{t} + \tau] \subset \mathbb{R}$ and vanish outside. If we denote by $\mathbb{1}_{I_\mu}$ the characteristic function of I_μ, $\mathbb{1}_{I_\mu}(t) = 1$ if $t \in I_\mu$ and $\mathbb{1}_{I_\mu}(t) = 0$ otherwise, then the phases are of the form $\delta_\eta(t) = \bar{\delta}_\mu \mathbb{1}_{I_\mu}(t)$ with some constants $\bar{\delta}_\mu$. Introducing the projectors P_μ which acts on functions $\phi(t)$ by multiplication with $\mathbb{1}_{I_\mu}$ and thus satisfies $P_\mu^2 = P_\mu$ it is

$$\tilde{\mathcal{Z}}_\mu[V_\mu^q] = \mathrm{Det}\left[\mathbb{1} + P_\mu\left(e^{i\bar{\delta}_\mu} - 1\right)f_\mu\right] = \mathrm{Det}\left[\mathbb{1} + P_\mu\left(e^{i\bar{\delta}_\mu} - 1\right)f_\mu P_\mu\right]. \tag{2.47}$$

The operator $g \equiv \mathbb{1} + P_\mu\left(e^{i\bar{\delta}_\mu} - 1\right)f_\mu P_\mu$ has a temporal "block structure" in the sense

$$g(t_1, t_2) = \begin{cases} \delta(t_1 - t_2) + \left(e^{i\bar{\delta}_\mu} - 1\right)f_\mu(t_1 - t_2) \equiv \tilde{g}(t_1 - t_2), & t_1, t_2 \in I_\mu, \\ \delta(t_1 - t_2), & \text{otherwise.} \end{cases} \tag{2.48}$$

It is nontrivial only if both t_1 and t_2 lie in the interval I_μ, in which case it depends solely on the difference $t_1 - t_2$. Its determinant will be given by the nontrivial block $\tilde{g}(t_1 - t_2)$. When applying the above mentioned hard cutoff procedure and discretizing times, $t_j = \bar{t} + (j-1)\pi/\Lambda$, the operator $\tilde{g}$ is converted into a large (but finite) $N \times N$-matrix $\left(g_{jk}\right)_{1 \le j, k \le N}$, $N = \tau/\Delta t = \Lambda\tau/\pi$, which is of *Toeplitz* form: Its elements depend on index differences, $g_{jk} = g_{j-k}$. Matrices of this form are ubiquitous in mathematical physics where they appear e.g. in the context of magnetism, random matrix theory,

and full counting statistics. Gutman et al.[21] showed that observables in a vast range of problems of nonequilibrium interacting fermions (and bosons) in 1D can be expressed in terms of Toeplitz determinants $\Delta_N = \det \left(g_{i-j} \right)_{1 \leq i,j \leq N}$ and computed their large-N asymptotic behavior. Generalizing known mathematical results (Szegö theorem, Fisher-Hartwig conjecture) the authors were also able to identify subleading contributions which are crucial to obtain an oscillatory dependence of Δ_N on N [21, 22]. The results are summarized in Appendix A.

They are applicable at zero temperature when distribution functions $f_\mu(\epsilon)$ are piecewise constant and exhibit sharp jumps. In partial equilibrium each of them has one single-step, $f_\mu(\epsilon) = \theta(eV_\mu - \epsilon)$, at corresponding chemical potentials eV_μ. Using (A.9) and (2.46) the Luttinger liquid Green's function (2.40) is

$$G_+^{\gtrless}(\xi = \xi_1 - \xi_2) \propto \Lambda^{-2\gamma} \; \frac{e^{-i\bar{c}(\Lambda+eV_+)(t-x/\bar{u})}}{\left[t - x/\bar{u}\right]^{1+\gamma}} \; \frac{e^{i\bar{s}(\Lambda+eV_-)(t+x/\bar{u})}}{\left[t + x/\bar{u}\right]^{\gamma}}$$

with equilibrium exponents, $\gamma \equiv (1 - K(0))^2/(4K(0)) = \bar{s}^2$. The results agrees with those obtained in the previous sections, Eqs. 2.8 and 2.36, up to the fast oscillating terms $e^{i\Lambda t}$ which stem from the hard cutoff Λ. By making use of the normalization (2.43) instead we obtain

$$G_+^{\gtrless}(\xi = \xi_1 - \xi_2) = \frac{\mp ia}{2\pi a v_F} \; e^{-i\bar{c}eV_+(t-x/\bar{u})+i\bar{s}eV_-(t+x/\bar{u})} \; \left(\frac{\mp ia}{t - x/\bar{u} \mp ia} \right)^{1+\gamma} \left(\frac{\mp ia}{t + x/\bar{u} \mp ia} \right)^{\gamma}$$

with short-time cutoff $a \sim \Lambda^{-1}$. Of course, the real power of the considered bosonization approach is reveiled in true nonequilibrium situations, especially in combination with spatially or temporally varying interacting strength where interaction gradients lead to backscattering of plasmons. In Chapter 7 we will apply the method to the problem of an interaction quench in a nonequilibrium Luttinger liquid.

3

Functional Bosonization of Quantum Wire Networks

In this chapter we develop a general approach to nonequilibrium nanostructures formed by one-dimensional channels which are coupled by tunnel junctions or impurity scattering. Possible one-dimensional elements are semiconducting and metallic quantum wires, carbon nanotubes and quantum Hall edge states.

The standard analytical approach to interacting one-dimensional systems (Luttinger liquids) is bosonization. In Chapter 2 we presented the commonly used operator bosonization technique and its recently developed nonequilibrium generalization. The latter provides an elegant technique to treat setups where the fermionic nonequilibrium distribution function is created outside the interacting region and "injected" into the Luttinger liquid. We will focus on a more complicated situation when the tunneling or the impurity backscattering takes place inside the interacting part of the system. Such coupling terms represent in general a very serious complication for the standard bosonization, and we are not aware of any way to solve the problem exactly. We choose instead an alternative route based on the functional bosonization formalism (see Sect. 2.2) that retains both fermionic and bosonic degrees of freedom. Combining the functional bosonization idea with the Keldysh nonequilibrium framework, we derive the Keldysh action for the considered class of problems. This action has a structure reminiscent of that of the generating function of the full counting statistics[23–25]. Our action generalizes that of Ref. [20] where a local scatterer under nonequilibrium conditions was explored.

As we will illustrate in Chapter 6 the formalism can be used for an exact treatment of specific setups. In general, this may not be possible and we present here an approximation scheme which applies for weak tunneling. The developed real-time instanton (saddle-point) method will allow us to determine Keldysh Green functions characterizing physical observables under interest (tunneling density of states, distribution functions, current-voltage characteristics, etc.).

While this chapter concentrates on the formal aspects of the model, a number of important applications such as quantum Hall interferometers and quantum wires with impurities will be the subject of the remainder of this thesis.

The results presented here have been published in Ref. [26].

3.1 Model and Keldysh Action

Let us consider a general model of a ballistic conductor which can be represented as a network of one-dimensional (1D) chiral channels and point scatterers, as shown in Fig. 3.1. It is assumed that electrons propagate along the channels, denoted by lower Greek index μ, with constant velocity v_μ from source to drain reservoirs located at coordinates x_μ^S and x_μ^D, respectively. In the physical world such channels are realized by quantum Hall (QH) edge states or right-/left-moving 1D states in quantum wires. At point scatterers, denoted by Latin index j, instantaneous tunneling between different channels occurs, which is described by the scattering matrix s^j. Typical examples of scatterers are quantum point contacts (QPCs) or impurities in nanowires. A somewhat less trivial type of scatterer is a multi-terminal junction that can be realized by a quantum dot under assumption that its Thouless energy is well above all typical energy scales of the problem such as the temperature and the voltage.

We also require that each chiral channel in the absence of tunneling is connected to one source and one drain reservoir (rather than forms a loop).

Albeit quite simple, our quantum-wire network model covers a broad class of mesoscopic ballistic devices, including QH interferometers and quantum wire junctions (See Fig. 3.1). We note also that the importance of network models has been well appreciated in the context of the integer QH effect, where the Chalker-Coddington network model [27] serves as a highly useful starting point for numerical and analytical investigation of the QH transition.
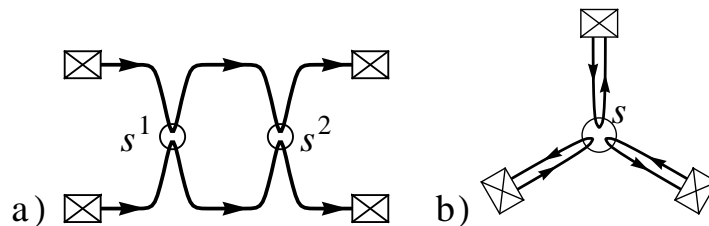

Figure 3.1: *Two possible realizations of our model:* (a) *Mach-Zehnder quantum Hall interferometer and* (b) *junction of three quantum wires. Channels are represented by solid lines, point scatterers by white circles, reservoirs by boxes. Arrows indicate directions of motion.*

In the absence of tunneling, i.e. when all scattering matrices are trivial, $s^j = \mathbb{1}$, different chiral channels are fully disconnected from each other. Unter the assumption that each channel is in a separate equilibrium state, interaction can be taken into account by the functional bosonization approach presented in Sect. 2.2.

Throughout this chapter we consider the zero temperature limit with different channels η having possibly different chemical potentials eV_η. In time representation the distribution functions of source reservoirs η read

$$f_\eta(t, t') = f_\eta(t - t') = e^{-ieV_\eta(t-t')} f_0(t - t')$$

with the equilibrium Fermi distribution function $f_0(\epsilon) = \theta(-\epsilon)$. For future reference we also define the "hole" distribution function $f_0^>(\epsilon) = 1 - f_0(\epsilon)$ and write also $f_0^< \equiv f_0$. In time representation we have

$$f_0^{\lessgtr}(t) = \pm \frac{i}{2\pi} \frac{1}{t \pm ia} \tag{3.1}$$

with the short-time cutoff $a \sim \Lambda^{-1}$.

Recapitulating Sect. 2.2, we remind us that interaction is encoded in an action $\mathcal{A}_{\text{int}}[\psi, \bar{\psi}]$, cf. (2.10), which is biquadratic in fermionic fields ψ, $\bar{\psi}$. It can be replaced by terms which are bilinear in ψ, $\bar{\psi}$ via a Hubbard-Stratonovich transformation at the expense of introducing a mediating (bosonic) field φ. The latter can be further decoupled from the fermionic degrees of freedom by a gauge transformation (2.15). The corresponding Jacobian (2.22) leads to corrections to the bosonic action which in the absence of tunneling is quadratic in φ and takes into account screening in random-phase approximation (2.25),

$$\mathcal{A}_0[\varphi] = \frac{1}{2} \sum_{\eta\nu} \int_{\mathcal{C}} \mathrm{d}\xi \mathrm{d}\xi' \, \varphi_\eta(\xi) V_{\eta\nu}^{-1}(\xi, \xi') \varphi_\nu(\xi') - \sum_\eta \int_{\mathcal{C}} \mathrm{d}\xi \, \varrho_{0\eta} \, \varphi_\eta(\xi) \tag{3.2}$$

with the effective interaction $V_{\mu\nu}^{-1} = U_{\mu\nu}^{-1} - \delta_{\mu\nu}\Pi_\mu$, the polarization operators (2.23),(2.24), and the mean charge density $\varrho_{0\eta} = eV_\eta/(2\pi|v_\eta|)$.

In Sect. 2.3 we observed that the Jacobian can contain higher-order contributions, which are encoded in a functonal determinant, if the 1D electrons are not in an equilibrium state. In this chapter we find a similar behavior for the connected quantum network when at least one node is characterized by a non-trivial scattering matrix $s^j \neq \mathbb{1}$. For the case of a single compact scatterer such an action has been constructed in Ref. [28] with the use of the nonequilibrium Green's function method. The result bears a strong resemblance with the solution of the problem of full counting statistics [20, 23]. In this chapter we generalize this approach to the situation with many scatterers. It turns out that the Keldysh action in this case can be written in terms of a full time-dependent single-particle scattering matrix (S-matrix) of the system in a given configuration of field φ^α, which we denote $S^\alpha = S[\varphi^\alpha](t, t')$, where $\alpha = f/b$ is the Keldysh index. Let us emphasize that the S-matrix is nonlocal in time and takes different values on the forward and backward branches of the Keldysh contour. Our result reads:

$$\mathcal{A}[\varphi] = \frac{1}{2} \sum_{\mu\nu} \int_{\mathcal{C}} \mathrm{d}\xi \, \mathrm{d}\xi' \, \varphi_\mu U_{\mu\nu}^{-1} \varphi_\nu - \sum_\mu \int \mathrm{d}\xi \, \mathrm{d}\xi' \, (\varphi_\mu^c, \varphi_\mu^q)_\xi \begin{pmatrix} 0 & \Pi_\mu^a(\xi - \xi') \\ \Pi_\mu^r(\xi - \xi') & 0 \end{pmatrix} \begin{pmatrix} \varphi_\mu^c \\ \varphi_\mu^q \end{pmatrix}_{\xi'}$$
$$- i \ln \mathrm{Det} \left[\mathbb{1} - f + S[\varphi^b]^\dagger S[\varphi^f] f \right]. \tag{3.3}$$

The last term in Eq. (3.3) is a functional determinant with respect to (real) time and channel indices. It is understood that f in the expression for the corresponding operator has the structure $f_{\mu\nu}(t, t') = \delta_{\mu\nu} f_\mu(t - t')$, i.e., it is diagonal in channel representation, with $f_\mu(t)$ being the Fourier transform of the source distribution function connected to channel μ. While the Keldysh components Π_μ^k of the polarization operators are encoded in the functional determinant in (3.3), the anomalous terms $\Pi_\mu^{r/a}$ (related to the Schwinger anomaly) are represented by the second term. It is written in the rotated Keldysh representation, $\varphi^{c(q)} = (\varphi^f \pm \varphi^b)/2$, and integration is performed along the real time axis.

A detailed derivation of the result (3.3), which employs ideas of Ref. [20], is presented in Sect. 3.4.1. In view of the importance of this result, we give also its alternative proof (Sect. 3.4.2), which follows closely the method of Ref. [28].

Construction of Scattering Matrix

Let us now discuss how the S-matrix for the systems under consideration is constructed. The elements of $S_{\nu\mu}^\alpha(t, t')$ give the amplitude that a wave packet incident from source μ at time t' leaves the system at time t through the drain ν. They are sums of amplitudes $S_{\nu\mu}^\alpha(t, t') = \sum_p A_{\nu\mu}^{(p)\alpha}(t, t')$ over all possible paths p formed by elements of the network.
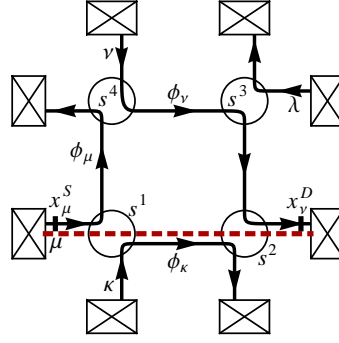
Figure 3.2: *Network built out of four channels $\mu, \kappa, \nu, \lambda$ and point scatterers $1, 2, 3, 4$. Counting fields measure outgoing currents. Along interior parts of channels classical phases $\phi_{\mu/\kappa/\nu}$, e.g. due to magnetic field, are accumulated. An exemplary path p is indicated by a dashed line.*

To see how the amplitudes $A_{\nu\mu}^{(p)\alpha}(t, t')$ are constructed let us consider Fig. 3.2, which shows an exemplary path p through a network of channels and point scatterers. It consists of an alternating sequence of two types of processes:

***a.* Electron propagation in the potential** φ_μ^α **between** x^i **and** x^j**,** leading to the accumulated phase

$$\vartheta_\mu^\alpha(x^j, x^i; t)(t) \equiv -v_\mu^{-1} \int_{x^i}^{x^j} dx \, \varphi_\mu^\alpha(x, t - (x^j - x)/v_\mu). \tag{3.4}$$

In addition to the Hubbard-Stratonovich field φ_μ^α, there may be other time-independent phases ϕ_μ^α (e.g., induced by a magnetic field) contributing to Eq. (3.4). Note that $\vartheta_\mu^\alpha(x, x^i)$ satisfies the same differential equation $(\partial_t + v_\mu \partial_x)\vartheta_\mu^\alpha(x, x^i; t) = -\varphi_\mu^\alpha(x, t)$ as $\Theta_\mu^\alpha(x, t)$, but has a simpler ("incomplete") Keldysh structure which involves only the retarded/advanced components of the bare particle-hole propagator $D_{0\mu}$. To take a finite flight time of electron between x^i and x^j into account, we introduce a "delay operator"

$$\Delta_\mu(x^j, x^i; t', t) = \delta(t' - t - (x^j - x^i)/v_\mu).$$

Then the amplitude of this process reads

$$\mathcal{M}_\mu^\alpha(x^j, x^i; t, t') \equiv e^{i\vartheta_\mu^\alpha(x^j, x^i; t)} \Delta_\mu(x^j, x^i; t, t'). \tag{3.5}$$

Indeed, consider the 1D version of the Schrödinger equation on a directed link $x^i \to x^j$,

$$i\partial_t \psi_\mu = (-iv_\mu \partial_x + \varphi_\mu^\alpha)\psi_\mu.$$

Using the definition of the phase (3.4), this equation can be solved independently on each branch of the Keldysh contour yielding the relation

$$\psi_\mu(x^j, t) = e^{i\vartheta_\mu^\alpha(x^j, x^i; t)} \psi_\mu(x^i, t - (x^j - x^i)/v_\mu), \tag{3.6}$$

which implies that the scattering matrix is given by Eq. (3.5).

***b.* Scattering/tunneling at point scatterer** j**:**   The amplitude of instantaneous scattering from channel μ to ν is

$$s^j_{\nu\mu}(t', t) = s^j_{\nu\mu}\delta(t' - t).$$

Passing the charge detector at drain μ**, which is described by the counting field** χ_μ**.**   As a special variant of *a.*, our formalism includes the theory of full counting statistics. A counting field residing in the drain lead μ measures the current flowing into that drain. The corresponding amplitude is

$$\mathcal{X}^\alpha_\mu(t', t) = e^{-i\frac{\alpha}{2}\chi_\mu}\delta(t' - t).$$

Then the action (3.3) enables us to express the cumulant generating function of the network as a functional integral over φ,

$$\mathcal{Z}(\vec{\chi}) = \int \prod_\mu \mathcal{D}\varphi^{f/b}_\mu(x, t)\, \exp\left\{i\mathcal{A}(\varphi, \vec{\chi})\right\}, \tag{3.7}$$

where the vector $\vec{\chi}$ combines the counting fields χ_μ in all drains.

Finally, the amplitude $A^{(p)\alpha}_{\nu\mu}$ of a path p is the path-ordered (real) time convolution ("latest to the left") of the amplitudes of its constituent processes. As an example, the amplitude indicated by the dashed line in Fig. 3.2 reads

$$A^{(p)\alpha}_{\nu\mu}(t, t') = \left[\mathcal{X}^\alpha_\nu\, \mathcal{M}^\alpha_\nu(x^D_\nu, x^2_\nu)\, s^2_{\nu\kappa}\, \mathcal{M}^\alpha_\kappa(x^2_\kappa, x^1_\kappa)\, s^1_{\kappa\mu}\, \mathcal{M}^\alpha_\mu(x^1_\mu, x^S_\mu)\right](t, t')$$

$$= \delta(t - t' - \tau)\, e^{-i\frac{\alpha}{2}\chi_\nu + i\phi_\kappa}\, s^2_{\nu\kappa}s^1_{\kappa\mu}\, \exp\left\{i\vartheta^\alpha_\nu(x^D_\nu, x^2_\nu; t) + i\vartheta^\alpha_\kappa(x^2_\kappa, x^1_\kappa; t - \tau_3) + i\vartheta^\alpha_\mu(x^1_\mu, x^S_\mu; t - \tau_3 - \tau_2)\right\},$$

where $\tau_{1/2/3}$ denote the flight times of the subpaths $x^S_\mu \to x^1_\mu$, $x^1_\kappa \to x^2_\kappa$, $x^2_\nu \to x^D_\nu$, and $\tau = \tau_1 + \tau_2 + \tau_3$ is the total flight time.

3.2 Weak Tunneling Expansion

Due to the complex temporal behavior of the scattering matrix analytical evaluation of the functional determinant (3.3) is not feasible in general. (Chapter 6 deals with an example which can be treated exactly.) An approximate treatment is possible if weak tunneling at the point scatterers is assumed (i.e. the scattering matrix $s^j_{\nu\mu}$ close to $\delta_{\nu\mu}$), and the ultimate goal of this section is the expansion of the action in the tunneling strength. Since in the absence of tunneling the network is described by the Gaussian action (3.2), one can introduce the tunneling action $\mathcal{A}_t[\varphi]$, so that $\mathcal{A}[\varphi] = \mathcal{A}_0[\varphi] + \mathcal{A}_t[\varphi]$, where the expansion of $\mathcal{A}_t[\varphi]$ starts from second-order terms with respect to the tunneling amplitudes at the point scatterers. In Sect. 3.4.3 we show that an exact representation of $\mathcal{A}_t[\varphi]$ is given in terms of a modified ("regularized") functional determinant

$$\mathcal{A}_t[\varphi] = -i\ln \mathrm{Det}\left[\mathbb{1} - f + \tilde{S}^{b\dagger}\tilde{S}^f f\right]. \tag{3.8}$$

The new, "regularized" scattering matrix $\tilde{S}$ here is constructed similarly to S. Each of its elements $\tilde{S}^\alpha_{\nu\mu}(t, t') = \sum_p \tilde{A}^{(p)\alpha}_{\nu\mu}(t, t')$ is a sum over the same paths p which contribute to $S^\alpha_{\nu\mu}(t, t')$ and connect the source μ with the drain ν. Full and regularized amplitudes, $A^{(p)}_{\nu\mu}$ and $\tilde{A}^{(p)}_{\nu\mu}$ respectively, differ in the partial amplitudes assigned to the elementary processes *a.* and *b.* which constitute a path p:

a. **Propagation between** x^i **and** x^j**.** Only the time delay is taken into account:

$$\tilde{\mathcal{M}}_\mu^\alpha(x^j, x^i) = \Delta_\mu(x^j, x^i),$$

while phase accumulation is shifted to

b. **Tunneling at point scatterers** j**.** The off-diagonal tunneling amplitudes become "dressed" by tunneling phases $\Phi_{\nu\mu}^\alpha(x^j, t) \equiv \Theta_\mu^\alpha(x_\mu^j, t) - \Theta_\nu^\alpha(x_\nu^j, t)$:

$$\tilde{s}_{\nu\mu}^{j\alpha}(t, t') = e^{i\Phi_{\nu\mu}^\alpha(x^j, t)} s_{\nu\mu}^j \delta(t - t').$$

The phases $\Theta_\mu = -D_{0\mu}\varphi_\mu$ are defined as in Sect. 2.2 and can be modified by additional time-independent phase contributions due to e.g. magnetic or counting fields as follows. If the additional phase accumulated by an electron which propagates along a channel μ from a position x to the drain lead μ is denoted as $\phi_{\mu.\mathrm{out}}^\alpha(x)$, then the phase Θ_μ^α is modified according to

$$\Theta_\mu^\alpha(x, t) \mapsto \Theta_\mu^\alpha(x, t) - \phi_{\mu.\mathrm{out}}^\alpha(x).$$

In our previous example, Fig. 3.2, the regularized scattering amplitudes read

$$\tilde{s}_{\kappa\mu}^{1\alpha}(t, t') = e^{i\Phi_{\kappa\mu}^\alpha(x^1, t) - i\left(\phi_\mu - \phi_\kappa\right) + i\frac{\alpha}{2}\left(\chi_\mu - \chi_\kappa\right)} s_{\kappa\mu}^2 \delta(t - t'),$$

$$\tilde{s}_{\nu\kappa}^{1\alpha}(t, t') = e^{i\Phi_{\nu\kappa}^\alpha(x^2, t) + i\frac{\alpha}{2}\left(\chi_\kappa - \chi_\nu\right)} s_{\nu\kappa}^2 \delta(t - t').$$

The regularized scattering matrix becomes trivial in the "clean" limit, $\tilde{S} = \mathbb{1}$, since all effects of interaction are now contained in the phases of the off-diagonal elements of the regularized scattering matrices $\tilde{s}_{\nu\mu}^j$ of connectors. Thus Eq. (3.8) can be expanded in (even) powers of the tunneling amplitudes:

$$\mathcal{A}_t[\varphi] = i \sum_{n=1}^\infty \frac{1}{n} \mathrm{Tr}\left[\left(\mathbb{1} - \tilde{S}^{b\dagger}\tilde{S}^f\right) f\right]^n.$$

We are now going to elaborate on the second-order terms in this series.

Second Order Expansion

Let us introduce the notation $\mathcal{P} \equiv \tilde{S}^{b\dagger}\tilde{S}^f$. Up to third order corrections in the tunneling amplitudes [that we denote as $\mathcal{O}(\mathrm{tun}^3)$] the tunneling action is

$$\begin{aligned}
\mathcal{A}_t[\varphi] =& i\,\mathrm{Tr}\left[(\mathbb{1} - \mathcal{P})f + \frac{1}{2}(\mathbb{1} - \mathcal{P})f(\mathbb{1} - \mathcal{P})f\right] + O(\mathrm{tun}^3) \\
=& i\,\mathrm{Tr}\left[(\mathbb{1} - \mathcal{P})_{\mu\mu}f_\mu + \frac{1}{2}\sum_{\mu\neq\nu}\mathcal{P}_{\mu\nu}f_\nu\mathcal{A}_{\nu\mu}f_\mu\right] + O(\mathrm{tun}^3).
\end{aligned} \tag{3.9}$$

In the last expression, the trace is only taken with respect to time. To reduce the tunneling action to this form, we used $(\mathbb{1} - \mathcal{P})_{\mu\mu} = O(\mathrm{tun}^2)$ and $\mathcal{A}_{\nu\mu} = O(\mathrm{tun})$.

It can be shown (see Sect. 3.4.4 for a detailed derivation) that $\mathcal{A}_t$ acquires contributions from paths which start in a certain source reservoir, evolve forward and backward in time, undergoing in total

exactly 2 tunneling events, and eventually return to the original source. Such paths involve exactly 2 different channels, μ and ν. Thus we can classify all paths according to the pair (μ, ν) of channels $\mu \neq \nu$ and the pair (i, j) of scatterers (possibly equal) at which the tunneling takes place: $\mu \to \nu$ at i and $\nu \to \mu$ at j. Of course, the class $(ij; \mu\nu)$ coincides with the class $(ji; \nu\mu)$. The second order expansion of the tunneling action then is a sum over these classes:

$$
\mathcal{A}_t[\varphi] = -i \sum_{(ij;\mu\nu)} \int \mathrm{d}t_1 \mathrm{d}t_2 \left(e^{-i\Phi^f_{\mu\nu}(x^i,t_1)} \quad e^{-i\Phi^b_{\mu\nu}(x^i,t_1)} \right) \begin{pmatrix} \Pi^T_{ij;\mu\nu}(t_{12}) & -\Pi^<_{ij;\mu\nu}(t_{12}) \\ -\Pi^>_{ij;\mu\nu}(t_{12}) & \Pi^{\tilde{T}}_{ij;\mu\nu}(t_{12}) \end{pmatrix} \begin{pmatrix} e^{i\Phi^f_{\mu\nu}(x^j,t_2)} \\ e^{i\Phi^b_{\mu\nu}(x^j,t_2)} \end{pmatrix},
\tag{3.10}
$$

$t_{12} \equiv t_1 - t_2$, where the tunneling polarization operators are given by

$$
\Pi^{\gtrless}_{ij;\mu\nu}(t) = -s^i_{\nu\mu} \bar{s}^j_{\nu\mu} \, e^{i\Delta\phi^{ij}_{\mu\nu}} e^{\pm i(\chi_\mu - \chi_\nu)} f^{\gtrless}_\mu(t + \tau^j_{\mu.\mathrm{in}} - \tau^i_{\mu.\mathrm{in}}) f^{\lessgtr}_\nu(\tau^i_{\nu.\mathrm{in}} - \tau^j_{\nu.\mathrm{in}} - t),
\tag{3.11}
$$

$$
\Pi^{T/\tilde{T}}_{ij;\mu\nu}(t) = \left[\theta(\pm t) \Pi^>_{ij;\mu\nu}(t) + \theta(\mp t) \Pi^<_{ij;\mu\nu}(t) \right]_{\chi \equiv 0},
\tag{3.12}
$$

where $\tau^k_{\lambda.\mathrm{in}}$ is the flight time from the source to the scatterer k along a channel λ, $\tau^k_{\lambda.\mathrm{in}} = (x^k_\lambda - x^S_\lambda)/v_\lambda$. We have also taken into account counting fields in the drain leads (which are not contained in $\Pi^{T/\tilde{T}}_{ij;\mu\nu}$) and classical phases,

$$
\Delta\phi^{ij}_{\mu\nu} \equiv \phi_{\nu.\mathrm{out}}(x^i) - \phi_{\mu.\mathrm{out}}(x^i) - \phi_{\nu.\mathrm{out}}(x^j) + \phi_{\mu.\mathrm{out}}(x^j).
$$

In the case $i = j$ we will also use the convention

$$
\Pi^T_{ii;\mu\nu}(t) = \Pi^{\tilde{T}}_{ii;\mu\nu}(t) = \frac{1}{2} \left[\Pi^>_{ii;\mu\nu}(t) + \Pi^<_{ii;\mu\nu}(t) \right].
\tag{3.13}
$$

The comparison of this expression with the Eq. (3.12) shows that they differ from each other by a singular term proportional to $\mathrm{sign}(t) h(t) \delta(t) = \pi \delta^2(t)$, where we put $h(t) = f^>_0(t) - f^<_0(t)$. It gives some constant (albeit infinite) contribution to the tunneling action (3.10) and therefore both representations for $\Pi^{T/\tilde{T}}_{ii;\mu\nu}$ are equivalent.

3.3 Real-Time Instanton Method

On the level of the second order expansion, the action $\mathcal{A}_t[\varphi]$ is expressed in terms of the tunneling phases Φ, which are linear functionals of φ:

$$
\Phi_{\mu\nu}(\xi) = \sum_\lambda \int_{\mathcal{C}} \mathrm{d}\xi' \, \mathcal{D}_{\mu\nu;\lambda}(\xi, \xi') \varphi_\lambda(\xi'), \quad \mathcal{D}_{\mu\nu;\lambda} \equiv D_{0\mu} \delta_{\mu\lambda} - D_{0\nu} \delta_{\nu\lambda}.
\tag{3.14}
$$

The action $\mathcal{A}_t[\varphi]$ is non-Gaussian in Φ and, in fact, is quite similar to the Ambegaokar-Eckern-Schön (AES) action [29]. The difference is that the kernel appearing in Eq. (3.10) is not only non-local in time (as in the case of AES) but in general is non-local in space as well. In view of the non-Gaussian character of the action an exact evaluation of physical quantities does not seem feasible in general. For this reason, we will use a saddle-point approximation that catches correctly the relevant interaction-induced physics, including both the renormalization and the dephasing phenomena.

To explain the idea of the method, let us consider some physical quantity $\mathcal{O}[\varphi] = \mathcal{O}_0 e^{i\mathcal{A}_J[\varphi]}$, where $\mathcal{A}_J[\varphi] = -\sum_\mu \int_\mathcal{C} \mathrm{d}\xi\, J_\mu(\xi)\varphi_\mu(\xi)$ is a linear functional of φ, and the prefactor $\mathcal{O}_0$ is independent on φ. Important examples, which are treated in the subsequent chapters, include the electronic Green's function and the current. The quantum average value of $\mathcal{O}$ is given by the functional integral

$$\langle \mathcal{O}[\varphi] \rangle = \int \mathcal{D}\varphi\, e^{i\mathcal{A}_0[\varphi] + i\mathcal{A}_t[\varphi] + i\mathcal{A}_J[\varphi]} \mathcal{O}_0, \tag{3.15}$$

which we estimate in the semiclassical approximation [30]. In this case the path integral is contributed by the saddle-point trajectory φ_{**} of the full action $\mathcal{A}_0[\varphi] + \mathcal{A}_t[\varphi] + \mathcal{A}_J[\varphi]$ and quantum fluctuations around it. Here free and tunneling actions $\mathcal{A}_0[\varphi]$, $\mathcal{A}_t[\varphi]$ are given by Eqs. (3.2) and (3.10), respectively. In the limit of weak tunneling between chiral channels the saddle-point trajectory ("instanton") can be found approximately by requiring that it minimizes the Gaussian contributions to the action $\mathcal{A}_0[\varphi] + \mathcal{A}_J[\varphi]$, which gives

$$\varphi_{*\mu}(\xi) = \sum_\nu \int_\mathcal{C} \mathrm{d}\xi'\, V_{\mu\nu}(\xi,\xi')(\varrho_{0\nu}(\xi') + J_\nu(\xi')). \tag{3.16}$$

As shown in Sect. 3.4.5, under such an approximation Eq. (3.15) simplifies to

$$\langle \mathcal{O}[\varphi] \rangle = \left\langle e^{i\mathcal{A}_J[\varphi]} \right\rangle_0 e^{i\tilde{\mathcal{A}}_t[\varphi_*]} \mathcal{O}_0\,, \tag{3.17}$$

with

$$\left\langle e^{i\mathcal{A}_J[\varphi]} \right\rangle_0 = \exp\left\{ i\left\langle \mathcal{A}_J[\varphi] \right\rangle_0 - \frac{1}{2}\left[\left\langle \left(\mathcal{A}_J[\varphi] - \left\langle \mathcal{A}_J[\varphi] \right\rangle_0 \right)^2 \right\rangle_0 \right] \right\}, \tag{3.18}$$

$$\tilde{\mathcal{A}}_t[\varphi_*] = -i \sum_{\{\mu,\nu\},(i,j)} \int \mathrm{d}t_1 \mathrm{d}t_2 \left(e^{-i\Phi^f_{*\mu\nu}(x^i,t_1)} \quad e^{-i\Phi^b_{*\mu\nu}(x^i,t_1)} \right) \begin{pmatrix} \tilde{\Pi}^T_{ij;\mu\nu}(t_{12}) & -\tilde{\Pi}^<_{ij;\mu\nu}(t_{12}) \\ -\tilde{\Pi}^>_{ij;\mu\nu}(t_{12}) & \tilde{\Pi}^{\tilde{T}}_{ij;\mu\nu}(t_{12}) \end{pmatrix} \begin{pmatrix} e^{i\Phi^f_{*\mu\nu}(x^j,t_2)} \\ e^{i\Phi^b_{*\mu\nu}(x^j,t_2)} \end{pmatrix}, \tag{3.19}$$

where $t_{12} \equiv t_1 - t_2$ and $\langle \ldots \rangle_0$ denotes averaging with respect to $\mathcal{A}_0[\varphi]$. We have introduced the instanton phases $\Phi_{*\mu\nu} = \mathcal{D}_{\mu\nu}\varphi_*$ and the *renormalized* tunneling polarization operators

$$\tilde{\Pi}^{\alpha\beta}_{ij;\mu\nu}(t_1 - t_2) = e^{i\left(D^{\alpha\beta}_{\Phi\mu\nu}(x^i,x^j;t_1-t_2) - D^{\alpha\alpha}_{\Phi\mu\nu}(0,0) \right)} \Pi^{\alpha\beta}_{ij;\mu\nu}(t_1 - t_2), \tag{3.20}$$

obtained by dressing of the bare tunneling polarization operators by phase-phase correlators

$$D_{\Phi\mu\nu}(\xi_1,\xi_2) = \sum_{\kappa\lambda} \int_C \mathrm{d}\xi'\, \mathrm{d}\xi''\, \mathcal{D}_{\mu\nu;\kappa}(\xi_1,\xi') V_{\kappa\lambda}(\xi',\xi'') \mathcal{D}_{\mu\nu;\lambda}(\xi'',\xi_2).$$

The meaning of Eq. (3.20) is that quantum fluctuations of tunneling phases renormalize the temporal dependence of tunneling polarization operators which lead to non-trivial (usually power-law) energy-dependence of tunneling coefficients.

Ttwo important applications of our general approach will be considered in Chapters 4 and 5.

3.4 Calculations

3.4.1 Derivation of Keldysh Action

This section and the following one are devoted to the proof of (3.3) and more specifically to the calculation of the Jacobian $J[\varphi, \psi, \bar{\psi}]$ corresponding to the gauge transformation $\psi_\mu^{f/b} \to e^{i\Theta_\mu^{f/b}} \psi_\mu^{f/b}$ with (2.16). Since this is a linear transformation in $\psi, \bar{\psi}$, its Jacobian is independent of $\psi, \bar{\psi}$ and can be therefore computed as

$$J[\varphi] \equiv e^{i\mathcal{A}_f[\varphi]} \equiv \int \mathcal{D}(\psi, \bar{\psi}) \, e^{i\mathcal{A}[\varphi, \psi, \bar{\psi}]} = \mathrm{Tr}\left\{ \hat{\varrho}_0 \hat{U}[\varphi^b]^\dagger \hat{U}[\varphi^f] \right\} \tag{3.21}$$

with density operator $\hat{\varrho}_0$ and the (many-particle) time evolution operators $\hat{U}[\varphi^{f/b}]$. The latter describes any *single-particle* dynamics the electrons undergo in the system *and the leads* (see Fig. 3.3), say scattering and propagation through time-dependent potentials $\varphi^\alpha(t)$. These potentials may have a non-trivial Keldysh structure, thus the superindex $\alpha = f/b$ which refers to the forward/backward branch of the Keldysh contour, respectively.
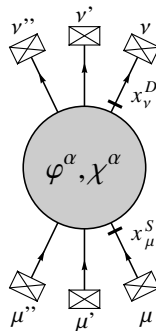

Figure 3.3: *Sketch of the system (shaded blob) which is connected to reservoirs (rectangles) via source (drain) leads, depicted by incoming (outgoing) lines. The leads μ (ν) enter (leave) the systems at contact positions x_μ^S (x_ν^D).*

Integrating out Fermions with Klich's Formula

There are several ways to evaluate the many-particle trace (3.21). Here we employ an approach that generalizes a derivation of the full counting statistics in Ref. [20]. In Sect. 3.4.2 we present an alternative derivation which keeps closely to the spirit of Ref. [28] where an analogous action was derived for the case of a single compact scatterer.

A central mathematical statement proven in Ref. [20] relates traces of certain *many*-particle operators with determinants of associated *single*-particle operators. We denote the (many-particle) Fock space representation of single-particle operators C by $\Gamma(C) \equiv \sum c_i^\dagger \langle i| \, C \, |j\rangle \, c_j$. Here, $\{|i\rangle\}_i$ is some single-particle basis, and c_i ($c_i^\dagger$) annihilates (creates) an electron in state $|i\rangle$. Then, the following identity holds:

$$\mathrm{Tr}\left(e^{\Gamma(A_1)} \cdots e^{\Gamma(A_n)} \right) = \det\left(\mathbb{1} + e^{A_1} \cdots e^{A_n} \right). \tag{3.22}$$

To proceed we write the density operator in the form

$$\hat{\varrho}_0 = \frac{e^{\Gamma(F)}}{\det\left(\mathbb{1} + e^F\right)} \tag{3.23}$$

where the single-particle operator $F = \sum \alpha_i N_i$ is a suitable linear combination of (single-particle!) "number operators" $N_i = |i\rangle\langle i|$ in the reservoirs. E.g. in thermal equilibrium $F = -\beta H_0$ with some appropriate Hamiltonian $H_0 = \sum \epsilon_i N_i$. The many-particle time-evolution operator is canonically discretized as

$$\hat{U}[\varphi^\alpha] = \text{Texp}\left[-i \int_{-\infty}^{\infty} \mathrm{d}t\, \hat{H}[\varphi^\alpha(t)]\right] = \lim_{\substack{\Delta t \to 0 \\ N \to \infty}} \prod_{i=1}^{N} e^{-i\Delta t\, \Gamma(H[\varphi^\alpha(t_i)])}.$$

Hence, Eq. (3.21) is a trace over a (infinite) product of operator exponentials which, according to (3.22), is

$$J[\varphi] = \frac{\text{Tr}\left[e^{\Gamma(F)}\hat{U}[\varphi^b]^\dagger \hat{U}[\varphi^f]\right]}{\det(\mathbb{1} + e^F)} = \frac{\det\left(\mathbb{1} + e^F U[\varphi^b]^\dagger U[\varphi^f]\right)}{\det(\mathbb{1} + e^F)}$$

$$= \det\left(\mathbb{1} + f\left(U[\varphi^b]^\dagger U[\varphi^f] - \mathbb{1}\right)\right) \tag{3.24}$$

with the single-particle time-evolution operator $U[\varphi^\alpha]$ (not to be confused with $\hat{U}[\varphi^\alpha]$) and the occupation number operator $f = \left[\mathbb{1} + e^{-F}\right]^{-1}$.

Wave packet representation

In a next step, we follow Landauer's original idea[31, 32] and represent the time-evolution operators with respect to the wave packet bases, relating them to the single-particle scattering matrices. Using a more compact notation for the single-particle time-evolution operator

$$U^\alpha(t_1, t_0) = \text{Texp}\left[-i \int_{t_0}^{t_1} \mathrm{d}t\, H[\varphi^\alpha(t)]\right], \qquad t_0 < t_1,$$

(hence $U[\varphi^\alpha] = U^\alpha(\infty, -\infty)$), Eq. (3.24) can be brought into the form

$$J[\varphi] = \lim_{t_\pm \to \pm\infty} \det\left\{\mathbb{1} + f\left[U^b(t_+, t_-)^\dagger U^f(t_+, t_-) - \mathbb{1}\right]\right\}. \tag{3.25}$$

We fix some time-*in*dependent reference Hamiltonian, say $H_0 \equiv H[\varphi \equiv 0]$, which contains the lead kinematics as well as scattering, but no interaction or current counting. Then the incoming/outgoing scattering states with respect to H_0 form two natural bases of the single-particle Hilbert space, see Fig. 3.4. Each state is characterized by its energy ϵ and the lead μ through which it enters/leaves the system: $H_0 |\epsilon\mu\rangle^{\text{in/out}} = \epsilon |\epsilon\mu\rangle^{\text{in/out}}$. The two bases are hence $\left(|\epsilon\mu\rangle^{\text{in}}\right)_{\epsilon;\mu}$ and $(|\epsilon\mu\rangle^{\text{out}})_{\epsilon;\mu}$.

For the sake of argument we will assume the lead channels μ to be one-dimensional (1D), semi-infinite and non-dispersive with constant velocity v_μ. We use the convention $v_\mu > 0$, i.e. for source channels $-\infty < x < x_\lambda^S$ and for drain channels $x_\lambda^D < x < \infty$, and choose the normalization such that $^{\text{in/out}}\left\langle \epsilon'\mu'|\epsilon\mu\right\rangle^{\text{in/out}} = \delta_{\mu\mu'}\delta(\epsilon - \epsilon')$ is satisfied.
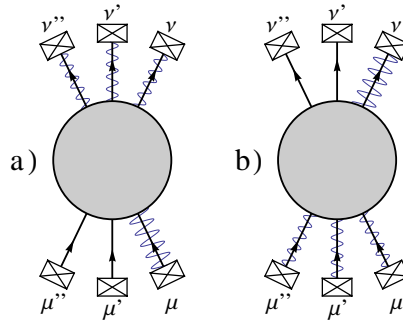
Figure 3.4: *(a) Spatial distribution of incoming scattering state $\left|\epsilon\mu\right\rangle^{\text{in}}$ (wavy lines). It extends in source lead μ and arbitrary drain leads ν, but in no other source leads. (b) Spatial distribution of outgoing scattering state $\left|\epsilon\nu\right\rangle^{\text{out}}$ (wavy lines). It extends in drain lead ν and arbitrary source leads μ, but in no other drain leads.*

The incoming state $\left|\epsilon\mu\right\rangle^{\text{in}}$ is a *plane wave* in source lead μ and spreads into drain leads ν. It vanishes in all other source leads μ': $^{\text{in}}\left\langle x\mu'|\epsilon\mu\right\rangle^{\text{in}} = \delta_{\mu'\mu}\frac{1}{\sqrt{2\pi v_\mu}}e^{i\epsilon x/v_\mu}$ (where $\left|x\mu\right\rangle$ is the eigenstate of the position operator in channel μ). Analogous statements hold for the outgoing states.

Let us now construct the incoming (outgoing) wave packet basis at reference time t_- (t_+). For that we define

$$\left|t\mu\right\rangle^{\text{in}} \equiv \int \frac{\mathrm{d}\epsilon}{\sqrt{2\pi}}\, e^{i\epsilon(t-t_- -x_\mu^S/v_\mu)}\left|\epsilon\mu\right\rangle, \quad \left|t\lambda\right\rangle^{\text{out}} \equiv \int \frac{\mathrm{d}\epsilon}{\sqrt{2\pi}}\, e^{i\epsilon(t-t_+ -x_\lambda^D/v_\lambda)}\left|\epsilon\lambda\right\rangle.$$

Note that t is not a parameter which describes the time-evolution of a state "$\left|\mu\right\rangle$" but labels the state $\left|t\mu\right\rangle$ similar to ϵ in $\left|\epsilon\mu\right\rangle$. The two new bases are thus $(\left|t\mu\right\rangle^{\text{in}})_{t;\mu}$ and $(\left|t\mu\right\rangle^{\text{out}})_{t;\mu}$.

To shed light on the meaning of label t, we study the time-evolution of the newly constructed states with respect to the reference Hamiltonian H_0. For time t' one has

$$^{\text{in}}\left\langle x\mu'\right|e^{-iH_0(t'-t_-)}\left|t\mu\right\rangle^{\text{in}} = \delta_{\mu'\mu}\,\sqrt{v_\mu}\delta(x-x_\mu^S+v_\mu(t-t')).$$
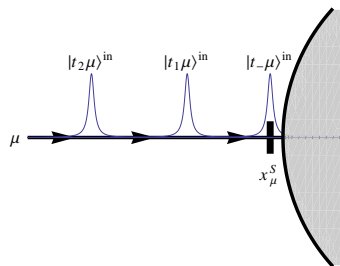
Figure 3.5: *Zoom into source lead μ: sketch of spatial distribution of wave packet states $\left|t_-\mu\right\rangle^{\text{in}}$, $\left|t_1\mu\right\rangle^{\text{in}}$, $\left|t_2\mu\right\rangle^{\text{in}}$ with $t_2 > t_1 > t_-$.*

This is a wave packet in source channel μ which propagates toward contact x_μ^S, arriving there at time t, see Fig. 3.5. After entering the system it may split and spread in some complicated way. Similarly,

the outgoing state $\left|t\lambda\right\rangle^{\text{out}}$ may be distributed in some complicated manner inside the system, however tuned such that at time t it arrives at drain contact x_λ^D and continues propagation as a single wave packet in drain channel λ. Summarizing,

$$e^{-iH_0(t-t_-)}\left|t\mu\right\rangle^{\text{in}} \equiv \sqrt{v_\mu}\left|x_\mu^S\right\rangle, \quad e^{-iH_0(t-t_+)}\left|t\lambda\right\rangle^{\text{out}} \equiv \sqrt{v_\lambda}\left|x_\lambda^D\right\rangle \tag{3.26}$$

are wave packets residing at contacts x_μ^S, x_λ^D, and thus being independent of $t_\mp$ and t.

Making the assumption that interaction, counting etc. is switched on and off adiabatically such that $H(t') = H_0$ for $t' \notin [t_-, t_+]$, we now argue that the same simple relations hold when taking the full Hamiltonian $H(t)$ into account,

$$U^\alpha(t, t_-)\left|t\mu\right\rangle^{\text{in}} = \sqrt{v_\mu}\left|x_\mu^S\right\rangle, \quad U^\alpha(t, t_+)\left|t\lambda\right\rangle^{\text{out}} = \sqrt{v_\lambda}\left|x_\lambda^D\right\rangle. \tag{3.27}$$

These relations are a direct consequence of (3.26) and the fact that potential φ^α is restricted spatially and temporally: For $t > t' > t_-$ incoming wave packet $U(t', t_-)\left|t\mu\right\rangle$ is completely contained in the source lead where we assume φ^α to be absent. For $t < t' < t_-$ potential $\varphi^\alpha(t')$ is again ineffective since not switched on yet. Therefore, $U(t, t_-)\left|t\mu\right\rangle^{\text{in}} = e^{-iH_0(t-t_-)}\left|t\mu\right\rangle$ for all t. The reasoning is analogous for outgoing states.

We are now able to give the operator $fU^b(t_+, t_-)^\dagger U^f(t_+, t_-)$ in the wave-packet representation. For source channels μ, μ' the matrix elements read

$$^{\text{in}}\left\langle t\mu\right|fU^b(t_+, t_-)^\dagger U^f(t_+, t_-)\left|t'\mu'\right\rangle^{\text{in}}$$
$$= \sum_{\mu''} \int \mathrm{d}t'' \, f_{\mu\mu''}(t, t'') \sum_\lambda \int \mathrm{d}t''' \, {}^{\text{in}}\left\langle t''\mu''\right|U^b(t_+, t_-)^\dagger\left|t'''\lambda\right\rangle^{\text{out}} \, {}^{\text{out}}\left\langle t'''\lambda\right|U^f(t_+, t_-)\left|t'\mu'\right\rangle^{\text{in}}. \tag{3.28}$$

Since the leads are populated by the reservoirs such that the occupation number of the *incoming* states is fixed, $^{\text{in}}\left\langle\epsilon\mu\right|f\left|\epsilon'\mu'\right\rangle^{\text{in}} = \delta_{\mu\mu'}\delta(\epsilon - \epsilon')f_\mu(\epsilon)$, the distribution function in time domain simplifies to

$$f_{\mu\mu'}(t, t') \equiv \left\langle t\mu\right|f\left|t'\mu'\right\rangle = \delta_{\mu\mu'} \int \frac{\mathrm{d}\epsilon}{2\pi} \, e^{-i\epsilon(t-t')} \, f_\mu(\epsilon).$$

The matrix elements of the time-evolution operator further reduce to

$$^{\text{out}}\left\langle t\lambda\right|U(t_+, t_-)\left|t'\mu\right\rangle^{\text{in}} = {}^{\text{out}}\left\langle t\lambda\right|U(t_+, t)U(t, t')U(t', t_-)\left|t'\mu\right\rangle^{\text{in}} = \sqrt{v_\lambda v_\mu}\left\langle x_\lambda^D\right|U(t, t')\left|x_\mu^S\right\rangle \equiv S_{\lambda\mu}(t, t') \tag{3.29}$$

which defines the scattering matrix $S = S[\varphi]$.

In the wave-packet representation Eq. (3.25) can be written

$$J[\varphi] = e^{i\mathcal{A}_f[\varphi]} = \det\left[\mathbb{1} - f + S^{b\dagger}S^f f\right]$$

where the determinant is to be taken with respect to source lead indices and arrival times. The log of this determinant appears in our general result stated in Eq. (3.3). The retarded and advanced parts of the polarization operator which are present in Eq. (3.3) are not reproduced within the method of this section since they represent itself the quantum anomaly. Their structure does not depend on the actual nonequilibrium state of the system and can be deduced from the analysis of the fermion action in the absence of tunneling as it discussed in Section 2.2.
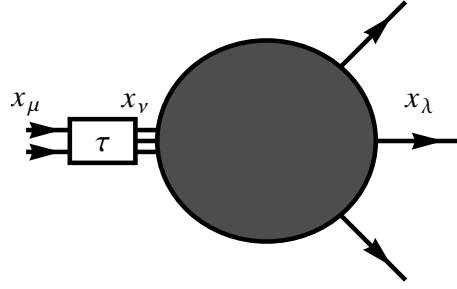
Figure 3.6: *Sketch of the system: a block characterized by the dwell time τ is connected to some part of the system (the shaded blob) via interface states $|x_\nu\rangle$.*

Construction of Scattering Matrix

According to (3.29) the scattering matrix element $S_{\lambda\mu}(t, t')$ is the transition amplitude for a peak residing in the (incoming) lead μ at time t' to a peak residing in the (outgoing) lead λ at time t. One expects that it is the summed amplitude for all possible trajectories which connect μ with λ. We will briefly demonstrate this assuming that the scatterer is a network of simple blocks which are connected to each other via "interface channels" which may be "outgoing" with respect to one block and "incoming" with respect to a neighboring one. The electronic state residing in the interface channel λ is denoted by $|x_\lambda\rangle$. It corresponds to a wave packet which is leaving one of the blocks and about to enter another one. We further assume that the blocks be simple enough such that each of them can be characterized by a unique dwell time τ (possibly different for each block), i.e. a wave packet which enters the block at time t will definitely leave it at (exactly) $t + \tau$, through whatever channel: $U(t + \tau, t) |x_i\rangle = \sum_f u_{fi}(t) |x_f\rangle$ where $|x_i\rangle$ is an incoming interface state and the sum extends over outgoing interface states $|x_f\rangle$. This defines the functions $u_{fi}(t)$ and the scattering matrix elements

$$s_{fi}(t', t) \equiv \delta(t' - t - \tau)\sqrt{\frac{v_i}{v_f}}u_{fi}(t) \tag{3.30}$$

where we have assigned a characteristic velocity v_λ to each interface channel λ. The full scattering matrix $S_{\lambda\mu}(t', t)$ can be constructed out of elements $s_{fi}(t', t)$ with the use of the following decomposition property. Consider the situation sketched in Fig. 3.6. Because of the decomposition property $U(t', t) = U(t', t + \tau)U(t + \tau, t)$ of the time-evolution operator, the amplitude for the transition from a peak at t in channel μ to one at t' in λ is

$$\sqrt{v_\lambda v_\mu} \langle x_\lambda | U(t', t) | x_\mu \rangle = \sum_\nu \int dt'' \sqrt{v_\lambda v_\mu} \langle x_\lambda | U(t', t'') | x_\nu \rangle \, s_{\nu\mu}(t'', t). \tag{3.31}$$

Obviously, the inner transition amplitude can be decomposed further in the same manner, and the full scattering matrix element $S_{\lambda\mu}$ turns out to be the sum of amplitudes $A_{\lambda\mu}^{(p)}$, each of them corresponding to a possible path p connecting the incoming state μ with the outgoing one λ. As p passes through a certain number of building blocks, $A_{\lambda\mu}^{(p)}$ is the product of the blocks' scattering matrix elements. For completeness we note that, since each trajectory will end in the outgoing leads, each decomposition will end with

$$\sqrt{v_{\lambda'} v_\lambda} \langle x_{\lambda'} | U(t', t) | x_\lambda \rangle = \delta(t' - t)\delta_{\lambda'\lambda} \tag{3.32}$$
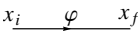
for $\lambda, \lambda' \in$ out.

Simple blocks

Having convinced ourselves of the usefulness of definition (3.30) we turn to simple two examples of building blocks: wires with fluctuating potentials and point scatterers. Simple as they are, a broad class of devices, including quantum wire junctions and electronic interferometers, can be modeled as a network of these construction units, and in the following we will restrict ourselves to such systems.

The corresponding scattering matrices are found by considering the time-evolution of wave packets $\psi(t,x) \equiv \langle x| U(t,t_0) |x_i\rangle$ which satisfy the Schrödinger equation

$$i\partial_t \psi(t) = H(t)\psi(t), \quad \text{with initial condition } \psi(t_0, x) = \delta(x - x_i). \tag{3.33}$$

We list the results here, giving all necessary definitions in the subsequent paragraphs:

Construction unit			*Scattering matrix*
Chiral wire	$x_i \quad \varphi \quad x_f$		$\mathcal{M}^\alpha(t', t) = e^{i\vartheta_{fi}^\alpha(t')}\Delta(t', t)$
Point scatterer	$i \rightarrow \boxed{s_{fi}} \leftarrow f$		$s_{fi}(t', t) = s_{fi}\,\delta(t' - t)$

***a.* Chiral wire with fluctuating potential** A possible block is a chiral non-dispersive wire where fermions propagate with constant velocity v in a fluctuating potential $\varphi^\alpha(t,x)$. Similar to the leads wires are described by a single coordinate x, extending from x_i to x_f, such that the dwell time is $\tau = \frac{x_f - x_i}{v}$. It is taken into account by the "delay operator" $\Delta(t', t) \equiv \delta(t' - t - \tau)$. The presence of the potential leads to accumulation of phase

$$\vartheta_{fi}(t) = -v^{-1} \int_{x_i}^{x_f} \mathrm{d}x'\, \varphi(x', t - (x_f - x')/v). \tag{3.34}$$

The wire connects exactly one incoming to one outgoing channel and the scattering matrix has just one entry $\mathcal{M}(t', t)$ in channel space.

***b.* Point scatterer** Another possible construction unit is the point scatterer which connects one-dimensional incoming (index i) and outgoing (index f) channels such that scattering occurs instantaneously (dwell time $\tau = 0+$). The scatterer is characterized by the unitary time-independent scattering matrix s_{fi}. If all channels λ have a linear dispersion with constant velocity v_λ, then according to (3.33) the wave packet incident from channel i (at time t_0) is

$$\psi(t, x, \lambda) = \delta_{\lambda i}\,\delta(x_i + v_i(t - t_0) - x)) + \sum_f \delta_{\lambda f}\, s_{fi}\, \sqrt{\frac{v_f}{v_i}}\, \delta(x_f + v_f(t - t_0) - x), \qquad t \approx t_0.$$

Since the state extends over several channels the wave function is a function of both channel index λ and channel coordinate x, and the sum is to be taken over all outgoing channels f.

Counting Fields   Up to now we have not addressed the issue of counting fields, claiming that they can be treated on the same footing as fluctuating potentials, a statement to be proven in this paragraph.

The number of electrons which flow through a certain point $\tilde{x}$ in the time interval $\tilde{t}_0 < t < \tilde{t}$ is described quantum-mechanically by the operator $N = \int_{\tilde{t}_0}^{\tilde{t}} \mathrm{d}t\, I(t)$. The current operator $I = v\psi^\dagger(\tilde{x})\psi(x)$ becomes time-dependent in Heisenberg representation, $I(t) = e^{iH(t-t_-)} I e^{-iH(t-t_-)}$ (t_- is some reference time at which the initial state of the system is fixed), v is the fermion velocity in the considered channel. According to Levitov and Lesovik [23] the correct generating functional of charge transfer through $\tilde{x}$ is

$$\mathcal{Z}(\chi) = \left\langle U_{-\chi}(\tilde{t},\tilde{t}_0)^\dagger U_\chi(\tilde{t},\tilde{t}_0) \right\rangle \quad \text{with } U_\chi(\tilde{t},\tilde{t}_0) = \mathrm{Texp}\left[i\frac{\chi}{2} \int_{\tilde{t}_0}^{\tilde{t}} \mathrm{d}t\, I(t) \right].$$

From the properties $U_\chi(\tilde{t}_0,\tilde{t}_0) = \mathbb{1}$ and $i\partial_{\tilde{t}} U_\chi(\tilde{t},\tilde{t}_0) = -\frac{\chi}{2} I(\tilde{t}) U_\chi(\tilde{t},\tilde{t}_0)$ we conclude that

$$U_\chi(\tilde{t},\tilde{t}_0) = e^{iH(\tilde{t}-t_-)} e^{-i(H-\frac{\chi}{2}I)(\tilde{t}-\tilde{t}_0)} e^{-iH(\tilde{t}_0-t_-)}$$

is a possible alternative representation. Thus,

$$\mathcal{Z}(\chi) = \left\langle T_\mathcal{C} \exp\left[-i \int_\mathcal{C} \mathrm{d}t'\, H_\chi(t') \right] \right\rangle$$

is the Keldysh partition sum with respect to the Hamiltonian $H_\chi^\alpha(t) \equiv H + v \int \mathrm{d}x\, A_\chi^\alpha(x,t)\psi^\dagger(x)\psi(x)$ where time integration and ordering are to be understood along the Keldysh contour $\mathcal{C}$ and we defined the local vector potential $A_\chi^{f/b}(t,x) = \pm\frac{\chi(t)}{2}\delta(x-\tilde{x})$ with the "time-dependent" counting field $\chi(t') \equiv \chi\theta(\tilde{t}-t)\theta(t-\tilde{t}_0)$.

The corresponding scattering matrix reads $s^{f/b}(t',t) = \delta(t'-t)\, e^{\pm\frac{i}{2}\chi(t)}$ and can be incorporated in the total scattering matrix.

3.4.2 Alternative Derivation of the Keldysh Action for 1D Systems

In this appendix we sketch an alternative derivation of the action $\mathcal{A}_f[\varphi]$ which holds for one-dimensional (1D) systems. As shown in Fig. 3.7 they may consist of several channels. Either direction of propagation is the same in all of them (in case of which the setup is referred to as "chiral") or there are two distinct possible directions: "right" (+) and "left"(-). The derivation generalizes that of Ref. [28] and some of the arguments given already there will be not reiterated here.
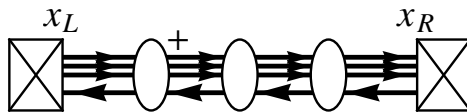

Figure 3.7: *Exemplary 1D system with 3 right-moving (+) and 1 left-moving (−) channels and 3 scatterers. The system extends $x_L < x < x_R$.*

We use a single coordinate system $x_L < x < x_R$ to describe all channels with left (right) contact position $x_{L(R)}$, i.e. velocities in right-(left-)moving channels are positive (negative): v_F ($-v_F$). The fermionic action is

$$\mathcal{A}_\mathrm{f}[\psi,\bar{\psi},\mathcal{V}] = \int \mathrm{d}x \int_\mathcal{C} \mathrm{d}t\, \Psi^\dagger \left(i\partial_t + i\tau_3 v_F \partial_x - \Sigma - \mathcal{V} \right) \Psi$$

where $\Psi = (\psi_\mu^\alpha)$ are vectors of Grassmannian fields with Keldysh and channel/direction indices α and μ, respectively, τ are Pauli matrices in direction space, v_F is the Fermi velocity, Σ is the self-energy correction due to the coupling to the reservoirs (see below), and $\mathcal{V}$ denotes the (temporally and spatially local) potential under the influence of which the electrons traverse the system. The latter may be the static scattering, Hubbard-Stratonovich or counting potential.

To obtain the integrated action $\mathcal{A}$, first its variation with respect to $\mathcal{V}$ is considered,

$$i\delta\mathcal{A} = -\int \mathrm{d}x \int \mathrm{d}t \, \mathrm{Tr}_\tau \left[\delta\mathcal{V}^f(t,x) G^T(x, t-0; x, t) - \delta\mathcal{V}^b(t,x) G^{\tilde{T}}(x, t+0; x, t) \right] \equiv -\int \mathrm{d}x \, \mathrm{Tr} \, \delta\mathcal{V}(x)\sigma_3 G(x,x) \tag{3.35}$$

where σ are Pauli matrices in Keldysh space, and the first trace Tr_τ is taken over Keldysh and channel indices, while the "full" trace Tr is additionally taken over real time. The full fermionic Green's function G is needed at coinciding spatial coordinates, where it is discontinuous because of linear dispersion. The above time shift regularization, which takes into account that fermion fields in the action are normal-ordered, is equivalent to the identification

$$G^{T(\tilde{T})}(x, t; x', t') \xrightarrow{x \to x'} \frac{1}{2iv_F} \left(g^{T(\tilde{T})}(x; t, t') - \delta\left(t - t'\right) \right) \tag{3.36}$$

with the quasiclassical Green's function

$$g^{\alpha\beta}(x, t, t') = iv_F \left(G^{\alpha\beta}(x+0, x; t, t') + G^{\alpha\beta}(x-0, x; t, t') \right).$$

Transfer matrices

The Green's function $G(x_1, x_2)$ is related to $G(x_1', x_2')$ via the the single-particle transfer matrices $\mathcal{M}(x, x')$ for spatial evolution from x' to x: $G^{\alpha\beta}(x_1, x_2) = \mathcal{M}^\alpha(x_1, x_1') G^{\alpha\beta}(x_1', x_2') \mathcal{M}^\beta(x_2', x_2)^\dagger$ or, for quasiclassical Green's functions, $g^{\alpha\beta}(x) = \mathcal{M}^\alpha(x, x') g^{\alpha\beta}(x') \mathcal{M}^\beta(x, x')^\dagger$. Defining $\mathcal{U}^\alpha(x; t, t') = iv_F^{-1}\delta(t-t')\tau_3(i\partial_{t'} - \mathcal{V}^\alpha(x, t'))$ (or more clearly in energy representation $\mathcal{U}^\alpha(x)(\epsilon, \epsilon') = iv_F^{-1}\tau_3(2\pi\delta(\epsilon - \epsilon')\epsilon - \mathcal{V}^\alpha(x, \epsilon - \epsilon'))$), the transfer matrices are given by

$$\mathcal{M}^\alpha(x, x') = \begin{cases} \mathcal{O}_{x_1} \exp\left[\int_{x'}^x \mathrm{d}x_1 \, \mathcal{U}^\alpha(x_1) \right], & x \geq' x, \\ \tilde{\mathcal{O}}_{x_1} \exp\left[\int_{x'}^x \mathrm{d}x_1 \, \mathcal{U}^\alpha(x_1) \right], & x \leq' x, \end{cases}$$

where $\mathcal{O}_x$ ($\tilde{\mathcal{O}}_x$) orders subsequent operators with respect to their space coordinate x, smaller (larger) coordinates ordered to the right. Consequently, transfer matrices are diagonal in Keldysh space (with $\mathcal{M}^\alpha$ being only related to $\mathcal{V}^\alpha$) and satisfy

$$\delta\mathcal{M}^\alpha(x_R, x_L) = \int_{x_L}^{x_R} \mathrm{d}x \, \mathcal{M}^\alpha(x_R, x) \left[-iv_F^{-1}\tau_3 \delta\mathcal{V}^\alpha(x) \right] \mathcal{M}^\alpha(x, x_L). \tag{3.37}$$

For short, we will also write for the total transfer matrix $\mathcal{M} \equiv \mathcal{M}(x_R, x_L)$. Note that in chiral systems considered in Ref. [28] scattering matrices S can be used. While coinciding with the transfer matrices in chiral systems, they differ in non-chiral ones, the two being related via

$$S = \tau_3 \left(\tau_+ + \mathcal{M}\tau_- \right)^{-1} \left(\mathcal{M}\tau_+ + \tau_- \right) \tau_3 \tag{3.38}$$

with the projectors $\tau_\pm = (\tau_0 \pm \tau_3)/2$ in direction space. In chiral, say right-moving, systems $\tau_3 = \tau_+ = \mathbb{1}$, $\tau_- = 0$ and indeed $S = \mathcal{M}$. Generally, S is unitary, $SS^\dagger = \mathbb{1}$, $\mathcal{M}$ is pseudo-unitary, $\mathcal{M}(x,x')\tau_3\mathcal{M}(x,x')^\dagger = \tau_3$. By defining $\bar{g} \equiv \sigma_3 g \tau_3$ spatial evolution amounts for the similarity transformation

$$\bar{g}(x) = \mathcal{M}(x,x')\bar{g}(x')\mathcal{M}(x,x')^{-1}.$$

The factor σ_3 ensures the normalization property $\bar{g}(x)^2 = \mathbb{1}$.

Using (3.36), (3.37) and $\bar{g}(x) = \mathcal{M}(x,x_L)\bar{g}(x_L)\mathcal{M}(x_R,x_L)^{-1}\mathcal{M}(x_R,x)$ the variation of the action (3.35) can be simplified to

$$
\begin{aligned}
i\delta\mathcal{A} &= -\int dx\, \mathrm{Tr}\, \tau_3 \delta\mathcal{V}(x)\, \frac{1}{2iv_F}\left(\bar{g}(x) - \sigma_3\tau_3\right) \\
&= -\frac{1}{2}\int dx\, \mathrm{Tr}\left[-iv_F{}^{-1}\tau_3\delta\mathcal{V}(x)\right]\mathcal{M}(x,x_L)\bar{g}(x_L)\mathcal{M}(x_R,x_L)^{-1}\mathcal{M}(x_R,x_L) + \mathrm{const.} \\
&= -\frac{1}{2}\mathrm{Tr}\,\bar{g}(x_L)\mathcal{M}^{-1}\delta\mathcal{M} + \mathrm{const.}
\end{aligned}
\tag{3.39}
$$

where we absorb all contributions to the action which are independent of distribution functions in "const.". We will show later on that they vanish.

Reservoir Green's Functions

In a next step, $\bar{g}(x_L)$ is expressed in terms of the quasiclassical Green's function

$$
g_{L(R)}(t-t') = \begin{pmatrix} g_{L(R)}^T & g_{L(R)}^< \\ g_{L(R)}^> & g_{L(R)}^{\tilde{T}} \end{pmatrix}_{t-t'} = \begin{pmatrix} \mathbb{1} - 2f_{L(R)} & -2f_{L(R)} \\ 2(\mathbb{1} - f_{L(R)}) & \mathbb{1} - 2f_{L(R)} \end{pmatrix}_{t-t'}
\tag{3.40}
$$

of the left (right) reservoirs (with distribution functions $f_{L(R)}$ which may have a non-trivial channel structure $f_{L(R)\mu}$). The Green's functions $\bar{g}_i = \sigma_3\bar{g}_i\tau_3$, $i = L, R$, are related to each other via a similarity transformation as follows: First, introducing the Keldysh matrices

$$
L \equiv \frac{1}{\sqrt{2}}\begin{pmatrix} \mathbb{1} & -\mathbb{1} \\ \mathbb{1} & \mathbb{1} \end{pmatrix}, \quad \tilde{U}_i = \begin{pmatrix} \mathbb{1} & (\mathbb{1} - 2f_i) \\ 0 & -\mathbb{1} \end{pmatrix} = \tilde{U}_i^{-1}
\tag{3.41}
$$

one easily finds

$$
L\bar{g}_iL^{-1} = \begin{pmatrix} \mathbb{1} & 2(\mathbb{1} - 2f_i) \\ 0 & -\mathbb{1} \end{pmatrix}\tau_3 = \tilde{U}_i^{-1}\sigma_3\tau_3\tilde{U}_i
\tag{3.42}
$$

and hence

$$
\bar{g}_i = U_i^{-1}\sigma_3\tau_3 U_i \quad \text{with} \quad U_i = \tilde{U}_i L = \frac{1}{\sqrt{2}}\begin{pmatrix} 2f_i^> & -2f_i^< \\ -\mathbb{1} & -\mathbb{1} \end{pmatrix}
\tag{3.43}
$$

with $f_i^< = f_i$, $f_i^> = \mathbb{1} - f_i$. Thus we have proven

$$
\bar{g}_R = U^{-1}\bar{g}_L U \quad \text{with} \quad U = U_L^{-1}U_R.
\tag{3.44}
$$

To relate the Green's function $\bar{g}(x_L)$ inside the system to its counterparts in the reservoirs one assumes that the dynamics inside the leads is governed by some relaxation process, say isotropization of momentum direction due to scattering off static white noise disorder. This is described by the self-energy contribution

$$\Sigma(t_1, x_1; t_2, x_2) = \delta(x_1 - x_2) \left(-\frac{i}{2\tau_{\text{rel}}} \right) \times \left\{ \begin{array}{ll} g_L(t_1, t_2), & x_1, x_2 < x_L \\ g_R(t_1, t_2), & x_1, x_2 > x_R \end{array} \right. .$$

Here τ_{rel} denotes the relaxation time. The requirement that $G(x + \Delta x, x)$ vanish for infinite distances Δx yields the boundary conditions[28],

$$(\mathbb{1} + \bar{g}_L)(\mathbb{1} - \bar{g}(x_-)) = 0, \qquad (\mathbb{1} - \bar{g}_R)(\mathbb{1} - \bar{g}(x_+)) = 0, \qquad (3.45)$$

again with $\bar{g} \equiv \sigma_3 g \tau_3$. Defining $\bar{\mathcal{M}} \equiv U\mathcal{M}$ the second equation is equivalent to $0 = \left(\mathbb{1} - \bar{\mathcal{M}}^{-1} \bar{g}_L \bar{\mathcal{M}} \right) (\mathbb{1} + \bar{g}(x_L))$. Combining it with the first equation gives

$$0 = \left(2\mathbb{1} + \bar{g}_L - \bar{\mathcal{M}}^{-1} \bar{g}_L \bar{\mathcal{M}} \right) - \left(\bar{g}_L + \bar{\mathcal{M}}^{-1} \bar{g}_L \bar{\mathcal{M}} \right) \bar{g}(x_L) \qquad (3.46)$$

and by inversion

$$\bar{g}(x_L) = \mathbb{1} + 2(\mathbb{1} - \bar{g}_L) \left(\bar{g}_L \bar{\mathcal{M}} + \bar{\mathcal{M}} \bar{g}_L \right)^{-1} \bar{\mathcal{M}} \qquad (3.47)$$

where we have made use of $\bar{g}_L^2 = \mathbb{1}$.

To rewrite this expression we choose a specific basis representation. Since $\bar{g}_L^2 = \mathbb{1}$ there exists one in which $\bar{g}_L = \text{diag}(\mathbb{1}, -\mathbb{1})$. In the very same representation we write

$$\bar{\mathcal{M}} = \begin{pmatrix} \bar{\mathcal{M}}_{11} & \bar{\mathcal{M}}_{12} \\ \bar{\mathcal{M}}_{21} & \bar{\mathcal{M}}_{22} \end{pmatrix}.$$

Then we have $\bar{g}_L \bar{\mathcal{M}} + \bar{\mathcal{M}} \bar{g}_L = 2 \, \text{diag}(\bar{\mathcal{M}}_{11}, -\bar{\mathcal{M}}_{22})$, which is readily inverted, as well as $\mathbb{1} + \bar{g}_L = 2 \, \text{diag}(\mathbb{1}, 0)$, $\mathbb{1} - \bar{g}_L = 2 \, \text{diag}(0, \mathbb{1})$, and (3.47) gives

$$\bar{g}(x_L) = \begin{pmatrix} \mathbb{1} & 0 \\ -2\bar{\mathcal{M}}_{22}^{-1} \mathcal{M}_{21} & -\mathbb{1} \end{pmatrix}. \qquad (3.48)$$

Defining

$$\mathcal{D} \equiv (\mathbb{1} + \bar{g}_L)/2 + \bar{\mathcal{M}}(\mathbb{1} - \bar{g}_L)/2 \qquad (3.49)$$

one may show that

$$\bar{g}(x_L) = \mathbb{1} - \left(\mathbb{1} - \bar{g}_L \right) \mathcal{D}^{-1} \bar{\mathcal{M}} \qquad (3.50)$$

is equivalent to (3.48). We have thus expressed $\bar{g}(x_L)$ entirely in terms of $\bar{g}_{L(R)}$ and the transfer matrix $\mathcal{M}(x_R, x_L)$.

Substituting this result into (3.39) and using $\mathcal{M}(x_R, x_L)^{-1} \delta \mathcal{M}(x_R, x_L) = \bar{\mathcal{M}}^{-1} \delta \bar{\mathcal{M}}$ yields

$$i\delta\mathcal{A} = \frac{1}{2} \text{Tr}(\mathbb{1} - \bar{g}_L) \mathcal{D}^{-1} \delta \bar{\mathcal{M}} + \text{const.} = \text{Tr} \, \mathcal{D}^{-1} \delta \mathcal{D} + \text{const.}$$

$$\Rightarrow i\mathcal{A} = \text{Tr} \, \text{Ln} \, \mathcal{D} + \text{const.} = \text{Tr} \, \text{Ln} \left[\frac{\mathbb{1} + \bar{g}_L}{2} + \bar{\mathcal{M}} \frac{\mathbb{1} - \bar{g}_L}{2} \right] + \text{const.} \quad (3.51)$$

Role of Drain Distribution Functions

So far we have not been concerned with the channel structure explicitly and merely stated that there are 2 directions of motion, right$(+)$ and left$(-)$, each of which is realized by a certain (not necessarily equal) number of channels (possibly even zero in chiral systems). In both left and right reservoirs to each channel μ was assigned a distribution function $f_{L\mu}$ and $f_{R\mu}$. For a right-(left-)moving channel $f_{R\mu}$ $(f_{L\mu})$ is the *drain* distribution function and one naturally wonders whether it should have an effect on the chiral fermions as long as the latter have not entered the drain reservoirs. We show here that this is not the case.

To this end we introduce the block decomposition with respect to channel indices, e.g.

$$
\mathcal{M} = \begin{pmatrix} \mathcal{M}_{++} & \mathcal{M}_{+-} \\ \mathcal{M}_{-+} & \mathcal{M}_{--} \end{pmatrix}, \quad f_i = \begin{pmatrix} f_{i+} & \\ & f_{i-} \end{pmatrix}, \quad i = L, R, \tag{3.52}
$$

where e.g. $\mathcal{M}_{+-}$, f_{i+}, f_{i-} still may have channel structure $\left(\mathcal{M}_{+-}\right)_{\mu\nu}$, $\left(f_{i+}\right)_\mu$, $\left(f_{i-}\right)_\nu$, however, with μ (ν) extending exclusively over right-(left-)moving channels.

Introducing

$$
Q \equiv U_R \mathcal{M} U_L^{-1} = \begin{pmatrix} Q_{11} & Q_{12} \\ Q_{21} & Q_{22} \end{pmatrix} = \begin{pmatrix} f_R^> \mathcal{M}^f + f_R^< \mathcal{M}^b & -2f_R^> \mathcal{M}^f f_L^< + 2f_R^< \mathcal{M}^b f_L^> \\ -\frac{1}{2}\mathcal{M}^f + \frac{1}{2}\mathcal{M}^b & \mathcal{M}^f f_L^< + \mathcal{M}^b f_L^> \end{pmatrix} \tag{3.53}
$$

and the projectors

$$
P_+ = \frac{1}{2}(1 + \sigma_3 \tau_3) = \begin{pmatrix} \tau_+ & 0 \\ 0 & \tau_- \end{pmatrix}, \quad P_- = \frac{1}{2}(1 - \sigma_3 \tau_3) = \begin{pmatrix} \tau_- & 0 \\ 0 & \tau_+ \end{pmatrix} \tag{3.54}
$$

the action (3.51) reads

$$
i\mathcal{A} = \ln \mathrm{Det}\left(P_+ + QP_-\right) + \mathrm{const.} = \ln \mathrm{Det}\left(P_+ + P_- QP_-\right) + \mathrm{const.}
$$

where

$$
P_- QP_- = \begin{pmatrix} \tau_- Q_{11} \tau_- & \tau_- Q_{12} \tau_+ \\ \tau_+ Q_{21} \tau_- & \tau_+ Q_{22} \tau_+ \end{pmatrix}.
$$

Writing out the direction structure explicitly yields

$$
i\mathcal{A} = \ln \mathrm{Det}\begin{pmatrix} f_{R-}^> \mathcal{M}_{--}^f + f_{R-}^< \mathcal{M}_{--}^b & -2f_{R-}^> \mathcal{M}_{-+}^f f_{L+}^< + 2f_{R-}^< \mathcal{M}_{-+}^b f_{L+}^> \\ -\frac{1}{2}\mathcal{M}_{+-}^f + \frac{1}{2}\mathcal{M}_{+-}^b & \mathcal{M}_{++}^f f_{L+}^< + \mathcal{M}_{++}^b f_{L+}^> \end{pmatrix} + \mathrm{const.}
$$

This proves that the action depends only on f_{L+} and f_{R-}, i.e. the source distribution functions.

Tracing out Keldysh Structure

We now return to the expression (3.51). Since we already know that the result does not depend on $f_{L,-}$ and $f_{R,+}$ we may make the choice $f_{L,-} = f_{R,-}$ and $f_{R,+} = f_{L,+}$. In other words, we put

$\bar{g}_L = \bar{g}_R = \mathrm{diag}\left(\bar{g}_{L+}, \bar{g}_{R-}\right) \equiv \bar{g}_{\mathrm{in}} \equiv \sigma_3 g_{\mathrm{in}} \tau_3$. As suggested by the subindex g_{in} contains the source (or incoming) distribution functions. It can be parametrized analogously to (3.43),

$$\sigma_3 g_{\mathrm{in}} = U_{\mathrm{in}}^{-1} \sigma_3 U_{\mathrm{in}} \quad \text{with } U_{\mathrm{in}} = \frac{1}{\sqrt{2}} \begin{pmatrix} 2f^> & -2f^< \\ -\mathbb{1} & -\mathbb{1} \end{pmatrix} \tag{3.55}$$

with f being the matrix of source distribution functions. Since U is not needed anymore and hence $\bar{\mathcal{M}} = \mathcal{M}$, we recall the definition of $\mathcal{D}$ given by Eq. (3.49) and of scattering matrix S (3.38) and obtain

$$\mathcal{D} = \frac{\mathbb{1} + \sigma_3 g \tau_3}{2} + \mathcal{M} \frac{\mathbb{1} - \sigma_3 g \tau_3}{2} = \left(\tau_+ + \mathcal{M}\tau_-\right) \tau_3 U_{\mathrm{in}}^{-1} \left[\frac{\mathbb{1} + \sigma_3}{2} + U_{\mathrm{in}} S U_{\mathrm{in}}^{-1} \frac{\mathbb{1} - \sigma_3}{2} \right] U_{\mathrm{in}}. \tag{3.56}$$

With

$$\tilde{Q} \equiv U_{\mathrm{in}} S\, U_{\mathrm{in}}^{-1} = \begin{pmatrix} Q^{ff} & Q^{fb} \\ Q^{bf} & Q^{bb} \end{pmatrix} = \begin{pmatrix} f^> S^f + f^< S^b & -2f^> S^f f^< + 2f^< S^f f^> \\ -\frac{1}{2} S^f + \frac{1}{2} S^b & S^f f^< + S^b f^> \end{pmatrix}$$

the action (3.51) is

$$i\mathcal{A} = \ln \mathrm{Det}\, \mathcal{D} + \text{const.} = \ln \mathrm{Det}\, Q^{bb} + \text{const.} = \mathrm{Tr}\, \mathrm{Ln}\left[\mathbb{1} - f + S^{b\dagger} S^f f \right] + \text{const.} \tag{3.57}$$

Up to anomalous terms, representing the r- and a-parts of the polarization operator, and contributions which are independent of distribution functions f, this proves Eq. (3.3)

Constant contributions

What are the "const."-contributions to the action we keep ignoring? All that we know so far about them is their independence of distribution function f. According to (3.57) they can be recovered by substituting $f = 0$ in the *full* action (where "const." is not neglected). So let us put $f \equiv 0$ in the rest of this section and recalculate the full action. Eq. (3.47) can be evaluated explicitly now, yielding $g^T(x_L) = g_0^-(x_L)$ and $g^{\tilde{T}}(x_L) = g_0^+(x_L)^\dagger$ with

$$g_0(x_L) = \begin{pmatrix} \mathbb{1} & 0 \\ 2S_{-+} & \mathbb{1} \end{pmatrix} = \mathbb{1} + 2 \begin{pmatrix} 0 & 0 \\ A_{-+}(x_L) & 0 \end{pmatrix}$$

where $A_{\nu\mu}(x; t', t)$ is defined as the amplitude for a μ-wave packet at position x and time t to end up as a ν-wave packet at time t' and the same position x (cf. Sect. 3.4.1). The above relation between $g^{T/\tilde{T}}$ and $g_0^\mp$ holds for all positions x with $g_0^\alpha(x) \equiv \mathcal{M}^\alpha(x, x_L) g_0^\alpha(x_L) \mathcal{M}^\alpha(x, x_L)^\dagger$. To calculate the latter we define (for given x) the "scattering matrix"

$$s \equiv \tau_3 \left(\tau_+ + \mathcal{M}(x, x_L)\tau_-\right)^{-1} \left(\mathcal{M}(x, x_L)\tau_+ + \tau_-\right) \tau_3$$

of the region between x_L and x which takes into account paths extending only within this region. Using the recursion relations (see Fig. 3.8)

$$S_{-+} = s_{-+} + s_{--} A_{-+}(x) s_{++},$$

$$A_{++}(x) = s_{+-} A_{-+}(x), \quad A_{+-}(x) = s_{+-} + s_{+-} A_{-+}(x) s_{+-}, \quad A_{--}(x) = A_{-+}(x) s_{+-}$$
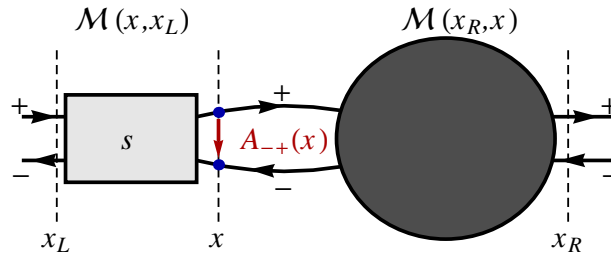
Figure 3.8: *Spatial evolution of g from x_L to x with $\mathcal{M}(x, x_L)$; s is the corresponding "scattering matrix"; the shaded blob represents the rest of the system. In contrast to s, paths contributing to $A_{-+}(x)$ may extend throughout the entire system.*

one obtains

$$g_0(x) = \mathbb{1} + 2 \begin{pmatrix} A_{++}(x) & A_{+-}(x) \\ A_{-+}(x) & A_{--}(x) \end{pmatrix}. \tag{3.58}$$

For a smooth potential $\mathcal{V}(x)$ all paths contributing to $A_{\nu\mu}(x)$ have a non-vanishing flight time such that $A_{\nu\mu}(x; t, t) = 0$. At point scatterers, which are a mere idealization, the Green's function $g(x)$ is not well-defined and we stay sufficiently far away from them. Concluding, for equal times the Green's function (3.36) vanishes. Substituting this result into Eq. (3.35) yields $\delta\mathcal{A}|_{f\equiv 0} = 0$, hence const. $= \mathcal{A}|_{f\equiv 0}$ is indeed a physically irrelevant constant.

3.4.3 Weak Tunneling Regularization

In general, the scattering matrix $S^\alpha = S[\varphi^\alpha]$ depends on time in a complicated manner which makes the exact evaluation of the functional determinant (3.3) unfeasible. In this section we present an approximation scheme which applies for systems with weak tunneling. A tunneling action $\mathcal{A}_t$ is derived by subtracting the clean action $\mathcal{A}_0$ from the full one $\mathcal{A}$. By construction $\mathcal{A}_t$ is small and may be therefore expanded. The crucial step, the separation of actions, can be performed at zero temperature where reservoirs may have differing chemical potentials. As it will turn out, interaction effectively leads to a dressing of the point scatterers by phases Φ.

Clean Limit

The clean limit was discussed in Sect. 2.2. The action $\mathcal{A}_0$ is obtained from (3.3) by replacing S by the clean scattering matrix $S_*^\alpha = \text{diag}\left(e^{i\vartheta_1^\alpha}\Delta_1, \ldots, e^{i\vartheta_N^\alpha}\Delta_N\right) \equiv e^{i\vartheta^\alpha}\Delta$ with the delay operators Δ_μ and the phases ϑ_μ accumulated along the complete paths $x_\mu^S \to x_\mu^D$.

The main step in the quest of the tunneling action

$$\mathcal{A}_t = \mathcal{A} - \mathcal{A}_0 = i\,\text{Tr}\,\text{Ln}\left[\left(\mathbb{1} - f + S^{b\dagger}S^f f\right)\left(\mathbb{1} - f + S_*^{b\dagger}S_*^f f\right)^{-1}\right]$$

is the inversion of the second bracket, a problem which was already dealt with in Ref. [33]. Since S_* is diagonal in channel space, the operator can be inverted for each channel separately. So we consider

$$\left(\mathbb{1} - f + S_*^{b\dagger}S_*^f f\right)_{\mu\mu} = \mathbb{1} - f_\mu + \Delta_\mu^{-1}e^{i\left(\vartheta_\mu^f - \vartheta_\mu^b\right)}\Delta_\mu f_\mu$$

where $\Delta_\mu(t', t) = \delta(t' - t - \tau_\mu)$ is an appropriate time delay operator. Note that it commutes with the stationary distribution function f_μ. For zero temperature we follow Ref.[33], according to which the inversion problem can be reformulated in terms of a certain Riemann-Hilbert problem, which is solved by defining the phases $\vartheta_\mu^\wedge$ and $\vartheta_\mu^\vee$ by

$$\vartheta_\mu^{\wedge\vee}(t) \equiv \frac{i}{2\pi} \int \mathrm{d}t' \, \frac{\vartheta_\mu^f(t') - \vartheta_\mu^b(t')}{t_\pm - t'} \equiv - \int \mathrm{d}t' \left[B(t - t') \mp \delta(t - t') \right] \left[\vartheta_\mu^f(t') - \vartheta_\mu^b(t') \right], \qquad (3.59)$$

with $t_\pm \equiv t \pm i0$. They satisfy $\vartheta^\wedge - \vartheta^\vee = \vartheta^f - \vartheta^b$, hence $\vartheta^f - \vartheta^\wedge = \vartheta^b - \vartheta^\vee \equiv \bar{\vartheta}$, and $f_\mu e^{i\vartheta_\mu^\wedge} f_\mu = e^{i\vartheta_\mu^\wedge} f_\mu$, $f_\mu e^{i\vartheta_\mu^\vee} f_\mu = f_\mu e^{i\vartheta_\mu^\vee}$. Thus, one obtains

$$\left(\mathbb{1} - f_\mu + \Delta_\mu^{-1} e^{i\left(\vartheta_\mu^f - \vartheta_\mu^b\right)} \Delta_\mu \, f_\mu \right)^{-1} = \Delta_\mu^{-1} \left[e^{-i\vartheta_\mu^\vee} \left(\mathbb{1} - f_\mu \right) + e^{-i\vartheta_\mu^\wedge} f_\mu \right] e^{i\vartheta_\mu^\vee} \Delta_\mu,$$

and, taking now the full channel structure into account,

$$\mathcal{A}_t = -i \operatorname{Tr} \operatorname{Ln} \left[\mathbb{1} - f + \tilde{S}^{b\dagger} \tilde{S}^f f \right] = i \sum_{n=1}^\infty \frac{1}{n} \operatorname{Tr} \left[\left(\mathbb{1} - \tilde{S}^{b\dagger} \tilde{S}^f \right) f \right]^n$$

with the "regularized" scattering matrix

$$\tilde{S}^{f/b} \equiv e^{-i\bar{\vartheta}} S^{f/b} \Delta^{-1} e^{-i\vartheta^{\wedge\vee}} \Delta. \qquad (3.60)$$

Defining in energy representation $N(\omega) = -\theta(-\omega)$ as the zero temperature limit of the Bose distribution function, we note that the function B introduced in (3.59) is the "generalized" distribution function $B(\omega) = 1 + 2N(\omega)$ ubiquitous in the bosonic Keldysh formalism. This fact allows us to endow the phases with a Keldysh structure. We address this issue in the next section before turning to the computation of the regularized scattering matrix in the subsequent one.

Phases and Keldysh Structure

Before we turn to the computation of the regularized scattering matrix let us consider the Keldysh structure of the phases ϑ. To this end we consider the clean path $x_\mu^S \to x_\mu^D$ containing the point x. An electron propagating from the source reservoir x_μ^S to x (arrival time t) accumulates the phase

$$\vartheta_{\mathrm{in}.\mu}^\alpha(t, x) \equiv -v_\mu^{-1} \int_{x_\mu^S}^x \mathrm{d}x' \, \varphi^\alpha(x', t - (x - x')/v_\mu) = -D_{0\mu}^r \varphi_\mu^\alpha(x, t); \qquad (3.61)$$

likewise when traveling from x (departure time t) to the drain reservoir x_μ^D it accumulates

$$\vartheta_{\mathrm{out}.\mu}^\alpha(t, x) \equiv -v_\mu^{-1} \int_x^{x_\mu^D} \mathrm{d}x \, \varphi^\alpha(x, t + (x' - x)/v_\mu) = D_{0\mu}^a \varphi_\mu^\alpha(x, t) \qquad (3.62)$$

where we introduced the retarded/advanced bare electron-hole pair propagators

$$D_{0\mu}^{r/a}(t; x', x) = \pm\theta(\pm t)\delta(x' - (x + v_\mu t))$$

along the the clean path. Quite obviously, the phase accumulated along the complete clean path satisfies

$$\vartheta_\mu^{f/b}(t) = \vartheta_{\mu.\text{in}}^\mp(x, t - (x_\mu^D - x)/v_\mu) + \vartheta_{\mu.\text{out}}^\mp(x, t - (x_\mu^D - x)/v_\mu) = -\left(D_{0\mu}^r - D_{0\mu}^a\right)\varphi_\mu^\mp(x, t - (x_\mu^D - x)/v_\mu).$$
(3.63)

The propagators $D_{0\mu}^{r/a}$ directly make reference to propagation velocity v_μ and thus encode spectral (kinematic) properties of the electron-hole pairs. As usual they lack information about the system's state which one expects to be contained in the missing Keldysh component $D_{0\mu}^k$ of the propagator. In this sense the phases ϑ are related to the potential φ via the linear operator D_0 which does not have the full Keldysh structure.

To overcome this "deficiency" we recall the definition made in the previous section

$$\bar{\vartheta}_\mu = \vartheta_\mu^\mp - \vartheta_\mu^{\wedge\vee} = \frac{1}{2}(B + 1)\vartheta_\mu^f - \frac{1}{2}(B - 1)\vartheta_\mu^b.$$
(3.64)

Combining now (3.63) and (3.64) and using the stationarity of $B(t, t') = B(t - t')$ we obtain

$$\bar{\vartheta}_\mu(t + (x_\mu^D - x)/v_\mu) = -\frac{1}{2}(B + 1)\left(D_{0\mu}^r - D_{0\mu}^a\right)\varphi_\mu^f(x, t) + \frac{1}{2}(B - 1)\left(D_{0\mu}^r - D_{0\mu}^a\right)\varphi_\mu^b(x, t) \quad (3.65)$$

With that the phase that an electron, traveling along a piece of wire between x^1 and x^2, accumulates is

$$\vartheta_{\mu 21}^\mp(t) = -\vartheta_{\mu.\text{out}}^\mp(x^2, t) + \vartheta_{\mu.\text{out}}^\mp(x^1, t - (x^2 - x^1)/v_\mu)$$
$$\equiv \Theta_\mu^\mp(x^2, t) - \Theta_\mu^\mp(x^1, t - (x^2 - x^1)/v_\mu)$$

with the phases

$$\Theta_\mu^\mp(x, t) \equiv -\vartheta_{\mu.\text{out}}^\mp(x, t) + \bar{\vartheta}_\mu(t + (x_\mu^D - x)/v_\mu) \tag{3.66}$$
$$= -\frac{1}{2}\left[(B + 1)D_{0\mu}^r - (B \mp 1)D_{0\mu}^a\right]\varphi_\mu^f(x, t) + \frac{1}{2}\left[(B - 1)D_{0\mu}^r - (B \mp 1)D_{0\mu}^a\right]\varphi_\mu^b(x, t)$$
$$= -\left[D_{0\mu}^{T/>}\varphi_\mu^f(x, t) - D_{0\mu}^{>/\tilde{T}}\varphi_\mu^b(x, t)\right].$$

We thus have managed to rewrite the scattering matrix of chiral wires $\mathcal{M}^\alpha(x_2, x_1) = e^{i\vartheta_{21}^\alpha}\Delta(x_2, x_1) = e^{i\Theta^\alpha(x_2)}\Delta(x_2, x_1)e^{i\Theta^\alpha(x_1)}$ in terms of phases with full Keldysh structure. Formally we started with expressions which did not contain any distribution functions whatsoever and somewhat artificially included them by redefining phases. The usefulness of such construction will become apparent in the next section.

Construction of "Regularized" Scattering Matrix

We have previously shown that the full scattering matrix S can be constructed out of simpler units. We prove in this subsection that the same statement holds for the regularized scattering matrix $\tilde{S}$.

Since the full scattering matrix elements are amplitude sums $S_{\nu\mu}^\alpha = \sum_p A_{\nu\mu}^{(p)\alpha}$ over all paths p connecting x_μ^S with x_ν^D, definition (3.60) directly implies that $\tilde{S}_{\nu\mu}^\mp = \sum_p \tilde{A}_{\nu\mu}^{(p)\mp}$ is the sum of the *regularized* amplitudes

$$\tilde{A}_{\nu\mu}^{(p)\mp} \equiv e^{-i\bar{\vartheta}_\nu}A_{\nu'\mu}^{(p)\mp}\Delta_\mu^{-1}e^{-i\vartheta_\mu^{\wedge\vee}}\Delta_\mu = e^{-i\Theta_\nu^\mp(x_\nu^D)}A_{\nu\mu}^{(p)\mp}e^{i\Theta_\mu^\mp(x_\mu^S)} \tag{3.67}$$

over the same paths p with phases $\Theta_{\mu(\nu)}$ along the clean paths $x_\mu^S \to x_\mu^D$ and $x_\nu^S \to x_\nu^D$. Note that $\vartheta_{\nu.\text{out}}^{\mp}(x_\nu^D, t) = 0$ and $\vartheta_{\mu.\text{out}}^{\mp}(x_\mu^S, t) = \vartheta_\mu^{\mp}(t + (x_\mu^D - x_\mu)/v_\mu)$, and thus definition (3.66) implies $\Theta_\nu^{\mp}(x_\nu^D, t) = \vartheta_\nu(t)$ and $\Theta_\mu^{\mp}(x_\mu^S, t) = -\vartheta_\mu^{\wedge\vee}(t + (x_\mu^D - x_\mu^S)/v_\mu)$.

We now consider a generic path p which starts at incoming lead channel μ, winds through an alternating sequence of wires and point scatterers (numbered $1, 2, \ldots, N$ with positions $x_1, x_2, \ldots, x_N$), eventually ends in outgoing channel ν'. The corresponding full amplitude is

$$
\begin{aligned}
A_{\nu\mu}^{(p)\mp} &= \mathcal{M}_\mu^{\mp}(x^D, x^N) s_{\nu\lambda}^N \cdots s_{\rho\kappa}^2 \mathcal{M}_\kappa^{\mp}(x^2, x^1) s_{\kappa\mu}^1 \mathcal{M}_\mu^{\mp}(x^1, x_\mu^S) \\
&= e^{i\Theta_\nu^{\mp}(x_\nu^D)} \Delta_\nu(x_\nu^D, x^N) e^{-i\Theta_\nu^{\mp}(x^N)} s_{\nu\lambda}^N \cdots s_{\rho\kappa}^2 e^{i\Theta_\kappa^{\mp}(x^2)} \Delta_\kappa(x^2, x^1) e^{i\Theta_\kappa^{\mp}(x^1)} s_{\kappa\mu}^1 e^{i\Theta_\mu^{\mp}(x^1)} \Delta_\mu(x^1, x_\mu^S) e^{-i\Theta_\mu^{\mp}(x_\mu^S)}
\end{aligned}
$$

and simply becomes

$$
\tilde{A}_{\nu\mu}^{(p)\mp} = \Delta_\nu(x_\nu^D, x^N) e^{-i\Theta_\nu^{\mp}(x^N)} s_{\nu\lambda}^N \cdots e^{i\Theta_\kappa^{\mp}(x^2)} \Delta_\kappa(x^2, x^1) e^{i\Theta_\kappa^{\mp}(x^1)} s_{\kappa\mu}^1 e^{i\Theta_\mu^{\mp}(x^1)} \Delta_\mu(x^1, x_\mu^S)
$$

upon regularization. This implies that regularization of the amplitudes amounts to regularization of the scattering matrices of the building blocks: The effect of fluctuating potentials (and counting fields) is removed from all wires and incorporated in the tunneling phases

$$
\Phi_{\nu\mu}^{\mp}(x^j, t) \equiv \Theta_\mu^{\mp}(x^j, t) - \Theta_\nu^{\mp}(x^j, t)
$$

which dress the point scattering amplitudes $s_{\nu\mu}^j$. This result is summarized in the table below:

Construction unit	Regularized scattering matrix
Chiral wire	$\Delta(t', t)$
Point scatterer	$\tilde{s}_{\nu\mu}^\alpha(t', t) = s_{\nu\mu}\, e^{i\Phi_{\nu\mu}^\alpha(t, \bar{x})}\, \delta(t' - t)$

3.4.4 Second Order Expansion

We prove the second order expansion (3.10) in tunneling strength ("tun") starting from (3.9). Obviously, $\mathcal{P}_{\nu\mu} \equiv \sum_\lambda (\tilde{S}_{\lambda\nu}^+)^\dagger \tilde{S}_{\lambda\mu}^f$ is the sum over all paths winding forward and along the forward Keldysh branch (i.e. with potentials φ^f) from source μ to some drain λ and then *backwards* along the backward branch (with potentials φ^b) to source ν (for short: "source $\mu \overset{-}{\to}$ drain $\lambda \overset{+}{\to}$ source ν"). The backward part $\bar{p}^b$ is obtained by time-reversal of a physical, forward path p^b (source $\nu \overset{+}{\to}$ drain λ) with amplitude $\tilde{A}_{\lambda\nu}^{(p^b)}$ and has amplitude $\tilde{A}_{\nu\lambda}^{\bar{p}^b} \equiv \tilde{A}_{\lambda\nu}^{(p^b)\dagger}$ (note that hermitian conjugation, $\dagger$, reverses the order of partial amplitudes in the product). Denoting with p^f the forward part of $p = p^f \oplus \bar{p}^b$, the total amplitude is $\tilde{A}_{\nu\mu}^{(p)} \equiv \tilde{A}_{\lambda\nu}^{(p^b)\dagger} \tilde{A}_{\lambda\mu}^{(p^f)}$.

In the chosen order of accuracy we only take paths with a total of 2 or less tunneling events into account. The expanded tunneling action is $\mathcal{A}_t = \mathcal{A}_1 + \mathcal{A}_2$ with

$$
\mathcal{A}_1 \equiv i \operatorname{Tr} \sum_\mu (\mathbb{1} - \mathcal{P})_{\mu\mu} f_\mu = i \sum_\mu \operatorname{Tr} \left[f_\mu - \sum_{p_1} \tilde{A}_{\mu\mu}^{(p_1)} f_\mu \right], \tag{3.68}
$$

$$
\mathcal{A}_2 \equiv \frac{i}{2} \operatorname{Tr} \sum_{\mu\neq\nu} \mathcal{P}_{\mu\nu} f_\nu \mathcal{P}_{\nu\mu} f_\mu = \frac{i}{2} \sum_{\mu\neq\nu} \sum_{p_2 = p_2' \oplus p_2''} \operatorname{Tr} \tilde{A}_{\mu\nu}^{(p_2'')} f_\nu \tilde{A}_{\nu\mu}^{(p_2')} f_\mu. \tag{3.69}
$$

The sum $\sum_p$ in (3.68) extends over paths p_1: "source $\mu \overset{-}{\to}$ drain $\nu \overset{+}{\to}$ source μ" with 2 or less tunneling events (obviously the number has to be even), while the sum in (3.69) extends over paths $p_2 = p_2' \oplus p_2''$:

$$\text{"}\underbrace{\text{source } \mu \overset{-}{\to} \text{drain } \kappa \overset{+}{\to} \text{source}}_{p_2'} \underbrace{\nu \overset{-}{\to} \text{drain } \lambda \overset{+}{\to} \text{source } \mu}_{p_2''}\text{"},$$

$$\text{or equivalently, "}\underbrace{\text{source } \nu \overset{-}{\to} \text{drain } \lambda \overset{+}{\to} \text{source}}_{p_2''} \underbrace{\mu \overset{-}{\to} \text{drain } \kappa \overset{+}{\to} \text{source } \nu}_{p_2'}\text{"}$$

where the equivalence is ensured by the cyclic invariance of the trace. Since $\mu \neq \nu$ subpaths p_2' and p_2'' each contain at least one tunneling event, i.e. in our approximation *exactly one*. Depending on whether tunneling occurs on the forward or backward Keldysh branch $\kappa, \lambda = \mu$ or ν. It is quite obvious that no matter how often a path evolves in time forward and backward (once for $\mathcal{A}_1$, twice for $\mathcal{A}_2$), as long as it starts and ends in the same reservoir and contains exactly 2 tunneling events, it exactly involves 2 different channels $\mu \neq \nu$. We will use this fact for a systematic classification of all paths.

To warm up we consider first the simplest (and least interesting) paths, which contribute to $\mathcal{A}_1$ and are of the form "source $\mu \overset{-}{\to}$ drain $\mu \overset{+}{\to}$ source μ" without any tunneling taking place. Time delay operators are canceled exactly (since forward and backward paths coincide geometrically) and no phases are accumulated (since after regularization they are carried only by the tunneling amplitudes). The total amplitude is thus a product of forward scattering amplitudes $s_{\mu\mu}^j$ of scatterers j along the clean path $x_\mu^S \to x_\mu^D$:

$$\prod_j |s_{\mu\mu}^j|^2 = \prod_j \left(\mathbb{1} - \sum_{\nu \neq \mu} |s_{\nu\mu}^j|^2 \right) = \mathbb{1} - \sum_j \sum_{\nu \neq \mu} |s_{\nu\mu}^j|^2 + \mathcal{O}(\text{tun}^4). \tag{3.70}$$

All other relevant paths contain exactly 2 tunneling events. Not surprisingly there is a whole plethora of them and we are well advised to proceed systematically. To this end and according to the observation made before we classify these paths with respect to the pair (μ, ν) of different channels $\mu \neq \nu$ involved and the two scatterers i and j (possibly $i = j$) at which tunneling $\mu \to \nu$ and $\nu \to \mu$ respectively occurs. Note that in this classification classes $(ij; \mu\nu)$ and $(ji, \nu\mu)$ are identical. What classes $(ij; \mu\nu)$ are possible, of course, depends on the topology of the considered network (since e.g. not all scatterers are even connected to a given channel μ). But, as we will show, once a class is fixed, its contribution to $\mathcal{A}_t$ is essentially independent of topology!
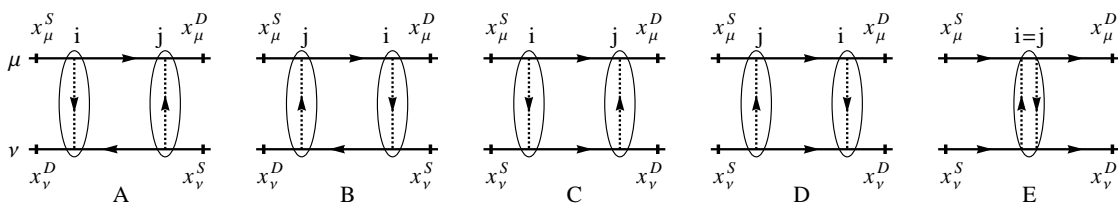

Figure 3.9: *The 5 topologically distinct configurations for class $(ij; \mu\nu)$. All channels except for μ, ν and all scatterers except for i, j ("distorted white circles") are dropped. Scatterers $i \neq j$ are different in A-D which allows for 4 different orderings along channels μ and ν. In E tunneling occurs twice at the same scatterer $i = j$.*

Fig. 3.9 shows the 5 topologically distinct configurations of channels μ, ν and scatterers i, j for given class $(ij; \mu\nu)$. Arrows at the scatterers indicate direction of tunneling. All scatterers except for i, j are dropped. They are involved only in forward scattering events and thus lead to corrections $\mathcal{O}(\text{tun}^3)$. In this way propagation from source x_μ^S to scatterer i just leads to an amplitude $\Delta_{i.\mu.\text{in}}$ which accounts for the finite flight time $\tau_{\mu.\text{in}}^i$. Analogously we define $\Delta_{j.\mu.\text{in}}$ and the same for ν, and further

$$\mathcal{X}_i^f \equiv \Delta_{i.\nu.\text{in}}^{-1} \tilde{s}_{\nu\mu}^{i-} \Delta_{i.\mu.\text{in}} = \Delta_{i.\nu.\text{in}}^{-1} e^{-i\Phi_{\mu\nu}^f(x^i)} \Delta_{i.\mu.\text{in}}\; s_{\nu\mu}^i,$$

$$\mathcal{X}_i^b \equiv \Delta_{i.\nu.\text{in}}^{-1} \left(s_{\mu\nu}^{i+}\right)^\dagger \Delta_{i.\mu.\text{in}} = \Delta_{i.\nu.\text{in}}^{-1} e^{-i\Phi_{\mu\nu}^b(x^i)} \Delta_{i.\mu.\text{in}}\; \bar{s}_{\mu\nu}^i,$$

$$\mathcal{X}_j^f \equiv \Delta_{j.\mu.\text{in}}^{-1} \tilde{s}_{\mu\nu}^{j-} \Delta_{j.\nu.\text{in}} = \Delta_{i.\nu.\text{in}}^{-1} e^{i\Phi_{\mu\nu}^f(x^j)} \Delta_{j.\nu.\text{in}}\; s_{\mu\nu}^j,$$

$$\mathcal{X}_j^b \equiv \Delta_{j.\mu.\text{in}}^{-1} \left(s_{\nu\mu}^{j+}\right)^\dagger \Delta_{j.\nu.\text{in}} = \Delta_{j.\mu.\text{in}}^{-1} e^{i\Phi_{\mu\nu}^b(x^j)} \Delta_{j.\nu.\text{in}}\; \bar{s}_{\nu\mu}^j.$$

For paths of given type p_1 or p_2 fixing the Keldysh branches on which the 2 tunneling events $\mu \to \nu$ (at i), $\nu \to \mu$ (at j) take place characterizes the corresponding paths uniquely provided they exist. Whether they exist or not depends on topology. Remarkably, they always do if the 2 tunneling events are required to occur on *different* Keldysh branches. Fig. 3.10 shows the paths for $i : \mu \to \nu$ occurring

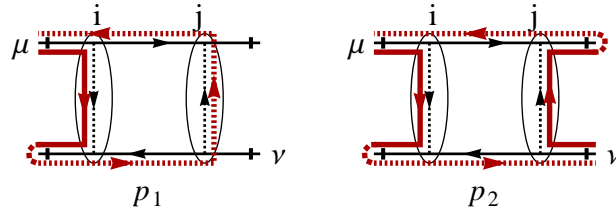**Figure 3.10:** *Paths for topology A with $i : \mu \to \nu$ on the forward, $j : \nu \to \mu$ on the backward branch. The forward parts are represented by solid thick lines; the backward parts by dashed lines. The first path is of type p_1, the second one of type p_2.*

on the forward, $j : \nu \to \mu$ on the backward branch for configuration A. Similar paths can be drawn for all other configurations. As an example, we consider the first path in Fig. 3.10 which is of type p_1. It starts at source μ, tunnels at i on the forward branch, arrives at drain ν, evolves backwards, tunnels at j on the backward branch and returns to source μ. Its amplitude is $\tilde{A}_{\mu\mu}^{(p_1)} = \mathcal{X}_j^b \mathcal{X}_i^f$. The contribution of both paths to $\mathcal{A}_t$ is

$$\mathcal{A}_{ij;\mu\nu}^< = -i\,\mathrm{Tr}\left[\mathcal{X}_j^b \mathcal{X}_i^f f_\mu - \mathcal{X}_j^b f_\nu \mathcal{X}_i^f f_\mu\right] = -i\,\mathrm{Tr}\left[e^{-i\Phi_{\mu\nu}^f(x^i)}\Pi_{ij;\mu\nu}^< e^{i\Phi_{\mu\nu}^f(x^j)}\right]$$

where tunneling polarization operators $\Pi_{ij;\mu\nu}$ are defined in (3.11) and we have made use of $s_{\mu\nu}^j = -\bar{s}_{\nu\mu}^j + \mathcal{O}(\text{tun}^2)$. Similarly $\mathcal{A}_{ij;\mu\nu}^>$ with $\Pi_{ij;\mu\nu}^>$ is obtained by considering paths with tunneling at i on the backward, at j on the forward branch. As mentioned previously the very same paths can be drawn for all topologies and yield the same action.

The story is less neat if both tunneling events occur on the same Keldysh branch: While p_2-type contributions to $\mathcal{A}_{ij;\mu\nu}^T$ and $\mathcal{A}_{ij;\mu\nu}^{\tilde{T}}$ are still independent from topology, p_1-type contributions are not as universal. Taking all paths carefully into account results in the table below

	$\Pi^{T}_{ij;\mu\nu}(t)/\left[-s^i_{\nu\mu}\bar{s}^j_{\nu\mu}\right]$	$\Pi^{\tilde{T}}_{ij;\mu\nu}(t)/\left[-s^i_{\nu\mu}\bar{s}^j_{\nu\mu}\right]$
A	$-\tilde{f}^<_\mu(t)\tilde{f}^<_\nu(-t)$	$\tilde{f}^>_\mu(t)\tilde{f}^<_\nu(-t) + \tilde{f}^<_\mu(t)\tilde{f}^>_\nu(-t) + \tilde{f}^<_\mu(t)\tilde{f}^<_\nu(-t)$
B	$\tilde{f}^>_\mu(t)\tilde{f}^<_\nu(-t) + \tilde{f}^<_\mu(t)\tilde{f}^>_\nu(-t) + \tilde{f}^<_\mu(t)\tilde{f}^<_\nu(-t)$	$-\tilde{f}^<_\mu(t)\tilde{f}^<_\nu(-t)$
C	$\tilde{f}^<_\mu(t)\tilde{f}^>_\nu(-t)$	$\tilde{f}^>_\mu(t)\tilde{f}^<_\nu(-t)$
D	$\tilde{f}^>_\mu(t)\tilde{f}^<_\nu(-t)$	$\tilde{f}^<_\mu(t)\tilde{f}^>_\nu(-t)$
E	$-f^<_\mu(t)f^<_\nu(-t) + \frac{1}{2}(f^<_\mu(t) + f^<_\nu(-t))\delta(t)$	$-f^>_\mu(t)f^>_\nu(-t) + \frac{1}{2}(f^<_\mu(t) + f^<_\nu(-t))\delta(t)$

with $\tilde{f}^{\gtrless}_\mu(t) \equiv f^{\gtrless}_\mu(t + \tau^i_{\mu.\text{in}} - \tau^j_{\mu.\text{in}})$, $\tilde{f}^{\gtrless}_\nu(t) \equiv f^{\gtrless}_\nu(t - \tau^j_{\nu.\text{in}} + \tau^i_{\nu.\text{in}})$. We have incorporated the tunneling-free contribution (3.70) into the case E which amounts to the $\delta(t)$-terms.

Quite miraculously, using the symmetry relation $f^{\gtrless}_{\mu/\nu}(t) = -f^{\lessgtr}_{\mu/\nu}(t)$ for $t \neq 0$, one can show that (3.12) holds, i.e. $\Pi^{T/\tilde{T}}_{ij;\mu}$ can be represented in a form which is independent of topology. We exemplify the proof, which is a straightforward calculation, on configuration A. In this situation, $\tau^j_{\mu.\text{in}} > \tau^i_{\mu.\text{in}}$ and $\tau^i_{\nu.\text{in}} > \tau^j_{\nu.\text{in}}$ and thus $\tilde{f}^>_\mu(t) = -\tilde{f}^<_\mu(t)$ for $t > 0$ and $\tilde{f}^>_\nu(-t) = -\tilde{f}^<_\nu(-t)$ for $t < 0$, hence,

$$-\tilde{f}^<_\mu(t)\tilde{f}^<_\nu(-t) = \theta(t)\tilde{f}^>_\mu(t)\tilde{f}^<_\nu(-t) + \theta(-t)\tilde{f}^<_\mu(t)\tilde{f}^>_\nu(-t),$$

$$\tilde{f}^>_\mu(t)\tilde{f}^<_\nu(-t) + \tilde{f}^<_\mu(t)\tilde{f}^>_\nu(-t) + \tilde{f}^<_\mu(t)\tilde{f}^<_\nu(-t) = \theta(-t)\tilde{f}^>_\mu(t)\tilde{f}^<_\nu(-t) + \theta(t)\tilde{f}^<_\mu(t)\tilde{f}^>_\nu(-t),$$

proving our statement. In the case E it is necessary to drop a constant (albeit infinite) and thus physically irrelevant contribution to the action to obtain (3.12) or (3.13). (See similar discussion after Eq. (3.13))

3.4.5 Saddle-Point Approximation

We prove here the formulas of Sect. 3.3. To keep things readable we resort on a rather symbolic notation, in which the contributions to the exponent in (3.15) read

$$\mathcal{A}_0[\varphi] = \frac{1}{2}\varphi V^{-1}\varphi - \varphi\varrho_0, \quad \mathcal{A}_t[\varphi] = -ie^{-i\Phi(1)}\Pi_{12}e^{i\Phi(2)}, \quad \mathcal{A}_J[\varphi] = -J\varphi$$

with the tunneling phases $\Phi = \mathcal{D}\varphi$ being linear functionals of φ. The saddle-points of $\mathcal{A}_0 + \mathcal{A}_t + \mathcal{A}_J$ and $\mathcal{A}_0 + \mathcal{A}_J$ are denoted φ_{**} and φ_*. We show first that up to the chosen accuracy $\mathcal{O}(\text{tun}^2)$ the former is not needed and calculation of the latter is sufficient, using that $\varphi_* - \varphi_{**} = \mathcal{O}(\text{tun}^2)$. A Gaussian expansion of the full action around φ_{**} reads

$$\left(\mathcal{A}_0 + \mathcal{A}_t + \mathcal{A}_J\right)[\varphi] \approx \left(\mathcal{A}_0 + \mathcal{A}_t + \mathcal{A}_J\right)[\varphi_{**}] + \frac{1}{2}(\varphi - \varphi_{**})\,\delta^2\left(\mathcal{A}_0 + \mathcal{A}_t + \mathcal{A}_J\right)[\varphi_{**}]\,(\varphi - \varphi_{**}). \quad (3.71)$$

Note that the first order term vanishes due to φ_{**} being the full saddle-point. We now successively replace φ_{**} by φ_* in the above expression. Expansion around φ_{**} and using $\delta^2(\mathcal{A}_0 + \mathcal{A}_J)[\varphi_{**}] = V^{-1} = \delta^2(\mathcal{A}_0 + \mathcal{A}_J)[\varphi_*]$ yields

$$\left(\mathcal{A}_0 + \mathcal{A}_t + \mathcal{A}_J\right)[\varphi_*] = \left(\mathcal{A}_0 + \mathcal{A}_t + \mathcal{A}_J\right)[\varphi_{**}] + \mathcal{O}(\text{tun}^4),$$

$$\delta^2(\mathcal{A}_0 + \mathcal{A}_t + \mathcal{A}_J)[\varphi_*] = \delta^2(\mathcal{A}_0 + \mathcal{A}_t + \mathcal{A}_J)[\varphi_{**}] + \mathcal{O}(\text{tun}^4).$$

Writing $\varphi - \varphi_{**} = (\varphi - \varphi_*) + (\varphi_* - \varphi_{**})$ and using again $\varphi_* - \varphi_{**} = \mathcal{O}(\text{tun}^2)$ Eq. (3.71) thus becomes

$$(\mathcal{A}_0 + \mathcal{A}_t + \mathcal{A}_J)[\varphi] \approx (\mathcal{A}_0 + \mathcal{A}_t + \mathcal{A}_J)[\varphi_*] + \frac{1}{2}(\varphi - \varphi_*)\,\delta^2\left(\mathcal{A}_0 + \mathcal{A}_t + \mathcal{A}_J\right)[\varphi_*]\,(\varphi - \varphi_*)$$
$$+ (\varphi_* - \varphi_{**})\,\delta^2(\mathcal{A}_0 + \mathcal{A}_t + \mathcal{A}_J)[\varphi_*]\,(\varphi - \varphi_{**}). \quad (3.72)$$

Only the last term, which is linear in $\varphi - \varphi_*$, contains φ_{**}. To proceed, we define $h \equiv (\varphi_* - \varphi_{**}) \, \delta^2(\mathcal{A}_0 + \mathcal{A}_t + \mathcal{A}_J)[\varphi_*] = \mathcal{O}(\mathrm{tun}^2)$ and perform the functional integration (3.15) in Gaussian approximation (3.72):

$$\int \mathcal{D}\varphi \, e^{i(\mathcal{A}_0 + \mathcal{A}_t + \mathcal{A}_J)[\varphi]} \approx e^{i(\mathcal{A}_0 + \mathcal{A}_t + \mathcal{A}_J)[\varphi_*]} \left(\mathrm{Det} \, \delta^2(\mathcal{A}_0 + \mathcal{A}_t + \mathcal{A}_J)[\varphi_*] \right)^{-1/2}$$

$$\times \exp[-\frac{i}{2} \underbrace{h \, \delta^2(\mathcal{A}_0 + \mathcal{A}_t + \mathcal{A}_J)[\varphi_*] \, h}_{=\mathcal{O}(\mathrm{tun}^4)}]$$

$$= e^{i(\mathcal{A}_0 + \mathcal{A}_J)[\varphi_*]} \exp \left[i\mathcal{A}_t[\varphi_*] - \frac{1}{2} \mathrm{Tr} \, \mathrm{Ln} \left(\mathbb{1} + V \delta^2 \mathcal{A}_t[\varphi_*] \right) \right]. \tag{3.73}$$

Hence, φ_* dropped out completely. The first exponential satisfies $e^{i(\mathcal{A}_0 + \mathcal{A}_J)[\varphi_*]} = \left\langle e^{i\mathcal{A}_J[\varphi]} \right\rangle_0$ where $\langle \ldots \rangle_0$ denotes the average with respect to the free action $\mathcal{A}_0[\varphi]$. This is shown using $\langle \varphi \rangle_0 = \bar{\varphi} \equiv V \varrho_0$ and $\langle (\varphi - \bar{\varphi})(\varphi - \bar{\varphi}) \rangle_0 = iV$. Since $\mathcal{A}_0[\varphi]$ is Gaussian we have the simple relation

$$\left\langle e^{i\mathcal{A}_J[\varphi]} \right\rangle_0 = \left\langle e^{-iJ\varphi} \right\rangle_0 = \exp \left[-iJ\bar{\varphi} - \frac{1}{2} \left\langle \left[J(\varphi - \bar{\varphi}) \right]^2 \right\rangle \right] = e^{-iJ\bar{\varphi} - \frac{i}{2} JVJ}.$$

On the other hand it is $i(\mathcal{A}_0 + \mathcal{A}_J)[\varphi_*] = -\frac{i}{2}(\varrho_0 + J)V(\varrho_0 + J) = -\frac{i}{2}JVJ - iJ\bar{\varphi} - \frac{i}{2}\varrho_0 V \varrho_0$. I.e. up to the last term $-\frac{i}{2}\varrho_0 V \varrho_0$, which is canceled by normalization, we have

$$e^{i(\mathcal{A}_0 + \mathcal{A}_J)[\varphi_*]} = e^{-iJ\bar{\varphi} - \frac{i}{2}JVJ} = \left\langle e^{i\mathcal{A}_J[\varphi]} \right\rangle_0$$

which proves (3.18).

To deal with the second exponential in (3.73) we expand the logarithm to leading order in V (again, a Gaussian expansion),

$$i\mathcal{A}_t[\varphi_*] - \frac{1}{2} \mathrm{Tr} \, \mathrm{Ln} \left(\mathbb{1} + V\delta^2 \mathcal{A}_t[\varphi_*] \right) \approx i\mathcal{A}_t[\varphi_*] - \frac{1}{2} \mathrm{Tr} \, V\delta^2 \mathcal{A}_t[\varphi_*] = i\mathcal{A}_t[\varphi_*] + \underbrace{i \left\langle \delta\mathcal{A}_t[\varphi_*](\varphi - \bar{\varphi}) \right\rangle_0}_{=0}$$

$$+ \frac{i}{2} \left\langle (\varphi - \bar{\varphi})\delta^2 \mathcal{A}_t[\varphi_*](\varphi - \bar{\varphi}) \right\rangle_0 \approx i \left\langle \mathcal{A}_t[\varphi - \bar{\varphi} + \varphi_*] \right\rangle_0.$$

Defining the phases $\bar{\Phi} = \mathcal{D}\bar{\varphi}$, $\Phi_* = \mathcal{D}\varphi_*$ it is

$$\left\langle \mathcal{A}_t[\varphi - \bar{\varphi} + \varphi_*] \right\rangle_0 = -i \left\langle e^{-i[\Phi(1) - \bar{\Phi}(1) + \Phi_*(1)]} \, \Pi_{12} \, e^{i[\Phi(2) - \bar{\Phi}(2) + \Phi_*(2)]} \right\rangle_0 = -ie^{-i\Phi_*(1)} \, \tilde{\Pi}_{12} \, e^{i\Phi_*(2)},$$

i.e. Eq. (3.19), where $\tilde{\Pi}_{12} \equiv e^{i\left(D_\Phi(1,2) - D_\Phi(0,0)\right)}\Pi_{12}$ are the renormalized tunneling polarization operators with the phase-phase correlator

$$D_\Phi(1,2) = -i \left\langle (\Phi(1) - \bar{\Phi}(1))(\Phi(2) - \bar{\Phi}(2)) \right\rangle_0 = - \left(\mathcal{D}V\mathcal{D} \right)(1,2).$$

3.5 Conclusions

In this chapter we developed a framework to study nonequilibrium networks of quantum wires. We combined the Keldysh and functional bosonization formalisms, the latter being more convenient to describe one-dimensional interacting systems than the commonly used standard (operator) bosonization

approach. In this formalism quartic interaction terms are decoupled by a Hubbard-Stratonovich (HS) transformation at the expense of introducing a bosonic field φ, which mediates the interaction. The HS field φ and the fermionic fields can be decoupled by means of a gauge transformation which gives rise to a nontrivial Jacobian. It is a Fredholm determinant and highly reminiscent of the full counting statistics. The bosonic Keldysh action obtained in this way is given by Eq. (3.3).

The dynamics of the electron system, including propagation in external fields and scattering, is encoded in the time-dependent scattering matrix $S[\varphi]$ and we illustrated its construction for the considered network model.

For the limit of weak tunneling we performed the second order expansion of the action, Eq. (3.10), in which every point of tunneling gives rise to contributions similar to the Ambegaokar-Eckern-Schön action[29]. In terms of bosonic excitations they can be interpreted as sites of plasmon production (due to inelastic electron tunneling), responsible for the population of a nonequilibrium plasmon bath in the system. We further presented a saddle-point (real-time instanton) approximation scheme to evaluate physical observables, such as Green's functions and current.

In the following chapters we will apply this formalism to important examples. Chapters 4, 5 deal with a Luttinger liquid and a quantum Hall Fabry-Pérot interferometer with weak backscattering/tunneling and thus are amenable to the developed approximation method. Tunneling in quantum Hall Mach-Zehnder interferometers, as considered in Chapter 6, is, in contrast, not weak. We will however see that under certain assumptions the simpler, chiral structure of the setup allows for an exact treatment.

4

Chapter 4

Tunneling Density of States of a Luttinger Liquid with Single Impurity

Over the last few decades tunneling spectroscopy has become a powerful tool to study interaction effects in mesoscopic systems. The zero bias anomaly, the suppression or enhancement of tunneling conductance at low bias[34, 35], is a key signature of interaction and was observed in various systems such as disordered metals[36, 37], high-mobility two-dimensional electron gases[38], quantum Hall edges[39], and arrays of quantum wires[40].

In Refs. [41–43] tunneling spectroscopy for nonequilibrium nanostructures was developed. By using a superconducting tunneling tip, with sharply peaked density of states, one cannot only measure the tunneling density of states, but as well infer the quasiparticle distribution function. This enables one to study energy relaxation and the underlying inelastic scattering processes.

Of particular interest in this context are one-dimensional systems where interaction leads to the emergence of the strongly correlated Luttinger liquid state. The characteristic power-law suppression of the tunneling conductance was the hallmark for the experimental confirmation of such a state in quantum Hall edges[39] and carbon nanotubes[44–46].

The effects of nonequilibrium on the tunneling density of states have been studied in a range of theoretical works[47–51]. It is known that due to integrability relaxation is absent in a uniform Luttinger liquid, and relaxation induced by inhomogenous interaction[52–57] or disorder[58, 59] was discussed in the literature.

In contrast, a single impurity is not expected to give rise to a complete thermal relaxation. In this chapter we will study the arising state by computing the tunneling density of states of a nonequilibrium quantum wire with a single weak impurity (see Fig. 4.1). Previous studies of this model focused on the nonlinear conductance and shot noise [60–63]. However, the tunnel spectroscopy of this problem, which requires the analysis of the single-particle Green's function, has never been addressed.
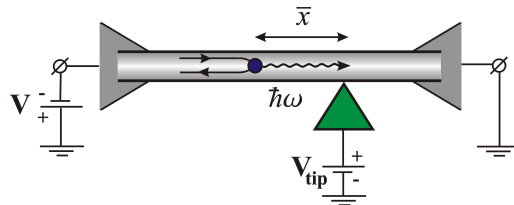

Figure 4.1: *Tunneling experiment with a voltage-biased quantum wire.*

The results and details of the calculation presented here have been published in Refs. [26, 64].

4.1 Model and Results

We apply the formalism developed in Chapter 3. The wire is modeled as a network of two channels: right-(left-) moving electrons, denoted by indices $\mu = +(-)$. Weak backscattering, i.e. tunneling between the two channels, occurs at the impurity (at $x = 0$). It is therefore represented as a point scatterer with reflection amplitude r_0, assumed to be small, $|r_0|^2 \ll 1$. Nonequilibrium is established by biasing the left and right reservoir by voltages $eV_+ = eV > 0$, $eV_- = 0$.

The interplay of interaction, nonequilibrium, and impurity scattering can be studied by placing a conducting tip near position $\bar{x}$ (say $\bar{x} > 0$) of the wire, held at a voltage V_{tip}, and measuring the current I_{tun} between tip and wire. Let us assume that the tip can be described in terms of fermionic quasiparticles with density of states $\nu_{\text{tip}}(\epsilon)$ and distribution function $f_{\text{tip}}(\epsilon)$, as is the case e.g. in the absence of interaction. If coupling $|t|^2$ between tip and wire is weak, a simple perturbative expansion yields the tunneling current

$$I_{\text{tun}} \propto |t|^2 \sum_{\mu=\pm} \int \mathrm{d}\epsilon \left[\Gamma_\mu^>(\epsilon) f_{\text{tip}}(\epsilon) - \Gamma_\mu^<(\epsilon)(1 - f_{\text{tip}}(\epsilon)) \right] \nu_{\text{tip}}(\epsilon).$$

The "rates" for tunneling into/out of the μ-channel of the wire are defined as

$$\Gamma_\mu^{\gtrless}(\epsilon) = \pm \frac{i}{2\pi} G_\mu^{\gtrless}(\bar{x}, \bar{x}, \epsilon). \tag{4.1}$$

Using a metallic tip with constant density of states ν_{tip}, measurement of the differential tunneling conductance in the limit of small temperature gives access to the *tunneling* density of states,

$$\left. \frac{\partial I_{\text{tun}}}{\partial V} \right|_{V_{\text{tip}}=\epsilon} \propto \Gamma_\mu^>(\epsilon) + \Gamma_\mu^<(\epsilon) = \nu_\mu(\epsilon) \equiv -\frac{1}{\pi} \text{Im} \, G_\mu^r(\bar{x}, \bar{x}, \epsilon). \tag{4.2}$$

If interaction is absent in the wire the rates simplify to $\Gamma_\mu^{\gtrless}(\epsilon) = f_\mu^{\gtrless}(\epsilon) \nu_\mu(\epsilon)$ with distribution functions $f_\mu(\epsilon) = f_\mu^<(\epsilon)$, $f_\mu^>(\epsilon) \equiv 1 - f_\mu(\epsilon)$, and density of states $\nu_\mu(\epsilon)$ of the channel μ.

We devote this chapter to the calculation of the rates for tunneling into a spinless Luttinger liquid. We consider point-like repulsive interaction, assuming for simplicity $g_2 = g_4 = V_0$ such that the interaction potential $U_{\mu\nu}(x, x') = V_0 \delta(x - x')$ does not discriminate between different channels. Interaction strength in the LL model is then characterized by the Luttinger constant $K = (1 + V_0/\pi v_F)^{-1/2}$, cf. (2.6). The free electron spectrum is linearized around the Fermi points, arising ultraviolet divergencies require the introduction of a high-energy cutoff $\Lambda \sim E_F$, which mimicks a finite bandwidth in the wire. In the absence of backscattering the tunneling rates exhibit the well-known zero bias anomaly, i.e. a power-law suppression near the Fermi edges,

$$\Gamma_\mu^{\gtrless}(\epsilon) = \frac{\nu_0}{\pi} \Gamma(1 + 2\gamma)^{-1} \times \theta(\pm(\epsilon - eV_\mu)) \left| \frac{\epsilon - eV_\mu}{\Lambda} \right|^{2\gamma} \quad \text{with exponent } \gamma = \frac{(1-K)^2}{4K} \tag{4.3}$$

where we have introduced the noninteracting density of states $\nu_0 = (2\pi v_F)^{-1}$.

As is shown in this chapter the tunneling rates change considerably upon including the impurity. For $eV > 0$ the rates are given by

$$\Gamma_\mu^{\gtrless}(\epsilon) = \pm\frac{\nu_0}{\pi}\left(\frac{eV}{\Lambda}\right)^{2\gamma}\Gamma(-2\gamma)\,\mathrm{Im}\,\left[(\mp z_\mu)^{2\gamma} + \mathcal{C}_\mu R_*(eV)(\pm 1)^{2\gamma}\Psi(-2\gamma, 1 - 2\gamma + 2\,\delta_\mu, -z_\mu)\right] \quad (4.4)$$

where we have used

$$\mathcal{C}_\pm = \frac{\Gamma(2K)}{\Gamma\left(1/2 \pm K/2\right)^2}, \quad \delta_+ = (1 - K)/2, \quad \delta_- = 1/2 - K, \quad z_\mu = (\epsilon - eV_\mu + \frac{i}{2}\tau_\varphi^{-1})/eV, \quad (4.5)$$

and $\Psi(a, b, c)$ is the confluent hypergeometric function[65]. We have also introduced the renormalized reflection coefficient

$$R_*(eV) = \frac{|r_0|^2}{\Gamma(2K)}\left|\frac{\Lambda}{eV}\right|^{2(1-K)} \quad (4.6)$$

and the nonequilibrium dephasing rate

$$\tau_\varphi^{-1} \equiv R_*(eV)\frac{2\sin^2 \pi\delta_+}{\pi}|eV|. \quad (4.7)$$

The energy dependence of the rates $\Gamma_\pm^{\gtrless}(\epsilon)$ is shown in Fig. 4.2. The main feature of these plots is that
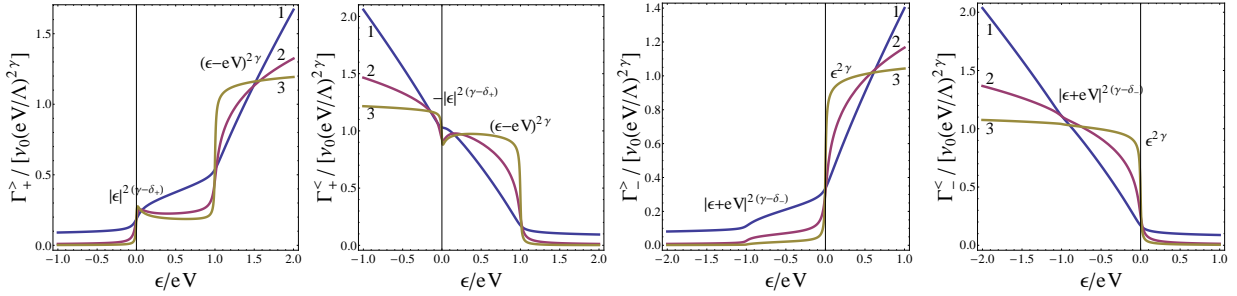

Figure 4.2: *Tunneling rates for right- and left-movers with different interaction strengths: $K = 0.4$ (1), $K = 0.4$ (2), and $K = 0.75$ (3). The Fermi edge for right-(left-) movers is at $eV_+ = eV$ ($eV_- = 0$).*

the tunneling rates have split power-law singularities which are characterized by different exponents and are smeared by the nonequilibrium dephasing rate $1/\tau_\varphi$. The main edges are located at corresponding chemical potentials – at $\epsilon = eV_\pm$ in the case of right-/left-moving states, respectively – having the equilibrium exponents γ. The formation of the second (side) edge due to scattering off the impurity occurs at $\epsilon = e(V_\pm - V)$. If the interaction is repulsive ($K < 1$) then the corresponding exponent $2(\gamma - \delta_-)$ for left-moving electrons is always positive, hence the correction at the side edge $\epsilon = -eV$ is smooth. For right-movers in the case of not too strong interaction, $K > 1/3$, the nonequilibrium exponent $2(\gamma - \delta_+)$ is negative, yielding a resonance in tunneling at the side edge $\epsilon = 0$.

The presence of side edges in the tunneling rates can be understood in the following way. Inelastic electron backscattering at the impurity at point $x = 0$ induces the emission of *real* nonequilibrium plasmons with typical frequencies $\omega \leq eV$, which in the non-dissipative LL can propagate to the

distant point of tunneling $\bar{x}$. Consequently, inelastic tunneling with absorption or stimulated emission of these real plasmons becomes possible. For example, an electron tunneling into a right-/left-moving state of the LL with the energy $\epsilon < eV_\pm$ can accommodate itself above the corresponding Fermi energy $(eV_\pm)$ by picking up the energy $\omega > eV_\pm - \epsilon$ from the nonequilibrium plasmon bath. Since the energy of out-of-equilibrium plasmons is limited by the applied voltage, we observe a threshold at $\epsilon \sim e(V_\pm - V)$, which exhibits a power-law singularity typical of the LL. The singularity at the side edge of the out-tunneling rate describes the inverse process — inelastic tunneling from the LL accompanied by the stimulated emission of nonequilibrium plasmons with typical energy $\omega \lesssim eV$. This side edge is pronounced in the case of right-moving states only, $\Gamma_+^<(\epsilon)$, and is not seen for the left-moving states, $\Gamma_-^<(\epsilon)$, since the associated exponent $2(\gamma - \delta_-)$ is always positive in the latter case.

4.2 Calculations

4.2.1 Action

Since interaction does not discriminate between channels $\mu, \nu = \pm$ it can be decoupled by a Hubbard-Stratonovich transformation introducing a single field φ, i.e. $\varphi_+ = \varphi_- = \varphi$. For weak backscattering, i.e. weak tunneling between right- and left-moving states at the impurity, the action $\mathcal{A}[\varphi] = \mathcal{A}_0[\varphi] + \mathcal{A}_t[\varphi]$ is obtained according to Sect. 3.2. The free action (3.2) is

$$\mathcal{A}_0[\varphi] = \frac{1}{2}\int_\mathcal{C} \mathrm{d}\xi \, \mathrm{d}\xi' \, \varphi(\xi)V^{-1}(\xi - \xi')\varphi(\xi') - \int_\mathcal{C} \mathrm{d}\xi \, \left(\varrho_{0+} + \varrho_{0-}\right)\varphi(\xi)$$

with $\xi = (x,t)$, non-local effective interaction $V^{-1}(\xi - \xi') = V_0^{-1}\delta(\xi - \xi') - \Pi(\xi - \xi')$, (summed) polarization operator $\Pi(\xi) = \Pi_+(\xi) + \Pi_-(\xi)$ and mean charge density $\varrho_{0\eta} = eV_\eta/(2\pi|v_\eta|)$. Using (2.23) we obtain for the retarded/advanced components of the effective interaction

$$V^{r/a}(\omega, p) = V_0\frac{\omega^2 - v_F^2 p^2}{\omega_\pm^2 - u^2 p^2} \tag{4.8}$$

with the plasmon velocity $u = v_F/K > v_F$.

   Since we are dealing with one scatterer, characterized by a scattering matrix s^1 with $r_0 = s_{+-}^1$, the tunneling or backscattering action $\mathcal{A}_t$, as given by (3.10), consists of one term (corresponding to class $(11; +-)$):

$$\mathcal{A}_t[\varphi] = -i\int \mathrm{d}t_1 \mathrm{d}t_2 \left(e^{-i\Phi^f(t_1)} \quad e^{-i\Phi^b(t_1)}\right)\begin{pmatrix} \Pi_{+-}^T & -\Pi_{+-}^< \\ -\Pi_{+-}^> & \Pi_{+-}^{\tilde{T}} \end{pmatrix}_{t_1 - t_2}\begin{pmatrix} e^{i\Phi^f(t_2)} \\ e^{i\Phi^b(t_2)} \end{pmatrix}, \tag{4.9}$$

where $\Phi^{f/b}(t) = \Theta_-^{f/b}(0,t) - \Theta_+^{f/b}(0,t)$ is the tunneling phase evaluated at the impurity, $x = 0$. The phases are related to the Hubbard-Stratonovich field φ according to (2.16). The tunneling polarization operator $\Pi_{+-} = \Pi_{11;+-}$ is given by (3.11), (3.13). Writing $|r_0|^2 = |s_{+-}^1|^2 = |s_{-+}^1|^2$, its components read

$$\Pi_{+-}^\gtrless(t) = -|r_0|^2 f_+^\gtrless(t) f_-^\lessgtr(-t) = -|r_0|^2 e^{-ieVt}\left[f_0^\gtrless(t)\right]^2, \tag{4.10}$$

$$\Pi_{+-}^{T/\tilde{T}}(t) = \frac{1}{2}\left[\Pi_{+-}^>(t) + \Pi_{+-}^<(t)\right]. \tag{4.11}$$

4.2.2 Green's Functions in Instanton Approximation

To find the tunneling rates we represent the electron Green's function at the point $\bar{x} > 0$ of tunneling as a path integral over the field φ,

$$G_\mu^{\gtrless}(\bar{x}, \bar{x}; \bar{t}) = \int \mathcal{D}\varphi \, e^{i\mathcal{A}[\varphi]} e^{i\Theta_\mu^{b/f}(\bar{x}\bar{t})} G_\mu^{\gtrless}(\bar{x}, \bar{x}; \bar{t}; [\varphi]) e^{-i\Theta_\mu^{f/b}(\bar{x},0)}.$$

Here, $G_\mu(\bar{x}, \bar{x}; \bar{t}, [\varphi])$ denotes the Green's function for a given configuration of φ. It satisfies the Dyson equation with the spatially local self-energy

$$\Sigma_\mu[\varphi](x, x'; t, t') = i\delta(x)\delta(x')(|r_0|^2 v_F/2) e^{i\mu\Phi(t)} g_{-\mu}(t - t') e^{-i\mu\Phi(t')}$$

where g_μ are the source reservoirs' quasiclassical Green's functions.

We solve the Dyson equation in first order in $|r_0|^2$:

$$G_\mu^{\alpha\beta}(\bar{x}, \bar{x}; \bar{t}) = \mathcal{G}_{0\mu}^{\alpha\beta} + \mathcal{G}_{1\mu}^{\alpha\beta} \quad \text{with} \tag{4.12}$$

$$\mathcal{G}_{0\mu}^{\alpha\beta} = \left\langle e^{i\Theta_\mu^\alpha(\bar{x}, \bar{t})} G_{0\mu}^{\alpha\beta}(\bar{x}, \bar{x}; \bar{t}) e^{-i\Theta_\mu^\beta(\bar{x},0)} \right\rangle,$$

$$\mathcal{G}_{1\mu}^{\alpha\beta} = i\frac{|r_0|^2 v_F}{2} \sum_{\gamma,\delta=f,b} \sigma_{\gamma\delta} \int dt_1\, dt_2 \left\langle e^{i\Theta_\mu^\alpha(\bar{x}, \bar{t})} G_{0\mu}^{\alpha\gamma}(\bar{x}, 0; \bar{t} - t_1) \right.$$

$$\left. \times e^{i\mu\Phi^\gamma(t_1)} g_{-\mu}^{\gamma\delta}(t_1 - t_2) e^{-i\mu\Phi^\delta(t_2)} G_{0\mu}^{\delta\beta}(0, \bar{x}; t_2) e^{-i\Theta_\mu^\beta(\bar{x},0)} \right\rangle$$

where $\sigma_{ff} = \sigma_{bb} = 1$, $\sigma_{fb} = \sigma_{bf} = -1$ and $G_{0\mu}^{\alpha\beta}$ are the Green's functions of free electrons, for instance

$$G_{0\mu}^{\gtrless}(x, t) = \pm f_\mu^{\gtrless}(t - \mu x/v_F)/iv_F. \tag{4.13}$$

All averages $\langle \ldots \rangle$ in Eq.(4.12) are taken with respect to the action $\mathcal{A}_0[\varphi] + \mathcal{A}_t[\varphi]$. They are of the form (3.15) and can be evaluated with the real-time instanton method described in Sect. 3.3. In this approximation the first term reads

$$\mathcal{G}_{0\mu}^{\alpha\beta} \approx e^{i\tilde{\mathcal{A}}_t[\varphi_{*0}]} \times \left\langle e^{i\Theta_\mu^{b/f}(\bar{x}, \bar{t})} G_{0\mu}^{\gtrless}(\bar{x}, \bar{x}; \bar{t}) e^{-i\Theta_\mu^{f/b}(\bar{x},0)} \right\rangle_0. \tag{4.14}$$

The second factor here is the full Green's function of a *clean* LL,

$$\tilde{G}_{0\mu}^{\gtrless}(\bar{x}, \bar{x}; \bar{t}) = e^{-\frac{1}{2}\left\langle \left[\Theta_\mu^{b/f}(\bar{x},\bar{t}) - \Theta_\mu^{f/b}(\bar{x},0)\right]^2 \right\rangle_0} \, G_{0\mu}^{\gtrless}(\bar{x}, \bar{x}; \bar{t}) = \pm \frac{a^{2\gamma}}{2\pi i v_F} e^{-ieV_\mu\bar{t}} \frac{1}{(a \pm i\bar{t})^{2\gamma+1}}. \tag{4.15}$$

The first factor in Eq. (4.14) gives dephasing corrections due to the interplay of tunneling and interaction. The instanton action $\tilde{\mathcal{A}}_t[\varphi_{*0}]$ is defined in (3.19) and obtained by substituting the dressed polarization operators into (4.9). The instanton phase Φ_* is generated by the source $\mathcal{A}_J[\varphi] = i\Theta_\mu^\alpha(\bar{x}, \bar{t}) - i\Theta_\mu^\beta(\bar{x}, 0)$,

$$\Phi_*^\gamma(t) = \left\langle \Phi^\gamma(t) \right\rangle_0 - D_{\Phi\Theta\mu}^{\gamma\alpha}(t - \bar{t}, -\bar{x}) + D_{\Phi\Theta\mu}^{\gamma\beta}(t, -\bar{x}), \quad \gamma = f, b, \tag{4.16}$$

with $iD_{\Phi\Theta\mu}^{\gamma\delta}(t,x) \equiv \left\langle \delta\Phi^\gamma(t,x)\delta\Theta_\mu^\delta(0,0) \right\rangle_0$, and depends on Keldysh indices α, β, direction μ of the tunneling electron, and time and position of tunneling $\bar{t}, \bar{x}$. Since the average value $\left\langle \Phi^\gamma(t) \right\rangle_0$, generated by the mean density $\varrho_{0\eta}$, does not depend on the Keldysh index γ and the time t it will drop out when the instanton phase is substituted into (4.9). Therefore it will be omitted in what follows.

The correlators $iD_{\Theta,\eta\nu}^{\alpha\beta}(t,x) = \left\langle \delta\Theta_\eta^\alpha(t,x)\delta\Theta_\nu^\beta(0,0) \right\rangle$ have been calculated in the introductory Section 2.2 on functional bosonization and the results are summarized in the Eqs. (2.34), (2.35) and (2.31). For the mixed phase-phase correlators they imply

$$iD_{\Phi\Theta\mu}^{\alpha\beta}(t,x) \equiv \left\langle \Phi^\alpha(t,x)\Theta_\mu^\beta(0,0) \right\rangle = i\left[D_{\Theta,-\mu}^{\alpha\beta}(t,x) - D_{\Theta,+\mu}^{\alpha\beta}(t,x) \right] \tag{4.17}$$

$$= -\mu\left[p\,\mathcal{L}_{\mu u}^{\alpha\beta}(t,x) - q\,\mathcal{L}_{-\mu u}^{\alpha\beta}(t,x) - \mathcal{L}_{\mu v_F}^{\alpha\beta}(t,x) \right] \tag{4.18}$$

and for those of the tunneling phases

$$iD_\Phi^{\alpha\beta}(t) = i\lim_{x\to 0}\left[D_{\Phi-}^{\alpha\beta}(t,x) - D_{\Phi+}^{\alpha\beta}(t,x) \right] = -2(1-K)\mathcal{L}_\Phi^{\alpha\beta}(t)$$

$$\text{with } \mathcal{L}_\Phi^{\gtrless}(t) = \ln\frac{\mp ia}{t\mp ia}, \quad \mathcal{L}_\Phi^{T/\tilde{T}}(t) = \frac{1}{2}\left[\ln\frac{-ia}{t-ia} + \ln\frac{ia}{t+ia} \right].$$

4.2.3 Instanton Action

With the above correlators we can evaluate the instanton action. First, we obtain for the "dressed" tunneling polarization operators (3.20)

$$\tilde{\Pi}_{+-}^{\gtrless}(t) = -|r_0|^2\frac{1}{(2\pi a)^2}e^{-ieVt}\left(\frac{a}{a\pm it} \right)^{2K}, \tag{4.19}$$

or in the frequency representation

$$\tilde{\Pi}_{+-}^{\gtrless}(\omega) = -\frac{R_*(eV)}{2\pi}\theta(\pm(\omega - eV))\left| \frac{\omega - eV}{eV} \right|^{2K-1}|eV|$$

where we used definition (4.6) for the renormalized reflection coefficient R_*. With the mixed phase-phase correlation function (4.17) at hand we are also in the position to write down the instanton trajectories (4.16),

$$i\Phi_*^{f/b}(t) = \mu\left\{ p\ln\left[\frac{t\pm ia + \mu\bar{x}/u}{t\pm ia - \bar{t} + \mu\bar{x}/u} \right] - q\ln\left[\frac{a - i\beta(t-\mu\bar{x}/u)}{a - i\alpha(t-\bar{t}-\mu\bar{x}/u)} \right] - \ln\left[\frac{t\pm ia + \mu\bar{x}/v_F}{t\pm ia - \bar{t} + \mu\bar{x}/v_F} \right] \right\}$$

for $\mu\bar{x} > 0$, and

$$i\Phi_*^{f/b}(t) = \mu\left\{ p\ln\left[\frac{a - i\beta(t+\mu\bar{x}/u)}{a - i\alpha(t-\bar{t}+\mu\bar{x}/u)} \right] - q\ln\left[\frac{t\pm ia - \mu\bar{x}/u}{t\pm ia - \bar{t} - \mu\bar{x}/u} \right] - \ln\left[\frac{a - i\beta(t+\mu\bar{x}/v_F)}{a - i\alpha(t-\bar{t}+\mu\bar{x}/v_F)} \right] \right\}$$

for $\mu\bar{x} < 0$, where we have introduced $p = (1+K)/2$ and $q = (1-K)/2$. These instantons are non-classical (or "quantum") solutions in the sense of the Keldysh nonequilibrium theory – the phases

$\Phi_*(t)$ are in fact different on the forward and backward branches of the Keldysh time contour, so that the quantum component is $\Phi_*^q(t) \neq 0$. Because of that the corresponding tunneling action $\tilde{\mathcal{A}}_t[\varphi_*]$, which we are going to evaluate, is non-zero.

Let us consider the case of tunneling into/out of a right-moving state with the tip being placed on the right from the impurity, $\mu = +$ and $\bar{x} > 0$, to exemplify how we evaluate the instanton action $\tilde{\mathcal{A}}_t[\varphi_*]$. The phase factor is

$$e^{i\Phi_*^{f/b}(t)} = \kappa_+^{f/b}(t)\kappa_-^{f/b}(t)\kappa_0^{f/b}(t) \tag{4.20}$$

with

$$\kappa_+^{f/b}(t) = \left(\frac{t \pm ia + \bar{x}/u}{t \pm ia - \bar{t} + \bar{x}/u}\right)^p, \quad \kappa_-^{f/b}(t) = \left(\frac{a - i\alpha(t - \bar{t} - \bar{x}/u)}{a - i\beta(t - \bar{x}/u)}\right)^q, \quad \kappa_0^{f/b}(t) = \left(\frac{t \pm ia - \bar{t} + \bar{x}/v_F}{t \pm ia + \bar{x}/v_F}\right). \tag{4.21}$$

The instanton action reads

$$i\tilde{\mathcal{A}}_t[\varphi_*] = \sum_{\zeta,\eta=f,b} \sigma_{\zeta\eta} \int dt_3 dt_4 \, \tilde{\Pi}_{+-}^{\zeta\eta}(t_3 - t_4) \, \mathcal{K}_+^{\zeta\eta}(t_3, t_4) \, \mathcal{K}_-^{\zeta\eta}(t_3, t_4) \, \mathcal{K}_0^{\zeta\eta}(t_3, t_4) \tag{4.22}$$

$$\text{with } \mathcal{K}_\sigma^{\zeta\eta}(t_3, t_4) = \kappa_\sigma^\zeta(t_3)^{-1}\kappa_\sigma^\eta(t_4) \quad \text{for } \sigma = +, -, 0.$$

Since the polarization factor $\tilde{\Pi}_{+-}(t_3 - t_4)$ comes with the factor $e^{-ieV(t_3-t_4)}$ the integral is dominated by the region $|t_3 - t_4| \lesssim |eV|^{-1}$. On the other hand, one may expect it to be dominated by the singularities of the phase factors as well; i.e. $t_3, t_4 \sim -\bar{x}/u, \bar{t} - \bar{x}/u$ for $\mathcal{K}_+$, $t_3, t_4 \sim \bar{x}/u, \bar{t} + \bar{x}/u$ for $\mathcal{K}_-$, and $t_3, t_4 \sim -\bar{x}/v_F, \bar{t} - \bar{x}/v_F$ for $\mathcal{K}_0$. These regions in the $t_3 - t_4$-planes are sketched in Fig. 4.3. To proceed we assume that they are well separated which imposes the condition
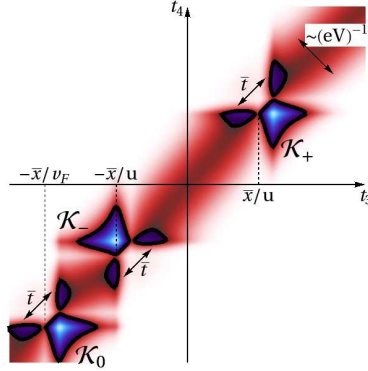

Figure 4.3: *Regions of dominance in $t_3 - t_4$-plane.*

$$|\bar{t}|, |eV|^{-1} \ll (1 - K)|\bar{x}|/v_F. \tag{4.23}$$

As it turns out the dephasing time τ_φ which defines the relevant times $\bar{t} \lesssim \tau_\varphi$ is $\sim |eV|^{-1}$, so that the above condition reduces to $|eV|^{-1} \ll (1 - K)|\bar{x}|/v_F$ which can be easily satisfied for sufficiently large voltage and tip-to-impurity distance.

Far from their singularities the phase factors become trivial, $\mathcal{K}_\sigma(t_3, t_4) \to 1$, and the integral (4.22)

approximately splits into

$$i\tilde{\mathcal{A}}_t[\varphi_*] \approx \mathcal{I}[\mathcal{K}_+] + \mathcal{I}[\mathcal{K}_-] + \mathcal{I}[\mathcal{K}_0]$$

$$\text{with } \mathcal{I}[\mathcal{K}_\sigma] = \sum_{\zeta,\eta=f,b} \sigma_{\zeta\eta} \int dt_3 dt_4 \, \tilde{\Pi}^{\zeta\eta}_{+-}(t_3-t_4) \left(\mathcal{K}^{\zeta\eta}_\sigma(t_3,t_4) - 1 \right).$$

We added -1 to the phase factor $\mathcal{K}_\sigma$ to make the integral manifestly convergent. "Manifestly" because convergence is already ensured by the relation $\sum_{\zeta\eta} \sigma_{\zeta\eta} \tilde{\Pi}^{\zeta\eta}_{+-}(t) = 0$. For the very same reason, the independence of $\mathcal{K}^{\zeta\eta}_-(t_3,t_4)$ of the Keldysh indices ζ, η implies $\mathcal{I}[\mathcal{K}_-] = 0$.

This is in contrast to $\mathcal{K}_+$, $\mathcal{K}_0$ which according to (4.21) have the form $\mathcal{K}^{\zeta\eta}(t_3,t_4) \equiv \kappa^\zeta(t_3)^{-1}\kappa^\eta(t_4)$ with $\kappa^{f/b}(t) = \left(\frac{t-t_a \pm ia}{t-t_b \pm ia} \right)^r$ and some exponent $r > 0$. For such phase factors $\mathcal{I}[\mathcal{K}]$ is dominated by the 2 regions $|t_3 - t_4| \lesssim |eV|^{-1}$ (singularity of $\tilde{\Pi}_{+-}$) and $|t_3 - t_a|, |t_4 - t_b| \lesssim |eV|^{-1}$ (singularity of $\mathcal{K}$) which determine the long-time asymptotics $|eV\bar{t}| \gg 1$. Keeping this observation in mind, we proceed by using the following approximation

$$\mathcal{I}[\mathcal{K}] \approx \int dt \sum_{\zeta\eta} \sigma_{\zeta\eta} \tilde{\Pi}_{+-}(t) \int dT \left(\kappa^\zeta(T)^{-1}\kappa^\eta(T) - 1 \right)$$

$$+ \sum_{\zeta\eta} \zeta\eta \, \tilde{\Pi}^{\zeta\eta}_{+-}(t_a - t_b) \Big|_{eV=0} \int dt_3 \, e^{-ieVt_3}\kappa^\zeta(t_3)^{-1} \int dt_4 \, e^{ieVt_4}\kappa^\eta(t_4)$$

$$\approx - R_*(eV) \left\{ \frac{|eV(t_b - t_a)|}{2\pi} \left(1 - e^{-2\pi i r \, \text{sign}[eV(t_b-t_a)]} \right) - \frac{\Gamma(2K)}{\Gamma(r)^2} e^{ieV(t_b-t_a)} \left[ieV(t_b - t_a) \right]^{2(r-K)} \right\}.$$

$$(4.24)$$

Considering right-movers $\mu = +$ and $\bar{x} > 0$ we thus obtain for the instanton action $i\tilde{\mathcal{A}}_t[\varphi_*] = \mathcal{I}[\mathcal{K}_+] + \mathcal{I}[\mathcal{K}_0]$. The first term,

$$\mathcal{I}[\mathcal{K}_+] = -\frac{|\bar{t}|}{2\tau_\varphi} - iR_*(eV) \frac{\sin 2\pi p}{2\pi} eV\bar{t} + \mathcal{C}_+ R_*(eV) e^{ieV\bar{t}}[ieV\bar{t}]^{2q}, \quad \mathcal{C}_+ = \Gamma(2K)/\Gamma(p)^2, \quad (4.25)$$

encodes effects of real plasmons on tunneling which are generated because of backscattering off the impurity. One of these effects is shot noise, which is represented by the first term in (4.25). This term is negative and linear in time $\bar{t}$ and thus accounts for dephasing with rate (4.7). The second term represents a perturbatively small renormalization of bias voltage and will be neglected in the following. The third term in (4.25) is subleading as compared to the first one and we will treat it perturbatively in R_*. It shows oscillatory behavior, accounting for the energy transfer $\sim eV$ between the nonequilibrium bath of plasmons and the tunneling electron. This point becomes more transparent and we refer the reader to the discussion of the tunneling rates $\Gamma^{\lessgtr}_\mu(\epsilon)$ in the end of Sect. 4.1.

We turn now to the contribution $\mathcal{I}[\mathcal{K}_0]$. In this case $r = 1$, so that the first term in (4.24) vanishes. Thus, the electron-hole pair contribution reads

$$\mathcal{I}[\mathcal{K}_0] = \sum_{\zeta\eta} \zeta\eta \, \tilde{\Pi}^{\zeta\eta}_{+-}(\bar{t}) \Big|_{eV=0} \int dt_3 \, e^{-ieVt_3}\kappa^\zeta_0(t_3)^{-1} \int dt_4 \, e^{ieVt_4}\kappa^\eta_0(t_4) \qquad (4.26)$$

$$= R_*(eV)\Gamma(2K)e^{-ieV\bar{t}} \left[-ieV\bar{t} \right]^{2(1-K)}. \qquad (4.27)$$

It is oscillatory and can be again treated perturbatively. In contrast to the plasmon contribution, however, it seemingly suggests an energy content of $\sim -eV$ and does not have a clear physical interpretation. We will see below that this term is an artefact of functional bosonization which will be canceled by the Born correction $\mathcal{G}_{1\mu}^{\alpha\beta}$. In total, we have

$$e^{i\tilde{\mathcal{A}}_t[\varphi_*]} \approx e^{-|\bar{t}|/2\tau_\varphi} \left(1 + \mathcal{C}_+ R_*(eV) \, e^{ieV\bar{t}} \left[ieV\bar{t} \right]^{2q} + \mathcal{I}[\mathcal{K}_0] \right) \quad \text{for } \bar{x} > 0, \, \mu = +. \qquad (4.28)$$

The same considerations can be applied to left-movers and one obtains

$$e^{i\tilde{\mathcal{A}}_t[\varphi_*]} \approx e^{-|\bar{t}|/2\tau_\varphi} \left(1 \, + \, \mathcal{C}_- R_*(eV) e^{ieV\bar{t}} [ieV\bar{t}]^{1-2K} \right), \quad \mathcal{C}_- = \Gamma(2K)/\Gamma(q)^2, \quad \text{for } \bar{x} > 0, \, \mu = -. \tag{4.29}$$

4.2.4 Born Correction

We evaluate the Born correction $\mathcal{G}_{1\mu}^{\alpha\beta}$ to the Green's function, (4.12), in leading order in $|r_0|^2$, which amounts to taking averages with respect to the clean action $\mathcal{A}_0[\varphi]$ only. Then Wick's theorem yields

$$\mathcal{G}_{1\mu}^{\alpha\beta} \approx i \frac{|r_0|^2 v_F}{2} \sum_{\gamma,\delta=f,b} \sigma_{\gamma\delta} \int \! dt_1 \, dt_2 \, G_{0\mu}^{\alpha\gamma}(\bar{x}, 0; \bar{t} - t_1) g_{-\mu}^{\gamma\delta}(t_1 - t_2) G_{0\mu}^{\delta\beta}(0, \bar{x}; t_2) \, \mathcal{J}_\mu^{\alpha\beta\gamma\delta}(\bar{x}, \bar{t}; t_1, t_2) \quad (4.30)$$

with

$$\begin{aligned}
\mathcal{J}_\mu^{\alpha\beta\gamma\delta}(\bar{x}, \bar{t}; t_1, t_2) &= \left\langle e^{i\Theta_\mu^\alpha(\bar{x},\bar{t})} e^{i\mu\Phi^\gamma(t_1)} e^{-i\mu\Phi^\delta(t_2)} e^{-i\Theta_\mu^\beta(\bar{x},0)} \right\rangle_0 \\
&= e^{-\frac{1}{2}\left\langle \left[\Theta_\mu^\alpha(\bar{x},\bar{t}) - \Theta_\mu^\beta(\bar{x},0)\right]^2 \right\rangle_0 - \frac{1}{2}\left\langle \left[\Phi^\gamma(t_1) - \Phi^\delta(t_2)\right]^2 \right\rangle_0} e^{i\mu\left(\Phi_*^\gamma(t_1) - \Phi_*^\delta(t_2)\right)} \quad (4.31)
\end{aligned}$$

and the instanton (4.16). The appearence of the instanton makes the integral (4.30) quite similar to the instanton action and we will use analogous approximations to deal with the time integrals.

We have already seen that the instanton phase factor factorizes into three contributions (4.20) – two governed by plasmons and one by electron-hole pair – and one might expect the integral (4.30) to split into three contributions in a way akin to the instanton action. However, it will turn out that the presence of the bare Green's functions $G_{0\mu}^{\alpha\gamma}(\bar{x}, 0; \bar{t} - t_1)$ and $G_{0\mu}^{\delta\beta}(0, \bar{x}; t_2)$ suppresses the plasmon contributions. Focusing again on $\mu = +$, $\bar{x} > 0$, we show that the remaining electron-hole pair term cancels $\mathcal{I}[\mathcal{K}_0]$ in (4.28).

The t_1, t_2-dependent contributions to (4.30) are

$$\begin{aligned}
&G_{0+}^{\alpha\gamma}(\bar{x}, 0; \bar{t} - t_1) g_-^{\gamma\delta}(t_1 - t_2) G_{0+}^{\delta\beta}(0, \bar{x}; t_2) e^{-\frac{1}{2}\left\langle \left[\Phi^\gamma(t_1) - \Phi^\delta(t_2)\right]^2 \right\rangle_0} e^{i\Phi_*^\gamma(t_1) - i\Phi_*^\delta(t_2)} \\
&\quad = e^{-ieV\bar{t}} e^{ieV(t_1 - t_2)} \times \tilde{g}_-^{\gamma\delta}(t_1 - t_2) \times \tilde{\kappa}_0^\delta(t_2)^{-1} \kappa_+^\delta(t_2)^{-1} \kappa_-^\delta(t_2)^{-1} \times \tilde{\kappa}_0^\gamma(t_1) \kappa_+^\gamma(t_1) \kappa_-^\gamma(t_1).
\end{aligned}$$

We combined terms with similar pole structure, defining

$$\tilde{g}_-^{\gamma\delta}(t_1 - t_2) \equiv e^{-\frac{1}{2}\left\langle \left[\Phi^\delta(t_2) - \Phi^\gamma(t_1)\right]^2 \right\rangle_0} g_-^{\gamma\delta}(t_1 - t_2) \bigg|_{eV=0},$$

$$\tilde{\kappa}_0^\delta(t_2)^{-1} \equiv G_{0+}^{\delta\beta}(-\bar{x}, t_2) \bigg|_{eV=0} \kappa_0^\delta(t_2)^{-1},$$

$$\tilde{\kappa}_0^\gamma(t_1) \equiv G_{0+}^{\alpha\gamma}(\bar{x}, \bar{t} - t_1) \bigg|_{eV=0} \kappa_0^\gamma(t_1).$$

Any voltage-dependence has been singled out in the phase factors explicitly.

Let us examine the pole structure: $\tilde{g}_-^{\gamma\delta}(t_1 - t_2)$ is divergent for $t_1 \approx t_2$. This is reminiscent of $\tilde{\Pi}_{+-}(t_3-t_4)$ in (4.22) which preferred $t_3 \approx t_4$. The plasmon contributions κ_+ and κ_- have been studied in the previous section where we already noted $\kappa_\pm(t) \to 1$ for t far from their singularities. This is not longer true for $\tilde{\kappa}_0$: Leaving the Keldysh indices and the corresponding short-time regularizations aside for a moment we have

$$G_{0+}(x,t)\Big|_{eV=0} = -\frac{1}{2\pi v_F}\frac{1}{t - x/v_F} \quad \text{and} \quad \kappa_0(t) = \frac{t - \bar{t} + \bar{x}/v_F}{t + \bar{x}/v_F},$$

hence,

$$\tilde{\kappa}_0^\delta(t_2)^{-1} \sim -\frac{1}{2\pi v_F}\frac{1}{t_2 - \bar{t} + \bar{x}/v_F}, \quad \tilde{\kappa}_0^\gamma(t_1) \sim \frac{1}{2\pi v_F}\frac{1}{t_1 + \bar{x}/v_F}.$$

Similarly to the original phase factors $\kappa_0^\delta(t_2)^{-1}$, $\kappa_0^\delta(t_1)$ these new ones have the poles $t_1 \sim -\bar{x}/v_F$, $t_2 \sim \bar{t} - \bar{x}/v_F$; however differently from $\kappa_0^\delta(t_2)^{-1}$, $\kappa_0^\delta(t_1)$, the phase factors $\tilde{\kappa}_0^\delta(t_2)^{-1}$, $\tilde{\kappa}_0^\delta(t_1)$ vanish far from these poles instead of converging to 1! Their poles are hence dominating the integral (4.30), while the plasmonic poles give subleading contributions (suppressed by the factor $v_F\bar{t}/(1 - K)\bar{x} \ll 1$). With only leading terms taken into account the integrals simplifies to

$$\mathcal{G}_{1+}^{\alpha\beta} \approx i\frac{|r_0|^2 v_F}{2}e^{-\frac{1}{2}\langle[\Theta_\mu^\alpha(\bar{x},\bar{t})-\Theta_\mu^\beta(\bar{x},0)]^2\rangle}$$
$$\sum_{\gamma,\delta=f,b} \sigma_{\gamma\delta} \; e^{-\frac{1}{2}\langle[\Phi^\delta(\bar{t})-\Phi^\gamma(0)]^2\rangle}\left[G_{0+}^{\alpha\gamma}(\bar{x},\bar{t}+\bar{x}/v_F)g_-^{\gamma\delta}(-\bar{t})G_{0+}^{\delta\beta}(-\bar{x},\bar{t}-\bar{x}/v_F)\right]_{eV=0}e^{-ieV\bar{t}}$$
$$\int\mathrm{d}t_2\, e^{-ieVt_2}\,\kappa_0^\delta(t_2)^{-1} \int\mathrm{d}t_1\, e^{ieVt_1}\,\kappa_0^\gamma(t_1) \quad (4.32)$$

For large times $|\bar{t}| \gg |eV|^{-1}$ short-time regularizations and thus the distinction between different Keldysh components becomes immaterial, e.g. $\Pi_{+-}^{\gamma\delta} = |r_0|^2 e^{-ieV\bar{t}}/(2\pi\bar{t})^2$, $G_{0+}^{\alpha\beta}(0,\bar{t}) = -1/(2\pi v_F\bar{t})$, and we can write

$$i\frac{|r_0|^2 v_F}{2}\left[G_{0+}^{\alpha\gamma}(\bar{x},\bar{t}+\bar{x}/v_F)g_-^{\gamma\delta}(-\bar{t})G_{0+}^{\delta\beta}(-\bar{x},\bar{t}-\bar{x}/v_F)\right]_{eV=0}e^{-ieV\bar{t}}$$
$$= i\frac{|r_0|^2 v_F}{2}\left(\frac{1}{2\pi v_F}\frac{1}{\bar{t}}\right)^2\left(-\frac{i}{\pi}\frac{1}{\bar{t}}\right)e^{-ieV\bar{t}} = -G_{0+}^{\alpha\beta}(\bar{x},\bar{x};\bar{t})\left[\Pi_{+-}^{\delta\gamma}(\bar{t})\right]_{eV=0}.$$

Substituting into (4.32), taking into account dressing of the Green's functions (4.15) and polarization operators by phase factors, and comparison with (4.26) yields

$$\mathcal{G}_{1+}^{\alpha\beta} \approx -\tilde{G}_{0+}^{\alpha\beta}(\bar{x},\bar{x};\bar{t}) \sum_{\delta\gamma}\delta\gamma\, \tilde{\Pi}_{+-}^{\delta\gamma}(\bar{t})\Big|_{eV=0} \int\mathrm{d}t_2\, e^{-ieVt_2}\,\kappa_0^\delta(t_2)^{-1} \int\mathrm{d}t_1\, e^{ieVt_3}\,\kappa_0^\gamma(t_1)$$
$$\approx -\tilde{G}_{0+}^{\alpha\beta}(\bar{x},\bar{x};\bar{t})\,\mathcal{I}[\mathcal{K}_0]. \quad (4.33)$$

The very same analysis can be performed for $\mu = -$. In this case, however, $\tilde{\kappa}_0^\gamma$ does not depend on the Keldysh index γ. Because of $\sum_{\gamma\delta}\sigma_{\gamma\delta}\,g_+^{\gamma\delta}(t_1 - t_2) = 0$ the contribution $\mathcal{G}_{1-}^{\alpha\beta}$ is negligible.

Concluding, we obtain

$$\mathcal{G}_{0+}^{\alpha\beta} \approx e^{-|\bar{t}|/2\tau_\varphi} \ \tilde{G}_{0+}^{\alpha\beta}(\bar{x},\bar{x};\bar{t}) \ \left(1 + \mathcal{C}_+ R_*(eV) e^{ieV\bar{t}} \left[ieV\bar{t}\right]^{2q} + \mathcal{I}[\mathcal{K}_0] \right), \tag{4.34}$$

$$\mathcal{G}_{0-}^{\alpha\beta} \approx e^{-|\bar{t}|/2\tau_\varphi} \ \tilde{G}_{0-}^{\alpha\beta}(\bar{x},\bar{x};\bar{t}) \ \left(1 \ + \ \mathcal{C}_- R_*(eV) \ e^{ieV\bar{t}} [ieV\bar{t}]^{1-2K} \right), \tag{4.35}$$

$$\mathcal{G}_{1+}^{\alpha\beta} \approx -\tilde{G}_{0+}^{\alpha\beta}(\bar{x},\bar{x};\bar{t}) \ \mathcal{I}[\mathcal{K}_0]. \tag{4.36}$$

In leading order in $|r_0|^2$, i.e. neglecting dephasing corrections, $G_{1+}^{\alpha\beta}$ cancels the $\mathcal{I}[\mathcal{K}_0]$ term of $\mathcal{G}_{0+}^{\alpha\beta}$, as was stated in the end of Sect. 4.2.3.

4.2.5 Tunneling Rates

We conclude this section by evaluating the Keldysh Green's function and the tunneling rates. Due to the tunneling actions (4.28), (4.29) the full Green's functions contain power-law terms $[ieV\bar{t}]^r$, $r > 0$, which have apparent branchcut singularities near $\bar{t} = 0$. However, these are only asymptotic expressions, valid in the long-time limit $|eV\bar{t}| \gg 1$. A regularization which takes this into account and does not violate the symmetry relation $\left[iG_\mu^{\gtrless}(\bar{x},\bar{x};\bar{t}) \right]^* = iG_\mu^{\gtrless}(\bar{x},\bar{x};-\bar{t}))$ is $[1+ieV\bar{t}]^r$, which yields the Green's functions

$$G_\mu^{\alpha\beta}(\bar{x},\bar{x};\bar{t}) = \tilde{G}_\mu^{\alpha\beta}(\bar{x},\bar{x};\bar{t}) e^{-|\bar{t}|/2\tau_\varphi} \left(1 \ + \ \mathcal{C}_\mu R_*(eV) e^{ieV\bar{t}} [1+ieV\bar{t}]^{r_\mu} \right) \tag{4.37}$$

$$\text{with} \quad \mathcal{C}_+ = \Gamma(2K)/\Gamma(p)^2, \quad \mathcal{C}_- = \Gamma(2K)/\Gamma(q)^2, \quad r_+ = 2q, \quad r_- = 1 - 2K. \tag{4.38}$$

The tunneling rates are obtained by Fourier transformation to energy representation. Using the aforementioned symmetry property of the Green's function they read

$$\Gamma_\mu^{\gtrless}(\epsilon) = \pm\frac{1}{2\pi} \int_0^\infty \mathrm{d}\bar{t} \left(e^{i\epsilon\bar{t}} \ iG_\mu^{\gtrless}(\bar{x},\bar{x};\bar{t}) + e^{-i\epsilon\bar{t}} \ iG_\mu^{\gtrless}(\bar{x},\bar{x};-\bar{t}) \right) = \mp\frac{1}{\pi}\mathrm{Im} \int_0^\infty \mathrm{d}\bar{t} \, e^{i\epsilon\bar{t}} G_\mu^{\gtrless}(\bar{x},\bar{x};\bar{t})$$

$$= \pm\frac{\nu_0}{\pi} \left[\mathcal{J}_0^{\gtrless}(\epsilon; eV_\mu) + \mathcal{C}_\mu R_*(eV) \ \mathcal{J}_{r_\mu}^{\gtrless}(\epsilon; eV_\mu - eV) \right] \tag{4.39}$$

with

$$\mathcal{J}_r^{\gtrless}(\epsilon; U) \equiv \pm ia^{2\gamma} \int_0^\infty \mathrm{d}\bar{t} \, e^{i(\epsilon-U+i/2\tau_\varphi)\bar{t}} \, (1+ieV\bar{t})^r (a \pm i\bar{t})^{-(2\gamma+1)},$$

Since $\mathcal{J}_r^{\gtrless}(\epsilon; U)$ is an analytic function of all parameters $\epsilon, r, \gamma, U, eV \in \mathbb{C}$ as long as $\mathrm{Im} \, (\epsilon-U+i/2\tau_\varphi) > 0$ and $\mathrm{Im} \, eV \leq 0$ we can consider here $\mathrm{Re} \, r > -1$, $\mathrm{Re} \, (2\gamma+1) < 1$, $\mathrm{Im} \, eV < 0$ and $\mathrm{Re} \, [(\epsilon-U+i/2\tau_\varphi)/eV] < 0$ and deduce all relevant cases by analytic continuation. Under these constraints we can evaluate the integral by rotating the integration contour, $\bar{t} = -is/eV$, $0 < s < \infty$, into the complex plane, and put $a \to 0$. Writing $z = (\epsilon - U + i/2\tau_\varphi)/eV$ we get

$$\mathcal{J}_r^{\gtrless}(\epsilon; U) = \pm\frac{a^{2\gamma}}{eV} \int_0^\infty \mathrm{d}s \, e^{zs} \, (1+s)^r (\pm s/eV)^{-(2\gamma+1)}$$

$$= \left(\pm\frac{eV}{\Lambda} \right)^{2\gamma} \Gamma(-2\gamma)\Psi(-2\gamma, 1-2\gamma+r, -z)$$

with the confluent hypergeometric function $\Psi(a, b, z)$. The result for physical (real) voltages eV, Eqn. (4.4), are obtained from (4.39) by substituting $eV - i0$. Close to the singularity $z \to 0$ we have $\Psi(-2\gamma, 1 - 2\gamma + 2r, z) \sim z^{2(\gamma - r)}$. Thus, the term $\mathcal{J}_0^{\gtrless}$ in Eq. (4.39) yields the equilibrium zero-bias anomaly. The impurity corrections $\Delta\Gamma_\mu^{\gtrless}$ to the tunneling rates, given by $\mathcal{J}_{r_\mu}^{\gtrless}$, are singular at $\epsilon = eV_\pm - eV$. Leaving dephasing smearing aside we have explicitly

$$\Delta\Gamma_\mu^<(\epsilon) \propto -R_*(eV)|\epsilon - eV_\mu + eV|^{2(\gamma - r_\mu)} \sin \begin{cases} 2\pi r_\mu, & \epsilon > eV_\mu - eV, \\ 2\pi\gamma, & \epsilon < eV_\mu - eV, \end{cases}$$

in the case of tunneling from the wire into the tip, and

$$\Delta\Gamma_\mu^>(\epsilon) \propto R_*(eV)\theta(\epsilon - eV_\mu - eV)|\epsilon - eV_\mu + eV|^{2(\gamma - r_\mu)}$$

in the case of tunneling from the tip into the wire. The result for $eV > 0$, Eqn. (4.4) is obtained by substituting $eV - i0$

4.3 Conclusions

In this chapter we studied tunneling into the nonequilibrium state of a biased Luttinger liquid with a single impurity. The tunneling rates, Fig. 4.2, that we found, exhibit two edges which are split by the bias voltage eV. Both support power-laws which are smeared by dephasing. The dephasing rate (4.7) is proportional to the effective reflection coefficient, which is renormalized in agreement with [11], and has thus a nontrivial power-law (not just linear) dependence on bias.

While the main edge at the Fermi energy is governed by the same power γ as the equilibrium density of states (4.3), the shifted side edge exhibits a modified power law. In the case of tunneling into a right-moving state (whose Fermi energy is increased by eV) and moderate interaction strength the exponent can be negative, thus yielding a resonance in tunneling.

In the physical picture, we suggested to understand the edge structure, inelastic scattering of electrons off the impurity leads to the creation of a nonequilibrium plasmon bath in the wire. In the tunneling experiment, through absorption of plasmons electrons can tunnel into the wire even if their initial energy is below the Fermi energy. The characteristic energy that can be absorbed is set by the bias voltage eV. Similarly, tunneling rates for the inverse process can be understood in terms of stimulated emission.

Naturally, such a plasmonic bath gives rise to decoherence, and the applied theory allows us to quantitatively understand the effect of the intrinsic noise, arising from the interplay of nonequilibrium and interaction. In the next chapters we will study systems in which coherence is of imminent importance, namely quantum Hall interferometers.

5 Chapter 5
Quantum Hall Fabry-Pérot Interferometers

In this chapter we study the role of Coulomb interaction in an electronic Fabry-Pérot interferometer realized with chiral edge states in the integer QHE regime. Electronic Fabry-Pérot (FPI) [66–69] and Mach-Zehnder (MZI) [8, 9, 70–81] interferometers are analogues of the optical interferometers, where the chiral edge states play the role of light beams while quantum point contacts (QPCs) act as beam splitters. Electron interferometry provides a powerful tool for studying the quantum interference and dephasing in mesoscopic semiconductor devices. Another motivation behind these experimental efforts stems from the recent interest in topological quantum computations, which propose to exploit the non-Abelian anyons in the fractional QHE regime [82].

The Coulomb interaction is of paramount importance in fractional QHE systems, where it gives rise to quasi-particles with fractional charge obeying anyonic statistics. It came as a surprise that e-e interaction plays a prominent role in integer QHE interferometers as well, even when their conductance is $\sim e^2/h$ so that the Coulomb blockade physics seems to be inessential. For instance, visibility in the MZIs and FPIs strongly depends on the source-drain voltage showing decaying oscillations, which have been termed "lobes". The search for a resolution of this puzzle in the case of MZI has triggered a lot of attention [83–89]. On the contrary, the extent of theoretical works on FPIs operating in the integer QHE regime is rather small [90–92].

In this chapter we develop a capacitance model of the e-e interaction in a FPI and apply it to study the transport properties of the FPI in and out of equilibrium in the limit of weak backscattering. Our approach is inspired by the previous theoretical work [91]. Its essential idea is that a compressible Coulomb island can be formed in the center of the FPI between two constrictions (Fig. 1), which strongly affects Aharonov-Bohm oscillations. Starting from this model, we demonstrate that depending on the strength of the e-e interaction the FPI can fall into "Aharonov-Bohm" (AB) or "Coulomb-dominated" (CD) regimes observed in the experiments [67, 69], see Fig. 5.1. We also analyze the suppression of nonequilibrium AB oscillations with the increase of a source-drain voltage and find regions of both power-law and exponential decays, which explains experiments of Refs. [66, 68].

The results and details of the calculation presented in this chapter have been published before in Refs. [93] and [26].

5.1 Model

We consider an electronic FPI of size L formed by a Hall bar with ν edge channels and two constrictions (QPCs) that allow for electron backscattering between the innermost right-/left-moving edge channels
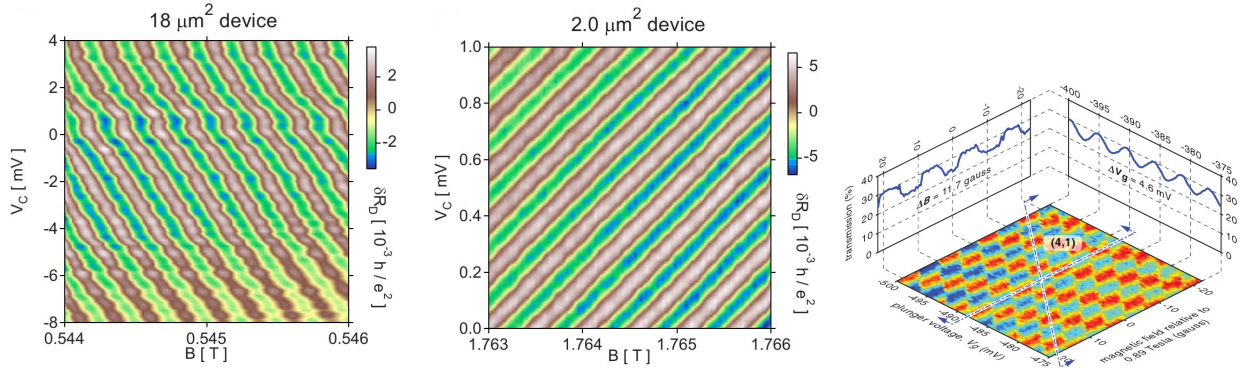
Figure 5.1: *Aharonov-Bohm conductances as function of magnetic field and gate voltages found in different experiments:* (left) *large device (area $\sim 18\,\mu\mathrm{m}^2$) with top gate[67];* (middle) *smaller device (area $\sim 2.0\,\mu\mathrm{m}^2$) without top gate[67];* (right) *device with one fully transmitted edge channel and four channels which are enclosed in the interferometer cell[69] (area $\sim 4.4\,\mu\mathrm{m}^2$ without top gate).*

with amplitudes $r_{1(2)}$ as shown in Fig. 5.2 (a). Right- and left-moving channels are connected to leads with different chemical potentials eV_+ and eV_-, respectively. In accordance with experimentalists' customs we asymmetric bias, where one edge is biases, $eV_+ = eV$, and the other one is grounded, $eV_- = 0$. In what follows, we take into account the backscattering in the lowest order, thus accounting for interference of maximally two different paths. For simplicity we assume the flight times along upper and lower arms (i.e. between two QPCs) to be the same, $\tau_+ = \tau_- = \tau = L/v_F$. We denote the magnetic flux threading the interferometer cell by ϕ, i.e. an electron which encircles the cell once accumulates the Aharonov-Bohm phase $2\pi\phi/\phi_0$, where $\phi_0 = hc/|e|$ is the flux quantum[10].

The 2DEG in the QHE regime is divided into compressible and incompressible strips [94, 95]. The filling factor in the n-th incompressible strip is integer. These strips are separated by much wider regions of compressible Hall liquid with a non-integer filling factor (compressible strips). The corresponding sketch the of electron density profile $\rho(y)$ in the FPI along y-axis is shown in Fig. 5.3. Let us denote by $y_k^\pm$ the boundaries between compressible and incompressible regions. Then $a_k = y_k^+ - y_k^-$ is the width of the k-th incompressible strip while $b_k = y_{k-1}^- - y_k^+$ is the width of the k-th compressible one. As it was shown in Ref. [94], in the situation of gate-induced confinement of the 2DEG in the QHE regime the widths $b_k \gg \lambda_B$, with λ_B being the magnetic length. At the same time a_k scales as $a_k \sim \left(b_k \lambda_B\right)^{1/2}$, so that in general the condition $b_k \gg a_k \gg \lambda_B$ is satisfied. In this picture compressible regions play the role of edge channels — the self-consistent electrostatic potential is constant through the compressible strips and can be controlled by connecting them to external leads.

We also assume that the filling fraction ν_0 in the center of the FPI exceeds ν, giving rise to a compressible droplet (Coulomb island). The reason for that can be smooth (on a scale λ_B) disorder potential fluctuations [96]. Let us denote by eN_i the excess charge on the island ($e < 0$), with N_i being integer. On the scheme in Fig. 5.3 the boundary of the island is given by y_ν^-. This value is quantized and changes abruptly when an electron tunnels between innermost compressible strips and the island through the incompressible strip. On the contrary, the boundaries of edge channels may change continuously upon a variation in external parameters, such as $eV_\pm$ and V_g, or due to quantum fluctuations of electrostatic potentials on these compressible regions (see also discussion later).
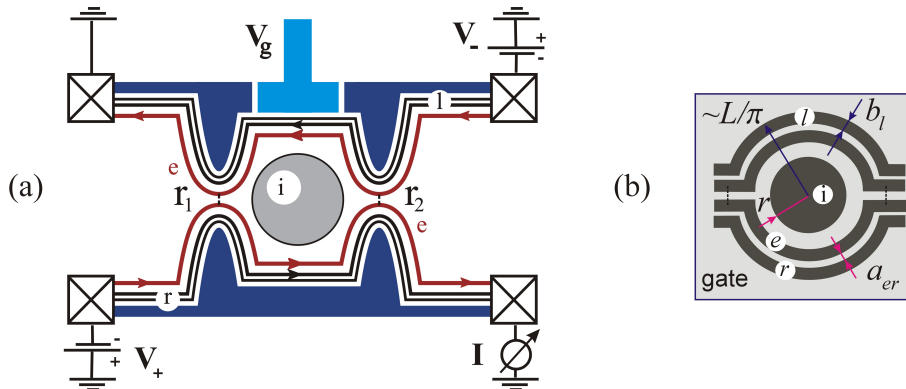
Figure 5.2: *(a) Fabry-Pérot interferometer with compressible island i. The innermost edge chan-*
nels e are subject to backscattering at the QPCs; the remaining $f_T = \nu - 1$ right(r)-
and left(l)- moving channels are fully transmitted; their role is in screening of the
interaction between the electrons of the channel e. Right- and left-moving channels
are connected to reservoirs with different chemical potentials eV_η, $\eta = \pm$. Here, the
gate g is depicted as a "plunger" gate. (b) Simple capacitance model, which uses
geometry of the compressible regions. Full transmitted right(r)- and left(l)-moving
channels are each joined into one conductor with the widths b_r and b_l, respectively.

Electrostatics of the FPI

In the framework of the above model, we treat the *e-e* interaction in the FPI by using the constant interaction model (see e.g. Ref. [97]) with mutual capacitances $C_{\alpha\beta}$ between four compressible regions — the interfering channel (e); right- and left-moving fully transmitted channels (r, l); the compressible island (i) — and the gate (g). These capacitances are denoted by C_{eg}, C_{ei} etc. We assume a large capacitance between counter-propagating innermost channels — thus they share the same electrostatic potential φ_e — and also consider $f_T = \nu - 1$ right- and left-moving channels as joint conductors with potentials φ_r (φ_l). Defining the capacitance matrix $\tilde{C}$ with elements $\tilde{C}_{\alpha\alpha} = \sum_\gamma C_{\alpha\gamma} + C_{\alpha g}$, and $\tilde{C}_{\alpha\beta} = -C_{\alpha\beta}$ ($\alpha \neq \beta$), where Greek indices span the set $\{e, r, l, i\}$ and $q_\alpha = -C_{\alpha g} V_g$ is an offset charge on conductor α, the electrostatic energy reads

$$E = \frac{1}{2} \sum_{\alpha\beta} \left(Q_\alpha - q_\alpha \right) \left(\tilde{C}^{-1} \right)_{\alpha\beta} \left(Q_\beta - q_\beta \right). \tag{5.1}$$

Total charge $Q_i = e \left(N_i + \nu\phi/\phi_0 \right)$ on the island is distributed on the highest partially filled Landau level (LL) and on ν fully occupied underlying LLs (cf. Fig. 5.3). Single electron tunneling is possible between interfering channels (e) and the island. We assume the rate Γ of such tunneling processes to be much smaller than all other energy scales in the problem, $\Gamma \ll v_F/L \lesssim eV$, hence N_i is quantized and is fixed for given external parameters ($\phi, V_g, eV_\pm$).

The mutual capacitances $C_{\alpha\beta}$ can be estimated from geometrical considerations [98]. We regard the island as a disc of radius r and represent the compressible edge channels as concentric rings of the width b_α and diameter L (here $\alpha = e, r, l$) as depicted in Fig. 5.2 (b). The edge channels are assumed to be thin, $b_\alpha \ll L$. Therefore for the estimation of capacitances we can neglect the difference between the radii of the island and those of edge channels, i.e. $L \simeq \pi r \simeq \pi y_k^\pm$. A top gate, if present, is modeled by a plane situated at distance d from the 2DEG. Since the size of FPI cell is much larger than d, we
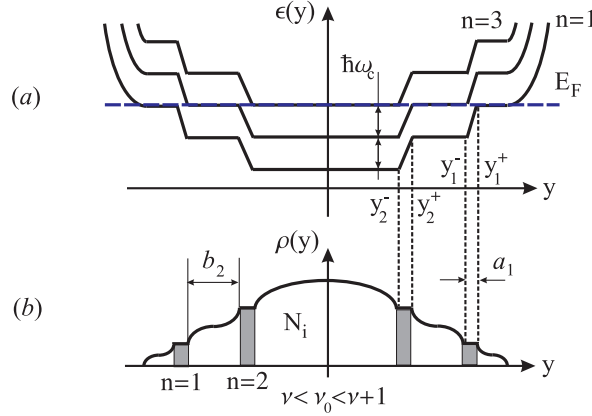
Figure 5.3: *The structure of the edge states in the FPI. Cut through the center of an interfe-rometer cell: (a) Landau level energies as the function of vertical coordinate y and (b) electron density $\rho(y)$ (see also Fig. 5.2). Besides ν completely filled LLs, the central region can sustain a partially filled Landau level whose occupation N_i changes by tunneling. Here we denoted by $a_k = y_k^+ - y_k^-$ the width of the k-th incompress-ible strip (shown in gray), which has the integer filling factor k. Compressible re-gions (white) represent the regions with non-integer filling fraction and have the width $b_k = y_{k-1}^- - y_k^+$. The picture above corresponds to the case $\nu = 2$.*

treat C_{ig}, C_{eg} and $C_{r(l)g}$ as parallel-plate capacitors and find the estimate

$$C_{ig} \simeq \epsilon \frac{r^2}{4d}, \qquad C_{eg} \simeq \epsilon \frac{Lb_e}{2\pi d}, \qquad C_{rg} \simeq \epsilon \frac{Lb_r}{4\pi d}, \tag{5.2}$$

where e.g. for GaAs the dielectric constant is $\epsilon = 12.6$. For the estimate of edge-to-edge (C_{er} and C_{el}) and edge-to-island (C_{ei}) capacitances we can use the mutual capacitance of two conducting rings. In the limit $b \ll a$ we obtain with logarithmic accuracy

$$C_{er} \simeq \frac{\epsilon L}{2\pi^2} \ln\left(\frac{b_e b_r}{a_{er}^2}\right), \quad C_{ei} \simeq \frac{\epsilon r}{\pi} \ln\left(\frac{rb_e}{a_{ei}^2}\right). \tag{5.3}$$

Here $b_{r(l)} = \sum_k^{\nu-1} b_k$ are the total widths of fully transmitted edge channels. Finding the mutual capacitance between a plunger gate and the island or the interfering edge channel is in general more difficult. Because of geometry, one can expect that C_{ig} and C_{eg} in this case will be substantially smaller than the above estimate (5.2) for the case of a top gate.

Let us now comment on the flux dependence of the electrostatic energy, Eq. (5.1). When the magnetic flux through the island is increased, $\delta\phi = \pi r^2 \delta B$, the LLs are squeezed and the charge on the island (for a fixed boundary y_ν^-) varies as $\delta Q_i = e\nu\, \delta\phi/\phi_0$. A similar effect of magnetic field on charges $Q_{e,r,l}$ distributed on compressible circular strips is negligibly small because of the condition $b \ll r$. Indeed, for a typical variation δB, such that $\delta\phi/\phi_0 \sim 1$, the corresponding modulations of these charges are

$$\frac{\delta Q_{e,r,l}}{e} \sim \frac{\delta\phi}{\phi_0}\left(\frac{2b}{r}\right) \ll 1, \tag{5.4}$$

and we do not include them into Eq. (5.1).

5.2 Results

In this subsection we summarize our results and give their physical interpretation. The detailed derivation is presented in the next subsection. The qualitative behavior of the FPI crucially depends on the relative coupling strength of the interfering edge (e) to the fully transmitted channels (l, r), to the island, and to the gate. The essential parameters are the number of transmitted channels ν^* which screen the bare e-e interaction in the interfering channel — as we demonstrate in the section 5.3, one has $\nu^* \simeq 1$ in the case of strong and $\nu^* \simeq \nu$ in the case of weak inter-edge interaction — and the effective edge capacitance $\bar{C}_e$ as defined below by Eq. (5.11). There are also two characteristic energy scales in our problem: (i) charging energy $E_C = e^2/\bar{C}_e$, or charge relaxation frequency $\omega_C = (\nu^*/\pi)E_C$; and (ii) the Thouless energy $\epsilon_{\text{th}} = \tau^{-1} = v_F/L$. The relation between these two parameters depends essentially on the geometry of the experiment (most importantly, on the geometry of the gates). We will assume that the condition $\epsilon_{\text{th}} \ll \omega_C$ is always satisfied, which simplifies a lot our subsequent calculations and enables us to get analytical results. This appears to be a proper assumption for most of available experiments. In particular, the value of the Thouless energy that can be deduced from the experiment of the Harvard group is $\epsilon_{\text{th}} \sim 50\,\mu\text{V}$ [66], whereas the charging energy is in the mV range [67].

5.2.1 Visibility, dephasing and the "lobe" structure

In the limit of weak backscattering, $R_j = |r_j|^2 \ll 1$, the dimensionless differential conductance of the FPI, $g = g_{\text{inc}} + g_{\text{AB}}$ – normalized with respect to the conductance quantum $G_0 = e^2/(2\pi)$ – is the sum of incoherent and coherent contributions. The incoherent contribution is

$$g_{\text{inc}}(V) = \nu - R_{1*}(eV) - R_{2*}(eV), \tag{5.5}$$

where $R_{j*}(eV)$ are the renormalized reflection coefficients (see Eq. (5.9) below). The dependence of the AB conductance on external parameters — the gate voltage V_g, the variation of the magnetic field ΔB and the bias V — factorizes into

$$g_{\text{AB}}(eV_+, eV_-, \phi, V_g) = \tilde{g}(V)\cos[\varphi_{\text{AB}}(V_g, \Delta B)]. \tag{5.6}$$

The AB phase φ_{AB} will be discussed in detail shortly. The amplitude of the oscillations is

$$\tilde{g}(V) = e^{-\tau/\tau_\varphi} R_{12*}(eV)\, 2\left|\cos\left(|eV\tau| + \frac{\pi}{4\nu^*}\right)\right| \tag{5.7}$$

with the nonequilibrium dephasing rate given by

$$\tau_\varphi^{-1} = |eV|\left(R_{1*}(eV) + R_{2*}(eV)\right)\frac{2}{\pi}\sin^2\frac{\pi}{2\nu^*}. \tag{5.8}$$

In Eqs. (5.5) and (5.7) we have introduced the renormalized reflection coefficients defined as

$$
\begin{aligned}
R_{j*}(eV) &= R_j \left|\frac{\omega_C}{eV}\right|^{1/\nu^*} \frac{e^{\gamma/\nu^*}}{\Gamma(2-1/\nu^*)} = R_{j*}(\epsilon_{\text{th}})\left|\frac{\epsilon_{\text{th}}}{eV}\right|^{1/\nu^*}, \\
R_{12*}(eV) &= |r_1 r_2|\,|\omega_C\tau|^{1/2\nu^*}\left|\frac{\omega_C}{eV}\right|^{1/2\nu^*}\frac{2^{1/2\nu^*}e^{\gamma/\nu}}{\Gamma(1-1/2\nu^*)} = R_{12*}(\epsilon_{\text{th}})\left|\frac{\epsilon_{\text{th}}}{eV}\right|^{1/2\nu^*}.
\end{aligned}
\tag{5.9}
$$

Remarkably, in the last equation the amplitudes r_1, r_2 do not renormalize separately, rather the renormalization operates non-locally. A similar result was found for FPIs in the fractional QHE regime in Ref. [90]. The relations (5.9) are valid for bias in the range $\epsilon_{\text{th}} \ll eV \ll \omega_C$. The above renormalization comes from *virtual* electron-hole excitations (being a precursor of weak Coulomb blockade [99, 100]) and stops at $eV \simeq \epsilon_{\text{th}}$. On the contrary, the dephasing rate τ_φ^{-1} is caused by *real* e-h pairs excited by backscattered electrons and is proportional to the shot noise of the QPCs. There a simple linear dependence of the shot noise on voltage, which is valid in the absence of interaction, is modified because of the renormalization of reflection coefficients.

An additional dependence of the conductance amplitude (5.7) on bias stems from an oscillatory prefactor which has the characteristic scale $\pi\epsilon_{\text{th}}$. As a consequence, the amplitude or, equivalently, the visibility $v(V) = |\tilde{g}(V)|/g_{\text{inc}}(V)$ vanishes for certain equidistantly distributed values of bias. The resulting characteristic "lobe" structure of visibility is shown in Fig. 5.4 and is in agreement with experiments reported in Refs. [66, 68].
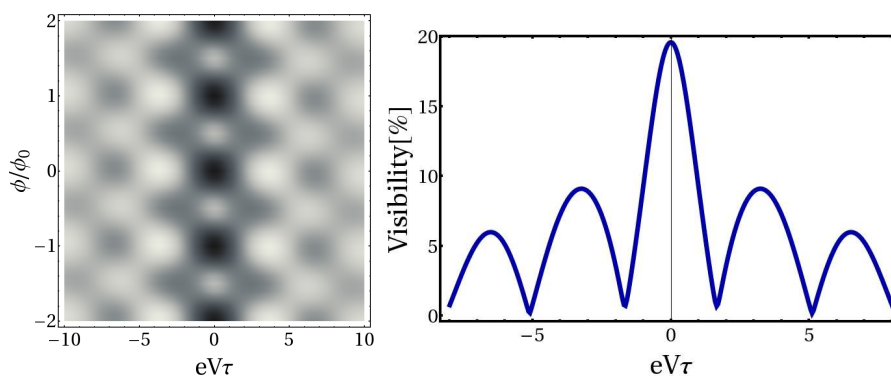

Figure 5.4: *Total differential conductance g as a function of bias and magnetic flux (left panel), and visibility (right panel). Parameters are: $\nu^* = 2$, $\omega_C\tau = 25$, $R_{1*}(\epsilon_{\text{th}}) = R_{2*}(\epsilon_{\text{th}}) = 0.2$.*

5.2.2 Aharonov-Bohm oscillations

In experiment one usually characterizes the FPI in terms of the pattern of its equilibrium conductance in the (B, V_g) - plane, which is governed by the AB phase. We have identified four different regimes where the behavior of AB oscillations is qualitatively different (see Table 5.1). In this table the parameter ν^* — the effective number of transmitted channels which screen the Coulomb interaction in the interfering channel — depends on the relative strength of the inter-edge *e-e* interaction. To distinguish between the limits of weak and strong *e-e* interaction we compare the inter-channel interaction energy $\sim e^2/C_{e\alpha}$ (here $\alpha = r, l$) with the screened-by-the-gate charging energy of the interfering edge itself given by $\sim e^2/C_{\alpha g}^*$. Here the edge-to-gate capacitance is effectively increased by the so-called "quantum capacitance":

$$C_{\alpha g}^* = C_{\alpha g} + (\nu - 1)\tau e^2/(\hbar\pi). \tag{5.10}$$

In the weak coupling limit one has $C_{e\alpha} \gg C_{\alpha g}^*$. In this case the electrostatic potentials on all edge channels (r, l, and e) are approximately equal to each other and $\nu^* \simeq \nu$. In the opposite strong coupling limit we have $C_{e\alpha} \ll C_{\alpha g}^*$. The potential φ_e here fluctuates independently of potentials on other edge channels (r and l), thus screening of *e-e* interaction by the latter channels is not effective and one gets

$\nu^* \simeq 1$. To make a distinction between the "Aharonov-Bohm" (AB) and "Coulomb-dominated" (CD)

Table 5.1: *"Phase diagram" of the FPI, which discriminates between two Aharonov-Bohm (AB and AB*) and two Coulomb-dominated (CD I and CD II) regimes.*

	$\boxed{C_{e\alpha} \gg C^*_{\alpha g}}$ $\nu^* = \nu$ $\bar{C}_{ei} = C_{ei} + C_{ri} + C_{li}$ $\bar{C}_{eg} = C_{eg} + C_{rg} + C_{lg}$	$\boxed{C_{e\alpha} \ll C^*_{\alpha g}}$ $\nu^* = 1$ $\bar{C}_{ei} = C_{ei}$ $\bar{C}_{eg} = C_{eg}$
$\bar{C}_{ei} \ll C_{ig}$	AB	AB*
$\bar{C}_{ei} \gg C_{ig}$	CD II	CD I

regimes we now define an effective edge-to-island capacitance $\bar{C}_{ei}$ by the relation $\bar{C}_{ei} = C_{ei} + C_{ri} + C_{li}$ in the weak coupling limit, i.e. at $\nu^* \simeq \nu$, and set it to be $\bar{C}_{ei} = C_{ei}$ in the opposite case of strong coupling. Then the FPI falls into AB or CD regimes depending on the ratio $\bar{C}_{ei}/C_{ig}$, as it is shown in the Table 5.1. As one can see from Eqs. (5.2) and (5.3), for the device with a top gate the capacitance C_{ig} scales like r^2 when the FPI size grows, while $\bar{C}_{ei}$ increases only as $r \ln r$. This suggests a simple rule of thumb: the AB regime occurs primarily in large FPIs with a top gate (in experiment "large" means a cell area $\sim 20 \mu \text{m}^2$). In this situation, i.e. at $\bar{C}_{ei}/C_{ig} \ll 1$, fluctuations of charge on the island are screened by the gate electrode and do not affect the AB conductance. In the opposite case of a large ratio between the capacitances ($\bar{C}_{ei}/C_{ig} \gg 1$), as one will see shortly, the AB conductance becomes linked to the Coulomb blockade on the compressible island, hence the naming – "Coulomb-dominated" – for this regime.

For a device without a top gate a bare edge-to-gate capacitance C_{eg} is only due to a plunger gate (see Fig. 5.2). Such a gate is used to control the size of the interference loop and for geometrical reasons C_{eg} is typically very small, so that one has $C^*_{eg} \simeq (\nu - 1)\tau e^2/(\hbar \pi)$. In this case our first condition of weak versus strong inter-edge *e-e* coupling can be simplified. Defining the dimensionless coupling constant as

$$\alpha_\nu \equiv \frac{(\nu - 1)e^2}{\epsilon \hbar v_F}$$

and using the estimate (5.3) for capacitances C_{er} and C_{el} one obtains the crossover value

$$\alpha^* \sim \frac{1}{2\pi} \ln \left(\frac{b_e b_r}{a_{er}^2} \right),$$

which sets the boundary between the weak and strong coupling regimes.

We name four regimes AB, AB*, CD I and CD II according to the Table 5.1 which lists the values of parameters ν^*, $\bar{C}_{ei}$ and $\bar{C}_{eg}$. The capacitance $\bar{C}_{eg}$ here is defined in analogy to $\bar{C}_{ei}$. In addition to these effective edge-to-island and edge-to-gate capacitances we now define full island and edge capacitances as

$$\bar{C}_i = \bar{C}_{ei} + C_{ig}, \quad \bar{C}_e = \bar{C}_{eg} + \bar{C}_{ei}C_{ig}/\bar{C}_i. \tag{5.11}$$

Then the AB phase in Eq. (5.6) reads

$$\varphi_{\mathrm{AB}} = 2\pi\phi/\phi_0 - \frac{2\pi}{\nu^*}\frac{\bar{C}_{ei}}{\bar{C}_i}(N_{i*} + \nu\phi/\phi_0) + \frac{|e|}{\omega_C}\left(2V_g - V_+ - V_-\right) \tag{5.12}$$

with integer N_{i*} minimizing the charging energy of the Coulomb island

$$E_i = \frac{e^2}{2\bar{C}_i}(N_{i*} + \nu\phi/\phi_0 - C_{ig}V_g/|e|)^2, \tag{5.13}$$

and we have defined $\omega_C = \nu^* E_C/\pi$ and $E_C = e^2/\bar{C}_e$.

In Fig. 5.5 we show the conductance $g_{\mathrm{AB}}(\phi, V_g)$ in the (B,V_g)–plane for three regimes: AB, CD I and CD II. The plots display significant differences. In particular, the lines of constant phase have a different slope in the AB and type-I CD regimes. The flux periodicity is also different in these two cases. The AB conductance in the case of type-II CD regime shows a "rhomb-like" pattern. The pattern of equilibrium conductance in the AB* case is the same as in the AB regime, provided one sets $\nu^* = 1$.
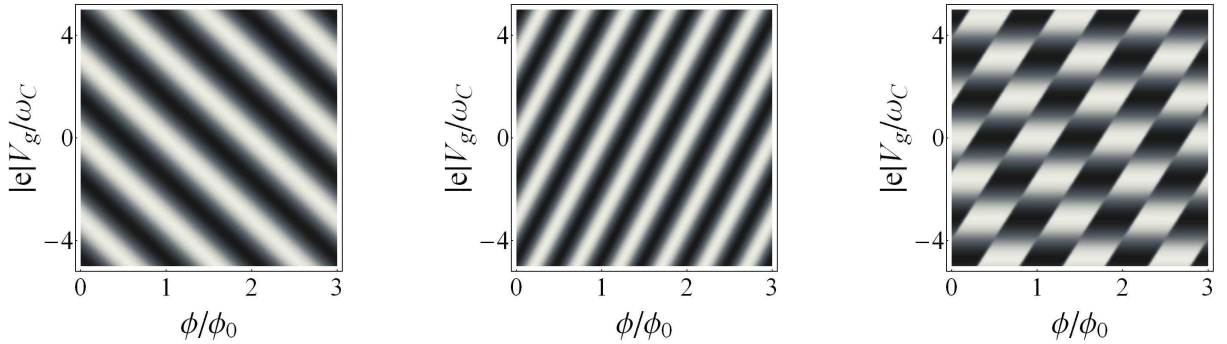

Figure 5.5: *Aharonov-Bohm conductance in different regimes.* AB regime (left): $\nu^* = \nu = 2$, *stripes of constant conductance have a negative slope, flux and gate voltage periods are* $\Delta\phi = \phi_0$ *and* $\Delta V_g = \nu E_C/|e|$. *Type-I CD regime (middle):* $\nu^* = 1$, $\nu = 3$, *stripes of constant conductance have now a positive slope, flux and gate voltage periods are* $\Delta\phi = \phi_0/(1 - \nu)$ *and* $\Delta V_g = E_C/|e|$. *Type-II CD regime (right):* $\nu^* = \nu = 2$, $C_{ig}/\bar{C}_e = 0.6$, *at fixed gate voltage* V_g *conductance depends discontinuously on flux – phase jumps occur at every* $\Delta\phi = \phi_0/\nu$.

5.2.3 Discussion and Comparison with Experiment

Noninteracting interferometer

Let us now discuss the physics which underlies the rich phenomenology of our rather simple model. To appreciate the role of interaction we consider first the noninteracting case, where the interfering channel couples neither to the fully transmitted ones nor to the island. Consider an electron which contributes to the tunneling current and which is, say, incident from the left source and leaks into the left drain. It may tunnel either at the left or right QPC. The latter path is longer than the first by $2L = 2v_F\tau$ and encircles a magnetic flux ϕ. Along this path the electron accumulates a dynamic ("Fabry-Pérot") phase $2\epsilon\tau$ (ϵ is the energy of the electron) and a magnetic AB phase $2\pi\phi/\phi_0$. According to quantum

mechanics, the current results from interference of both paths. Integration over all energies in the range $eV_- < \epsilon < eV_+$ gives the backscattering current

$$I_b = -e \int_{eV_-}^{eV_+} \frac{d\epsilon}{2\pi} \left| r_1 + e^{2\pi i\phi/\phi_0 + 2i\epsilon\tau} r_2 \right|^2 = I_{\text{inc}} + I_{\text{AB}}, \tag{5.14}$$

that we split into incoherent and coherent contributions,

$$I_{\text{inc}} = -\frac{e^2}{2\pi} V(R_1 + R_2), \quad I_{\text{AB}} = -\frac{e}{2\pi\tau} 2r_1 r_2 \cos[e(V_+ + V_-)\tau + 2\pi\phi/\phi_0] \sin[eV\tau] \tag{5.15}$$

where we assumed for simplicity that r_1, r_2 are real. While the incoherent part of the current I_{inc} is expected already on the classical level, I_{AB} stems from interference and is sensitive to magnetic flux. The dynamic phase accumulated by an electron depends on its "absolute" energy ϵ, and hence the current I_{AB} depends on both chemical potentials eV_+, eV_- and not just on their difference $eV = eV_+ - eV_-$. Clearly, the sum $(V_+ + V_-)$ enters only the phase shift of the AB pattern, but not the amplitude. However, this independence of the amplitude of oscillations on the bias does not in general hold for the differential conductance g_{AB}. Specifically, when the differential conductance is calculated in the framework of the model of noninteracting electrons, the amplitude of the corresponding AB oscillations $\tilde{g}$ does depend on the manner in which bias is applied.

Experimentally, the bias is applied asymmetrically: $eV_+ = eV$, $eV_- = 0$. The expected dimensionless conductance then is

$$g_{\text{AB}} = G_0^{-1} \partial_V I_{\text{AB}} = -2r_1 r_2 \cos[2eV\tau + 2\pi\phi/\phi_0],$$

i.e. bias merely controls the phase shift of the AB oscillation pattern. The amplitude $\tilde{g} = 2|r_1 r_2|$ is independent of bias. This clearly contradicts our results, presented above, as well as experimental observations.

The situation would change essentially if the bias were applied symmetrically: $eV_+ = eV/2$, $eV_- = -eV/2$. Then the conductance would be

$$g_{\text{AB}} = -2r_1 r_2 \cos[eV\tau] \cos[2\pi\phi/\phi_0]. \tag{5.16}$$

Now, the amplitude would oscillate with bias on the scale $\pi\epsilon_{\text{th}}$, yielding a visibility with a "lobe" structure. This result is apparently much more similar to our findings (albeit without dephasing and renormalization of $r_1 r_2$) as well as to the experimental observations. On the basis of the similarity between Eq. (5.16) and the experimental observations it was conjectured in Ref. [67] that the electron-electron interaction effectively symmetrizes the bias even if the latter is applied asymmetrically.

Mean field potential and contracting edge

To see how this works, assume that a charge within the interferometer cell produces a (for simplicity constant) self-consistent potential φ_0. An electron which propagates in this potential during a time 2τ accumulates the "electrostatic" AB phase $-2\varphi_0\tau$. Hence, the dynamic phase would be $2(\epsilon - \varphi_0)\tau$ and instead of the bare chemical potentials the relative potentials $(eV_\pm - \varphi_0)$ enter the result (5.15). Such a mean-field potential is indeed generated within our model. For instance, in the generic limit of large charging energy $E_C \gg \epsilon_{\text{th}}$ our calculations in the subsection 5.3 yield $\varphi_0 \simeq e(V_+ + V_-)/2$ in the case of AB regime. Therefore without any need of any fine tuning, the bias is effectively symmetrized, which explains the appearance of the "lobe" structure.

The mean-field potential φ_0 on the compressible strip corresponding to the interfering edge channel is in general a function of the applied chemical potentials $eV_\pm$, the gate voltage V_g and the magnetic flux ϕ. The most general expression found in subsection 5.3 reads

$$\varphi_0(eV_\pm, V_g, \phi) = \frac{1}{1 + \omega_C \tau} \left[eV_g + \frac{eV_+ + eV_-}{2} \omega_C \tau + E_C \frac{\bar{C}_{ei}}{\bar{C}_i} (N_{i*} + \nu\phi/\phi_0) \right]. \qquad (5.17)$$

Here N_{i*}, as before, provides the minimum for the Coulomb energy E_i of the island given by Eq. (5.13). If we introduce the "mean electrochemical potential"

$$-\tilde{\varphi}_0 = (eV_+ + eV_-)/2 - \varphi_0, \qquad (5.18)$$

then the "total" AB phase is

$$\varphi_{AB}(eV_\pm, V_g, \phi) = 2\pi\phi/\phi_0 - 2\tau\tilde{\varphi}_0(eV_\pm, V_g, \phi) \qquad (5.19)$$

and becomes (5.12) in the limit $\omega_C \tau \gg 1$. The first contribution here is the magnetic AB phase accumulated along a fixed reference loop with area A_0, i.e. $\phi = A_0 \delta B$, with $\delta B \ll B$ being a weak modulation of magnetic field on top of the high field B which drives the 2DEG into the QHE regime. Because of the condition $b \ll L$ (see Fig. 5.2 b) imposed in our model, and since a typical variation δB is such that ϕ changes on a scale of a few flux quanta only, one can use any boundary $y_k^\pm$ to define A_0. For example, one can set $A_0 = \pi(y_\nu^+)^2$. Let us further show that the second "electrostatic" contribution $(-2\tau\tilde{\varphi}_0)$ to the phase φ_{AB} can be interpreted in terms of the motion of edge states which leads to a variation of the relevant FPI area when the magnetic field B or gate voltage V_g are varied.
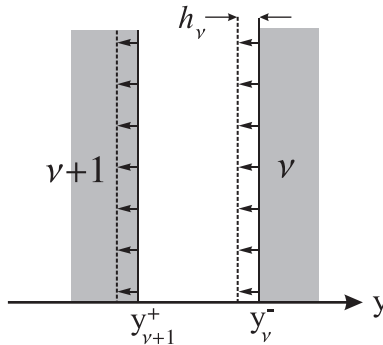

Figure 5.6: *When the boundaries of the compressible strip (white) separating incompressible regions (gray) with filling factors ν and $\nu + 1$ move toward the $(\nu + 1)$-liquid (indicated by arrows), the latter shrinks while the ν-liquid's area grows: as the result the charge on the incompressible strip, defined by the boundaries $y_{\nu+1}^-$ and y_ν^+, decreases (in this figure $h_\nu < 0$).*

First, we note that in the stationary limit an imbalance of electron density on the interfering edge channel $\delta\rho_e$ is related to the corresponding electrochemical potential (5.18) via the simple relation $\delta\rho_e = -\tilde{\varphi}_0/(2\pi v_F)$, since $(2\pi v_F)^{-1}$ is the 1D thermodynamic density of states in our model. As it is always the case in QHE systems, this charge density can be translated into the variation h_ν of the boundary between the compressible and incompressible strips (Fig. 5.6), $\delta\rho_e = n_L h_\nu$, where $n_L = B/\phi_0 = (2\pi\lambda_B^2)^{-1}$ is the electron concentration of one completely filled LL, and we have assumed the

fluctuations of inner and outer boundaries of the compressible strip to be the same, $\delta y_{\nu+1}^{+} = \delta y_{\nu}^{-} = h_{\nu}$. Therefore the "electrostatic" part of the AB phase reads

$$- 2\tau \tilde{\varphi}_0 = 4\pi L \delta \rho_e = 4\pi n_L (Lh_{\nu}) = 2\pi (B/\phi_0)\delta A. \tag{5.20}$$

Here $\delta A = 2Lh_{\nu}$ is the change in area enclosed by interfering edge state. To recapitulate the logic, we have thus related the self-consistent electrostatic potential φ_0 to a variation of the FPI area. With these arguments at hand one can now rewrite Eqs. (5.17) and (5.19) in the equivalent form

$$\phi_{AB} = 2\pi \Big(A_0 \delta B + B \delta A \Big)/\phi_0 + \text{const}\,, \tag{5.21}$$

where the variation of area reads

$$\delta A = -\frac{1}{\nu^*} \frac{\bar{C}_{ei}}{\bar{C}_i} \left(\nu \frac{A_0}{B} \delta B + \frac{\phi_0}{B} \Delta N_i \right) + \frac{|e|}{\omega_C} \frac{\phi_0}{\pi B} \delta V_g. \tag{5.22}$$

The integer ΔN_i denotes the deviation of the electron number on the Coulomb island from the initial reference value. We have also taken into account that the source-drain bias is small on a scale of the charging energy, $|eV| \ll E_C$.

Regimes and experiments

Let us now discuss our theory of the FPI in relation to the recent experiments by considering separately each of the four regimes in the Table 5.1. In the *AB regime* one has $\bar{C}_{ei}/\bar{C}_i \ll 1$, thus the coupling of the interfering edge to the Coulomb island is negligible and the area A does not change with B. The AB phase then simplifies to

$$\varphi_{\text{AB}} = 2\pi \phi/\phi_0 + \frac{2\pi}{\nu} \frac{|e|V_g}{E_C}, \tag{5.23}$$

yielding the lines of constant phase with a negative slope (Fig. 5.5, left) and a magnetic field period $\Delta B = \phi_0/A_0$ which is independent of ν. The second term in the above equation describes the spatial shift of the electron trajectory upon varying the gate voltage. If $\delta V_g > 0$ then the interfering edge state moves outwards and thus encloses a larger flux as it is seen from Eq. (5.22). The AB regime was observed in large devices (cell area $\sim 18\mu\text{m}^2$) with a top gate [66, 67, 69], where the condition $\bar{C}_{ei} \ll C_{gi}$ is satisfied. In Ref. [67] it has been also found that the magnetic field period ΔB is independent of B, while the gate voltage periodicities (both top- and plunger- ones) scale as $\Delta V_g \propto 1/B \propto \nu$. These observation are consistent with our Eq. (5.23) if the charging energy $E_C = e^2/\bar{C}_e$ is ν-independent. This is the case provided the full edge capacitance $\bar{C}_e \simeq \bar{C}_{eg} + \bar{C}_{ei}$ stays approximately the same at each Hall plateau.

In the *CD regime* one has $\bar{C}_{ei}/C_i \simeq 1$ and the area of the interfering loop shrinks with increasing magnetic field. This is because the interfering edge is now electrostatically coupled to the charge $Q_i = e(N_i + \nu\phi/\phi_0)$ on the Coulomb island, which depends explicitly on flux. The AB phase in this regime reads

$$\varphi_{\text{AB}} = 2\pi(1 - \nu/\nu^*)\phi/\phi_0 - \frac{2\pi}{\nu^*}N_i + \frac{2\pi}{\nu^*} \frac{|e|V_g}{E_C},$$

In the *type-II* CD regime $\nu^* \simeq \nu$ and at fixed V_g the AB phase stays piecewise constant when the magnetic field is varied. Its dependence on B exclusively enters via N_i. Indeed, as it follows from

Eq. (5.22) the shrinkage of the interfering loop in this case, $\delta A = -(A_0/B)\delta B$, exactly compensates a change in magnetic phase $\varphi = A_0 \delta B$. When the FPI is brought close to a charge degeneracy point of the island by varying V_g or B, electron tunneling becomes possible between the droplet and interfering channels (i.e. $\Delta N_i = \pm 1$) resulting in abrupt change of A. This creates a phase lapse (or jump) $\Delta \phi_{AB} = \pm 2\pi/\nu$ giving rise to the "rhomb-like" pattern shown in Fig. 5.5 (right) at $\nu \geq 2$.

In the *type-I* CD regime $\nu^* \simeq 1$ and a change in AB phase caused by area shrinkage when rising B overcompensates the growing of the magnetic part ϕ, since now $\delta A = -\nu(A_0/B)\delta B$. Counterintuitively, the phase decreases when increasing the magnetic field. At the same time, whenever an electron tunnels into the island from the interfering edge channel (e), the boundary of this edge state contracts so as to expel exactly one flux quantum from the AB loop. The phase lapse, being equal to $\Delta \phi_{AB} = -2\pi$ in this tunneling process, is therefore invisible in the interference conductance. As a result, one has the diagonal stripe pattern with lines of constant phase having positive slope (Fig. 5.5, middle). The periods are $\Delta B = \phi_0/(f_T A)$ and $\Delta V_g = e/(C_{eg} + C_{gi})$, with $f_T = \nu - 1$ being the number of fully transmitted edge channels (note, that at $\nu = 1$ the lines of constant phase are vertical).

In the limit of weak backscattering at QPCs, the Coulomb-dominated regime has been observed in Ref. [69]. In this work measurements were performed with a large range of edge state configurations (including fractional fillings), classified by the bulk filling f_b and the number f_T of fully transmitted edges. We focus on the results obtained with a $4.4\,\mu\mathrm{m}^2$-device without a top (but with plunger-) gate. They indicate that interaction plays a major role (i.e. CD I and CD II regimes). For integer f_b and $f_T = f_b - 1$ the results coincide with our Fig. 5.5 (middle), including a period in magnetic field which scales as $\Delta B \propto 1/f_T$.The gate period in Ref. [69] was found to be weakly increasing with f_T. We can explain this dependence if we assume that the full edge capacitance, which equals to $\bar{C}_e = C_{gi} + C_{eg}$ in the CD I regime, decreases with f_T, because, for geometric reason, the mutual coupling of the plunger gate and the inner interfering edge channel (C_{eg}) becomes less efficient at high ν. A quite "exotic" behavior was observed, when more than one channel were trapped in the interferometer cell. In the case of $f_b = 4$ and $f_T = 1$ experimental findings resemble very much Fig. 5.5 (middle) corresponding to our CD II regime. In such a setting one fully transmitted and one partially reflected edge channel can be described by our model with $\nu = 2$ assuming that the other two trapped inner channels can be treated as a compressible island, where the excess charge is quantized.

Nonequilibrium transport measurements in the FPIs in the AB regime have been performed in Refs. [66, 68]. Their main findings can be summarized as follows: (i) the dependence of the AB conductance on B and the bias V factorizes into a product of two terms yielding a "checkerboard" pattern in the (B, V)-plane (cf. Fig. 5.4, left); (ii) the scale of the "lobe" structure is set by $\epsilon_{\mathrm{Th}} \sim v_D/L$; (iii) the visibility decay with bias is stronger at higher magnetic fields. The results of our theory, Eqs. (5.6) - (5.9), are in full accord with these observations. In particular, the suppression of visibility in our model at $|r_j|^2 \ll 1$ is mainly due to a power-law decay with the *negative* exponent $(-1/2\nu^*)$. Since in the AB regime $\nu^* = \nu \propto 1/B$, this decay is stronger in the case of a small number of edge channels, i.e. at higher B, in agreement with Ref. [66].

It is interesting to note that our theory predicts a fourth regime (AB*, see Table 5.1). It is characterized by the same equilibrium conductance pattern as the AB regime (Fig. 5.5, left), but in contrast to the latter, the power-law decay of the visibility oscillations corresponds to $\nu^* = 1$, and thus is independent of B. Such a behavior of the FPI has not yet been observed in the experiment.

Closing this section we have to mention that a crossover from the AB to the type-I CD regime (in our) terminology has been recently discussed in details in Ref. [92]. We note that our capacitance model is very similar in spirit to the one used in that paper. However, the important difference is that our approach takes explicitly into account quantum corrections to classical geometrical capacitances,

given by Eq. (5.10). As a result we obtain the extra type-II CD regime which may arise because of screening of Coulomb interaction by the fully transmitted edge channels.

5.3 Calculations

This section is devoted to the derivation of the above results using the formalism developed in Chapter 3. For simplicity we assume all edge channels to have the same length L and same velocity $|v_\mu| = v_F$ (with $v_\mu > 0$ in right-moving channels and $v_\mu < 0$ in left-moving ones). Consequently, all flight times $\tau = L/v_F$ are the same. Further, the scatterer 1 has the coordinate x^1 and scatterer 2 has the coordinate $x^2 = x^1 + L$ for each of the edges, see Fig. 5.7.
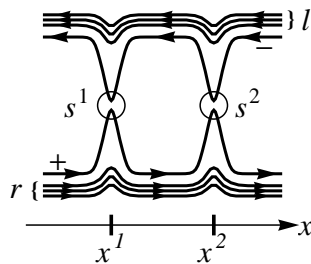
Figure 5.7: *Network model of the FPI.*

We remind us that two characteristic energy scales play an important role in our analysis, namely, Thouless energy $\epsilon_{\text{th}} = \tau^{-1}$ and charging energy $E_C = e^2/\bar{C}_e$ (or charge relaxation frequency $\omega_C = \frac{\nu^*}{\pi} E_C$), see Sec. 5.2. As has been discussed there, we will assume that the charging energy is much higher than the Thouless energy, and will consider voltages in the intermediate range between these two scales, $\omega_C \gg |eV| \gg \epsilon_{\text{th}}$.

5.3.1 Electrostatic Action

Our network consists of ν right-moving and ν left-moving chiral channels which we label with the subindex μ, see Fig. 5.7. The innermost right-moving channel ($\mu = +$) is coupled to the innermost left-moving channel ($\mu = -$) by two scatterers $i = 1, 2$ with 2×2-scattering matrices s^i. The remaining chiral channels (right-moving ones labeled $\mu = r1, \ldots, r(\nu-1)$, left-moving ones by $\mu = l1, \ldots, l(\nu-1)$) connect sources to drains without any possibility of tunneling.

Interaction is taken into account by the electrostatic model (5.1) described in the beginning. For simplicity we assumed that electrostatic coupling between all fully transmitted right-moving channels ($\mu = r1, \ldots, r(\nu-1)$) is strong such that they share a common electrostatic potential V_r. This enables us to merge them into one conductor (labeled $\alpha = r$). We proceeded in the same way with the fully transmitted left-moving channels ($\mu = l1, \ldots, l(\nu - 1)$ are now merged into $\alpha = l$) and the two innermost ones ($\mu = +, -$ are merged into $\alpha = e$). This reduces the number of charge degrees of freedom characterizing the edge channels down to three:

$$Q_e = \int \mathrm{d}x\, \bar{\psi}_+ \psi_+ + \int \mathrm{d}x\, \bar{\psi}_- \psi_-, \quad Q_r = \sum_{\kappa=1}^{\nu-1} \int \mathrm{d}x\, \bar{\psi}_{r\kappa} \psi_{r\kappa}, \quad Q_l = \sum_{\kappa=1}^{\nu-1} \int \mathrm{d}x\, \bar{\psi}_{l\kappa} \psi_{l\kappa}.$$

As a fourth conducting element, we introduce a central compressible island with total charge $Q_i = e(N_i + \nu\phi/\phi_0)$. While the second contribution, the charge in the ν fully occupied LLs of the central

region, is fixed by external parameters, the occupation N_i of the partially filled LL of the island is an (integer) degree of freedom to begin with. Since it is assumed to fluctuate via very slow tunneling, $\Gamma \ll \epsilon_{\text{th}}$, we will, however, treat it in a mean-field approximation.

The fermionic action we start with reads as follows

$$\mathcal{A}_0[\psi, \bar{\psi}, N_i] = \sum_\mu \int_{\mathcal{C}} \mathrm{d}t\mathrm{d}x \, \bar{\psi}_\mu \left(i\partial_t + iv_\mu\partial_x \right) \psi_\mu - \frac{1}{2} \sum_{\alpha\beta} \left(Q_\alpha - q_\alpha \right) \left(\tilde{C}^{-1} \right)_{\alpha\beta} \left(Q_\beta - q_\beta \right),$$

where the first sum extends over the 2ν chiral channels $\mu = r1, \ldots, r(\nu-1), l1, \ldots, l(\nu-1), +, -$ and the second one over the 4 conductors $\alpha, \beta = e, r, l, i$. The electrostatic part of $\mathcal{A}_0[\psi, \bar{\psi}, N_i]$ is, of course, a direct consequence of (5.1) and we refer to the corresponding section for definitions of q_α and $\tilde{C}$. Charges Q_α are, of course, dynamic, i.e. time-dependent, quantities, but for the sake of readability we leave time-dependence implicit (as we did with time integration in the above electrostatic action).

Our interest lies in interference effects which manifest themselves in tunneling corrections to current. Tunneling phases respond only to the Hubbard-Stratonovich field $\varphi = eV_e$ on the interfering edges (note that the electrostatic merging of channels $\mu = +, -$ allows us to use just one field $\varphi = \varphi_+ = \varphi_-$). The short-term goal of the present section is to integrate out all other degrees of freedom.

Potentials $V_c = (V_e, V_r, V_l)^t$**:**   First, we decouple the quadratic charge terms via a (multidimensional) Hubbard-Stratonovich transformation, thereby (re)introducing the potentials V_α on the conductors. Since we do not need the potential V_i on the island, we single out the island degrees of freedom beforehand, writing

$$\tilde{C}^{-1} = \begin{pmatrix} p_{cc} & p_{ci} \\ p_{ic} & p_{ii} \end{pmatrix}, \; V_{ci} = p_{ci}(Q_i - q_i). \tag{5.24}$$

The index c refers to the 3 indices e, r, l, that means p_{cc}, $p_{ci} = p_{ic}^t$, p_{ii} are 3×3-, 3×1-, and 1×1-matrices. With that the electrostatic contribution to the action reads

$$\mathcal{A}_{\text{int}}[\psi, \bar{\psi}, N_i] = -\frac{1}{2}(Q_i - q_i)^2 p_{ii} - \frac{1}{2}(Q_c - q_c)^t p_{cc}(Q_c - q_c) - V_{ci}^t(Q_c - q_c)$$

and becomes upon Hubbard-Stratonovich decoupling:

$$\mathcal{A}_{\text{int}}[\psi, \bar{\psi}, V_c, N_i] - \frac{1}{2}(Q_i - q_i)^2 p_{ii} + \frac{1}{2}(V_c - V_{ci})^t p_{cc}^{-1}(V_c - V_{ci}) - V_c^t(Q_c - q_c)$$
$$\text{with } V_c = (V_e, V_r, V_l)^t.$$

Integrating out Q_e**,** Q_r**,** Q_l**:**   Next, we integrate out the charges Q_e, Q_r, Q_l. As explained in Sections 2.2 and 3.1 charges and potentials are decoupled by a gauge transformation (2.15) which generates a tunneling term $\mathcal{A}_t$ (see below) and, according to the Dzyaloshinskii-Larkin theorem, quadratic and linear (in voltages) terms $V_\alpha^2 S_\alpha$ and $\bar{Q}_\alpha V_\alpha$. The former is given by the polarization operators (2.23), (2.24) and amounts for screening, thus an "enhancement" of the capacitances (in fact, the capacitances become complex, "Keldysh"- and energy-dependent, but in the static limit the corrections are indeed

positive). Then the retarded/advanced components of the "screening capacitances" read

$$S_\alpha^{r/a}(\omega) = -e^2 \sum_{\kappa=1}^{\nu-1} \int \mathrm{d}\xi_1 \mathrm{d}\xi_2 \, \Pi_{\alpha\kappa}^{r/a}(\omega,\xi_1,\xi_2) = \pm i(\nu-1)e^2 \frac{1-e^{\pm i\omega\tau}}{2\pi\omega}, \quad \alpha = r,l,$$

$$S_e^{r/a}(\omega) = -e^2 \sum_{\mu=\pm} \int \mathrm{d}\xi_1 \mathrm{d}\xi_2 \, \Pi_\mu^{r/a}(\omega,\xi_1,\xi_2) = \pm i2e^2 \frac{1-e^{\pm i\omega\tau}}{2\pi\omega}.$$

(5.25)

Charges injected from the reservoirs due to nonequilibrium boundary conditions (in excess of the equilibrium charge which is canceled by the positive background charge) are

$$\bar{Q}_r = (\nu-1)e\frac{eV_+\tau}{2\pi}, \quad \bar{Q}_l = (\nu-1)e\frac{eV_-\tau}{2\pi}, \quad \bar{Q}_e = e\frac{(eV_+ + eV_-)\tau}{2\pi}.$$

(5.26)

We collect them in the diagonal matrix $S = \mathrm{diag}\,(S_e, S_r, S_l)$ and the vector $\bar{Q}_c = (\bar{Q}_e, \bar{Q}_r, \bar{Q}_l)^t$. Subsequent elimination of charge degrees of freedom transforms $\mathcal{A}_{\mathrm{int}}[\psi, \bar{\psi}, V_c, N_i]$ into

$$\mathcal{A}_0[V_c, N_i] = -\frac{1}{2}\bar{p}_{ii}(Q_i - q_i)^2 + \frac{1}{2}V_c^t(p_{cc}^{-1} + S)V_c - V_c^t(\bar{Q}_c - q_c + p_{cc}^{-1}V_{ci})$$

$$\text{with } \bar{p}_{ii} = p_{ii} - p_{ic}p_{cc}^{-1}p_{ci}.$$

(5.27)

Integrating out V_r, V_l: The final and somewhat cumbersome step is to integrate out the voltages V_r, V_l. In order to do that we again split the degrees of freedom, writing

$$p_{cc}^{-1} = \begin{pmatrix} c_{ee} & c_{et} \\ c_{te} & c_{tt} \end{pmatrix}, \quad S = \begin{pmatrix} S_e & \\ & S_t \end{pmatrix},$$

(5.28)

where the index t refers to the 2 indices r, l, and c_{ee}, $c_{et} = c_{te}^t$, c_{tt} are corresponding 1×1-, 1×2-, and 2×2-matrices. The action then reads

$$\mathcal{A}_0[V_c, N_i] = -\frac{1}{2}\bar{p}_{ii}(Q_i - q_i)^2 + \frac{1}{2}(c_{ee} + S_e)V_e^2 - V_e(\bar{Q}_e - q_e + c_{ee}V_{ei} + c_{et}V_{ti})$$

$$+ \frac{1}{2}V_t^t(c_{tt} + S_t)V_t - V_t^t(\bar{Q}_t - q_t + c_{te}V_{ei} + c_{tt}V_{ti} - c_{te}V_e).$$

Performing the Gaussian integration over V_r, V_l is a straightforward, albeit cumbersome calculation which in the end yields,

$$\mathcal{A}_0[V_e, N_i] = -\frac{1}{2\bar{C}_i}(Q_i - q_i)^2 - (\bar{Q}_t - q_t)^t \bar{p}_{ti}(Q_i - q_i) + \frac{1}{2}\bar{C}_e^* V_e^2 - V_e(\bar{Q}_e - q_e + x_{et}(\bar{Q}_t - q_t) + x_{ei}(Q_i - q_i))$$

(5.29)

where we have introduced the effective capacitances and coupling strengths

$$\bar{C}_i^{-1} \equiv p_{ii} - p_{ic}p_{cc}^{-1}p_{ci} + (p_{ie}c_{et} + p_{it}c_{tt})(c_{tt} + S_t)^{-1}(c_{te}p_{ei} + c_{tt}p_{ti}),$$

$$\bar{C}_e^* \equiv c_{ee} + S_e - c_{et}(c_{tt} + S_t)^{-1}c_{te}, \quad \bar{C}_e \equiv \bar{C}_e^*\Big|_{S_e = S_r = S_l = 0}$$

$$x_{et} \equiv -c_{et}(c_{tt} + S_t)^{-1},$$

$$x_{ei} \equiv c_{ee}p_{ei} + c_{et}p_{ti} - c_{et}(c_{tt} + S_t)^{-1}(c_{te}p_{ei} + c_{tt}p_{ti}),$$

$$\bar{p}_{ti} \equiv (c_{tt} + S_t)^{-1}(c_{te}p_{ei} + c_{tt}p_{ti}).$$

Regimes AB, CD I, CD II: In the limits of very strong, i.e. $C_{\alpha e} \ll C_{eg} + S_e$, and very weak, i.e.

$$C_{\alpha e} \gg \frac{(C_{\alpha g} + S_\alpha)^2}{C_{eg} + C_{rg} + C_{lg} + S_e + S_r + S_l},$$

coupling between fully transmitted edges $\alpha = r, l$ and interfering edge e the expressions simplify to

	Strong coupling	Weak coupling
$\bar{C}_i$	$C_{ei} + C_{ig}$	$C_{ei} + C_{ri} + C_{li} + C_{ig}$
$\bar{C}_e^*$	$C_{eg} + S_e + C_{ig} - C_{ig}^2/\bar{C}_i$	$C_{eg} + C_{rg} + C_{lg} + S_e + S_l + S_r + C_{ig} - C_{ig}^2/\bar{C}_i$
x_{et}	$\begin{pmatrix} 0 & 0 \end{pmatrix}$	$\begin{pmatrix} 1 & 1 \end{pmatrix}$
x_{ei}	$C_{ei}/\bar{C}_i$	$(C_{ei} + C_{ri} + C_{li})/\bar{C}_i$
$\bar{p}_{ti}$	0	$0,$

and using Eqs. (5.24)-(5.28), the action becomes

$$\mathcal{A}_0[\varphi, N_i] = \frac{1}{2} \int_{\mathcal{C}} dt\, dt'\, \varphi(t) V^{-1}(t-t') \varphi(t') - \int_{\mathcal{C}} dt\, \varphi(t) N_0(t) - \frac{1}{2\bar{C}_i}(Q_i - q_i)^2 \tag{5.30}$$

$$\text{with} \quad V^{r/a}(\omega) = E_C \frac{\omega}{\omega \pm i\omega_C(1 - e^{\pm i\omega\tau})},$$

$$N_0 \equiv \frac{\nu^*}{\pi} \frac{eV_+ + eV_-}{2} \tau - \frac{|e|V_g}{E_C} - \frac{\bar{C}_{ei}}{\bar{C}_i} Q_i/|e| \tag{5.31}$$

Here $\bar{C}_i$, $\bar{C}_e$, $\bar{C}_{eg}$, $\bar{C}_{ei}$, and ν^* are given in Sect. 5.2.2 (Eq. (5.11) and Table 5.1).

5.3.2 Tunneling Action

To construct the tunneling action $\mathcal{A}_t[\varphi]$ in lowest order we use Eq. (3.10) which makes it necessary to identify the paths $(ij; \mu\nu)$. Only the innermost chiral channels $\mu, \nu = \pm$ allow for tunneling between each other at scatterers $i, j = 1, 2$ which gives 4 classes: $(11; +-)$, $(22; +-)$, $(12; +-)$, and $(21; +-)$. Classical phases are accumulated due to magnetic flux ϕ:

$$\Delta\phi_{+-}^{11} = \Delta\phi_{+-}^{22} = 0, \quad \Delta\phi_{+-}^{12} = -\Delta\phi_{+-}^{21} = -2\pi\phi/\phi_0.$$

At zero temperature the distribution functions read $f_\pm^{\gtrless}(t) = e^{-ieV_\pm t} f_0^{\gtrless}(t)$ with Fermi distribution function $f_0^{\gtrless}(t)$. Writing for short $r_i \equiv s_{-+}^i$, $\chi \equiv \chi_+ - \chi_-$, $\epsilon_{ij} = \epsilon_{ij3}$ (the right-hand side being the 3-dimensional Levi-Civita symbol), and $\Pi_{ij} \equiv \Pi_{ij;+-}$ we obtain the tunneling operators (3.11, 3.12)

$$\Pi_{ij}^{\gtrless}(t) = -r_i \bar{r}_j\, e^{\pm i\chi}\, e^{-i\epsilon_{ij}\left[2\pi\phi/\phi_0 + (eV_+ + eV_-)\tau\right]}\, e^{-ieVt} f_0^{\gtrless}(t + \epsilon_{ij}\tau) f_0^{\lessgtr}(t - \epsilon_{ij}\tau), \tag{5.32}$$

$$\Pi_{ij}^{T/\tilde{T}}(t) = \left[\theta(\pm t)\Pi_{ij}^{>}(t) + \theta(\mp t)\Pi_{ij}^{<}(t)\right]_{\chi\equiv 0}. \tag{5.33}$$

Writing the tunneling phases $\Phi \equiv \Phi_{+-}$ the tunneling action reads

$$\mathcal{A}_t[\varphi] = -i \sum_{i,j=1,2} \int dt_1 dt_2 \begin{pmatrix} e^{-i\Phi^f(x^i, t_1)} & e^{-i\Phi^b(x^i, t_1)} \end{pmatrix} \begin{pmatrix} \Pi_{ij}^T(t_{12}) & -\Pi_{ij}^{<}(t_{12}) \\ -\Pi_{ij}^{>}(t_{12}) & \Pi_{ij}^{\tilde{T}}(t_{12}) \end{pmatrix} \begin{pmatrix} e^{i\Phi^f(x^j, t_2)} \\ e^{i\Phi^b(x^j, t_2)} \end{pmatrix} \tag{5.34}$$

with $t_{12} \equiv t_1 - t_2$. According to Sect. 3.2 and Eq. (2.16) the tunneling phases are related to the potential φ via

$$\Phi(x^i, t) = \Theta_-(x^i, t) - \Theta_+(x^i, t) = \int_{\mathcal{C}} \mathrm{d}t' \, \mathcal{D}_{+-}(x^i; t, t')\varphi(t') \tag{5.35}$$

$$\text{with} \quad \mathcal{D}_{+-}(x; t, t') \equiv - \int_{x_1}^{x_2} \mathrm{d}x' \, D_{0-}(x - x'; t, t') + \int_{x_1}^{x_2} \mathrm{d}x' \, D_{0+}(x - x'; t, t')$$

with bare particle-hole propagator $D_{0\mu}$ (Eq. (2.18)). Note that x' is integrated over because the potential $\varphi(x', t) = \varphi(t)$ in our model does not vary in space.

Defining $\epsilon_i = \pm$ for $i = 1, 2$ retarded and advanced components of $\mathcal{D}_{+-}$ read in energy representation

$$\mathcal{D}_{+-}^{r/a}(\omega; x^i) = \pm i\epsilon_i \frac{e^{\pm i\omega\tau} - 1}{\omega}. \tag{5.36}$$

5.3.3 Current in Instanton Approximation

Current is measured via the counting fields χ in the tunneling polarization operators (5.32). We use the adiabatic approximation where measuring time t_0 is much larger than all intrinsic time scales of the system and transient effects due to switching of the counting fields are negligible. The tunneling correction to current is the derivative

$$I_t = -i\frac{e}{t_0}\partial_\chi \ln \mathcal{Z}\Big|_{\chi=0} = \sum_{i,j=1,2} \left(I_{ij}^< - I_{ij}^> \right) \tag{5.37}$$

$$\text{with} \quad I_{ij}^{\alpha\beta} = \frac{e}{t_0} \int \mathrm{d}t_1 \mathrm{d}t_2 \int \mathcal{D}\varphi \sum_{\{N_i\}} e^{i\mathcal{A}_0[\varphi, N_i] + i\mathcal{A}_t[\varphi]} \, e^{-i\Phi^\alpha(x^i, t_1)} \Pi_{ij}^{\alpha\beta}(t_{12}) e^{i\Phi^\beta(x^j, t_2)}\Big|_{\chi=0}. \tag{5.38}$$

The average $\int \mathcal{D}\varphi \sum_{\{N_i\}}$ is treated in real-time instanton approximation as outlined in Sect. 3.3:

$$I_{ij}^{\alpha\beta} \approx \frac{e}{t_0} \int \mathrm{d}t_1 \mathrm{d}t_2 \, e^{i\tilde{\mathcal{A}}_t[\varphi_*]} \left\langle e^{-i\Phi^\alpha(x^i, t_1)} \Pi_{ij}^{\alpha\beta}(t_{12}) e^{i\Phi^\beta(x^j, t_2)} \right\rangle_0 \bigg|_{\chi=0, \, N_i=N_{i*}}$$

$$= \frac{e}{t_0} \int \mathrm{d}t_1 \mathrm{d}t_2 \, e^{i\tilde{\mathcal{A}}_t[\varphi_*]} e^{-i\Phi_0(x^i) + i\Phi_0(x^j)} \, \tilde{\Pi}_{ij}^{\alpha\beta}(t_{12}) \bigg|_{\chi=0, \, N_i=N_{i*}} \tag{5.39}$$

As always $\langle \ldots \rangle_0$ denotes averaging with respect to $\mathcal{A}_0[\varphi, N_{i*}]$ given in (5.30). Because of the linear-in-φ contribution potential φ and hence tunneling phase Φ have non-vanishing expectation values $\varphi_0 = \varphi_0[N_i]$, $\Phi_0 = \Phi_0[N_i]$ which minimize $\mathcal{A}_0[\varphi, N_i]$ for given N_i. At the saddle-point N_{i*} in turn minimizes $\mathcal{A}_0[\varphi_0[N_i], N_i]$. For strong coupling $\omega_C\tau \gg 1$ the mean-field reads

$$\varphi_0 = \frac{1}{1 + \omega_C\tau} \left[eV_g + \frac{eV_+ + eV_-}{2}\omega_C\tau + E_C\frac{\bar{C}_{ei}}{\bar{C}_i}(N_{i*} + \nu\phi/\phi_0) \right], \tag{5.40}$$

$$\Phi_0(x^{1/2}) = \mp\tau\varphi_0 \quad \Rightarrow \quad -i\Phi_0(x^k) + i\Phi_0(x^l) = 2i\epsilon_{kl}\tau\varphi_0$$

with $N_{i*} \in \mathbb{Z}$ minimizing the electrostatic energy E_i, (5.13).

Due to the presence of the source term $i\mathcal{A}_J[\varphi] = -i\Phi^\alpha(x^i, t_1) + i\Phi^\beta(x^j, t_2)$ the instanton phase $\Phi_* = \Phi_0 + \delta\Phi_*$, (3.16), deviates from the mean-field by

$$\delta\Phi_*^\gamma(x^k, t) = D_\Phi^{\gamma\alpha}(t - t_1, x^k, x^i) - D_\Phi^{\gamma\beta}(t - t_2, x^k, x^j). \tag{5.41}$$

The instanton action thus reads

$$i\tilde{\mathcal{A}}_t[\varphi_*] = \sum_{kl}\sum_{\gamma\delta} \sigma_{\gamma\delta} \int \mathrm{d}t_3 \mathrm{d}t_4 \, e^{-i\Phi_0(x^k)+i\Phi_0(x^l)} e^{-i\delta\Phi_*^\gamma(x^k,t_3)+i\delta\Phi_*^\delta(x^l,t_4)} \tilde{\Pi}_{kl}^{\gamma\delta}(t_3-t_4) \tag{5.42}$$

We will evaluate the time integrals in (5.39) and (5.42) approximately. They will be dominated by the singularities of the instanton and the polarization operators. To identify and characterize them more precisely it is indispensable to compute the phase correlator $D_\Phi \equiv -i\left\langle (\Phi-\Phi_0)(\Phi-\Phi_0) \right\rangle_0$. It will turn out that the singularities (branchcuts) of $\tilde{\Pi}_{kk}(t)$ around $t \sim 0$ and of $\tilde{\Pi}_{kl}(t)$, $k \neq l$, around $t \sim \pm\tau$ dominate all integrals.

5.3.4 Correlation Functions

In this section we calculate the correlation function of the tunneling phases $\Phi(x^i)$ which according to (5.35) is $D_\Phi = -\mathcal{D}_{+-}V\mathcal{D}_{+-}$. Details of the calculation are not important for the rest of the paper and may be safely skipped. The final results for zero temperature and the strong coupling limit, $\omega_C\tau \gg 1$, are

$$D_\Phi^{\gtrless}(t=0,x^i,x^j) = D_\Phi^{T/\tilde{T}}(0,x^i,x^j) \equiv D_\Phi(0;x^i,x^j) = A_{ij}\frac{i}{\nu^*}\left(\gamma + \ln[\omega_C\tau]\right) \tag{5.43}$$

and

$$D_\Phi^{\gtrless}(t,x^i,x^j) = A_{ij}\frac{i}{2\nu^*}\left\{ \ln\left[\frac{a \pm i(t-\tau)}{a \pm it}\right] + \ln\left[\frac{a \pm i(t+\tau)}{a \pm it}\right]\right\}. \tag{5.44}$$

for large times, $|\omega_C t| \gg 1$.

We start the computation by combining (5.31) and (5.36),

$$D_\Phi^r(\omega,x_i,x_j) = -\mathcal{D}_{+-}^r(\omega;x^i)V^r(\omega)\mathcal{D}_{+-}^r(\omega;x^j) = -iA_{ij}\frac{\pi}{\nu^*}\frac{i\omega_C\left(1-e^{i\omega\tau}\right)}{\omega\left[\omega+i\omega_C\left(1-e^{i\omega\tau}\right)\right]}\left(e^{i\omega\tau}-1\right)$$

with $A_{ij} = \epsilon_i\epsilon_j$. In time representation the relevant correlation functions are the $\gtrless$-components which, at zero temperature, read

$$D_\Phi^{\gtrless}(t) = \pm \int\frac{\mathrm{d}\omega}{2\pi} e^{-i\omega t}\left[D_\Phi^r(\omega) - D_\Phi^a(\omega)\right]\theta(\pm\omega)$$

$$= -A_{ij}\frac{i}{2\nu^*}\left\{ J^{\gtrless}(t-\tau) - J^{\gtrless}(t) + \left[J^{\gtrless}(-t^*-\tau)\right]^* - \left[J^{\gtrless}(-t^*)\right]^*\right\} \tag{5.45}$$

$$\text{with}\quad J^{\gtrless}(t) \equiv \int\mathrm{d}\omega\left[\pm\theta(\pm\omega)\right]\frac{i\omega_C\left(1-e^{i\omega\tau}\right)}{\omega\left[\omega+i\omega_C\left(1-e^{i\omega\tau}\right)\right]}\left(e^{-i\omega t}-1\right). \tag{5.46}$$
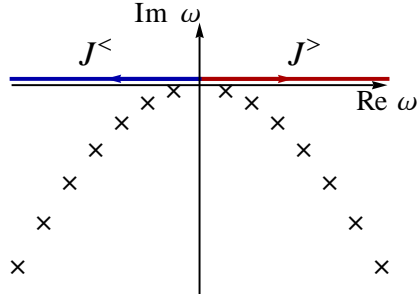
Figure 5.8: *Analytic structure of the integrand in (5.46): it is analytic in the upper half of the ω-plane and possesses poles in the lower half. Contours of integration for $J^>$ and $J^<$ are indicated by arrows.*

The integral defining $J^>$ ($J^<$) is perfectly convergent for all times with non-positive (non-negative) imaginary part, $\mathrm{Im}\, t \leq 0$ ($\mathrm{Im}\, t \geq 0$), thus ensuring the analyticity of $J^{\gtrless}$ in this region. Apparently, we have $J^{\gtrless}(t)^* = J^{\lessgtr}(t^*)$.

First, we perform the integration for $\mathrm{Re}\, t < 0$. Under this assumption the contour of integration can be rotated into the upper half of the complex ω-plane where the integrand is analytic (see Fig. 5.8). Defining dimensionless time and charging frequency, $z \equiv -t/\tau$, and $y \equiv \omega_C \tau$, respectively, and integrating along the imaginary axis, one obtains for $y \gg 1$

$$J^{\gtrless}(t) = \int_0^\infty \mathrm{d}s \left(e^{-zs} - 1 \right) \frac{y\left(1 - e^{-s}\right)}{s\left[s + y\left(1 - e^{-s}\right)\right]} \approx \int_0^\infty \mathrm{d}s \left(e^{-zs} - 1 \right) \frac{y}{s\left(s + y\right)}$$

$$= -e^{yz}\Gamma(0, yz) - \gamma - \ln yz \equiv g(yz) \quad (5.47)$$

with the incomplete Gamma function $\Gamma(\alpha, x) = \int_x^\infty \mathrm{d}s\, e^{-s} s^{\alpha-1}$, $x \in \mathbb{R}$, and the Euler-Mascheroni constant γ.

The asymptotic behavior of g is

$$g(yz) \equiv \to (-1 + \gamma + \ln yz)yz, \qquad\qquad yz \to 0+,$$

$$\to -\gamma - \ln yz - \frac{1}{yz}, \qquad\qquad yz \to \infty. \quad (5.48)$$

We now proceed with the case $\mathrm{Re}\, t > 0$ where the contour of integration can be rotated into the lower half of the complex ω-plane. In contrast to the previous case the integrand does possess poles in this region (see Fig. 5.8), around which, therefore, the integral has to be taken additionally. Since both pole and imaginary axis contributions, $J_0^{\gtrless}$ and $J_1^{\gtrless}$ respectively, separately diverge for large ω we have to introduce an auxiliary ultraviolet cutoff, $e^{\mp a\omega}$, $a = \tilde{a}\tau$. Then, defining $z \equiv t/\tau$, the imaginary axis contribution reads for $y = \omega_C \tau \gg 1$

$$J_1^{\gtrless}(t) = -y \int_0^\infty \mathrm{d}s \frac{1 - e^s}{s\left[s - y\left(1 - e^s\right)\right]} \left(e^{-sz} - 1 \right) e^{\pm is\tilde{a}} \approx \int_0^\infty \mathrm{d}s \frac{e^{-sz} - 1}{s} e^{\pm is\tilde{a}} = -\ln \frac{\tilde{a} \pm iz}{\tilde{a}}.$$

The poles are defined as roots of equation $\omega + i\omega_C\left(1 - e^{i\omega\tau}\right) = 0$, $\omega \neq 0$, and writing $x = i\omega\tau$, they are given by $x_n = y - W_{-n}(ye^y)$, $n \in \mathbb{Z}\backslash\{0\}$, where the product log function is defined by

$W_n(x)e^{W_n(x)} = x$. We choose the numbering such that $\operatorname{Im} x_{n+1} > \operatorname{Im} x_n$, $\operatorname{Im} x_1 > 0 > \operatorname{Im} x_{-1}$. As can be deduced already from the defining equation the roots satisfy $\operatorname{Re} x_n \geq 0$. One may show that in two limiting cases one has

$$x_n \to 2\pi i n \frac{y}{1+y} + 2\left(\frac{n\pi}{y}\right)^2, \qquad\qquad |n| \ll \frac{y}{2\pi}, \qquad (5.49)$$

$$\to 2\pi i n + \ln\left[-i\frac{2\pi n}{y}\right], \qquad\qquad |n| \gg \frac{y}{2\pi}. \qquad (5.50)$$

To proceed further, we note that $\frac{\mathrm{d}}{\mathrm{d}\omega}\left[\omega + i\omega_C\left(1 - e^{i\omega\tau}\right)\right]_{\omega_n} = 1 + y - x_n$. Therefore the residues read

$$\operatorname{Res}_{\omega_n}\left[\frac{i\omega_C\left(1 - e^{i\omega\tau}\right)}{\omega\left[\omega + i\omega_C\left(1 - e^{i\omega\tau}\right)\right]}\left(e^{-i\omega\tau} - 1\right)e^{\mp a\omega}\right] = -\frac{1}{1+y-x_n}\left(e^{-zx_n} - 1\right)e^{\pm i\tilde{a}x_n}.$$

Taking into account that for $J^>$ $(J^<)$ only poles ω_n with positive (negative) real part contribute, $n \geq 1$ $(n \leq -1)$, we obtain for the pole contribution

$$J_0^{\gtrless}(t) = -\sum_{n=1}^{\infty}\frac{\mp 2\pi i}{1+y-x_n}\left(e^{-zx_{\pm n}} - 1\right)e^{\pm i\tilde{a}x_{\pm n}}.$$

This expression cannot be evaluated analytically further, but analytical approximations are possible by substituting the poles x_n by their asymptotic behavior, Eqs. (5.49), (5.50).

We convince ourselves that the short-time divergence, which forced us to introduce the ultraviolet cutoff $\tilde{a}$, is in fact merely an artifact of our method of calculation, and is cured by taking the sum of $J_1^{\gtrless} + J_0^{\gtrless}$. In other words, $J_0^{\gtrless}$ has to diverge logarithmically for $z \to 0$ as well. Of course, any divergence originates from terms with large $|n| \to \infty$, such that for our present purpose we may safely use the approximation (5.50) which yields for $z \to 0$

$$J_0^{\gtrless}(t) \sim -\sum_{n=1}^{\infty}\left[\left(\pm i\frac{2\pi n}{y}\right)^z e^{-2\pi n(\tilde{a}\pm iz)} - e^{-2\pi n\tilde{a}}\right]\frac{1}{n} \approx -\ln\frac{1 - e^{-2\pi\tilde{a}}}{1 - e^{-2\pi(\tilde{a}\pm iz)}} \approx \ln\frac{\tilde{a} \pm iz}{\tilde{a}},$$

which is exactly what we expected to find. Although the approximation is good enough to estimate the divergency, it is not reliable for obtaining finite offsets. Using $\ln\tilde{a} = \ln\frac{1-e^{-2\pi\tilde{a}}}{2\pi}$ we can single out all $\tilde{a}$-dependances,

$$J_0^{\gtrless}(t) + J_1^{\gtrless}(t) = -\ln\left[\pm 2\pi iz\right] - \sum_{n=1}^{\infty}\frac{\mp 2\pi i}{1+y-x_{\pm n}}e^{-zx_{\pm n}}$$

$$+ \sum_{n=1}^{\infty}\left[\frac{\mp 2\pi i}{1+y-x_{\pm n}}\left(e^{\pm i\tilde{a}(x_{\pm n}\mp 2\pi in)} - 1\right) + \frac{x_{\pm n}\mp 2\pi in - 1 - y}{\left(1+y-x_{\pm n}\right)n}\right]e^{-2\pi\tilde{a}n}.$$

The $\tilde{a}$-contribution is just a constant about which we will not care too much presently. For the moment we will fix it manually, by requiring a good agreement between $J_0^{\gtrless}(t) + J_1^{\gtrless}(t)$ and the analytical
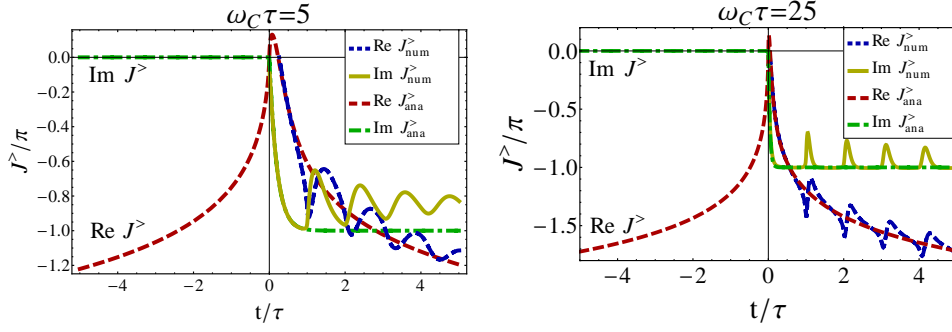
Figure 5.9: $J^>$ *(real (*blue*) and imaginary (*yellow*) part), numerically evaluated and manually fixed, and analytical continuation $\sim g(-\omega_C(t-i0))$ (real (*red*) and imaginary (*green*) part).*

continuation $g(-\omega_C(t\mp i0))$ of the result (5.47) obtained for $\mathrm{Re}\, t < 0$. Fig. 5.9 shows the corresponding plots for $y = 5$ and $y = 25$.

A numerical study shows that the oscillating contributions decrease in width for large y (while their amplitude remains in the order of unity) and may be therefore neglected in the following. We approximate $J^{\gtrless}$ by smooth functions $g^{\gtrless}$, required to be analytical for $\mathrm{Im}\, t \le 0$ ($\mathrm{Im}\, t \ge 0$) and

$$g^{\gtrless}(t) = -\, e^{-\omega_C t}\Gamma(0, -\omega_C t) - \gamma - \ln\left[-\omega_C t\right], \qquad\qquad \mathrm{Re}\, t < 0.$$

Since the voltage is assumed to be low $|eV| \ll \omega_C$ one needs correlation functions for long times $|\omega_C t| \gg 1$ only and we can use the asymptotic expression (5.48) for g. Therefore introducing a short-time cutoff $a \sim \omega_C^{-1}$ and writing $t_\mp \equiv t \mp ia$ we use the following approximate relation in our subsequent analysis

$$J^{\gtrless}(t) \approx g^{\gtrless}(t) = -\gamma - \ln[-\omega_C t_\mp],$$

which together with (5.45) and $J^{\gtrless}(t = 0) = 0$ gives Eqs. (5.44) and (5.43).

5.3.5 Renormalized Polarization Operators

In the real-time instanton approximation, Sect. 3.3, virtual fluctuations around the instanton are taken into account by dressing the tunneling polarization operators, Eq. (3.20). The phase factor is

$$e^{i\left[D^{\gtrless}_{\Phi\infty}(t,x_k,x_l)-D_\Phi(0)\right]} = e^{\frac{\gamma}{\nu^*}}\,(\omega_C\tau)^{\frac{1}{\nu^*}}\left[\frac{a \pm it}{a \pm i(t-\tau)}\right]^{\frac{A_{kl}}{2\nu^*}}\left[\frac{a \pm it}{a \pm i(t+\tau)}\right]^{\frac{A_{kl}}{2\nu^*}}.$$

and dressing of the bare polarization operators (5.32) yields (f_0 can be found in (3.1); χ is put to 0)

$$\tilde{\Pi}^{\gtrless}_{kl}(t) = -r_k\bar{r}_l\frac{(\omega_C\tau)^{\frac{1}{\nu^*}}}{(2\pi)^2}e^{\frac{\gamma}{\nu^*}}e^{-i\epsilon_{kl}\left[2\pi\phi/\phi_0+(eV_++eV_-)\tau\right]}e^{-ieVt}$$

$$\times \begin{cases} \left[a \pm it\right]^{\frac{1}{\nu^*}-2}\left[a \pm i(t-\tau)\right]^{-\frac{1}{2\nu^*}}\left[a \pm i(t+\tau)\right]^{-\frac{1}{2\nu^*}}, & k = l, \\ \left[a \pm it\right]^{-\frac{1}{\nu^*}}\left[a \pm i(t-\tau)\right]^{\frac{1}{2\nu^*}-1}\left[a \pm i(t+\tau)\right]^{\frac{1}{2\nu^*}-1}, & k \ne l, \end{cases}$$
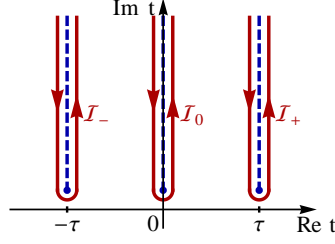
Figure 5.10: *Analytic structure of $\mathcal{I}$ in the complex t-plane: while the function is analytic in the lower half, it has poles or branchcuts in the upper half, residing at $t^* = 0, \tau, -\tau$. Integrating $\tilde{\Pi}_{kl}^{\gtrless}(t)$ "around" these, i.e. along drawn contours, gives $\tilde{P}_{kl}^{\gtrless}(t^*)$.*

The dressed polarization operators exhibit non-analytic behavior (poles or branchcuts) around $t \approx 0, \pm\tau$. The double time-integrals (5.39) and (5.42) can be approximately expressed in terms of the integrals $\tilde{P}_{kl}^{\gtrless} \equiv \int \mathrm{d}t\, \tilde{\Pi}_{kl}^{\gtrless}(t)$. Before we demonstrate this statement in the next section, we will devote the remainder of the current section to the evaluation of $\tilde{P}_{kl}^{\gtrless}$.

We focus first on $\tilde{P}_{kl}^{>}$. To deal with both $k = l$ and $k \neq l$ simultaneously we generically consider the function

$$\mathcal{I}(t, eV) \equiv e^{-ieVt} \left[a + it\right]^\eta \left[a + i(t - \tau)\right]^\lambda \left[a + i(t + \tau)\right]^\lambda,$$
$$0 > \eta > -2, \quad 0 > \lambda > -1, \quad 2\lambda + \eta = -2.$$

Apparently, $\mathcal{I}$ has branchcuts only in the upper half of the complex t-plane (Fig. 5.10), i.e. the integral $\int \mathrm{d}t\, \mathcal{I}(t, eV)$ vanishes whenever the integration contour can be closed in the lower half. Therefore, we assume the nontrivial case $eV < 0$. The real-time integrals $\int \mathrm{d}t\, \mathcal{I}(t, eV) = \mathcal{I}_- + \mathcal{I}_0 + \mathcal{I}_+$ consist of three contributions which correspond to integrals along closed contours in the complex t-plane. With $z \equiv |eV\tau| \gg 1$ the contour integral around $-\tau$ is

$$\mathcal{I}_- \approx -2\pi \frac{2^\lambda}{\Gamma(-\lambda)} e^{-iz} e^{i\frac{\pi}{2}\lambda} |eV| z^{-2-\lambda}.$$

Similarly, one obtains the integral around $+\tau$, $\mathcal{I}_+ = \mathcal{I}_-^*$.

The situation is slightly less trivial for the integral around $t \approx 0$, since it may be that $\eta = -1$, i. e. we have a first order pole, or $\eta > -1$, giving rise to a strong divergence. In the first case the integral gives

$$\mathcal{I}_0 = 2\pi \left[a - i\tau\right]^\lambda \left[a + i\tau\right]^\lambda \approx \frac{2\pi}{\tau}.$$

In the second case we have to go around the singularity with care. We explicitly kept the distance $\delta \ll a$ to the integration contour from the branchcut in the calculations. After weakening the degree of divergence by partial integration we may safely put $\delta \to 0$ and obtain

$$\mathcal{I}_0 \approx 2\pi \Gamma(-\eta)^{-1} |eV| z^{2\lambda}.$$

Note that in this approximation $\mathcal{I}_0$ is continuous in $\eta = -1$.

For the direct terms, $k = l$, we have $\eta = \frac{1}{\nu^*} - 2$, $\lambda = -\frac{1}{2\nu^*}$, i. e. $\eta + \lambda = \frac{1}{2\nu^*} - 2$, $2\lambda = -\frac{1}{\nu^*}$, hence for large voltages, $z \gg 1$, $\mathcal{I}_0$ is dominant. For the interference terms, $k \neq l$, we set $\eta = -\frac{1}{\nu^*}$, $\lambda = \frac{1}{2\nu^*} - 1$, i. e. $\eta + \lambda = -\frac{1}{2\nu^*} - 1$, $2\lambda = \frac{1}{\nu^*} - 2$, hence the contributions $\mathcal{I}_\pm$ dominate over $\mathcal{I}_0$ if and only if $\nu^* > \frac{3}{2}$.

As $\int dt\, \mathcal{I}(t, eV)$ splits into three contributions, so do $\tilde{P}_{kl}^{\gtrless} = \tilde{P}_{kl}^{\gtrless}(-\tau) + \tilde{P}_{kl}^{\gtrless}(0) + \tilde{P}_{kl}^{\gtrless}(+\tau)$. Note that $\tilde{\Pi}^{<}(t) = \tilde{\Pi}^{>}(-t)\Big|_{eV \mapsto -eV}$ implies $\tilde{P}_{kl}^{<}(t^*) = \tilde{P}_{kl}^{>}(-t^*)\Big|_{eV \mapsto -eV}$.

Summarizing, for $z \gg 1$ the dominant integrals of the dressed polarization operators are

$$\tilde{P}_{kk}^{\gtrless}(t^* = 0) = -\,\theta(\mp eV)\frac{|eV|}{2\pi}\, R_{k*}(eV), \tag{5.51}$$

$$\tilde{P}_{kl}^{\gtrless}(t^* = \kappa\tau) = -\,\theta(\mp eV)\frac{1}{2\pi\tau}\, R_{12*}(eV)\, \frac{1}{2}e^{i\kappa\left[|eV\tau| - \frac{\pi}{2}\left(1 + \frac{1}{2\nu^*}\right)\right]}e^{-i\epsilon_{kl}\left[2\pi\phi/\phi_0 + (eV_+ + eV_-)\tau\right]}, \tag{5.52}$$

$$\tilde{P}_{kl}^{\gtrless}(t^* = 0) = -\,\theta(\mp eV)\frac{1}{2\pi\tau}\, r_k\bar{r}_l\, |eV\tau|^{\frac{1}{\nu^*} - 1}\frac{(\omega_C\tau)^{\frac{1}{\nu^*}}e^{\frac{\gamma}{\nu^*}}}{\Gamma(\frac{1}{\nu^*})}\, e^{-i\epsilon_{kl}\left[2\pi\phi/\phi_0 + (eV_+ + eV_-)\tau\right]} \tag{5.53}$$

with $k \neq l$, $\kappa = \pm$. In the case of $\nu^* > \frac{3}{2}$ the contribution (5.52) is dominant, while in the case $\nu^* < \frac{3}{2}$ it is (5.53). We have used definitions (5.9) of the renormalized reflection coefficients and assumed for simplicity $r_1\bar{r}_2$ to be real.

5.3.6 Instanton Action and Current

We have now everything in place to finalize the calculation of the instanton action (5.42) and the current (5.39). The instanton phases $\delta\Phi_*^\gamma(x^k, t) = D_\Phi^{\gamma\alpha}(t - t_1, x^k, x^i) - D_\Phi^{\gamma\beta}(t - t_2, x^k, x^j)$ and thus $i\tilde{\mathcal{A}}_t[\varphi_*]$ are functions of the times t_1, t_2 over which to integrate in (5.39). A shift of integration variables $t_{3/4} \mapsto t_{3/4} + t_2$ in (5.42) immediately shows that the action $i\tilde{\mathcal{A}}_t[\varphi_*]$ is a function of the difference $t \equiv t_1 - t_2$. Hence, the whole integrand of (5.39) is purely a function of $t = t_1 - t_2$. Performing a change of integration variables $(t_1, t_2) \mapsto (t = t_1 - t_2, T = (t_1 + t_2)/2)$, the integral over the center-of-mass time T is seemingly divergent. This simply amounts to infinite transferred charge $Q = \int_0^{t_0} dT\, I$ for a steady current I and an infinite measuring time $t_0 \to \infty$. Since our interest lies in the steady current (not on transient effects due to switching of the measuring device) we identify $\int dt_1 dt_2 = \int dT\, dt = t_0 \int dt$ upon which the current becomes

$$I_{ij}^{\alpha\beta} = e \int dt\, e^{i\tilde{\mathcal{A}}_t[\varphi_*]}\Big|_{t_1 - t_2 = t}\, e^{2i\epsilon_{ij}\tau\varphi_0}\, \tilde{\Pi}_{ij}^{\alpha\beta}(t)\Big|_{\chi = 0}. \tag{5.54}$$

Given that $i\tilde{\mathcal{A}}_t[\varphi_*]$ is non-divergent, large contributions to this current stem from the singularities of $\tilde{\Pi}_{ij}^{\alpha\beta}(t)$ which we identified in the previous section. The case $\nu^* = 1$, i.e. $\nu^* < \frac{3}{2}$, needs to be treated more carefully and will be considered toward the end of this section. Focusing for now on $\nu^* \geq 2$, dominant contributions are then

$$e^{-1}I_{ij}^{\alpha\beta} \approx \begin{cases} e^{i\tilde{\mathcal{A}}_t[\varphi_*]}\Big|_{t_1 - t_2 \approx 0} \tilde{P}_{ii}^{\alpha\beta}(t^* = 0), & i = j, \\[2mm] e^{i\tilde{\mathcal{A}}_t[\varphi_*]}\Big|_{|t_1 - t_2| \approx \tau} e^{2i\epsilon_{ij}\tau\varphi_0}\left(\tilde{P}_{ij}^{\alpha\beta}(t^* = +\tau) + \tilde{P}_{ij}^{\alpha\beta}(t^* = -\tau)\right), & i \neq j. \end{cases} \tag{5.55}$$

We evaluate the t_3, t_4-integrals in (5.42) using a similar approximation scheme. Within the given constraints $t_1 - t_2 \approx 0$ for $i = j$ and $|t_1 - t_2| \approx \tau$ for $i \neq j$, the singularity of

$$\tilde{\Pi}_{kk}(t_3 - t_4) \sim \frac{1}{(t_3 - t_4)^{2 - 1/\nu^*}}$$

dominates over the ones of

$$\tilde{\Pi}_{kl}(t_3 - t_4) \sim \frac{1}{\left[(t_3 - t_4 - \tau)(t_3 - t_4 + \tau)\right]^{1-1/2\nu^*}}, \quad k \neq l,$$

and of the instantons

$$e^{i\delta\Phi_*(x^k, t'+t_2)} = e^{iD_\Phi(t'-t_1+t_2, x^k, x^i) - iD_\Phi(t', x^k, x^j)}$$

$$\sim \left(\frac{(t'-t_1+t_2)^2}{(t'-t_1+t_2-\tau)(t'-t_1+t_2+\tau)}\right)^{A_{ki}/2\nu^*} \left(\frac{(t'-\tau)(t'+\tau)}{t'^2}\right)^{A_{kj}/2\nu^*}.$$

Hence, again transforming to relative and center-of-mass times, $t = t_3 - t_4$, $T = (t_3 + t_4)/2$, the dominant contribution to the instanton action stems from the $t \approx 0$-singularity of $\tilde{\Pi}_{kk}(t)$:

$$i\tilde{\mathcal{A}}_t[\varphi_*] \approx \sum_{k=1,2} \sum_{\gamma,\delta=\mp} \gamma\delta \int \!dt\, \tilde{\Pi}_{kk}^{\gamma\delta}(t) \int \!dT\, e^{-i\delta\Phi_*^\gamma(x^k, T) + i\delta\Phi_*^\delta(x^k, T)}$$

$$= -\sum_{k=1,2} \sum_{\gamma\neq\delta} \int \!dt\, \tilde{\Pi}_{kk}^{\gamma\delta}(t) \int \!dT\, \left(e^{iJ^{\gamma\delta}(T)} - 1\right) \quad \text{with } J^{\gamma\delta}(T) = -\delta\Phi_*^\gamma(x^k, T) + \delta\Phi_*^\delta(x^k, T)$$

$$\approx \sum_{k=1,2} \sum_{\gamma\neq\delta} \tilde{P}_{kk}^{\gamma\delta}(t^* = 0) \int \!dT\, \left(e^{iJ^{\gamma\delta}(T)} - 1\right).$$

The second equality follows from $\tilde{\Pi}_{kl}^>(t) + \tilde{\Pi}_{kl}^<(t) = \tilde{\Pi}_{kl}^T(t) + \tilde{\Pi}_{kl}^{\tilde{T}}(t)$. The integrals $\tilde{P}_{kl}^{\gamma\delta} = \int \!dt\, \tilde{\Pi}_{kl}^{\gamma\delta}(t)$ have been studied in the previous section.

Using the definition (5.41) of the instanton and the relation $(D_\Phi^T - D_\Phi^>)(t, x^k, x^l) = (D_\Phi^< - D_\Phi^{\tilde{T}})(t, x^k, x^l) = A_{kl}\frac{\pi}{\nu^*}\theta(-t)\theta(t+\tau)$ one obtains (independent of α and β!)

$$J^{\gtrless}(T) = \pm\frac{\pi}{\nu^*}\left[A_{ki}\theta(t_1 - T)\theta(T - t_1 + \tau) - A_{kj}\theta(t_2 - T)\theta(T - t_2 + \tau)\right] \tag{5.56}$$

With constraints $|t_1 - t_2| \ll \tau$ for $i = j$ and $|t_1 - t_2| = \tau$ for $i \neq j$ (cf. Eq. (5.55)), the instanton action thus reads

$$i\tilde{\mathcal{A}}_t[\varphi_*] = \begin{cases} -|t_1 - t_2|/\tau_\varphi, & i = j \\ -\tau/\tau_\varphi - ieV\tau\epsilon_{ij}(R_{1*}(eV) - R_{2*}(eV))\pi^{-1}\sin\frac{\pi}{\nu^*}, & i \neq j \end{cases} \tag{5.57}$$

with dephasing rate

$$\tau_\varphi^{-1} = -4\sin^2\frac{\pi}{2\nu^*}\sum_{k=1,2}\left(\tilde{P}_{kk}^>(0) + \tilde{P}_{kk}^<(0)\right) \tag{5.58}$$

which due to (5.51) becomes the expression (5.8) in the limit $|eV\tau| \gg 1$; see Fig. 5.11. The purely imaginary contributions to (5.57) correspond to (perturbatively small) renormalization corrections to bias voltage and will be neglected further on. We will also neglect the instanton action for $i = j$.

Combining these results with (5.55) we obtain for the incoherent and interference corrections to current due to tunneling

$$\Delta I_{\text{inc}} = I_{11} + I_{22} = -\frac{e^2}{2\pi}\left(R_{1*}(eV) + R_{2*}(eV)\right)V, \tag{5.59}$$

$$I_{\text{AB}} = -\frac{e}{\pi\tau}R_{12*}(eV)\,\text{sign}\,V\,e^{-\tau/\tau_\varphi}\sin(|eV\tau| - \pi/4\nu^*)\cos\varphi_{\text{AB}} \tag{5.60}$$
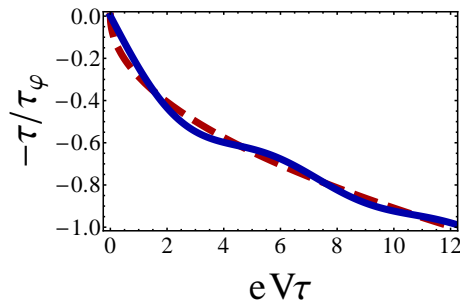
Figure 5.11: *The dephasing rate as a function of the source-drain voltage shown for $\nu^* = 2$, $\omega_C \tau = 25$ and $R_{1*}(\epsilon_{\text{th}}) = R_{2*}(\epsilon_{\text{th}}) = 0.2$. The solid line gives the numerical result for (5.58). The dashed line is the power-law asymptotic given by Eq. (5.8).*

with Aharonov-Bohm phase

$$\varphi_{\text{AB}} = 2\pi\phi/\phi_0 + (eV_+ + eV_-)\tau - 2\tau\varphi_0 \tag{5.61}$$

which in the limit $\omega_C \tau \gg 1$ gives (5.12). For large bias, $\omega_C \gg |eV| \gg \epsilon_{\text{th}}$, this yields the dimensionless conductances given in (5.5) and (5.6).

Concluding this section we turn to the case $\nu^* = 1$. According to Eq. (5.53) the dominant contribution to current is

$$e^{-1}I_{ij}^{\alpha\beta} \approx e^{i\tilde{\mathcal{A}}_t[\varphi_*]}\Big|_{t_1-t_2\approx 0} e^{2i\epsilon_{ij}\tau\varphi_0}\tilde{P}_{ij}^{\alpha\beta}(t^* = 0). \tag{5.62}$$

The $i \neq j$-contribution of Eq. (5.55) is also present, but subleading. The instanton action $i\tilde{\mathcal{A}}_t[\varphi_*]$ can be evaluated following the same line of reasoning as for $\nu^* \geq 2$, yielding $i\tilde{\mathcal{A}}_t[\varphi_*] = -|t_1 - t_2|/\tau_\varphi$ which can be neglected. The dominant contribution to current is thus

$$I_{\text{AB}}^{\nu^*=1} = -\frac{e}{\pi\tau} \, r_1\bar{r}_2 \, \omega_C\tau e^{\gamma} \, \cos\varphi_{\text{AB}}.$$

In the limit $\omega_C \tau \gg 1$ its bias dependence is negligible, in contrast to the contribution I_{AB}, Eq. (5.60). Therefore, while the latter is subleading in *current* for $\nu^* = 1$, it yields the leading contribution to *conductance*: $g_{\text{AB}} = \partial I_{\text{AB}}^{\nu^*=1}/\partial V + \partial I_{\text{AB}}/\partial V \approx \partial I_{\text{AB}}/\partial V$, i.e. giving the previous result (5.6).

5.4 Conclusions

In this chapter we provided a theory of a Fabry-Pérot interferometer (FPI) realized with the edge states of a two-dimensional electron gas in the integer quantum Hall regime. We took into account a compressible island in the center of the interferometer cell and described the Coulomb coupling with the edge states by a simple capacitive interaction model.

This model accounts for the observed visibility of the Aharonov-Bohm conductance oscillations, Fig. 5.4. The lobe structure appears to be a simple mean field effect, arising due to the effective symmetrization of the applied bias by interaction. As we argued, already in a noninteracting interferometer a symmetrically applied bias would give rise to visibility lobes. Further, we calculated the dephasing rate (5.8) which due to renormalization of the QPC tunneling coefficients, Eq. (5.9), has a power-law dependence on bias.

Depending on the relative strengths of the mutual capacitances between the Coulomb island, the interfering edge states, the fully transmitted edge channels and the gates, the FPI falls into different regimes which we listed in Table 5.1. Each regime is characterized by distinct Aharonov-Bohm conductance patterns as functions of gate voltages and magnetic field, Fig. 5.5. As we extensively discussed, our results are in good agreement with experiments.

Quantum Hall interferometers are also realized in the Mach-Zehnder geometry. In contrast to the FPI tunneling coefficients of the QPCs are close to 1/2, and a weak tunneling expansion is not justified. However, as we demonstrate in the following chapter the chirality of the setup allows for an *exact* treatment under the assumption that interaction is absent outside the interferometer cell.

6 Chapter 6
Quantum Hall Mach-Zehnder Interferometers

Electronic Mach-Zehnder interferometers (MZIs) realized with edge states in the integer quantum Hall (QH) regime have attracted a lot of attention recently because of a striking interplay between the quantum coherence and effects of electron-electron interaction observed in these mesoscopic devices [8, 9, 70–81]. Similarly to the electronic Fabry-Pérot interferometers considered in the previous chapter, the chiral edge states in the electronic MZI, are coupled by quantum point contacts (QPCs), which act as electron beam-splitters (see Fig. 6.1). The differential conductance measured in the above experiments shows strong Aharonov-Bohm (AB) oscillations. The most remarkable experimental observation is that the out-of-equilibrium visibility does not monotonically decreases with voltage but rather exhibits decaying oscillations ("lobes"). Such a dependence cannot be explained under the assumption of noninteracting electrons (which yields a constant visibility) and therefore is a hallmark of Coulomb interaction.

This puzzling behavior has triggered a lot of theoretical works [83–85, 87–89, 101–103] . They can be conventionally separated into approaches with contact [85, 101, 103] and long-range [83, 84, 88, 89, 102] Coulomb interaction. Despite the fact that the model of contact e-e interaction may successfully describe the related experiments on the energy relaxation in the quantum Hall edge states at filling factor ν=2 [104–108] , results of Refs. [89, 103] indicate that the account of the long-range character of Coulomb interaction is important to fully understand the nonequilibrium effects in MZIs.

The natural choice for a theoretical approach to one-dimensional interacting electrons in the QH edge states is that of bosonization [109]. However, with this method one faces a serious obstacle when describing electron scattering at QPCs. Namely, electron tunneling between two edge channels yields a non-Gaussian cosine term in the Hamiltonian if the latter is translated into the bosonic representation, impeding a solution of the problem. Therefore almost all recent theories of MZIs consider the limit of weakly coupled edge states where a perturbative treatment of electron tunneling at QPCs is justified. This is rather unfortunate since in the experiment transmission coefficients of both QPCs are close to 1/2.

In the case of a single QPC connecting two fractional QHE edge states at filling factor $\nu = 1/m$ (with m being odd) the exact solution via the Bethe ansatz is available [60]. The latter method can be generalized to the case of the fractional edge state MZI with equal arm lengths [110, 111]. However, quantum interference in such a setup has not been yet observed experimentally, and the Bethe-ansatz solution cannot be directly extended to the case of integer filling factors, especially under

the assumption of a long-range *e-e* interaction.

In this chapter we consider the model of the MZI operating at integer filling factor ν where electrons interact only when they are *inside* the interferometer. The model is specified by two single-particle scattering matrices of the QPCs defining the interferometer and the electrostatic charging energy E_c which takes into account the Coulomb interaction. Thus within our model *e-e* interaction is taken to be maximally long-ranged so that the interaction energy depends only on two total charges collected on different arms of the MZI. We show that this model is exactly solvable at any value of charging energy E_c and transmission coefficients of both QPCs. This simplified approach is much broader than the one based on the Bethe-ansatz solution since it offers a possibility to combine the exact description of electron scattering at QPCs with, in principle, an arbitrary form of *e-e* interaction within the interior region of the MZI.

In the special case of filling factor $\nu=1$ the numerically exact solution to the above model was obtained in Refs. [102] using a combination of bosonization and refermionization techniques. Our way to solve the same model is different in many aspects. We use the nonequilibrium functional bosonization approach developed in Chapter 3. Within this framework we demonstrate that the interfering current can be expressed in terms of a Fredholm functional determinant of the single-particle "counting" operator which is highly reminiscent of the problem of electron full counting statistics (FCS) of mesoscopic transport [24]. In the limit of strong interaction $E_c \gg 1/\tau$, where τ is the electron flight time through the MZI, the "counting" operator is reduced to the determinant of generalized Toeplitz form. Under this condition a fully analytical treatment becomes possible. It rests upon the conjecture of Ref. [22], which provides the asymptotic formula for such class of determinants. At moderate charging energy $E_c \sim 1/\tau$ we obtain the numerically exact solution.

We reveal that the "lobe" pattern in visibility is the many-body interference effect resulting from the quantum superposition of (at least) two many-particle scattering amplitudes with a mutual phase difference which is linear in voltage. In the limit of strong interaction we find the scaling exponents which govern the power-law dependences of these amplitudes on voltage and obtain the nonequilibrium dephasing rate governing the exponential suppression of visibility with bias (or the arms length of the MZI). Both power-exponents and the dephasing rate depend on the transmission coefficient of the first QPC and the filling factor ν. They happen to be intrinsically related to the cumulant generating function of the FCS describing the charge transfer through the first QPC.

Our analytical findings are corroborated by exact numerical evaluations of the Fredholm determinants. At $E_c \gg 1/\tau$ they provide further support to the aforementioned conjecture of Ref. [22]. At moderate charging energy $E_c \gtrsim 1/\tau$ and $\nu=2$ the obtained results match experimental observations. We also consider the role of external dephasing due to the quantum shot noise emitted from an extra QPC0 placed outside the MZI (Fig. 6.1). This study supports the conclusion of Ref. [101] that non-Gaussian shot noise leads to the disappearance of multiple side lobes in the visibility if the transmission T_0 of the QPC0 exceeds 1/2.

It is worth mentioning that the aforementioned simplification of the problem to a single-particle one is a special feature of the MZI topology, where electrons are scattered at most twice between the two quantum Hall edges. Thus, unfortunately the method developed in the present chapter is not applicable to treat the non-chiral quantum Hall Fabry-Perot interferometers.
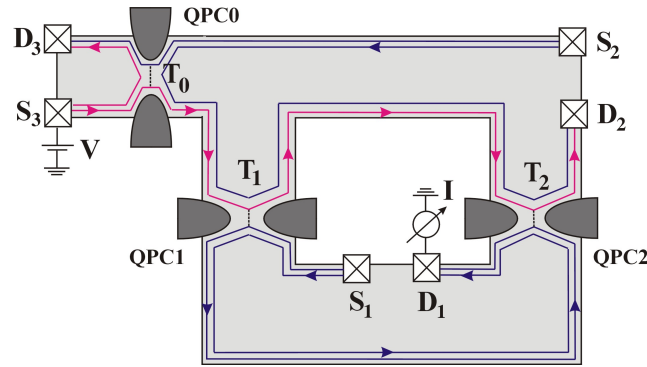
Figure 6.1: *Layout of an electronic Mach-Zehnder interferometer built on quantum Hall edge states at filling factor $\nu = 2$. Quantum point contact (QPC1 and QPC2) characterized by transparencies $T_{1(2)}$ are used to partially mix the outer edge channels. All ohmic contacts are grounded, except for the source terminal S_3 which is kept at voltage V. The current is measured in the drain terminal D_1. The QPC0 can be used to dilute the incoming current in the outer channel by changing the transparency T_0.*
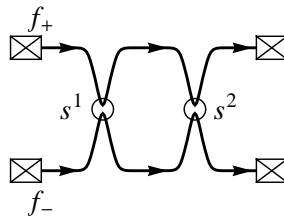
Figure 6.2: *Scheme of an MZI at filling factor ν. Two quantum point contacts are characterized by the scattering matrices s^1 and s^2, which connect the outer channels. Inner channels are fully reflected.*

6.1 Model

We consider a Mach-Zehnder interferometer (MZI) realized in a two-dimensional electron gas (2DEG) in the quantum Hall regime with integer filling factor ν. Fig. 6.1 shows a sketch, while Fig. 6.2 shows an even further simplified network model of the MZI. Each edge carries ν channels, modeled as chiral 1D fermions with drift velocity v_D, which serve as electron beams. Electrons are injected and detected via ohmic contacts ("sources" S_j and "drains" D_j). The Mach-Zehnder geometry requires a topologically nontrivially shaped 2DEG sample with contacts S_1 and D_1 placed between two edges. We refer to them as "upper" (denoted by subindex $+$) and "lower" (subindex $-$) edges. The area enclosed by the edges is threaded by a magnetic flux Φ which gives rise to a proportionate Aharonov-Bohm (AB) phase $\phi = 2\pi\Phi/\Phi_0$ with flux quantum $\Phi_0 = hc/|e|$.

The interferometer is formed by two quantum point contacts QPC1 and QPC2 which tunnel-couple the outer channels of the two edges, while the inner channels are fully reflected. The scattering can be thus described by 2×2-scattering matrices in the space of outer channels,

$$s^j = \begin{pmatrix} ir_j & t_j \\ t_j & ir_j \end{pmatrix} \quad \text{with } r_j^2 + t_j^2 = 1. \tag{6.1}$$

For simplicity we assume that the distance L between the two QPCs is the same along both edges, as is predominantly the case in experiments.

The "upper" edge is biased by the voltage V applied to the source S_3. All other contacts are grounded. An additional QPC0 can be tuned such that it fully reflects all inner channels which originate from S_3, as is shown in Fig. 6.1, while the outer channel is fully transmitted, $T_0 = 0$. This situation, where all inner channels are unbiased ($V_0 = 0$), exhibits the most interesting experimental features and will be considered mainly in this work. By closing QPC0 further, $T_0 > 0$, the outer channel is diluted and brought into a nonequilibrium state. Alternatively, QPC0 can be completely opened in which case the inner channels of the upper edge are biased, $V_0 = V$.

In our work we consider the effects of long-range interaction in the edges on the one hand, and, in view of large edge distances and strong screening by surrounding metallic gates on the other hand, we neglect interaction between the edges. Further, exact solutions can be obtained, if we disregard interaction of electrons outside the interferometer cell. Thus, if $N_\pm$ denotes the total electron number in the outer and inner channels along the upper/lower edge between QPC1 and QPC2, then the interaction Hamiltonian reads

$$H_{\text{int}} = \frac{1}{2} E_C \left(N_+^2 + N_-^2 \right)^2 \tag{6.2}$$

where $E_C = e^2/C$ is the charging energy with electron charge $e < 0$ and edge capacitance C.

This model is exactly solvable for any value of the charging energy E_C and transmission coefficients t_j^2. In the limit $E_C\tau \gg 1$, where $\tau = L/v_F$ is the electron dwell time in the MZI, a fully analytical treatment is possible. For the more general case $E_C\tau \sim 1$ we have developed a numerically exact scheme to evaluate the visibility in the MZI as a function of voltage. Before going into the details of the calculation in Sect. 6.3, we summarize first the results.

6.2 Results and Discussion

Within the described model we calculated the current $I = I_{\text{inc}} + I_{\text{coh}}$ into the drain contact D2 as function of bias V and AB phase ϕ. It consists of an incoherent, flux-independent contribution,

$$I_{\text{inc}} = \frac{e^2 V}{2\pi} \left(r_1^2 t_2^2 + t_1^2 r_2^2 \right)$$

which in our model is not affected by interaction. Interference of two trajectories, either along the upper or lower edge, gives rise to the flux-dependent, coherent, contribution

$$I_{\text{coh}} = \frac{e}{2\pi\tau} r_1 t_1 r_2 t_2 \, 2\text{Re}\, e^{i\phi} \mathcal{I}_0. \tag{6.3}$$

Here, the bias-dependent quantity $\mathcal{I}_0$ encodes interaction-induced effects such as charging, dephasing and renormalization. It is sensitive to the nonequilibrium state in the interferometer cell, established by scattering at QPC1, and in turn completely independent of QPC2. In the noninteracting case it is simply $\mathcal{I}_0 = eV\tau$. The corresponding differential conductances are

$$G_{\text{inc}} \equiv \partial_V I_{\text{inc}} = \frac{e^2}{2\pi} \left(r_1^2 t_2^2 + t_1^2 r_2^2 \right),$$
$$G_{\text{coh}} \equiv \partial_V I_{\text{coh}} = v G_{\text{inc}} \cos(\phi + \alpha_{\text{AB}})$$

where the differential visibility v and the phase α_{AB} of the AB oscillations are

$$v = v_0 |\partial_{eV\tau} \mathcal{I}_0|, \quad \alpha_{\mathrm{AB}} = \arg \left(\partial_{eV\tau} \mathcal{I}_0 \right). \tag{6.4}$$

The noninteracting value of visibility is simply the constant $v_0 = 2r_1 t_1 r_2 t_2 / \left(r_1^2 t_2^2 + t_1^2 r_2^2 \right)$ with $T_j = t_j^2 = 1 - R_j$.

6.2.1 Limit of strong interaction

Unbiased inner channels

First, we discuss the results in the limit $E_c\tau \gg 1$ and with QPC0 tuned such that inner channels are unbiased, $V_0 = 0$.
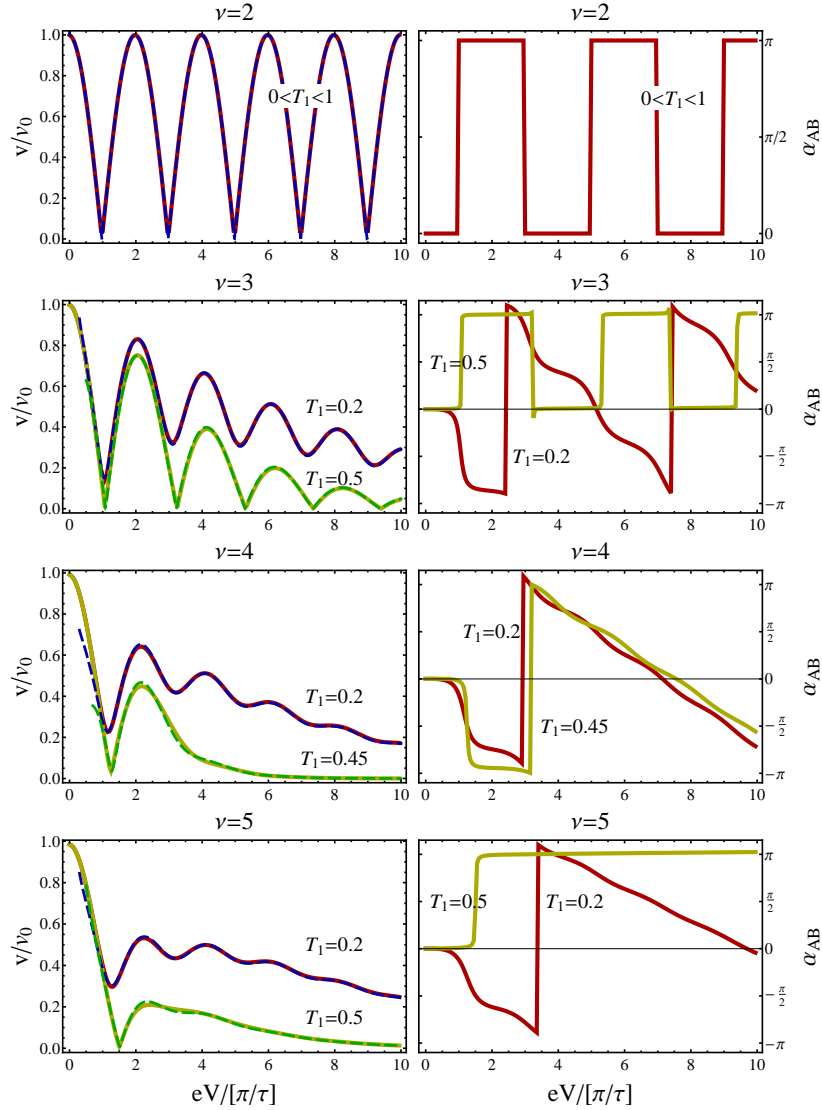
Figure 6.3: *AB oscillations in the conductance of the quantum Hall Mach-Zehnder interferometer with unbiased inner channels: visibility v and phase α_{AB}. Solid lines show numerically exact curves, dashed lines are the result of the analytical asymptotic expansion.*

In the case of not too low voltages, namely at $eV\tau \gtrsim 1$, our model predicts the asymptotic expansion for the current,

$$\mathcal{I}_0 = e^{ieV\tau(\beta_1 + 1/\nu)}\left(C_1(eV\tau)^{\lambda_1} + C_2(eV\tau)^{\lambda_2}e^{\pm ieV\tau}\right). \tag{6.5}$$

The different terms in this expression can be interpreted as follows. The coefficient

$$\beta_1 = \frac{1}{2\pi i}\ln\left(R_1 e^{-4\pi i/\nu} + T_1\right) \tag{6.6}$$

describes the nonequilibrium dephasing of the AB oscillations induced by a combined effect of inelastic *e-e* scattering and the quantum shot noise generated at QPC1. If $\nu \geq 3$ then $\mathrm{Im}\beta_1 > 0$ and, by defining the out-of-equilibrium dephasing rate as $1/\tau_\varphi = eV\,\mathrm{Im}\beta_1$, we see that AB oscillations are suppressed by the factor $e^{-\tau/\tau_\varphi}$ in the high-bias limit $eV \gg 1/\tau$.

It is worth stressing that the exponential suppression of the interference current is directly related to the full counting statistics (FCS) of electrons passing through the QPC1 during the time interval τ. Indeed, defining the FCS cumulant generating function (CGF) [24]

$$\kappa_\tau(\chi_*) = \left[1 + T_1(e^{i\chi_*} - 1)\right]^{eV\tau/2\pi}, \tag{6.7}$$

where χ_* is the so-called "counting field", we see that the damping factor equals

$$e^{i\beta_1 eV\tau} = \kappa_\tau(-4\pi/\nu). \tag{6.8}$$

The exponents $\lambda_{1,2}$, which determine the power-law dependence of the interference current on bias, are due to the Anderson orthogonality catastrophe which happens each time when an electron enters or leaves the interior part of the MZI where it strongly interacts with all other electrons. In our simplified model, where *e-e* interaction is present only inside MZI, the orthogonality catastrophe is absent for the incoherent contribution to the current, which stays linear in voltage as in the case of noninteracting fermions.
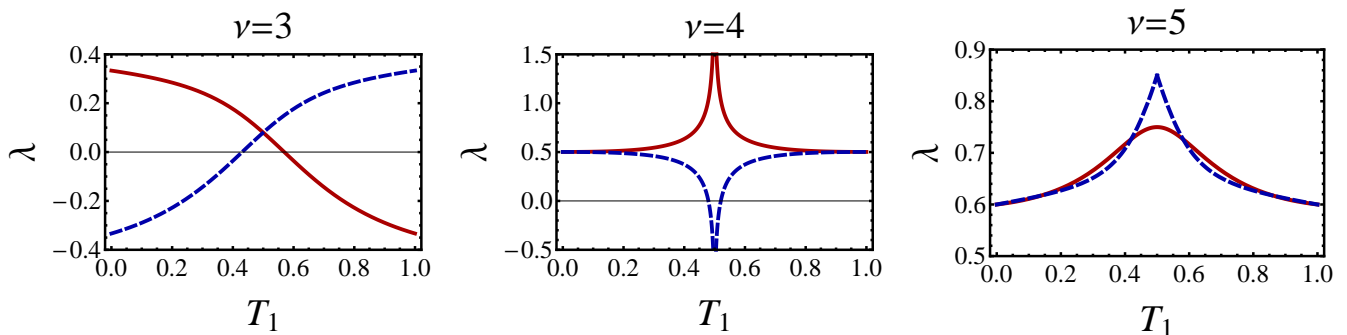

Figure 6.4: *Power law exponents shown as a function of transmission coefficient T_1. Solid line shows $\mathrm{Re}\,\lambda_1$, dashed line shows $\mathrm{Re}\,\lambda_2$ in the case of $\nu = 3$, and $(-\mathrm{Re}\,\lambda_2)$ in the case of $\nu = 4, 5$.*

The exponents $\lambda_{1,2}$ are functions of both the filling factor ν and the transparency T_1 of the first QPC and are shown in Fig. 6.4. The explicit expressions read

$$\lambda_{1,2} = -2\left(\frac{\nu-2}{2\nu} \mp \frac{1}{2} - \beta_1\right)^2 + 1 - \frac{2}{\nu} + \frac{2}{\nu^2}, \qquad 2 \leq \nu < 4, \tag{6.9}$$

for low filling factors and

$$\lambda_1 = -2\left(\frac{1}{\nu} + \beta_1\right)^2 + 1 - \frac{2}{\nu} + \frac{2}{\nu^2},$$

$$\lambda_2 = -2\left(\frac{1}{\nu} + \beta_1 \pm \frac{1}{2}\right)^2 - \frac{1}{2} + \frac{2}{\nu^2}, \quad \nu \geq 4$$

(6.10)

in case of higher ν. In the case $2 \leq \nu < 4$ the voltage dependent phase factor in Eq. (6.5) has to be taken with the sign $(-)$. For $\nu \geq 4$ the signs $\pm$ correspond to the cases $T_1 > 1/2$ and $T_1 < 1/2$, respectively. The coefficients $C_{1,2}$ in Eq. (6.5) are some bias independent complex numbers which depend solely on ν and T_1 and can be found from the fit of this asymptotic expansion to its numerically exact counterpart. In the limit of strong interaction $E_c\tau \gg 1$ the case $\nu = 1$ is very special. One has $\mathcal{I}_0 = (eV\tau)$ and the MZI behaves the same as in the absence of e-e interaction.

In Fig. 6.3 we show the lobe structure in the visibility and the phase of the AB oscillations as a function of bias for different filling factors ν and transmission T_1. For each plot we have fitted the asymptotic visibility to its exact numerical dependence on the variable $eV\tau$ using the two free parameters C_1 and C_2. Though Eq. (6.5) is strictly speaking valid in the high voltage limit $eV\tau \gg 1$, one sees from Fig. 6.3 that the obtained fit is almost perfect in the much broader region $eV\tau \gtrsim 1$. At smaller voltages the visibility saturates to the noninteracting value v_0.

At $\nu = 2$ we have $\lambda_1 = \lambda_2 = 0$ and $C_1 = -C_2 = i$. This gives the oscillatory visibility $v = v_0 \cos(eV\tau/2)$ which is independent of the transparency T_1 and does not decay with bias. The behavior of the MZI in this case is completely analogous to the one treated within the model of short-range electron interaction. The latter model is also exactly solvable at $\nu = 2$ by means of the method of refermionization, as it has been recently shown in Ref. [103].

In the case $\nu = 3$ an infinite number of lobes is present and at half transmission ($T_1 = 1/2$) the visibility reaches zeros — at this special point the two exponents coincide: $\lambda_1 = \lambda_2$. For $\nu \geq 4$ our model predicts only one central and one side lobe. Note, that at $\nu = 4$ the exponents $\lambda_{1,2}$ logarithmically diverge at $T_1 \to 1/2$. The asymptotic result (6.5) does not hold in this case anymore (the numerical evaluation of v, however, is always possible). This is the reason why we plot $v(V)$ and $\alpha_{AB}(V)$ for $T_1 = 0.45$ in Fig. 6.3.

In agreement with experimental findings the appearence of zeros in the visibility in the cases $\nu = 2$ and for $\nu \geq 3$ at half-transmission comes with a "stick-slip" behavior of the phase shift α_{AB}: The latter is constant as bias is varied within the lobes and jumps by π whenever the visibility dips to zero.

The "phase diagram" shown in Fig. 6.5 summarizes the obtained results. The main qualitative features depend on the counting parameter $\chi_* = -4\pi/\nu$ and QPC1 transmission T_1. For $\pi < -\chi < 3\pi$ the exponents $\operatorname{Re}\lambda_1 \approx \operatorname{Re}\lambda_2$ are close to each other with $\operatorname{Re}\lambda_1 = \operatorname{Re}\lambda_2$ at $T_1 = 1/2$. The current $\mathcal{I}_0$ is thus a superposition of two contributions with similar scaling behavior, which gives rise to pronounced oscillations of visibility with an infinite number of zeros at $T_1 = 1/2$ with the corresponding stick-slip behavior of the phase shift α_{AB}. For other values of χ_* the λ_1-term decreases for high bias significantly more slowly than the λ_2-term and oscillations in the visibility are weaker. A single zero appears at most at $T_1 = 1/2$.

The special feature of our model is the absence of dephasing at $\nu = 2$ in the limit $E_c\tau \gg 1$. On the mathematical level it comes from the fact that the suppression factor given by the CGF $\kappa_\tau(\chi_*)$ is evaluated at the counting parameter $\chi_* = -2\pi$ and thus it is equal to one. At moderate charging energy $E_c\tau \sim 1$ the counting parameter becomes time-dependent and deviates from -2π at $\nu = 2$ and dephasing is restored (see the following subsection 6.2.2).
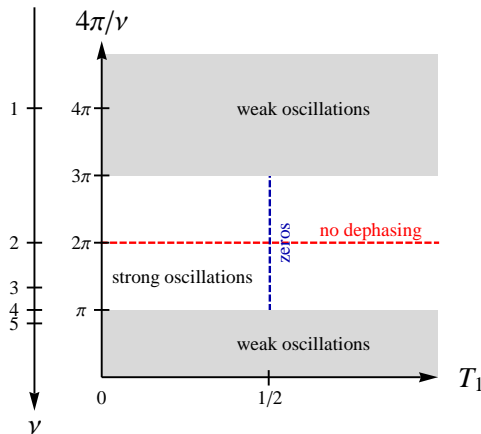
Figure 6.5: *"Phase diagram" of Mach-Zehnder interferometer with strong interaction. Pronounced zeros appear for $\pi < 4\pi/\nu < 3\pi$ with an infinite number of zeros at $T_1 = 1/2$. Dephasing is absent for $\nu = 2$.*
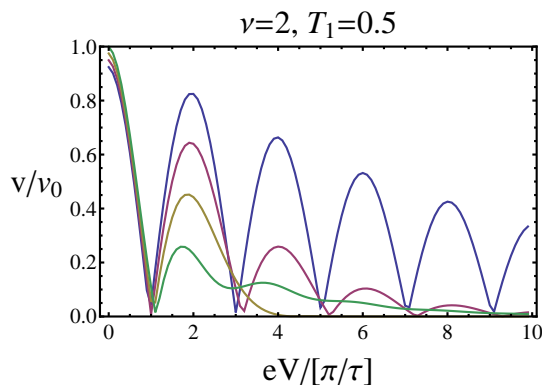

Figure 6.6: *Dephasing of the visibility due to the quantum shot noise generated at the QPC0. The curves from up to down were evaluated numerically for $R_0 = 0.9, 0.7, 0.5$ and 0.3.*

An alternative source of dephasing can be provided by the dilution of the impinging current due to the electron scattering at the QPC0 which is put outside the interferometer. At $R_0 < 1$ the QPC0 generates the double-step distribution function $f_+(\epsilon) = T_0\theta(-\epsilon) + R_0\theta(eV - \epsilon)$ for incoming electrons. Visibility plots at half-transmission of the first QPC ($T_1 = 1/2$) and different reflectivity R_0 are shown in Fig. 6.6. In the case $R_0 > 1/2$ the suppression of visibility with voltage can be roughly characterized by the dephasing rate $1/\tau_\varphi = (eV/2\pi)\ln(2R_0 - 1)$, which diverges logarithmically at $R_0 \to 1/2$. At this point the behavior of the MZI visibility changes from the regime with multiple side lobes, characterized by periodic oscillations in $v(V)$ with a typical period $\sim 2\pi/\tau$, to the regime with only one node. The same transition in the behavior of visibility under variation of R_0 has been first predicted in Ref. [101], albeit in the framework of the short-range *e-e* interaction model. Concerning the experimental verification of such a transition, we refer to the recent work [81].

It is evident from the Eq. (6.5), which gives the interference current, that the appearance of the visibility fringes in our model stems from the superposition of two *multi-particle* amplitudes having

the relative phase shift $eV\tau$. Based on our analytical calculations presented in Sect. 6.3, the following quantitative picture underlying these two most probable many-body scattering processes can be drawn. At $\nu \geq 4$ the amplitude with the exponent λ_1 corresponds to the multi-particle process where an electron enters the MZI through the QPC1 and another electron leaves the MZI shortly afterwards on a time scale $\sim \hbar/eV$ via the QPC2. Such amplitude is non-zero solely due to the strongly non-local character of Coulomb interaction in our model. The second amplitude with exponent λ_2 is associated with the more conventional process when the same electron enters and leaves the MZI. In this case the interferometer is excited in a virtual charge state for a long time $\simeq \tau$, which results in the appearance of the phase factor $\propto e^{ieV\tau}$ relative to the first amplitude. At $\nu = 2$ and 3 both amplitudes (with exponents $\lambda_{1,2}$) describe the real process of the fast e-e collision between the two electrons entering and leaving the MZI via different QPCs. The relative phase shift between the two amplitudes is due to the fact that the e-e collision associated with the second amplitude is accompanied by the creation/destruction of a real electron-hole pair with energy $\pm eV$, which is subsequently recombined on a larger time scale $\simeq \tau$.

Biased inner channels: $V_0 = V$

While the peculiar interaction effects in visibility arise in MZIs where an additional QPC0 fully reflects all biased inner channels, some (including the earliest) experiments were performed on MZIs without the QPC0 and show qualitatively different visibilities for $\nu = 1, 2$, lacking the lobe structure [9, 79].

The visibility lobe structure and the stick-slip behavior of α_{AB} are intimately linked to a phase rigidity of $\mathcal{I}_0$ upon variation of bias. Biased inner channels $V_0 = V$ lead to additional charging effects. Within our strong coupling assumption they give rise to a phase factor: $\mathcal{I}_0 \mapsto e^{-i(1-1/\nu)eV\tau}\mathcal{I}_0$. Obviously, phase rigidity is broken and, as shown in Fig. 6.7, the lobe structure is destroyed.

The constant visibility in case of $\nu = 2$ is an artifact of the strong coupling limit of our model and corrected in more realistic interaction models. The qualitative features shown for $\nu \leq 3$, including the increase of visibility with $v/v_0 > 1$ for small bias voltages, are compatible with experimental findings for $\nu = 2$ [79].

6.2.2 The case of moderate strength of interaction

In this subsection we discuss the results for visibility in the case of not too strong e-e interaction, $E_C\tau \gtrsim 1$. The majority of experimental data for MZIs was collected for filling factor $\nu = 2$, which motivated us to consider this case only. The numerically calculated plots of visibility for transparencies $T_1 = 0.5$ and $T_1 = 0.2$ are shown in Fig. 6.9. The finite charging energy E_C gives rise to the decay of visibility $v(V)$ with bias contrary to its behavior at $E_C\tau \to \infty$ discussed in the previous subsection 6.2.1. Note also that nodes in $v(V)$ are generally present only in the case $T_1 = 1/2$. At the transmission coefficient close (but not equal) to one-half the nodes are superseded by deep minima. At the same time the typical period of oscillations increases as long as E_C decreases. However, the estimate $e(\Delta V) \sim 2\pi/\tau$ for the scale of oscillations is valid up to the moderate charging energy $E_C \sim 1/\tau$.

We do not know the analytical formula describing the AB conductance for the arbitrary dimensionless parameter $E_C\tau$. Nevertheless, the dephasing rate $1/\tau_\varphi$ describing the exponential suppression ($\propto e^{-\tau/\tau_\varphi}$) of the visibility with bias can be found explicitly. As in the previous discussion, it is expressed in terms of the cumulant generating function of the FCS,

$$\tau_\varphi^{-1} = -\frac{eV}{2\pi} \int_{-\infty}^{\tau+\bar{t}} \mathrm{Re}\left[\ln\left(1 + R_1(e^{4i\vartheta_+(t)} - 1)\right)\right] dt \tag{6.11}$$
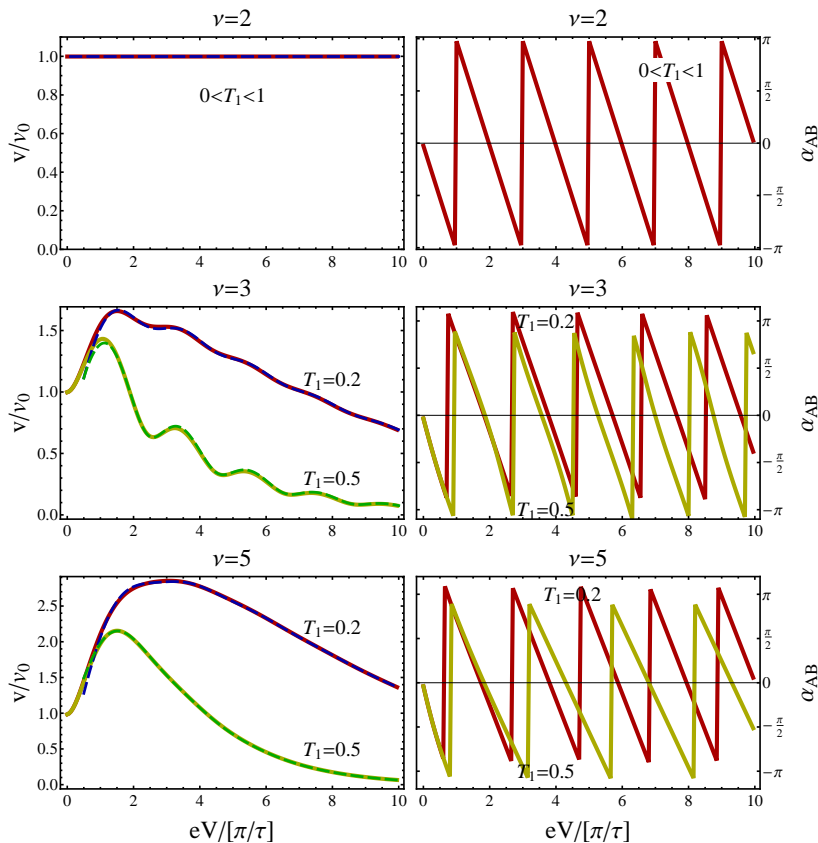
Figure 6.7: *AB oscillations in the conductance of the quantum Hall Mach-Zehnder interferometer with $V_0 = V$: visibility v and phase α_{AB}. Solid lines show numerically exact curves, dashed lines are the result of the analytical asymptotic expansion.*

through the time-dependent "counting" phase $\vartheta_+(t)$ shown in Fig. 6.8. In the limit $E_c\tau \gg 1$ the time dependence of $\vartheta_+(t)$ approaches the window function

$$\vartheta_+(t) = \begin{cases} -\pi/\nu, & t \in [\bar{t}, \bar{t} + \tau] \\ 0, & t \notin [\bar{t}, \bar{t} + \tau], \end{cases} \tag{6.12}$$

causing the dephasing rate to vanish at $\nu = 1, 2$.

If we introduce the effective charge $e^*(t)/e = \vartheta_+(t)/2\pi$ then it can be interpreted as the optimal charge fluctuation on the MZI which promotes the scattering of the transport ("trial") electron from one arm of the interferometer into another.[1]

Loosely speaking, if such a scattering event happens to start at the time instant $\bar{t}$, then it finishes no later than $\bar{t} + \tau$ (cf. the upper bound of the time integral in Eq. (6.11)). It means that an electron entering the MZI at time $\bar{t}$ cannot be influenced by those electrons which enter behind at times larger than $\bar{t} + \tau$, since by the latter time the trial electron leaves the interior interacting region

---

[1]We note that in view of the specific chiral geometry of the MZI the charge from the internal interacting region of the interferometer can always freely leak into the source or drain, and thus the issue of Coulomb blockade phenomenon is not relevant here.
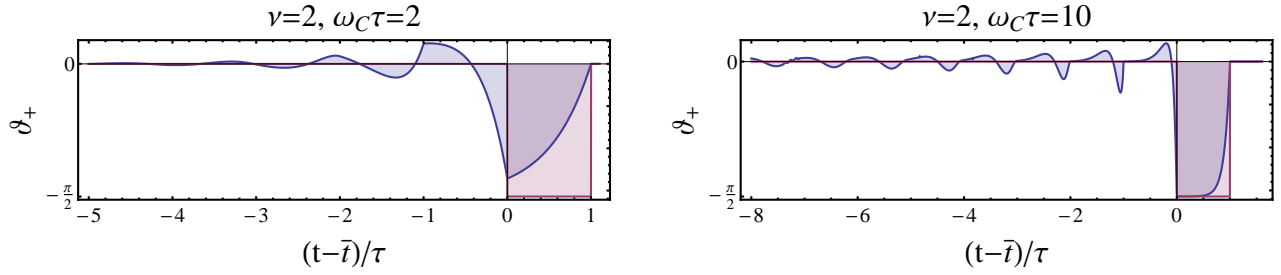
Figure 6.8: *Time-dependent "counting" phase shown for two strengths of Coulomb interaction. It approaches the "window" function, Eq. (6.12), in the limit $E_c \to \infty$. The charge relaxation frequency is defined as $\omega_c = \nu E_c / \pi$.*
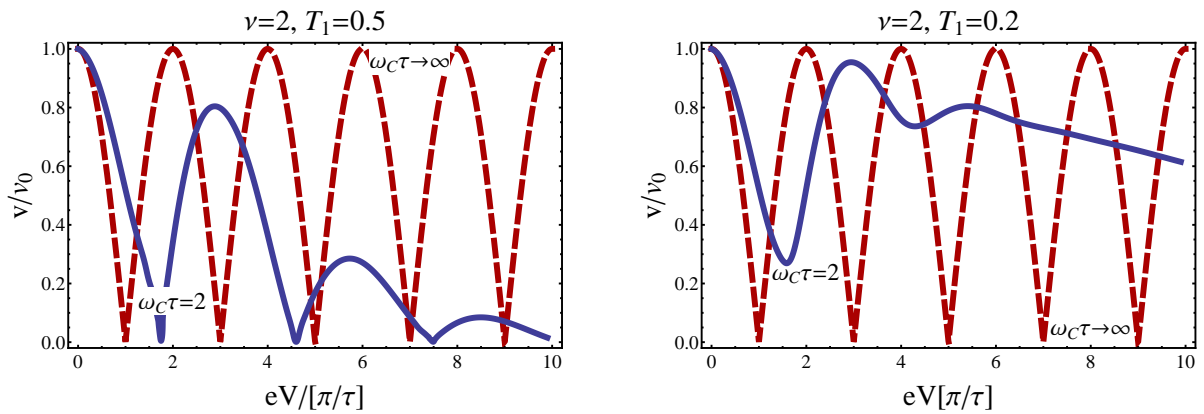

Figure 6.9: *Bias dependence of visibility for the moderate interaction strength (solid blue curve) in comparison to the one in the limit of strong interaction (dashed red line). The charge relaxation frequency $\omega_c = \nu E_c / \pi$.*

of the system through the second QPC. Counter-intuitively, typical arm-to-arm electron scattering is generally preceded by a rearrangement of the charge $e^*(t)$ on the MZI at all times $t < \bar{t}$. We thus see that the single electron transfer through the MZI in the presence of *e-e* interaction is a collective many-body process involving many electrons.

6.3 Calculations

6.3.1 Keldysh Action

As depicted in Fig. 6.2 we model the MZI as a quantum wire network and treat it in functional bosonization, cf. Chapter 3. Each of the two edges supports ν chiral channels – 1D fermions of velocity v –, of which the outermost channels (labeled by $+$ and $-$) are tunnel-coupled by two point-scatterers. These are separated by a distance L and described by scattering matrices s^j, cf. (6.1).

We consider zero temperature and assume the lower edge to be grounded, $V_- = 0$, while along the upper edge the outer channel is biased, $V_+ = V$, and, depending on the tuning of QPC0, the inner ones are either biased as well, $V_0 = V$, or grounded, $V_0 = 0$. In time representation the distribution functions

of the outer channels are $f_{\pm}(t) = e^{-ieV\pm t}f_0(t)$ with equilibrium distribution function $f_0(t) = \frac{i}{2\pi}\frac{1}{t+ia}$; the inner channels are characterized by $f_\lambda(t) = e^{-ieV_0t}f_0(t)$ along the upper edge, and $f_\lambda(t) = f_0(t)$ along the lower one.

In the functional bosonization approach we introduce the Hubbard-Stratonovich potential $\varphi^{f/b}$ which leads to the accumulation of the phase

$$\vartheta_\lambda^{f/b}(t) = -v_D^{-1}\int_{x^1}^{x^2}\mathrm{d}x'\,\varphi_\lambda^{f/b}(t+(x'-x^1)/v_D) = -\int_t^{t+\tau}\mathrm{d}t'\,\varphi_\lambda^q(t')$$

along the channel λ. An additional Aharonov-Bohm phase $\phi_\pm$ is accumulated along the upper/lower edges in the presence of the magnetic field.

The entire dynamics of an electron in the system is encoded in the time-dependent scattering or transfer matrices $S^{f/b}$. For an electron in an inner channel λ of the upper/lower edge they are plainly

$$S_\lambda^{f/b}(t_2,t_1) = \Delta^{21}(t_2,t_1)\,e^{i\phi_\pm}e^{i\vartheta_\lambda^{f/b}(t_1)}s^1$$

with the time delay operator $\Delta^{21}(t_2,t_1) = \delta(t_2-t_1-\tau)$. In contrast, the two outer channels are tunnel-coupled, and hence simultaneously described by the 2×2-matrix

$$\hat{S}^{f/b}(t_2,t_1) = s^2\,\Delta^{21}(t_2,t_1)\,e^{i\hat{\phi}}e^{i\hat{\vartheta}^{f/b}}s^1$$

where we combined the phases into matrices

$$\hat{\phi} = \begin{pmatrix} \phi_+ & \\ & \phi_- \end{pmatrix}, \quad \hat{\vartheta}^{f/b} = \begin{pmatrix} \vartheta_+^{f/b} & \\ & \vartheta_-^{f/b} \end{pmatrix}.$$

In order to compute the current into drain reservoir D_1 (see Fig. 6.1), we include a time-dependent counting field $\chi\mathbb{1}_{(-t_0/2,t_0/2)}(t)$ into the lower outer edge. We are not interested in transient effects of switching on the measuring device and will subsequently work in the adiabatic limit $t_0 \to \infty$. Again we define the 2×2-matrix

$$\hat{\chi}(t) = \begin{pmatrix} 0 & \\ & \chi\mathbb{1}_{(-t_0/2,t_0/2)} \end{pmatrix}.$$

Let us turn to the interaction (6.2). In each of the two edges a quantum-dot-like interaction is effective and thus all channels of one edge share the same Hubbard-Stratonovich potential $\varphi_\eta^{f/b}(t,x) = \varphi_\eta^{f/b}(t)$, $\eta = \pm$, which furthermore is constant in space. Its quadratic action (2.25) is determined by the screened interaction $V_{\mu\nu}^{-1}(t,t') = \int_{x^1}^{x^2}\mathrm{d}x\mathrm{d}x'\,V_{\mu\nu}^{-1}(t,t';x,x')$. In frequency representation its retarded and advanced components are

$$V_\eta^a(\epsilon) = \frac{2\pi}{\nu}\omega_C\frac{\epsilon}{\epsilon - i\omega_C(1-e^{-i\epsilon\tau})}, \quad V_\eta^r(\epsilon) = V_\eta^a(\epsilon)^* \tag{6.13}$$

with charge relaxation frequency $\omega_C = \frac{\nu}{2\pi}E_C$. Note that the filling factor ν enters due to the fact that all ν channels along the edge η contribute to the screening.

The full Keldysh action (3.3), including the counting field, thus reads $\mathcal{A} = \mathcal{A}_{\text{int}} + \mathcal{A}_{\text{ferm}}$ with $\mathcal{A}_{\text{ferm}} = \mathcal{A}_{\text{inner}} + \mathcal{A}_{\text{outer}}$, and

$$i\mathcal{A}_{\text{int}} = 2i \sum_{\eta=\pm} \int \mathrm{d}t \mathrm{d}t'\, \varphi_\eta^c(t) V_\eta^{a-1}(t,t')\varphi_\eta^q(t'),$$

$$i\mathcal{A}_{\text{inner}} = \sum_{\text{inner channels } \lambda} \text{Tr}_t \left[\text{Ln} \left[\mathbb{1} - f_\lambda + S_\lambda^{b\dagger} S_\lambda^f f_\lambda \right] - 2i\vartheta_\lambda^q f_0 \right],$$

$$i\mathcal{A}_{\text{outer}} = \text{Tr} \left[\text{Ln}\, \mathcal{D} - 2i\hat{\vartheta}_\eta^q f_0 \right] \quad \text{with } \mathcal{D} \equiv \mathbb{1} - \hat{f} + \hat{S}^{b\dagger} e^{i\hat{\chi}} \hat{S}^f \hat{f}.$$

Here, the trace Tr_t is to be taken with respect to times while Tr also extends over channel indices. Note that we also subtract singular terms of the form $\text{Tr}\, \vartheta^q f_0$ which cancel UV divergent contributions in the $\text{Tr}_t\, \text{Ln}$ arising due to the lack of a lower band edge in our theory.

6.3.2 Exact Current

The current is obtained by taking the derivative of the generating functional with respect to the counting field. Assuming adiabatic measurement with long measurement time t_0 we obtain

$$I = \frac{e}{t_0} \left\langle \frac{\partial}{i\partial\chi} i\mathcal{A} \bigg|_{\chi=0} \right\rangle = -i\frac{e}{t_0} \left\langle \text{Tr}\, \mathcal{D}^{-1} \partial_\chi \mathcal{D} \bigg|_{\chi=0} \right\rangle.$$

The average $\langle \ldots \rangle$ is to be taken with respect to the full action $\mathcal{A}$ with the counting field put to zero, $\chi = 0$. In this case $i\mathcal{A}_{\text{outer}} = \text{Tr} \left[\text{Ln}\, \tilde{\mathcal{D}} - 2i\hat{\vartheta} f_0 \right]$ with

$$\tilde{\mathcal{D}} \equiv s_1 \mathcal{D} s_1^\dagger = \mathbb{1} - \tilde{f} + e^{2i\hat{\vartheta}^q} \tilde{f} \text{ with } \tilde{f} \equiv s_1 \hat{f} s_1^\dagger = \begin{pmatrix} R_1 f_+ + T_1 f_- & ir_1 t_1 (f_+ - f_-) \\ -ir_1 t_1 (f_+ - f_-) & T_1 f_+ + R_1 f_- \end{pmatrix}, \tag{6.14}$$

and the action only contains s^1, not s^2. This is due to the chirality of the system: the nonequilibrium state is not affected by what happens with the electrons "downstream". Using $\tilde{\mathcal{D}}$ the current reads

$$I = \frac{e}{t_0} \left\langle \text{Tr}\, e^{-i\hat{\vartheta}^b} e^{-i\hat{\phi}} \Delta^{21\,-1} s^{2\dagger} |-\rangle \langle -| s^2 \Delta^{21} e^{i\hat{\vartheta}^f} e^{i\hat{\phi}} \tilde{f} \tilde{\mathcal{D}}^{-1} \right\rangle = \frac{e}{t_0} \sum_{\mu,\kappa=+,-} N_{\mu\kappa}$$

with

$$N_{\mu\kappa} = \langle -| s_2 |\mu\rangle \langle\kappa| s^{2\dagger} |-\rangle \left\langle \int \mathrm{d}\bar{t}\, e^{i\vartheta_\mu^f(\bar{t}) - i\vartheta_\kappa^b(\bar{t})}\, e^{i\phi_\mu - i\phi_\kappa}\, \langle\mu| \tilde{f}\tilde{\mathcal{D}}^{-1}(\bar{t},\bar{t}) |\kappa\rangle \right\rangle. \tag{6.15}$$

What simplifies the many-body average considerably is the fact that the operator $\tilde{\mathcal{D}}$ and hence $\mathcal{A}_{\text{outer}}$ (like $\mathcal{A}_{\text{inner}}$) is independent of ϑ^c and φ^c. These classical fields only appear linearly in $\mathcal{A}_{\text{int}}$ and $\vartheta_\varrho^{f/b} = \vartheta_\varrho^c \pm \vartheta_\varrho^q$. Therefore φ^c can be exactly integrated over. To this end let us denote the "source term"

$$i\vartheta_\mu^c(\bar{t}) - i\vartheta_\kappa^c(\bar{t}) \equiv i\mathcal{A}_{J;\mu\kappa} \equiv i \sum_\varrho \int \mathrm{d}t'\, J_{\varrho;\mu\kappa}^q(\bar{t};t')\varphi_\varrho^c(t'). \tag{6.16}$$

The particle numbers (6.15) then read

$$N_{\mu\kappa} = \langle-|\,s^2\,|\mu\rangle\,\langle\kappa|\,s^{2\dagger}\,|-\rangle \int \mathcal{D}\varphi^c \mathcal{D}\varphi^q \int \mathrm{d}\bar{t}\ e^{i\mathcal{A}_{\mathrm{int}}+i\mathcal{A}_{J;\mu\kappa}}e^{i\mathcal{A}_{\mathrm{ferm}}}\ \mathcal{A}_{\mu\kappa}(\bar{t},\bar{t}), \tag{6.17}$$

$$\text{with } \mathcal{A}_{\mu\kappa}(t_1,t_2) = e^{i\vartheta_\mu^q(t_1)+i\vartheta_\kappa^q(t_2)}\ e^{i\phi_\mu - i\phi_\kappa}\ \langle\mu|\,\tilde{f}\tilde{\mathcal{D}}^{-1}(t_1,t_2)\,|\kappa\rangle. \tag{6.18}$$

Functional integration over φ^c yields, in symbolic notation,

$$\int \mathcal{D}\varphi^c \exp\left[i\mathcal{A}_{\mathrm{int}}+i\mathcal{A}_{J;\mu\kappa}\right] = \int \mathcal{D}\varphi^c \exp\left[2i\varphi^c V^{a-1}\varphi^q + iJ^q\varphi^c\right] \propto \delta\left(\varphi^q - \varphi_*^q\right) \tag{6.19}$$

$$\text{with } \varphi_{*\varrho}^q(t) = -\frac{1}{2}\int \mathrm{d}t'\,V_\varrho^a(t,t')J_{\varrho;\mu\kappa}^q(\bar{t},t') \tag{6.20}$$

which renders the φ^q-integration trivial. Taking the average $\langle\ldots\rangle$ therefore reduces to merely evaluating the integrand $e^{i\mathcal{A}_{\mathrm{ferm}}}\mathcal{A}_{\mu\kappa}$ at $\varphi^q = \varphi_*^q$. In what follows we will therefore set $\varphi^q = \varphi_*^q$. The particle numbers are then

$$N_{\mu\kappa} = \langle-|\,s^2\,|\mu\rangle\,\langle\kappa|\,s^{2\dagger}\,|-\rangle \int \mathrm{d}\bar{t}\ e^{i\mathcal{A}_{\mathrm{ferm}}}\ \mathcal{A}_{\mu\kappa}(\bar{t},\bar{t}+\tau_\mu-\tau_\kappa)\Big|_{\vartheta^q=\vartheta_*^q}. \tag{6.21}$$

In the following we will not distinguish ϑ_ϱ^q and

$$\vartheta_{*\varrho}^q(t) = -\int_t^{t+\tau}\mathrm{d}x'\,\varphi_{*\varrho}^q(t') \tag{6.22}$$

any longer.

Obviously, $N_{\mu\kappa} \propto e^{i\phi_\mu - i\phi_\kappa}$ are contributions to currents arising from interference of paths along the edges μ and κ. For $\mu = \kappa$ we recover the classical, *incoherent* contributions: in this case $J_{\sigma;\mu\mu}^q = 0$, hence $\vartheta_*^q = 0$, $\tilde{\mathcal{D}} = \mathbb{1}$, $\mathcal{A}_{\mathrm{ferm}} = 0$, $\mathcal{A}_{\mu\mu} = R_1 f_\mu + T_1 f_{-\mu}$ and thus

$$N_{++} = T_2\,\mathrm{Tr}\left[R_1 f_+ + T_1 f_-\right], \quad N_{--} = R_2\,\mathrm{Tr}\left[R_1 f_- + T_1 f_+\right]. \tag{6.23}$$

Remarkably they are not sensitive to interaction (e.g. no renormalization). This statement is true for any interaction (as long as absent outside the interferometer cell).

That is in contrast to the *coherent* contributions, $\kappa = -\mu$, to current where interaction gives rise to dephasing and an oscillatory dependence of conductance on bias. In this case the source terms are

$$J_{\mu;\mu\kappa}^q(t') = -\mathbb{1}_{[\bar{t},\bar{t}+\tau]}(t') = -J_{-\mu;\mu\kappa}^q(t'), \tag{6.24}$$

giving rise to the instanton potential (6.20)

$$\varphi_\eta^q(t) = -\frac{1}{2}\eta\kappa\int_{\bar{t}}^{\bar{t}+\tau}\mathrm{d}t'\,V_\eta^a(t'). \tag{}$$

Using (6.13) we obtain the instanton phase

$$\vartheta_\eta^q(t) = \frac{1}{2}\eta\kappa\int_t^{t+\tau}\mathrm{d}t'\int_{\bar{t}}^{\bar{t}+\tau}\mathrm{d}t''\,V_\eta^a(t'-t'') \tag{6.25}$$

$$= \frac{\kappa\eta}{\nu}\mathrm{Im}\left[J^>(\bar{t}-t) - J^>(\tau-t+\bar{t})\right]. \tag{6.26}$$

The integral

$$J^{\lessgtr}(t) = \int_0^{\mp\infty} d\epsilon \frac{i\omega_C(1 - e^{i\epsilon\tau})}{\epsilon\left[\epsilon + i\omega_C(1 - e^{i\epsilon\tau})\right]} \left(e^{-i\epsilon t} - 1\right)$$

$$\stackrel{\omega_\eta\tau\gg 1}{\to} -\gamma - \ln\left[-\frac{t \pm ia}{a}\right], \quad a \sim \omega_\eta^{-1},$$

was already discussed at length in Sect. 5.3.4 in the context of the quantum Hall Fabry-Pérot interferometer. We found that

$$J^{\lessgtr}(t) \stackrel{\omega_\eta\tau\gg 1}{\to} -\gamma - \ln\left[-\frac{t \pm ia}{a}\right], \quad a \sim \omega_\eta^{-1},$$

in the strong interaction limit and for long times $\omega_\eta|t| \gg 1$, such that for $|\bar{t} - t|, |\bar{t} + \tau - t| \gg \omega_C^{-1}$ the instanton phase simplifies to the window function

$$\vartheta_\eta^q(t) = -\frac{\kappa\eta}{\nu}\mathrm{Im}\left[\ln\frac{t - \bar{t} + ia}{a} - \ln\frac{t - (\bar{t} + \tau) + ia}{a}\right] = -\frac{\kappa\eta}{\nu}\pi\left[\theta(\bar{t} - t) - \theta(\bar{t} + \tau - t)\right] \qquad (6.27)$$

$$= \bar{\vartheta}_\eta \mathbb{1}_{[\bar{t},\bar{t}+\tau]}(t) \qquad (6.28)$$

with the $\kappa(= -\mu)$-dependent constant $\bar{\vartheta}_\eta = \kappa\eta\pi/\nu$. In this limit we can proceed fully analytically. Moderate interaction strength requires numerical evaluation.

Summarizing, the coherent contributions to currents are

$$N_{+-} = -ir_2 t_2\, e^{i\phi} \int d\bar{t}\, e^{i\mathcal{A}_{\mathrm{ferm}}^{(0)}}\, \frac{\mathrm{Det}\,\tilde{\mathcal{D}}}{\mathrm{Det}\,\tilde{\mathcal{D}}^{(0)}}\, \langle+|\,\tilde{f}\tilde{\mathcal{D}}^{-1}(\bar{t},\bar{t})\,|-\rangle, \qquad (6.29)$$

evaluated at the phase $\vartheta_\eta^q(t) = \bar{\vartheta}_\eta \mathbb{1}_{[\bar{t},\bar{t}+\tau]}(t)$, $\bar{\vartheta}_\eta = -\eta\pi/\nu$, and $N_{-+} = N_{+-}^*$. We further defined the clean action $\mathcal{A}_{\mathrm{ferm}}^{(0)} = \mathcal{A}_{\mathrm{ferm}}\big|_{T_1=0}$ and operator $\tilde{\mathcal{D}}^{(0)} = \tilde{\mathcal{D}}\big|_{T_1=0}$.

The next two somewhat formal sections are devoted to the evaluation of the determinant and inverse of $\tilde{\mathcal{D}}$.

6.3.3 Reduction to single-channel problems

In addition to the double-time dependence, the operators $\tilde{\mathcal{D}}$ and $\tilde{f}$ have a nontrivial channel structure: for given times t_1, t_2 it is $\tilde{\mathcal{D}}(t_1, t_2), \tilde{f}(t_1 - t_2) \in \mathbb{C}^{2\times 2}$. The double index structure (times and channels) complicates matters (the computation of the determinant and inverse of $\tilde{\mathcal{D}}$) quite considerably.

In fact, inversion of similar operators without double-channel structure was achieved by solving an appropriate *Riemann-Hilbert (RH) problem* in Refs. [33, 112]. In this section we will elaborate on this technique and demonstrate its usefulness for our present problem. Specifically, we will rewrite our problem in terms of determinants and inverses of single-channel operators. Their computation will be the subject of the subsequent section.

The Riemann-Hilbert problem

Let us consider for the moment a simpler problem, namely the inversion of

$$\mathcal{D}^{(0)} = \mathbb{1} - \hat{f} + e^{-2i\vartheta_+^q}\hat{f}.$$

As well having a 2×2-channel structure, in contrast to $\tilde{\mathcal{D}}$, this operator is diagonal and can be inverted by means of a RH problem, as demonstrated in this subsection. For this purpose we write

$$\hat{f}(t_1 - t_2) = \hat{\Lambda}(t_1) f_0(t_1 - t_2) \hat{\Lambda}(t_2)^{-1}, \quad \hat{}(t) \equiv \begin{pmatrix} \Lambda_+(t) & \\ & 1 \end{pmatrix} \equiv \begin{pmatrix} e^{-ieVt} & \\ & 1 \end{pmatrix}. \tag{6.30}$$

We further note that $f_0^<(\epsilon) \equiv f_0(\epsilon) = \theta(-\epsilon)$, $f_0^>(\epsilon) \equiv 1 - f_0(\epsilon) = \theta(\epsilon)$ are projection operators in energy domain. In time representation they project onto functions which are analytic in the upper/lower half of the complex time plane: i.e. it is

$$\left(f_0^{\lessgtr} g \right)(t) = \pm \frac{i}{2\pi} \int dt' \frac{g(t')}{t - t' \pm ia}$$

for functions g which decay sufficiently fast as $|t'| \to \infty$. By making use of this property we can invert $\mathcal{D}_0 = \hat{\Lambda} \left(f_0^> + e^{-2i\vartheta_+^q} f_0^< \right) \hat{\Lambda}^{-1}$. To this end we decompose the kernel $\mathcal{K}(t) = e^{-2i\vartheta_+^q(t)}$ into positive and negative energy contributions. More specifically, we solve the Riemann-Hilbert problem of finding a complex matrix-valued function $Y(t) \in \mathbb{C}^{2 \times 2}$ of complex time t which has the properties

1. $Y(t)$ is analytic on $\mathbb{C} \setminus [\bar{t}, \bar{t} + \tau]$;

2. $Y(t)$ has a branchcut discontinuity along $[\bar{t}, \bar{t} + \tau]$ such that $Y_\pm(t) \equiv \lim_{\delta \to +0} Y(t \pm i\delta)$ satisfy $Y_-(t)^{-1} Y_+(t) = \mathcal{K}(t)$;

3. $Y(t)$ has integrable singularities at $t = \bar{t}, \bar{t} + \tau$ and $\lim_{|t| \to \infty} Y(t) = 1$.

This function Y then has the projection properties

$$f_0^< Y_+ f_0^< = Y_+ f_0^<, \quad f_0^> Y_- f_0^> = Y_- f_0^>, \tag{6.31}$$

which, loosely speaking, allow to "commute" projectors and functions $Y_\pm$ and get rid of redundant projectors. The same relations hold for the inverses $Y_\pm^{-1}$, from which one can deduce that the inverse of $\mathcal{D}_0 = \hat{\Lambda} Y_-^{-1} \left(Y_- f_0^> + Y_+ f_0^< \right) \hat{\Lambda}^{-1}$ is

$$\mathcal{D}_0^{-1} = \hat{\Lambda} \left(Y_-^{-1} f_0^> + Y_+^{-1} f_0^< \right) Y_- \hat{\Lambda}^{-1}. \tag{6.32}$$

In fact, for the diagonal kernel $\mathcal{K}(t) = e^{-2i\vartheta_+^q(t)}$ the solution to the RH problem is straightforwardly given by

$$Y_\pm(t) = \exp \left\{ \mp 2i \int dt' f_0^{\lessgtr}(t - t') \vartheta_+^q(t') \right\} = \exp \left\{ \frac{\bar{\vartheta}_+}{\pi} \ln \frac{t - \bar{t} \pm i0}{t - \bar{t} - \tau \pm i0} \right\}. \tag{6.33}$$

The same projection relations (6.31) also allow for a decomposition of $\tilde{\mathcal{D}}$.

Removing the double-channel structure

First, let $Y(t) = \exp \left[\frac{\bar{\vartheta}_+}{\pi} \ln \frac{t - \bar{t}}{t - \bar{t} - \tau} \right]$ be the above RH solution with branchcut behavior $Y_-^{-1} Y_+ = e^{-2i\vartheta_+^q}$ along the real time axis. With $\vartheta_-^q = -\vartheta_+^q$ and thus

$$\Lambda^{-1} s_1^\dagger \begin{pmatrix} e^{2i\vartheta_+^q} & 0 \\ 0 & e^{2i\vartheta_-^q} \end{pmatrix} s_1 \Lambda = \Lambda^{-1} s_1^\dagger \begin{pmatrix} e^{4i\vartheta_+^q} & 0 \\ 0 & \mathbb{1} \end{pmatrix} s_1 \Lambda \, Y_-^{-1} Y_+ \tag{6.34}$$

we obtain

$$\tilde{\mathcal{D}} = s_1 \Lambda Y_-^{-1} \left[Y_- f_0^> + \Lambda^{-1} s_1^\dagger \begin{pmatrix} e^{4i\vartheta_+^q} & 0 \\ 0 & \mathbb{1} \end{pmatrix} s_1 \Lambda Y_+ f_0^< \right] \Lambda^{-1} s_1^\dagger \tag{6.35}$$

$$= Y_-^{-1} s_1 \Lambda \left[f_0^> + \Lambda^{-1} s_1^\dagger \begin{pmatrix} e^{4i\vartheta_+^q} & 0 \\ 0 & \mathbb{1} \end{pmatrix} s_1 \Lambda f_0^< \right] \Lambda^{-1} \Lambda \left[Y_- f_0^> + Y_+ f_0^< \right] \Lambda^{-1} s_1^\dagger \tag{6.36}$$

$$= Y_-^{-1} \mathcal{D}_* s_1 \Lambda \left[Y_- f_0^> + Y_+ f_0^< \right] \Lambda^{-1} s_1^\dagger \tag{6.37}$$

$$= Y_-^{-1} \mathcal{D}_* s_1 Y_- \mathcal{D}_0 s_1^\dagger \tag{6.38}$$

with

$$\mathcal{D}_* \equiv \mathbb{1} + \begin{pmatrix} e^{4i\vartheta_+^q} - \mathbb{1} & 0 \\ 0 & 0 \end{pmatrix} \tilde{f} = \begin{pmatrix} \mathcal{D}_{**} & \left(e^{4i\vartheta_+^q} - \mathbb{1} \right) f_{+-} \\ 0 & \mathbb{1} \end{pmatrix}, \quad \mathcal{D}_{**} \equiv \mathbb{1} + \left(e^{4i\vartheta_+^q} - \mathbb{1} \right) f_{++}, \tag{6.39}$$

$$\mathcal{D}_0 = \mathbb{1} + \left(e^{-2i\vartheta_+^q} - \mathbb{1} \right) \hat{f} = \begin{pmatrix} \mathbb{1} + \left(e^{-2i\vartheta_+^q} - \mathbb{1} \right) f_+ & 0 \\ 0 & \mathbb{1} + \left(e^{2i\vartheta_-^q} - \mathbb{1} \right) f_- \end{pmatrix}. \tag{6.40}$$

Determinant of $\tilde{\mathcal{D}}$ The operators $\mathcal{D}_0$ and $\mathcal{D}_*$ are diagonal and upper triangular matrices with respect to channel indices which allows to represent $\mathrm{Det}\,\tilde{\mathcal{D}}$ in terms of single-channel operators. From (6.38) follows:

$$\mathrm{Det}\,\tilde{\mathcal{D}} = \mathrm{Det}\,\mathcal{D}_*\ \mathrm{Det}\,\mathcal{D}_0 = \mathrm{Det}\,\mathcal{D}_{**}\ \mathrm{Det}\left[\mathbb{1} + (e^{-2i\vartheta_+^q} - \mathbb{1}) f_+ \right] \mathrm{Det}\left[\mathbb{1} + (e^{2i\vartheta_-^q} - \mathbb{1}) f_- \right]. \tag{6.41}$$

The second of these determinants can be rewritten by solving a different Riemann-Hilbert problem with branchcut behavior $\tilde{Y}_-^{-1} \tilde{Y}_+ = e^{-4i\vartheta_+^q}$ on the real time axis. Noting

$$\tilde{Y}_- f_0^> + \tilde{Y}_+ f_0^< = \left[\tilde{Y}_-^{-1} f_0^> + \tilde{Y}_+^{-1} f_0^< \right]^{-1} = \left[f_0^> + e^{4i\vartheta_+^q} f_0^< \right]^{-1} \tilde{Y}_- \tag{6.42}$$

we obtain

$$\mathbb{1} + (e^{-2i\vartheta_+^q} - \mathbb{1}) f_+ = \Lambda_+ \tilde{Y}_-^{-1} \left[\tilde{Y}_- f_0^> + e^{2i\vartheta_+^q} \tilde{Y}_+ f_0^< \right] \Lambda_+^{-1} \tag{6.43}$$

$$= \Lambda_+ \tilde{Y}_-^{-1} \left[f_0^> + e^{2i\vartheta_+^q} f_0^< \right] \left[\tilde{Y}_- f_0^> + \tilde{Y}_+ f_0^< \right] \Lambda_+^{-1} \tag{6.44}$$

$$= \tilde{Y}_-^{-1} \left[\mathbb{1} + \left(e^{2i\vartheta_+^q} - \mathbb{1} \right) f_+ \right] \left[\mathcal{D}_{**}^{(0)} \right]_{T_1 \to 0}^{-1} \tilde{Y}_- \tag{6.45}$$

where the superindex (0) denotes the limit $T_1 \to 0$ and we used

$$\Lambda_+ \left[\tilde{Y}_- f_0^> + \tilde{Y}_+ f_0^< \right] \tilde{Y}_-^{-1} \Lambda_+^{-1} = \left\{ \Lambda_+ \tilde{Y}_- \left[\tilde{Y}_-^{-1} f_0^> + \tilde{Y}_+^{-1} f_0^< \right] \Lambda_+^{-1} \right\}^{-1}$$

$$= \left[\mathbb{1} + \left(e^{4i\vartheta_+^q} - \mathbb{1} \right) f_+ \right]^{-1} = \left[\mathcal{D}_{**}^{(0)} \right]^{-1} \tag{6.46}$$

since $f_{++} \to f_+$, $f_{--} \to f_-$ for $T_1 \to 0$. This implies

$$\text{Det}\left[\mathbb{1} + (e^{-2i\vartheta_+^q} - \mathbb{1})f_+\right] = \text{Det}\left[\mathbb{1} + (e^{2i\vartheta_+^q} - \mathbb{1})f_+\right] / \text{Det}\,\mathcal{D}_{**}^{(0)} \tag{6.47}$$

and

$$\frac{\text{Det}\,\tilde{\mathcal{D}}}{\text{Det}\,\tilde{\mathcal{D}}^{(0)}} = \text{Det}\,\mathcal{D}_{**}\left[\text{Det}\,\tilde{\mathcal{D}}/\text{Det}\,\mathcal{D}_{**}\right]_{T_1 \to 0}. \tag{6.48}$$

Inversion of $\tilde{\mathcal{D}}$ Returning to Eq. (6.37) with the Riemann-Hilbert problem $Y_-^{-1}Y_+ = e^{-2i\vartheta_+^q}$ the inverse of $\tilde{\mathcal{D}}$ is

$$\tilde{\mathcal{D}}^{-1} = s_1\hat{\Lambda}\left[Y_-^{-1}f_0^> + Y_+^{-1}f_0^<\right]\hat{\Lambda}^{-1}s_1^\dagger\mathcal{D}_*^{-1}Y_-. \tag{6.49}$$

Convolution with the rotated distribution function $\tilde{f}$ yields

$$\tilde{f}\tilde{\mathcal{D}}^{-1} = s_1\hat{\Lambda}f_0\hat{\Lambda}^{-1}s_1^\dagger\tilde{\mathcal{D}}^{-1} = Y_+^{-1}\tilde{f}\mathcal{D}_*^{-1}Y_- \tag{6.50}$$

the $(+,\bar{t};-,\bar{t})$-component of which is

$$\langle+|\,\tilde{f}\tilde{\mathcal{D}}^{-1}(\bar{t},\bar{t})\,|-\rangle = \left(Y_+^{-1}Y_-\right)(\bar{t})\,\langle+|\,\tilde{f}\mathcal{D}_*^{-1}(\bar{t},\bar{t})\,|-\rangle = e^{2i\bar{\vartheta}_+}\,\langle+|\,\tilde{f}\mathcal{D}_*^{-1}(\bar{t},\bar{t})\,|-\rangle. \tag{6.51}$$

Inversion of the operator $\mathcal{D}_*$ is not exactly trivial, but simplified by its triangular structure in channel space:

$$\mathcal{D}_*^{-1} = \begin{pmatrix} \mathcal{D}_{**}^{-1} & -\mathcal{D}_{**}^{-1}\left(e^{4i\vartheta^q} - \mathbb{1}\right)f_{+-} \\ 0 & \mathbb{1} \end{pmatrix}. \tag{6.52}$$

Note that the relation $\mathcal{D}_{**}(t_1, t_2) = \delta(t_1 - t_2)$ for $t_1 \notin [\bar{t}, \bar{t} + \tau]$ implies the same for the inverse, $\mathcal{D}_{**}^{-1}(t_1, t_2) = \delta(t_1 - t_2)$ for $t_1 \notin [\bar{t}, \bar{t}+\tau]$ (this can be seen by block matrix representation or reformulation in terms of a Riemann-Hilbert problem). One therefore obtains

$$\langle+|\,\tilde{f}\tilde{\mathcal{D}}^{-1}(\bar{t},\bar{t})\,|-\rangle = e^{2i\bar{\vartheta}_+}\left[-f_{++}\mathcal{D}_{**}^{-1}\left(e^{4i\vartheta_+^q} - \mathbb{1}\right)f_{+-} + f_{+-}\right](\bar{t},\bar{t})$$

$$= e^{2i\bar{\vartheta}_+}\int_{\bar{t}}^{\bar{t}+\tau}\text{d}t'\,\mathcal{D}_{**}^{-1}(\bar{t},t')f_{+-}(t',\bar{t}). \tag{6.53}$$

In the previous subsection it was shown how the operator $\mathcal{D}_{**}$ is inverted in the limit $T_1 \to 0$, Eq. (6.46). With $\tilde{Y}(t) = (\frac{t-\bar{t}}{t-\bar{t}-\tau})^{2\bar{\vartheta}_+/\pi}$ one obtains for $t \in [\bar{t}, \bar{t}+\tau]$, $t - \bar{t}, \bar{t}+\tau - t \gg \Lambda^{-1}$ (Λ being the UV cutoff)

$$\left[\mathcal{D}_{**}^{(0)}\right]^{-1}(\bar{t},t) = \tilde{Y}_-(\bar{t})\left[\mathbb{1} + \left(e^{-4i\vartheta_+^q} - \mathbb{1}\right)f_+\right]_{\bar{t},t}\tilde{Y}_-^{-1}(t) \tag{6.54}$$

$$= -\frac{\Lambda}{\pi}\,e^{-2i\bar{\vartheta}_+}\sin(2\bar{\vartheta}_+)\,e^{-ieV(\bar{t}-t)}\left|t - \bar{t}\right|^{-2\bar{\vartheta}_+/\pi-1}\left|\bar{t}+\tau-t\right|^{2\bar{\vartheta}_+/\pi}\tau^{-2\bar{\vartheta}_+/\pi}\Lambda^{-2\bar{\vartheta}_+/\pi-1} \tag{6.55}$$

where the regularization $\tilde{Y}_-(\bar{t}) = \tilde{Y}_-(\bar{t} + \Lambda^{-1})$ was chosen.

For arbitrary $T_1 > 0$ the operator $\mathcal{D}_{**}$, though scalar in channel space, contains a nontrivial nonequilibrium distribution function $f_{++} = R_1 f_+ + T_1 f_-$ (which has two discontinuities in energy representation) and thus cannot be easily inverted by means of the Riemann-Hilbert problem. In the next section we will relate the inversion problem to determinants of operators of (generalized) *Toeplitz* form.

6.3.4 Toeplitz matrices and generalizations

Fredholm determinants of the form

$$\text{Det}\,\mathcal{D}_{**} = \text{Det}\left[\mathbb{1} + \left(e^{4i\vartheta_+^q} - \mathbb{1}\right)f_{++}\right]$$

with a window function $\vartheta_+^q(t) = \bar{\vartheta}_+\mathbb{1}_{[\bar{t},\bar{t}+\tau]}(t)$ and a stationary distribution function f_{++} were already encountered in the context of nonequilibrium bosonization of Luttinger liquids, cf. e.g. end of Sect. 2.3. Their asymptotic behavior for large times τ is the topic of Appendix A. The basic observation is that due to the special form of $\vartheta_+^q(t)$ the determinant $\text{Det}\,\mathcal{D}_{**}$ can be related to a Toeplitz determinant. Indeed, by introducing an UV cutoff Λ and discretizing times $t_j = \bar{t} + (j-1)\Delta t$ into steps $\Delta t = \pi/\Lambda$ the operator $\mathcal{D}_{**}(t_1, t_2)$ can be mapped onto a finite $N \times N$-Toeplitz matrix $(g_{j,k}) = (g_{j-k})$ of size $N = \Lambda\tau/\pi$. Most conveniently one starts with the "symbol"

$$g(\epsilon) = e^{2i\bar{\vartheta}_+\epsilon/\Lambda}\left[1 + \left(e^{4i\bar{\vartheta}_+} - 1\right)f_{++}(\epsilon)\right], \quad -\Lambda < \epsilon \leq \Lambda,$$

essentially the energy representation of $\mathcal{D}_{**}$. The slow prefactor $e^{2i\bar{\vartheta}_+\epsilon/\Lambda}$ prevents the arising of artificial Fermi edge singularity effects at $\epsilon = \pm\Lambda$ due to the hard cutoff. The discretized version g_{j-k} of $\mathcal{D}_{**}(t_1, t_2)$ is then obtained by Fourier transformation

$$g_{j-k} = \int_{-\Lambda}^{\Lambda} \frac{d\epsilon}{2\Lambda}\, e^{-i\epsilon(j-k)\Delta t}g(\epsilon) = \frac{i}{2\pi}\frac{1}{j-k-2\bar{\vartheta}_+/\pi}\left(e^{4i\bar{\vartheta}_+} - 1\right)\left[R_1 e^{-i\pi eV/\Lambda[j-k-2\bar{\vartheta}_+/\pi]} + T_1\right].$$

$$\tag{6.56}$$

Using the results of Appendix A, Eq. (A.14), we obtain for $eV\tau \gg 1$ the asymptotic expansion

$$\frac{\text{Det}\,\mathcal{D}_{**}}{\text{Det}\,\mathcal{D}_{**}^{(0)}} = \frac{\Delta\left[4\vartheta_+^q, f_{++}\right]}{\Delta\left[4\vartheta_+^q, f_+\right]} = \exp\left\{\frac{eV\tau}{2\pi}\left[-i2\bar{\vartheta}_+ + \ln\left[R_1 e^{4i\bar{\vartheta}_+} + T_1\right]\right]\right\}$$

$$\times \sum_{n=-\infty}^{\infty} e^{-ieV\tau n}(eV\tau)^{2(\beta_0+n)(\beta_1-n)}\frac{G(1+\beta_0+n)G(1-\beta_0-n)G(1+\beta_1-n)G(1-\beta_1+n)}{G(1+2\bar{\vartheta}_+/\pi)G(1-2\bar{\vartheta}_+/\pi)} \quad (6.57)$$

with $\beta_1 = -\frac{i}{2\pi}\ln\left[R_1 e^{4i\bar{\vartheta}_+} + T_1\right]$ and $\beta_0 = -2\bar{\vartheta}_+/\pi - \beta_1$ and the Barnes G-function G.

Inversion of $\mathcal{D}_{**}$

Remarkably, the same relations are also useful to invert Toeplitz matrices. We show here how $\mathcal{D}_{**}^{-1}(\bar{t}, t)$ can be related to a *generalized* Toeplitz determinant the asymptotic behavior of which can be estimated by generalizing known results about Toeplitz determinants. We start with Laplacian expansion of $\det(g)$ which shows that the inverse g^{-1} is

$$\left(g^{-1}\right)_{jk} = (-1)^{j+k}\frac{\det g^\sharp(k,j)}{\det(g)}, \tag{6.58}$$

where $g^{\sharp}(k,j)$ is a $(N-1) \times (N-1)$-matrix derived from g by removing its k-th row and j-th column. Specifically for $j = 1$ (corresponding to the continuous time $\bar{t}$) its elements are

$$
\left(g^{\sharp}(k,1)\right)_{lm} = \begin{cases} g_{l,m+1}, & 1 \leq l < k, \\ g_{l,m}, & k \leq l \leq N-1 \end{cases} \tag{6.59}
$$

$$
= \frac{i}{2\pi} \frac{1}{l - m - \frac{2}{\pi}\vartheta_{+}(t_l;t_k)} \left(e^{4i\vartheta_{+}(t_l;t_k)} - 1 \right) \left[R_1 e^{-i\pi U/\Lambda[j-k-\frac{2}{\pi}\vartheta_{+}(t_l;t_k)]} + T_1 \right] \tag{6.60}
$$

with the time-dependent phase $(t_l = \bar{t} + (l-1)\Delta t)$

$$
\vartheta_{+}(t_l;t_k) = \begin{cases} \bar{\vartheta}_{+} + \pi/2, & \bar{t} \leq t_l < t_k, \\ \bar{\vartheta}_{+}, & t_k \leq t_l < \bar{t} + \tau. \end{cases} \tag{6.61}
$$

Hence, $g^{\sharp}(k,j)$ differs from g in the time-dependence of the phase $\vartheta_{+}(t;t_k)$ (and the size) which prevents it to be a Toeplitz matrix. Numerical studies however suggest, that known results about Toeplitz determinants can be generalized to our case, see Appendix A. Then it is

$$
\left(g^{-1}\right)_{1k} = (-1)^{1+k} \frac{\Delta[4\vartheta_{+}(\bullet;t_k), f_{++}]}{\Delta[4\bar{\vartheta}_{+}, f_{++}]}, \tag{6.62}
$$

where the denominator, a Toeplitz determinant, can be evaluated with (A.14) and the numerator with (A.21).

It is instructive to apply these relations to invert (6.56) and thus $\mathcal{D}_{**}$ in the limit $T_1 \to 0$ for which the computation can be done via the Riemann-Hilbert problem. For $\mathcal{D}_{**}^{-1}(\bar{t}, t_k)$ and thus $\left(g^{-1}\right)_{1k}$ one needs to consider the generalized Toeplitz problem with three jumps in time domain, $\tau_1 = \bar{t}$, $\tau_2 = t_k$, $\tau_3 = \bar{t}+\tau$, and just 1 jump in in energy domain $\mu_1 = eV$. Further it is $c_{10} = 2\bar{\vartheta}_{+}/\pi + 1$ and $c_{20} = 2\bar{\vartheta}_{+}/\pi$ and hence $p_{12} = -2\bar{\vartheta}_{+}/\pi - 1$, $p_{13} = -\left(2\bar{\vartheta}_{+}/\pi + 1\right) 2\bar{\vartheta}_{+}/\pi$ and $p_{23} = 2\bar{\vartheta}_{+}/\pi$. The asymptotic behavior of $\det(g) = \Delta[4\vartheta_{+}^{q}, f_{+}]$ is known and one obtains

$$
\left[\left(g^{-1}\right)_{1k}\right]_{T_1 \to 0} = \Gamma e^{-ieV(\bar{t}-t_k)} \left|\frac{\Lambda(t_k - \bar{t})}{\pi}\right|^{-2\bar{\vartheta}_{+}/\pi - 1} \left|\frac{\Lambda(\bar{t} + \tau - t_k)}{\pi}\right|^{2\bar{\vartheta}_{+}/\pi} \left|\frac{\Lambda\tau}{\pi}\right|^{-2\bar{\vartheta}_{+}/\pi}. \tag{6.63}
$$

Except for the dimensionless unknown factor Γ and the dimensionful prefactor $\Lambda/\pi = \left(\Delta t\right)^{-1}$ which arises due to discretization, the above asymptotics agrees in all power-laws with the exact result (6.55).

Now we turn to the less trivial case of arbitrary $0 < T_1 < 1$. Now, the distribution function is f_{++} instead of f_{+} which adds a discontinuity at $\mu_1 = 0$ (the one at eV is now denoted μ_2). The asymptotics of $\Delta[4\vartheta_{+}(\bullet;t_k)]$ is determined by

$$
c_{10} = \alpha_1 + 1, \quad c_{20} = \alpha_1; \qquad\qquad \alpha_1 \equiv 2\bar{\vartheta}_{+}/\pi, \tag{6.64}
$$

$$
c_{k1} = \beta_1 + n_k \quad (k = 1, 2); \qquad\qquad \beta_1 \equiv \frac{1}{2\pi i} \ln\left[R_1 e^{4i\bar{\vartheta}_{+}} + T_1 \right], \tag{6.65}
$$

and the exponents

$$
\begin{aligned}
p_{12} =& -(\alpha_1 + 1 - \beta_1) + n_1(\alpha_1 - 2\beta_1) - n_2(\alpha_1 + 1 - 2\beta_1) - 2n_1(n_1 - n_2 - 1), \\
p_{23} =& \,\alpha_1 - \beta_1 - n_1(\alpha_1 - 2\beta_1) + n_2(\alpha_1 + 1 - 2\beta_1) - 2n_2(n_2 - n_1 + 1), \\
p_{13} =& -(\alpha_1 + 1 - \beta_1)(\alpha_1 - \beta_1) - \beta_1^2 + n_1(\alpha_1 - 2\beta_1) + n_2(\alpha_1 + 1 - 2\beta_1) - 2n_1n_2, \\
q_{12} =& \,(\alpha_1 + 1 - \beta_1)\beta_1 + (\alpha_1 - \beta_1)\beta_1 + n_1(\alpha_1 - 2\beta_1) + n_2(\alpha_1 + 1 - 2\beta_1) \\
& + 2(n_1n_2 + n_1 - n_2) - 2n_1^2 - 2n_2^2.
\end{aligned}
\tag{6.66}
$$

One then has

$$
(-1)^{1+k}\Delta[4\vartheta_+(\bullet; t_k), f_{++}] = \sum_{n_1, n_2} \Gamma_{(n_1, n_2)} e^{i\alpha_1\Lambda\tau + i\beta_1 eV\tau} e^{ieV[n_1(t_k - \bar{t}) + n_2(\bar{t} + \tau - t_k)]}
$$

$$
\times \left|\frac{\Lambda(t_k - \bar{t})}{\pi}\right|^{p_{12}} \left|\frac{\Lambda(\bar{t} + \tau - t_k)}{\pi}\right|^{p_{23}} \left|\frac{\Lambda\tau}{\pi}\right|^{p_{13}} \left|\frac{\pi eV}{\Lambda}\right|^{q_{12}}.
\tag{6.67}
$$

This expression is valid when all time differences $|t_k - \bar{t}|$, τ, $|\bar{t} + \tau - t_k|$ are large as compared to the time scales defined by Λ and eV; notably $\bar{t} + (eV)^{-1} \ll t_k \ll \bar{t} + \tau - (eV)^{-1}$, which is the regime I in Fig. 6.10. For intermediate times such as in the regime IIb, $\bar{t} + \Lambda^{-1} \lesssim t_k \lesssim \bar{t} + (eV)^{-1}$ the powers are expected to cross over to different values. We study the modified powers in the next paragraph.
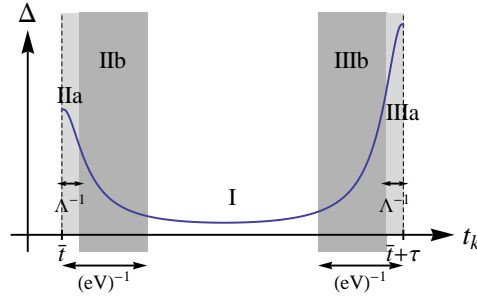

Figure 6.10: *Sketch of the determinant Δ as function of time t_k. The asymptotic expansion (6.67) is valid in region I. A crossover to different powers is expected in regions IIa,...,IIIb, defined by the time scales $(eV)^{-1}$ and Λ^{-1}.*

Short-time crossover Let us consider the behavior for t_k close to $\bar{t}$. In the regime IIa, $t_k - \bar{t} \lesssim \Lambda^{-1}$, the system is unable to resolve the phase jump at t_k, hence $\vartheta_+(\bullet; t_k) \to \bar{\vartheta}_+$, and we expect

$$
(-1)^{1+k}\Delta[4\vartheta_+(\bullet; t_k), f_{++}] \to \sum_{n'} \Gamma'_0(n') \, e^{i\alpha_1\Lambda\tau + i\beta_1 eV\tau - ieV\tau n'}
$$

$$
\times \left|\frac{\Lambda\tau}{\pi}\right|^{-(\alpha_1 - \beta_1 + n')^2 - (\beta_1 - n')^2} \left|\frac{\pi eV}{\Lambda}\right|^{2(\alpha_1 - \beta_1 + n')(\beta_1 - n')}
\tag{6.68}
$$

with $\Gamma'_0(n') = G(1 + \alpha_1 - \beta_1 + n')G(1 - \alpha_1 + \beta_1 - n')G(1 + \beta_1 - n')G(1 - \beta_1 + n')$. In the intermediate regime IIb, $\Lambda^{-1} \lesssim t_k - \bar{t} \lesssim |eV|^{-1}$, the powers can be modified,

$$
(-1)^{1+k}\Delta[4\vartheta_+(\bullet; t_k), f_{++}] \sim \sum \mathcal{K}' \left|\frac{\Lambda(t_k - \bar{t})}{\pi}\right|^{p'_{12}} \left|\frac{\Lambda\tau}{\pi}\right|^{p'_{13}} \left|\frac{\pi eV}{\Lambda}\right|^{q'_{12}}
\tag{6.69}
$$

Matching these asymptotics at $t_k \sim \bar{t} + |eV|^{-1}$ and $t_k \sim \bar{t} + \Lambda^{-1}$ requires

$$q'_{12} - p'_{12} = q_{12} - p_{12} = 2(\alpha_1 - \beta_1 - n_2)(\beta_1 + n_2) + 1 + \alpha_1, \tag{6.70}$$

$$p'_{13} = p_{23} + p_{13} = -(\alpha_1 - \beta_1 - n_2)^2 - (\beta_1 + n_2)^2, \tag{6.71}$$

$$q'_{12} = 2(\alpha_1 - \beta_1 + n')(\beta_1 - n'), \tag{6.72}$$

$$p'_{13} = -(\alpha_1 - \beta_1 + n')^2 - (\beta_1 - n')^2 \tag{6.73}$$

which is satisfied by setting $p'_{12} = -1 - \alpha_1$ and $n_2 = -n'$. Similarly, in the regime IIIa, $|\bar{t} + \tau - t_k| \lesssim \Lambda^{-1}$ we expect

$$(-1)^{1+k} \Delta[4\vartheta_+(\bullet; t_k), f_{++}] \to e^{-i\Lambda\tau} \Delta[4\bar{\vartheta}_+ + 2\pi, f_{++}]$$

$$= \sum_{n''} \Gamma''_0(n'') \, e^{i\alpha_1\Lambda\tau + i\beta_1 eV\tau - ieV\tau n''} \left| \frac{\Lambda\tau}{\pi} \right|^{-(\alpha_1+1-\beta_1+n')^2-(\beta_1-n')^2} \left| \frac{\pi eV}{\Lambda} \right|^{2(\alpha_1+1-\beta_1+n')(\beta_1-n')} \tag{6.74}$$

with $\Gamma''_0(n'') = G(2 + \alpha_1 - \beta_1 + n'')G(-\alpha_1 + \beta_1 - n'')G(1 + \beta_1 - n'')G(1 - \beta_1 + n'')$, while for the intermediate range IIIb, $|eV|^{-1} \lesssim \bar{t} + \tau - t_k \lesssim \Lambda^{-1}$, we make the ansatz

$$(-1)^{1+k} \Delta[4\vartheta_+(\bullet; t_k), f_{++}] \sim \sum \mathcal{K}'' \left| \frac{\Lambda(\bar{t} + \tau - t_k)}{\pi} \right|^{p''_{23}} \left| \frac{\Lambda\tau}{\pi} \right|^{p''_{13}} \left| \frac{\pi eV}{\Lambda} \right|^{q''_{12}}. \tag{6.75}$$

Matching at points $t_k \sim \bar{t} + \tau - |eV|^{-1}$ and $t_k \sim \bar{t} + \tau - \Lambda^{-1}$ requires

$$q''_{12} - p''_{23} = q_{12} - p_{23} = 2(\alpha_1 + 1 - \beta_1 - n_1)(\beta_1 + n_1) - \alpha_1, \tag{6.76}$$

$$p''_{13} = p_{12} + p_{13} = -(\alpha_1 + 1 - \beta_1 - n_1)^2 - (\beta_1 + n_1)^2, \tag{6.77}$$

$$q''_{12} = 2(\alpha_1 + 1 - \beta_1 + n'')(\beta_1 - n''), \tag{6.78}$$

$$p''_{13} = -(\alpha_1 + 1 - \beta_1 + n'')^2 - (\beta_1 - n'')^2 \tag{6.79}$$

which are satisfied by setting $n'' = -n_1$ and $p''_{23} = \alpha_1$. Then the summation in (6.75) extends over the integer $n_1 = -n''$.

6.3.5 Strong Coupling Results

Combining Eqs. (6.29),(6.53),(6.57) we obtain for the interference contributions to current

$$N_{+-} = N^*_{+-} = -ir_2 t_2 \int d\bar{t} \, \frac{\text{Det}\,\tilde{\mathcal{D}}}{\text{Det}\,\tilde{\mathcal{D}}^{(0)}} e^{i\mathcal{A}^{(0)}_{\text{ferm}}} \, e^{i\phi + 2i\bar{\vartheta}_+} \int_{\bar{t}}^{\bar{t}+\tau} dt' \, \mathcal{D}^{-1}_{**}(\bar{t}, t') f_{+-}(t' - \bar{t}) \tag{6.80}$$

$$= -ir_2 t_2 e^{i\phi + 2i\bar{\vartheta}_+} \int d\bar{t} \, e^{i\mathcal{A}^{(0)}_{\text{ferm}}} \int_{\bar{t}}^{\bar{t}+\tau} dt_k \left[\frac{\mathcal{D}^{-1}_{**}(\bar{t}, t_k)}{\left(g^{-1}\right)_{1k}} \right]_{T_1 \to 0} \frac{(-1)^{1+k} \Delta[4\vartheta_+(\bullet; t_k), f_{++}]}{\Delta[4\vartheta_+, f_+]} f_{+-}(t_k - \bar{t}) \tag{6.81}$$

with the phase $\bar{\vartheta}_\eta = -\eta\pi/\nu$. It turns out that the integrand is in fact independent of time $\bar{t}$ and thus the integral is formally divergent. This amounts to an infinite number of electrons counted during an

infinite measuring time in a stationary situation. The stationary current is obtained by dropping the $\bar{t}$-integral and putting, say, $\bar{t} = 0$,

$$e^{-1} I_{+-} = r_1 t_1 r_2 t_2 \; e^{i\phi + 2i\bar{\vartheta}_+} e^{i\mathcal{A}^{(0)}_{\text{ferm}}}$$

$$\times \int_0^\tau \mathrm{d}t_k \left[\frac{\mathcal{D}_{**}^{-1}(0, t_k)}{\left(g^{-1} \right)_{1k}} \right]_{T_1 \to 0} \frac{(-1)^{1+k} \Delta[4\vartheta_+(\bullet; t_k), f_{++}]}{\Delta[4\vartheta_+, f_+]} (f_+(t_k) - f_-(t_k)). \quad (6.82)$$

The t_k-integral

The nontrivial part

$$\mathcal{J} \equiv (-1)^{1+k} \Delta[4\vartheta_+(\bullet; t_k), f_{++}](f_+(t_k) - f_-(t_k)) \quad (6.83)$$

of the integrand has power-law singularities at $t_k \sim 0$ and $t_k \sim \tau$ which contribute dominantly to the integral provided that the real part of the corresponding exponents are negative. For $|eVt|, |eV(\tau - t_k)| \gg 1$ according to (6.67) the relevant powers are

$$\mathcal{J} \sim t_k^{p_{12}-1} (\tau - t_k)^{p_{23}} \tau^{p_{13}} (eV)^{q_{12}}. \quad (6.84)$$

Eq. (6.66) shows that by choosing $|n_1|$ and $|n_2|$ sufficiently large, $\operatorname{Re} p_{12}$ and $\operatorname{Re} p_{23}$, respectively, can be easily made negative. Before proceeding we remind ourselves that power laws are modified as one goes closer to the singularities. In general, in all regions of $(0, \tau)$ the integrand is a superposition of powers,

$$\mathcal{J} \sim t_k^{\tilde{p}_{12}} (\tau - t_k)^{\tilde{p}_{23}} \tau^{\tilde{p}_{13}} (eV)^{\tilde{q}_{12}} \Lambda^{\tilde{\gamma}+1}, \quad (6.85)$$

where $\tilde{\gamma} \equiv \tilde{p}_{12} + \tilde{p}_{23} + \tilde{p}_{13} - \tilde{q}_{12}$ ensures the correct dimensionality (which is inverse time). The powers have been discussed in the previous section for different asymptotic regions, separated by the time scales $0 < \Lambda^{-1} \ll (eV)^{-1} \ll \tau - (eV)^{-1} \ll \tau - \Lambda^{-1} < \tau$.

For instance, very close to the left singularity, $0 < t_k \lesssim \Lambda^{-1}$, it is

$$f_+(t_k) - f_-(t_k) = \frac{i}{2\pi} \frac{e^{-ieVt_k} - 1}{t_k} \approx \frac{eV}{2\pi}, \quad (6.86)$$

and the powers are $\tilde{p}_{12} = 0$, $\tilde{p}_{23} = 0$, $\tilde{p}_{13} = p'_{13}$, and $\tilde{q}_{12} = q'_{12} + 1$. Integration over these regimes will lead to another superposition of powers

$$\int \mathrm{d}t_k \, \mathcal{J} \sim (eV\tau)^{\tilde{p}} (eV/\Lambda)^{\tilde{r}}. \quad (6.87)$$

The leading terms are those with large $\operatorname{Re} \tilde{p}$ and small $\operatorname{Re} \tilde{r}$. In our example

$$\int_0^{\Lambda^{-1}} \mathrm{d}t_k \, \mathcal{J} \sim (eV\tau)^{p'_{13}} (eV/\Lambda)^{q'_{12}+1-p'_{13}} \sim (eV\tau)^{p'_{13}} (eV/\Lambda)^{1+\alpha_1^2}. \quad (6.88)$$

Due to $\alpha_1 = -2/\nu$, the second exponent is constant (independent of any integer n_1 or n_2), thus it suffices to minimize the real part of

$$p'_{13} = -2 \left(n_2 - \frac{\alpha_1 - 2\beta_1}{2} \right)^2 - \frac{\alpha_1^2}{2}. \quad (6.89)$$

The property that the exponent of (eV/Λ) and thus of Λ is constant is convenient and not a coincidence: It encodes renormalization effects due to high-energy virtual excitations. In contrast, the arbitrary integers which encode different branches of $\ln \tilde{g}$ are relevant for intermediate energies $0 < \epsilon < eV$ only, and thus do not affect the high energy scale Λ. For $\Lambda^{-1} \lesssim t_k \lesssim (eV)^{-1}$ the approximation $f_+(t_k) - f_-(t_k) \approx eV/(2\pi)$ is still reliable which gives the powers $\tilde{p}_{12} = p'_{12}$, $\tilde{p}_{23} = 0$, $\tilde{p}_{13} = p'_{13}$, and $\tilde{q}_{12} = q'_{12} + 1$ and the integral

$$\int_{(eV)^{-1}}^{\Lambda^{-1}} dt_k \, \mathcal{J} \sim (eV\tau)^{p'_{13}} (eV/\Lambda)^{q'_{12}+1-p'_{13}} (\Lambda t_k)^{p'_{12}+1} \Big|_{(eV)^{-1}}^{\Lambda^{-1}} \tag{6.90}$$

$$\sim (eV\tau)^{p'_{13}} \left[(eV/\Lambda)^{1+\alpha_1^2} - (eV/\Lambda)^{1+\alpha_1^2-2/\nu} \right] \tag{6.91}$$

$$\sim (eV\tau)^{p'_{13}} (eV/\Lambda)^{1+\alpha_1^2-2/\nu} \tag{6.92}$$

where we kept only the dominant contribution.

We study now the limit $t_k \searrow (eV)^{-1}$ where $f_+(t_k) - f_-(t_k) \sim 1/t_k$ and powers are $\tilde{p}_{12} = p_{12} - 1$, $\tilde{p}_{23} = p_{23}$, $\tilde{p}_{13} = p_{13}$, and $\tilde{q}_{12} = q_{12}$. For some intermediate time $(eV)^{-1} \lesssim t \ll \tau$ the integral is

$$\int_{(eV)^{-1}}^{t} dt_k \, \mathcal{J} \sim (eV\tau)^{p_{13}+p_{23}} (eV/\Lambda)^{q_{12}-p_{13}-p_{23}} (\Lambda t_k)^{p_{12}} \Big|_{(eV)^{-1}}^{t}. \tag{6.93}$$

Assuming $\mathrm{Re}\, p_{12} < 0$ the upper boundary t is irrelevant and

$$\int_{(eV)^{-1}}^{t} dt_k \, \mathcal{J} \sim (eV\tau)^{p'_{13}} (eV/\Lambda)^{1+\alpha_1^2-2/\nu}. \tag{6.94}$$

Let us now turn to the singularity $t_k \sim \tau$ where $f_+(t_k) - f_-(t_k) \sim \tau^{-1}$. The same line of reasoning gives the integrals

$$\int_{\tau-\Lambda^{-1}}^{\tau} dt_k \, \mathcal{J} \sim (eV\tau)^{p''_{13}-1} (eV/\Lambda)^{2+\alpha_1^2-4/\nu}, \tag{6.95}$$

$$\int_{\tau-(eV)^{-1}}^{\tau-\Lambda^{-1}} dt_k \, \mathcal{J} \sim (eV\tau)^{p''_{13}} (eV/\Lambda)^{2+\alpha_1^2-4/\nu} (\Lambda(\tau - t_k))^{1-2/\nu} \Big|_{\tau-(eV)^{1}}^{\tau-\Lambda^{-1}} \tag{6.96}$$

$$\sim \begin{cases} (eV\tau)^{p''_{13}-1} (eV/\Lambda)^{2+\alpha_1^2-4/\nu}, & \nu < 2, \\ (eV\tau)^{p''_{13}-1} (eV/\Lambda)^{1+\alpha_1^2-2/\nu}, & \nu \geq 2. \end{cases} \tag{6.97}$$

Introducing again some intermediate time $(eV)^{-1} \ll t < \tau - (eV)^{-1}$ (which for $\mathrm{Re}\, p_{23} < -1$ will be irrelevant as integral boundary) one obtains

$$\int_{t}^{\tau-(eV)^{-1}} dt_k \, \mathcal{J} \sim (eV\tau)^{p''_{13}-1} (eV/\Lambda)^{1+\alpha_1^2-2/\nu}. \tag{6.98}$$

Around $t_k \sim \tau$, the exponent which is to be maximized in all subintegrals is

$$p''_{13} - 1 = -2 \left(n_1 - \frac{\alpha_1 + 1 - 2\beta_1}{2} \right)^2 - \frac{(\alpha_1 + 1)^2}{2} - 1. \tag{6.99}$$

In the following we are interested in the integers n_2 and n_1 which maximize $\operatorname{Re} p'_{13}$ and $\operatorname{Re} p''_{13} - 1$. To this end we write $\alpha_1 = M + m$ with $M \in \mathbb{Z}$ and $|m| \leq 1/2$. Then for even M leading contributions come from $n_2 = M/2$ and $n_1 = (M+1)/2 \pm 1/2$, and for odd M they come from $n_2 = M/2 \pm 1/2$ and $n_1 = (M+1)/2$. For all integer ν in all these contributions $\operatorname{Re} p'_{13} \geq \operatorname{Re} p''_{13} - 1$.

These observations lead us to the conclusion that, with all oscillatory terms $e^{ieV\tau n_2} e^{i\alpha_1 \Lambda \tau}$ and t_k-independent contributions,

$$\left[\frac{\mathcal{D}_{**}^{-1}(0, t_k)}{\left(g^{-1} \right)_{1k}} \right]_{T_1 \to 0} \propto \frac{\Lambda}{\pi}, \tag{6.100}$$

$$\Delta[4\bar{\vartheta}_+, f_+]^{-1} \propto e^{-i\alpha_1 (\Lambda + eV)\tau} \left(\frac{\Lambda \tau}{\pi} \right)^{\alpha_1^2}, \tag{6.101}$$

taken into account, the leading terms of the t_k-integral for $\nu \geq 2$ are

$$\int dt_k \ldots = \frac{\Lambda}{\pi} \, e^{-i\alpha_1 eV\tau + i\beta_1 eV\tau} \left(\sum_{n_2} \Gamma'_{n_2} e^{ieV\tau n_2} (eV\tau)^{p'_{13} + \alpha_1^2} \right.$$

$$\left. + \sum_{n_1} \Gamma''_{n_1} \left(e^{-ieV\tau} - 1 \right) e^{ieV\tau n_1} (eV\tau)^{p''_{13} - 1 + \alpha_1^2} \right) (eV/\Lambda)^{1 - 2/\nu} \tag{6.102}$$

where Γ'_{n_2} and Γ''_{n_2} are some unknown dimensionless constants. This expansion contains all terms in leading order of (eV/Λ) (also those subleading in $(eV\tau)$).

Action $\mathcal{A}_{\text{ferm}}^{(0)}$ in the absence of tunneling

We first calculate the clean action

$$i\mathcal{A}_{\text{ferm}}^{(0)} = \left[\operatorname{Tr} \operatorname{Ln} \left[\mathbb{1} - \check{f} + e^{2i\check{\vartheta}^q} \check{f} \right] - 2i \operatorname{Tr} \check{\vartheta}^q f_0 \right] \tag{6.103}$$

Here the traces extend over all ν upper and ν lower inner channels. We combined all 2ν distribution functions f_λ and phases ϑ_λ^q into 2×2-matrices $\check{f}$ and $\check{\vartheta}^q$. Due to the Dzyaloshinskii-Larkin theorem we anticipate that only first-and-second-order-in-ϑ terms are non-vanishing and we expand

$$i\mathcal{A}_0 = \operatorname{Tr} \left[\operatorname{Ln} \left[\mathbb{1} + \left(2i\vartheta^q - 2\vartheta^{q2} \right) \hat{f} \right] - 2i\vartheta^q f_0 \right] \tag{6.104}$$

$$= 2i \operatorname{Tr} \vartheta^q \left(\hat{f} - f_0 \right) - 2 \operatorname{Tr} \vartheta^q (\mathbb{1} - \hat{f}) \vartheta^q \hat{f}. \tag{6.105}$$

For local operators A, B, C, i.e. $A(t_1 - t_2) = A(t_1)\delta(t_1 - t_2)$ etc., we use the relation

$$\operatorname{Tr}_t A[B, f_0]C = \int dt_2 \lim_{t_1 \to t_2} A(t_1) \frac{i}{2\pi} \frac{B(t_1) - B(t_2)}{t_1 - t_2 + i0} C(t_2) = \frac{i}{2\pi} \int dt \, A(t) \dot{B}(t) C(t), \tag{6.106}$$

which implies for nonequilibrium distribution functions, $f_1(t) = e^{-ieV_1 t} f_0(t)$,

$$\text{Tr}_t A(f_1 - f_0)B = \frac{eV_1}{2\pi} \int \mathrm{d}t\, A(t)B(t). \tag{6.107}$$

We assumed that along upper edge the outer channel is biased by V and the inner ones by V_0 while the lower edge is grounded. This gives for the first, zero mode, contribution

$$2i\,\text{Tr}\,\check{\vartheta}^q \left(\check{f} - f_0\right) = i\frac{e\left[V + (\nu - 1)V_0\right]\tau}{2\pi}\,2\bar{\vartheta}_+. \tag{6.108}$$

The quadratic contribution to $i\mathcal{A}_{\text{ferm}}^{(0)}$ is UV divergent and needs to be cutoff by ω_C. It is

$$-2\,\text{Tr}\,\vartheta^q \left(\mathbb{1} - \hat{f}\right)\vartheta^q \hat{f} = -\frac{1}{2\pi^2}\nu\,4\bar{\vartheta}_+^2 \ln \omega_C \tau = -\frac{2}{\nu} \ln \omega_C \tau. \tag{6.109}$$

Note that $i\mathcal{A}_{\text{ferm}}^{(0)}$ is a purely Gaussian contribution,

$$e^{i\mathcal{A}_{\text{ferm}}^{(0)}} = \left\langle e^{i\vartheta_+^f(0) - i\vartheta_-^b(0)} \right\rangle_0 = \exp\left\{ i\left\langle \vartheta_+^f(0) - \vartheta_-^b(0) \right\rangle_0 - \frac{1}{2}\left\langle \delta\left[\vartheta_+^f(0) - \vartheta_-^b(0)\right]^2 \right\rangle_0 \right\} \tag{6.110}$$

where averaging is performed with respect to the full action with $T_1 \to 0$.

Current, Conductivity and Visibility

Setting $V_+ = Vx$ and $V_- = 0$ and defining the exponents

$$p'(n_2) \equiv -2\left(n_2 - \frac{\alpha_1 - 2\beta_1}{2}\right)^2 + 1 + \frac{1}{2}\left(\frac{2}{\nu}\right)^2 - \frac{2}{\nu}, \tag{6.111}$$

$$p''(n_1) \equiv -2\left(n_1 - \frac{\alpha_1 + 1 - 2\beta_1}{2}\right)^2 - \frac{1}{2} + \frac{1}{2}\left(\frac{2}{\nu}\right)^2, \tag{6.112}$$

the coherent current contribution $I_{\text{coh}} = 2\text{Re}\,I_{+-}$ is $I_{\text{coh}} = \frac{e}{2\pi\tau} r_1 t_1 r_2 t_2\, 2\text{Re}\,e^{i\phi}\,\mathcal{I}_0$ with

$$\mathcal{I}_0 = 2e^{-2\pi i/\nu} \exp\left\{ i\frac{eV\tau[1 - (\nu - 1)x]}{\nu} \right\} e^{i\beta_1 eV\tau}$$

$$\times \left(\sum_{n_2} \Gamma'_{n_2} e^{in_2 eV\tau} \left(eV\tau\right)^{p'(n_2)} + \sum_{n_1} \Gamma''_{n_1} e^{in_1 eV\tau} \left(e^{-ieV\tau} - 1\right) \left(eV\tau\right)^{p''(n_1)} \right). \tag{6.113}$$

The following table shows the two dominant powers for each filling factor ν:

ν	leading powers
2	$p'(0) = p'(-1) = 0 = p''(0)$
3	$p'(-1),\, p'(0)$
≥ 4	$p'(0);\, p''(0)$ if $T_1 < 1/2$, $p''(1)$ if $T_1 > 1/2$

Taking these two leading terms into account we obtain the results presented in Sect. 6.2, namely Eq. (6.5) with the exponents (6.9), (6.10).

6.4 Conclusions

In this chapter we applied the functional bosonization framework of Chapter 3 to study the quantum Hall Mach-Zehnder interferometer for arbitrary integer filling factors ν. Taking into account only interaction inside the interferometer cell we found that the model is exactly solvable, and that the current is related to the full counting statistics of the first quantum point contact (QPC) with interaction-induced time-dependent nonvanishing "counting field" $\vartheta_+(t)$. In other words, the interferometer couples strongly to the noise of the QPC.

We considered the effect of long-range (quantum-dot-like) interaction within each interferometer arm. In the limit of large charging energy $E_C\tau \gg 1$ (with τ being the flight time along the arms) the counting field is piecewise constant, being $-\pi/\nu$ during a time interval τ and 0 otherwise. In this case current was expressed in terms of (block) Toeplitz determinants and amenable to an entirely analytical evaluation. We found the asymptotic expansion (6.5) for high bias with the leading powers shown in Fig. 6.4. The resulting visibility and phase of the Aharonov-Bohm conductance oscillations are presented in Fig. 6.3.

For the experimentally most important situation of filling $\nu = 2$, the strong coupling limit happens to yield a counting phase of exactly $-\pi/2$ for which renormalization and dephasing are completely absent. Dephasing is restored either when deviating from $-\pi/2$ by considering moderate interaction strength or diluting the incident electron beam via an additional QPC and thus introducing a supplemental source of noise. These cases can be dealt with numerically and yield Figs. 6.9 and 6.6.

7 Chapter 7
Interaction Quench in Nonequilibrium Luttinger Liquids

One of the central assumptions of statistical mechanics is the ergodicity hypothesis that closed systems with a sufficiently high number of degrees of freedom sample the accessible microstates of their phase space with equal probability. Generally, it is expected that such systems, prepared in some initial state, relax due to inelastic processes to a thermal equilibrium state, which has little or no memory of the initial state beyond the average energy (or a finite number of additional conserved quantities).

The Luttinger liquid is an integrable system with infinitely many integrals of motion, say the occupation numbers of the plasmonic modes. Thus, its dynamics is highly constrained. Starting from a given initial state it cannot relax into the thermal equilibrium, if the integrals of motion are not compatible in both states.

Indeed the nonequilibrium dynamics of the similar Lieb-Liniger model (a bosonic model with short-range repulsive interaction which flows to the Luttinger model under renormalization) was studied numerically by [113]. The steady state obtained was compatible with a generalized Gibbs ensemble, which satisfies the maximum entropy principle under the constraints set by integrability.

Questions about the nonequilibrium dynamics of such integrable systems, whether they relax into a steady state and how much memory they retain from the initial state, are of great theoretical interest. Their study has become experimentally accessible with the recent advent of ultracold atom systems in optical traps. They are highly controllable and very weakly coupled to the environment and represent an ideal laboratory to realize models originally developed for solid state systems. A prominent example is Ref. [114] where the dynamics of a trapped one-dimensional Bose gas (consisting of ^{87}Rb atoms), initially prepared out of equilibrium, and specifically the time-dependent momentum distribution function $n(k, t)$, was considered. Even after thousands of collisions no equilibration could be observed, and integrability of the underlying Lieb-Liniger model was conjectured to be the cause.

In experiment, the nonequilibrium initial state is usually the stationary state of some Hamiltonian H_0. Relaxation is initiated by a *quantum quench*: H_0 is suddenly switched to the Hamiltonian H which drives the time-evolution of interest. A conceptually simple quench is considered by Ref. [115, 116] where a Luttinger model with suddenly switched interaction was studied. As suggested by the authors this model can be realized with dipolar fermionic atoms in one-dimensional traps. The effective dipolar interaction is sensitive to the relative angle between the dipole moments and the direction of motion, and its amplitude and sign can be tuned via an orienting external electric field. The authors found that the Luttinger model retains Fermi-liquid-like correlations and quasiparticle-like discontinuities in

the momentum distribution function at finite times $t > 0$ after the quench and relaxes to a steady state with Luttinger-liquid-like power-law correlations. The latter are governed by different exponents than in the equilibrium case.

In this chapter we use the nonequilibrium bosonization approach, presented in Sect. 2.3, to consider the quench of a Luttinger liquid out of an nonequilibrium initial state with double-step distribution functions. Similarly to the equilibrium quench case, we find that at finite times momentum distribution functions exhibit discontinuities (here with two edges). Differently, the corresponding quasiparticle weights are not merely suppressed algebraically, but also exponentially. The steady state as well exhibits two edges, reminiscent of the original nonequilibrium state, which in analogy with the equilibrium Luttinger liquid support power-laws, smeared by dephasing. We find that all exponents are sensitive to the inital state. Let us go into the details after specifying the model and discussing the nonequilibrium quench results.

7.1 Model and Equilibrium Results

We consider a spinless single-channel Luttinger liquid with right-moving (index $\eta = +$) and left-moving ($\eta = -$) fermion species. Their respective velocities and distribution functions are $v_\eta = \eta v_F$ and $f_\eta(\epsilon)$. We focus on temperature $T = 0$; in a possible nonequilibrium setup distribution functions may be of double-step form

$$f_\eta(\epsilon) = R\,\theta(U - \epsilon) + (1 - R)\,\theta(-\epsilon), \quad 0 < R < 1,\ U > 0. \tag{7.1}$$

In the equilibrium Luttinger liquid short-range interaction, giving rise to forward scattering between fermions of the same (g_4) and different (g_2) species, is entirely characterized by 2 constants (2.6): the Luttinger parameter K and the plasmon velocity u. At $T = 0$ the equal-time fermionic Green's functions, for instance, read

$$G_{0\eta}^{\gtrless}(t_1 = t_2, x = x_1 - x_2) = G_{0\eta}^{\gtrless}(0, \bar{x}) \left(\frac{a}{\sqrt{x^2/u^2 + a^2}} \right)^{2\gamma} \tag{7.2}$$

with non-interacting Green's function $G_{0\eta}^{\gtrless}(t_1 - t_2, x_1 - x_2)$, short-time cutoff $a \sim \Lambda^{-1}$ and exponent $\gamma = (1 - K)^2/(4K)$. The instantaneous momentum distribution function, defined as the Fourier transform

$$n_\pm(p, \bar{t}) \equiv -i \int \mathrm{d}\bar{x}\, e^{-i(p \pm p_F)\bar{x}} G_\pm^<(\bar{x}, 0; t_1 = t_2 = \bar{t}), \tag{7.3}$$

is $\propto |p|^{2\gamma}$.

In this chapter we consider a nonequilibrium quantum quench, realized by suddenly switching on interaction at time $t = 0$. Prior to the quench, $t < 0$, the fermionic system is assumed to be ideal ($g_2(t) = 0 = g_4(t)$, $K(t) = 1$) and set in the nonquilibrium state described by the distribution functions (7.1). After the quench, $t > 0$, $g_j(t) = g_j > 0$, $K(t) = K < 1$.

Equilibrium Quench

To appreciate the importance of the initial state, starting from which the quench is performed, let us review first the results of [115, 116] for the equilibrium quench at $T = 0$. Calculations there

were performed with a finite interaction range $R_0 \sim v_F/\Lambda$ as short-distance regularization. At long distances $\bar{x} \gg R_0$ results are insensitive to the regularization scheme, and momentum-dependent coupling parameters (associated with finite interaction range) can be replaced by their zero momentum values, $g_j(q) \approx g_j(q = 0)$. The equal-time correlation function then is

$$G_+^<(\bar{t}; \bar{x}, 0) = G_{0+}^<(0, \bar{x}) \left| \frac{R_0}{\bar{x}} \right|^{\tilde{\gamma}^2} \left| \frac{(2u\bar{t})^2 - \bar{x}^2}{(2u\bar{t})^2} \right|^{\tilde{\gamma}^2/2} \tag{7.4}$$

where the exponent is determined by $\tilde{\gamma} \equiv \frac{1-K^2}{4K}$.

For short times such that $2u\bar{t} \ll \bar{x}$ the correlation function $G_+^<(\bar{t}; \bar{x}, 0) \approx Z(\bar{t}) G_{0+}^<(\bar{x}; 0)$ can be interpreted as the Green's function of an effective time-dependent Fermi liquid with "Landau quasiparticle weight"

$$Z(\bar{t}) = \left(\frac{R_0}{2u\bar{t}} \right)^{\tilde{\gamma}^2} \tag{7.5}$$

which gives rise to a discontinuity in the momentum distribution function $n_+(p)$ at Fermi momentum $p = p_F$. According to (7.5) the jump decays algebraically with time $\bar{t}$.

For large times $\bar{t} \to \infty$ the system reaches a time-independent steady state with power-law correlations

$$G_+^<(\bar{t} \to \infty; \bar{x}, 0) = G_{0+}^<(0, \bar{x}) \left| \frac{R_0}{\bar{x}} \right|^{\tilde{\gamma}^2}.$$

The corresponding momentum distribution function no longer exhibits a discontinuity at $p = p_F$, but instead has a power-law singularity $\sim |p - p_F|^{\tilde{\gamma}^2}$. This behavior is very similar to that observed in an equilibrium Luttinger liquid (cf. Eqn. (7.2)), however with different exponents $\tilde{\gamma}^2 \neq 2\gamma$. Hence, while interactions drive relaxation processes, which destroy the Fermi-liquid-likeness of the system, its integrability prevents it from relaxing into thermal equilibrium.

7.2 Nonequilibrium Results

It is then little surprising that the steady state differs significantly in nonequilibrium, $0 < R < 1$. In contrast to the equilibrium situation, the correlation function now is a linear combination of different powers of $|\bar{x}|$, $|2u\bar{t} + \bar{x}|$, $|2u\bar{t} - \bar{x}|$, and $2u\bar{t}$. The powers are derived and presented in detail in Section 7.3. Here, let us focus on the long-distance behavior at finite times and the stationary limit.

Finite time quasiparticle weights

For finite times $\bar{t}$ and long distances $\bar{x} \gg 2u\bar{t} \gg v_F U^{-1}$, and for moderate interaction, $\sqrt{2} - 1 < K < 1$, the correlation function is

$$G_+^<(\bar{t}; \bar{x}, 0) = G_{0+}^<(0; \bar{x}) \, e^{-\bar{t}/(2\tau_\varphi)} \sum_{n_1, n_2, n_4, n_5} e^{i(n_1 + n_2 + n_4 + n_5)2U\bar{t}u/v_F}$$

$$\times \left(\tilde{\Gamma}_1'(n_1, n_2, n_4, n_5) \left(\frac{2u\bar{t}\Lambda}{\pi v_F} \right)^{T_1'} \left(\frac{\pi U}{\Lambda} \right)^{V_1'} + \tilde{\Gamma}_2'(n_1, n_2, n_4, n_5) \left(\frac{2u\bar{t}\Lambda}{\pi v_F} \right)^{T_2'} \left(\frac{\pi U}{\Lambda} \right)^{V_2'} e^{i(\bar{x} - 2u\bar{t})U/v_F} \right)$$
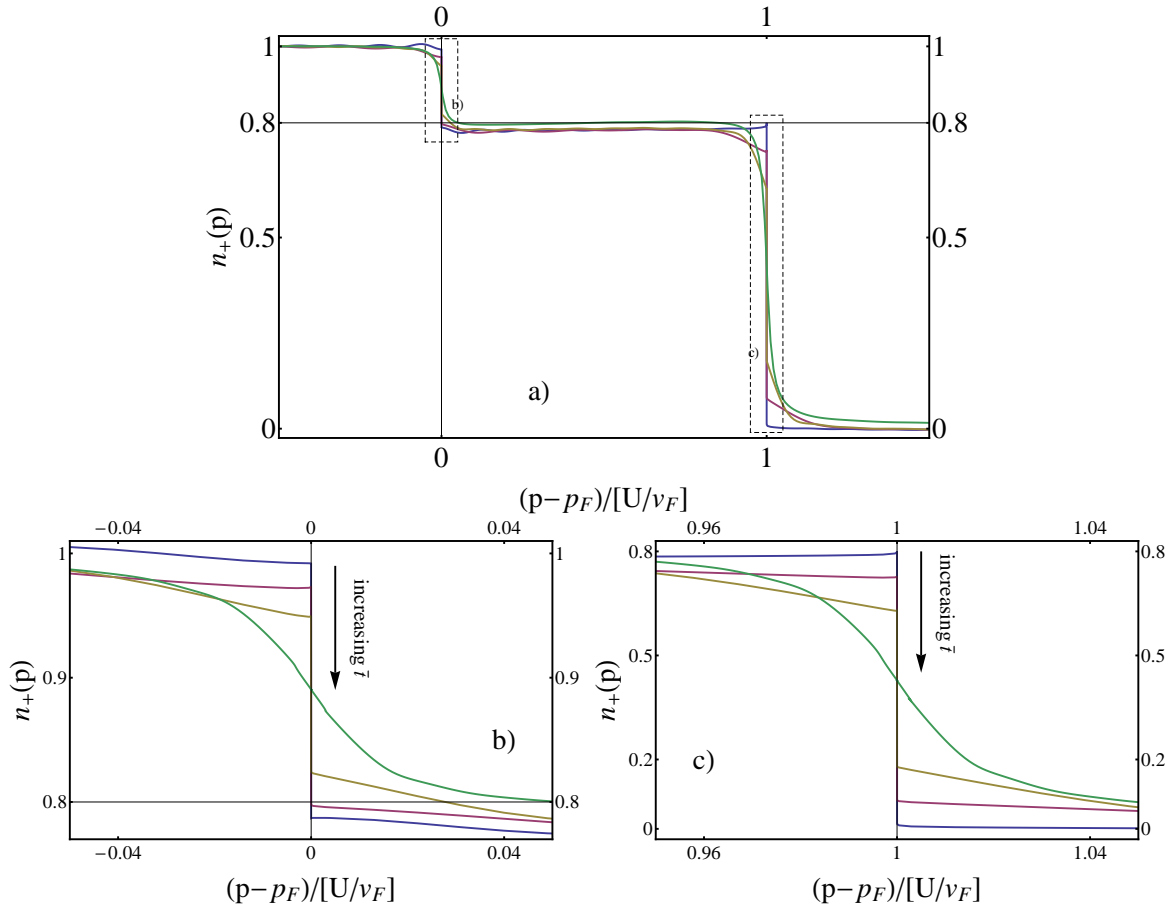
Figure 7.1: *Sketch of momentum distribution function for $K = 0.8$ and $a = 0.8$ at times $\bar{t}/[v_F/(2uU)] =$0.001, 2, 20, 50, 100, and in the stationary limit $\bar{t} \to \infty$; b) and c) are zooms into a) around edges $p = p_F$ and $p = p_F + U/v_F$. Clear discountinuities are visible which decrease with time $\bar{t}$ and eventually vanish.*

with some numerical prefactors $\tilde{\Gamma}'_j$, decay rate

$$\tau_\varphi^{-1} = -\frac{2U}{\pi}\frac{u}{v_F}\ln\left[\left(1 - 2(1-a)a\left(1 - \cos 2\pi c^2\right)\right)\left(1 - 2(1-a)a\left(1 - \cos 2\pi cs\right)\right)\right] \tag{7.6}$$

and exponents $T'_1 = T'_+ + T'_-$, $V'_1 = V'_+ + V'_-$ (with $T'_\pm$, $V'_\pm$ from Eqns. (7.8), (7.10)) and $T'_2 = T'_+ + T'_-$, $V'_2 = V'_+ + V'_-$ (with $T_\pm$, $V_\pm$ from Eqns. (7.9), (7.10)).

For simplicity we focus only on the most dominant contributions which are, for moderate repulsive interaction, $1 > K \gtrsim 0.6$, given by $n_1 = n_4 = n_5 = 0$ and $n_2 = 0$ for T'_1, V'_1 and $n_2 = 1$ for T'_2, V'_2:

$$T'_j(V'_j) = -\frac{1}{2}\left[\left(\frac{3}{2} - j + s^2 + 2\beta_1\right)^2 + \left(\frac{3}{2} - j + s^2 - 2\beta_2\right)^2 + \left(cs + 2\beta_3\right)^2 + \left(cs - 2\beta_4\right)^2 - \frac{1}{2} \pm 4c^2s^2\right]$$

Similar to the equilibrium quench, the entire $\bar{x}$-dependence of the full Green's function is given by the noninteracting contribution, $G^>_{0+} \propto \bar{x}^{-1}$, and correlations drop off with distance in a Fermi liquid-
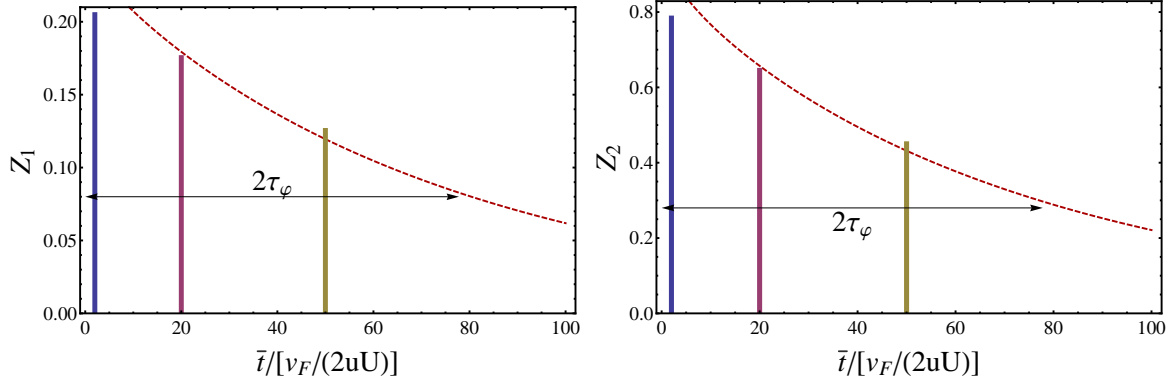
Figure 7.2: *Sketch of time evolving quasiparticle weights Z_1 and Z_2 for $K = 0.8$ and $a = 0.8$ around $p = p_F$ and $p = p_F + U/v_F$, respectively.*

like manner. Correspondingly, the momentum distribution function has discontinuities at $p = p_F$ and $p = p_F + U/v_F$, signaling the existence of Landau quasiparticle states (see Fig. 7.1 for $K = 0.8$ and $a = 0.8$). In the nonequilibrium setup each of the two "Fermi edges" exhibits quasiparticles with possibly different weights $Z_1 \propto e^{-\bar{t}/(2\tau_\varphi)}\bar{t}^{T_1'}U^{V_1'}$, $Z_2 \propto e^{-\bar{t}/(2\tau_\varphi)}\bar{t}^{T_2'}U^{V_2'}$. In striking contrast to the equilibrium situation, the quasiparticle weights are not only algebraically suppressed, but dominantly exponentially with decay time τ_φ. Their time evolution is sketched in Fig. 7.2.

Stationary Limit
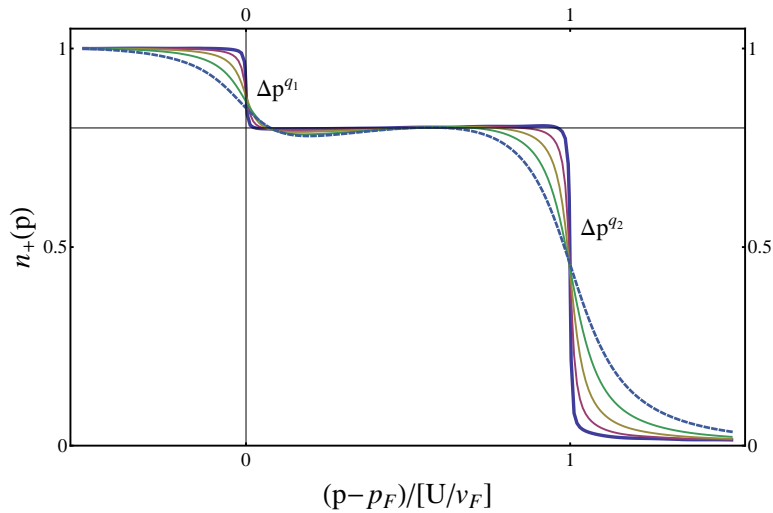
Figure 7.3: *Steady-state momentum distribution function for $a = 0.8$ and different K. At edges $p = p_F$ and $p = p_F + U/v_F$ the initial discontinuites are replaced by power laws $\Delta p^{q_{1/2}}$ which are smeared by dephasing.*

For long times, $\bar{t} \to \infty$, the quenched system relaxes to a stationary state without the Fermi liquid signatures, but with critical power-law correlations characteristic for Luttinger liquid. For $\bar{x} \gg v_F U^{-1}$
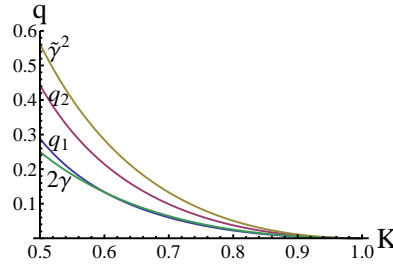
Figure 7.4: *Luttinger liquid exponents governing of power-law singularities of the momentum distribution functions: q_1 at $p = p_F$ and q_2 at $p = p_F + U/v_F$ for quenched nonequilibrium, $\tilde{\gamma}^2$ for quenched equilibrium, and 2γ for equilibrium for $a = 0.8$.*
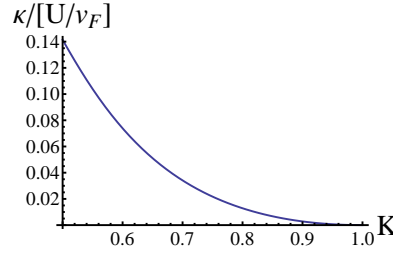
Figure 7.5: *Inverse decay length κ at $a = 0.8$ as function of K.*

and moderate repulsive interaction $\sqrt{2} - 1 \leq K \leq 1$ the correlation function is in leading order

$$G_+^<(\bar{t}; \bar{x}, 0) = G_{0+}^<(0; \bar{x}) \, e^{-\kappa|\bar{x}|} \left(\tilde{\Gamma}_1 \left| \frac{\Lambda \bar{x}}{\pi v_F} \right|^{1+X_1} \left| \frac{\pi U}{\Lambda} \right|^{V_1} + \tilde{\Gamma}_2 \, e^{iU\bar{x}/v_F} \left| \frac{\Lambda \bar{x}}{\pi v_F} \right|^{1+X_2} \left| \frac{\pi U}{\Lambda} \right|^{V_2} \right) \quad (7.7)$$

with known numerical prefactors $\tilde{\Gamma}_j$, exponents

$$X_j(V_j) = -\frac{1}{2} \left[\left(s^2 - 2\beta_1 \right)^2 - \left(s^2 - 2 + j - 2\beta_2 \right)^2 - \left(cs - 2\beta_3 \right)^2 - \left(cs + 2\beta_4 \right)^2 \pm (c^2 + s^2)^2 \right],$$

$j = 1, 2$, decay length $\kappa^{-1} = 4u\tau_\varphi$, and

$$\beta_1 \equiv \frac{1}{2\pi i} \ln \left[ae^{-2\pi is^2} + 1 - a \right], \qquad \beta_2 \equiv \frac{1}{2\pi i} \ln \left[ae^{2\pi ic^2} + 1 - a \right] = -\beta_1^*,$$

$$\beta_3 \equiv \frac{1}{2\pi i} \ln \left[ae^{2\pi ics} + 1 - a \right], \qquad \beta_4 \equiv \frac{1}{2\pi i} \ln \left[ae^{-2\pi ics} + 1 - a \right] = -\beta_3^*.$$

Like in quenched equilibrium the exponents differ from the equilibrium situation. The stationary state retains information about the system's prehistory, including the initial state prior to the quench: even long after the quench the momentum distribution function exhibits a double-step structure reminiscent of the original nonequilibrium state (cf. Fig. 7.3); similar to the equilibrium Luttinger liquid the sharp discontinuities are replaced by power laws $|p - p_F|^{q_1}$ and $|p - p_F - U/v_F|^{q_2}$. Exponents differ both from equilibrium and quenched equilibrium and are in general different at the two edges (cf. Fig. 7.4).

7.3 Calculations

We use the nonequilibrium version of canonical bosonization, which is presented in Section 2.3. In this framework nonequilibrium corrections to the right-movers' equal-time Green's function $G_+^{\gtrless}(\bar{t};\bar{x},0)$,(2.40), (2.42) are expressed in terms of Fredholm determinants

$$\Delta_\mu \equiv \mathrm{Det}\left[\mathbb{1} + \left(e^{i\delta_\mu} - \mathbb{1} \right) f_\mu \right].$$

Counting phases δ_μ (2.41) measure incoming charge in the leads for given trajectory $\varrho_\mu^q(x,t)$. The charge configuration $\varrho_\mu^q(x,t)$ is the "advanced charge response" to the injection of a right-moving fermion at $\xi_2 = (\bar{t},0)$ and its removal at $\xi_1 = (\bar{t},\bar{x})$ and satisfies the equations of motion (2.44). The sudden temporal switch-on of interaction at $t=0$ does not make the equations singular in any way (as sharp *spatial* changes would); time evolution of density is required to be continuous at $t=0$. For $t>0$ interaction couples the bare right- and left-moving charge modes $\varrho_\pm^q$. The eigenmodes of the interacting systems, the plasmon modes $\tilde{\varrho}_\eta^q$, are obtained by the Bogoliubov transformation

$$\begin{pmatrix} \varrho_+^q \\ \varrho_-^q \end{pmatrix} = \begin{pmatrix} c & s \\ s & c \end{pmatrix} \begin{pmatrix} \tilde{\varrho}_+^q \\ \tilde{\varrho}_-^q \end{pmatrix}, \quad \text{with } c = \frac{1+K}{2\sqrt{K}}, \quad s = -\frac{1-K}{2\sqrt{K}}.$$

Their time evolution decouples,

$$\tilde{\varrho}_+^q(x,t) = -\frac{1}{2}\, c\, \theta(\bar{t}-t) \left\{ \delta[x - u(t-\bar{t})] - \delta[x - \bar{x} - u(t-\bar{t})] \right\},$$

$$\tilde{\varrho}_-^q(x,t) = \frac{1}{2}\, s\, \theta(\bar{t}-t) \left\{ \delta[x + u(t-\bar{t})] - \delta[x - \bar{x} + u(t-\bar{t})] \right\}.$$

Requiring continuity at $t=0$ and inverting the Bogoliubov transformation we obtain the charge density prior to the quench, $t<0$,

$$\varrho_+^q(x,t) = -\frac{1}{2}\left\{ c^2 \left(\delta[x + u\bar{t} - v_F t] - \delta[x - \bar{x} + u\bar{t} - v_F t] \right) - s^2 \left(\delta[x - u\bar{t} - v_F t] - \delta[x - \bar{x} - u\bar{t} - v_F t] \right) \right\},$$

$$\varrho_-^q(x,t) = -\frac{1}{2}cs \left\{ \left(\delta[x + u\bar{t} + v_F t] - \delta[x - \bar{x} + u\bar{t} + v_F t] \right) - \left(\delta[x - u\bar{t} + v_F t] - \delta[x - \bar{x} - u\bar{t} + v_F t] \right) \right\}.$$

which yields the counting phases

$$\delta_+(t) = 2\pi \left\{ c^2 \left(\theta\left[t - \frac{-\bar{x} + u\bar{t}}{v_F} \right] - \theta\left[t - \frac{u\bar{t}}{v_F} \right] \right) - s^2 \left(\theta\left[t - \frac{-\bar{x} - u\bar{t}}{v_F} \right] - \theta\left[t - \frac{-u\bar{t}}{v_F} \right] \right) \right\},$$

$$\delta_-(t) = -2\pi cs \left\{ \left(\theta\left[t - \frac{-u\bar{t}}{v_F} \right] - \theta\left[t - \frac{\bar{x} - u\bar{t}}{v_F} \right] \right) - \left(\theta\left[t - \frac{u\bar{t}}{v_F} \right] - \theta\left[t - \frac{\bar{x} + u\bar{t}}{v_F} \right] \right) \right\}.$$

Fig. 7.6 depicts the density trajectories in the $x-t$-plane the accumulation of corresponding phases.

The phases are shown in Fig. 7.7: For $|\bar{x}| < 2u\bar{t}$ each phase $\delta_\pm = \delta_{1\pm} + \delta_{2\pm}$ consists of two rectangular-shaped pulses of width $|\bar{x}|/v_F$ separated by the distance $(2u\bar{t} - |\bar{x}|)/v_F$. The pulses overlap in the case

$|\bar{x}| > 2u\bar{t}$. In the long-time limit $2u\bar{t} \gg |\bar{x}|$ the pulses are well separated and each of the two Fredholm determinants in (2.40),

$$\Delta_\mu \approx \text{Det}\left[\mathbb{1} + \left(e^{i\delta_{1\mu}} - \mathbb{1}\right)f_\mu\right] \text{Det}\left[\mathbb{1} + \left(e^{i\delta_{2\mu}} - \mathbb{1}\right)f_\mu\right],$$

factorizes into two Toeplitz determinants which may be evaluated with (A.9) or more general forms following from (A.4).

Let us consider first the equilibrium situation with distribution functions $f_+(\epsilon) = f_-(\epsilon) = f_0(\epsilon) = \theta(-\epsilon)$. Eqn. (A.21) yields

$$\Delta_+ = G(1-s^2)G(1+s^2)G(1-c^2)G(1+c^2) \; e^{i\Lambda\bar{x}/v_F} \left|\frac{\Lambda\bar{x}}{\pi v_F}\right|^{-c^4-s^4} \left|\frac{(2u\bar{t})^2 - \bar{x}^2}{(2u\bar{t})^2}\right|^{s^2c^2},$$

$$\Delta_- = G(1-cs)^2 G(1+cs)^2 \; \left|\frac{\Lambda\bar{x}}{\pi v_F}\right|^{-2c^2s^2} \left|\frac{(2u\bar{t})^2 - \bar{x}^2}{(2u\bar{t})^2}\right|^{s^2c^2}.$$

The prefactor, containing the Barnes G-functions G, do not follow from (A.21), but from the long-time limit where the factorization into Toeplitz determinants makes (A.9) applicable.

The Green's function following the equilibrium interaction quench is thus

$$G_+^<(\bar{t}; \bar{x}, 0) \propto e^{i\Lambda\bar{x}/v_F} \left|\frac{\Lambda\bar{x}}{\pi v_F}\right|^{-(c^2+s^2)^2} \left|\frac{(2u\bar{t})^2 - \bar{x}^2}{(2u\bar{t})^2}\right|^{2s^2c^2}.$$

Since $2cs = \tilde{\gamma}$ and $-(c^2 + s^2)^2 = -1 - \tilde{\gamma}^2$ the power laws are in perfect agreement with the exact result (7.4) of Ref. [115]. In the following we will use the equilibrium quench as reference case to normalize our Fredholm determinants.

The situation becomes more complicated when turning to nonequilibrium, (7.1). Using (A.21) we obtain

$$G_+^<(\bar{t}; \bar{x}, 0) = G_{0+}^<(0, \bar{x}) \; \tilde{\Delta}_+ \; \tilde{\Delta}_-$$

for $|\bar{x}|, |2u\bar{t} - |\bar{x}||, |2u\bar{t}| \gg v_F/U$ with equilibrium-normalized determinants

$$\tilde{\Delta}_+ = \sum_{n_1, n_2, n_3} \tilde{\Gamma}_+(n_1, n_2, n_3) \, e^{i(\beta_1+\beta_2)U|\bar{x}|/v_F} e^{i(n_1+n_2-n_3)U|\bar{x}|/v_F} e^{in_3 2U\bar{t}u/v_F}$$

$$\times \left|\frac{\Lambda}{\pi v_F}\right|^{1+\gamma_++V_+} |\bar{x}|^{1+X_+} \left(2u\bar{t} - |\bar{x}|\right)^{D_+} \left(2u\bar{t} + |\bar{x}|\right)^{S_+} (2u\bar{t})^{T_+} \left|\frac{\pi U}{\Lambda}\right|^{V_+},$$

$$\tilde{\Delta}_- = \sum_{n_4, n_5, n_6} \tilde{\Gamma}_-(n_4, n_5, n_6) \, e^{i(\beta_3+\beta_4)U|\bar{x}|/v_F} e^{i(n_4+n_5-n_6)U|\bar{x}|/v_F} e^{in_6 2U\bar{t}u/v_F}$$

$$\times \left|\frac{\Lambda}{\pi v_F}\right|^{\gamma_-+V_-} |\bar{x}|^{X_-} \left(2u\bar{t} - |\bar{x}|\right)^{D_-} \left(2u\bar{t} + |\bar{x}|\right)^{S_-} (2u\bar{t})^{T_-} \left|\frac{\pi U}{\Lambda}\right|^{V_-}$$

for $2u\bar{t} > \bar{x} > 0$ and

$$\tilde{\Delta}_+ = \sum_{n_1,n_2,n_3} \tilde{\Gamma}'_+(n_1,n_2,n_3)\, e^{i(\beta_1+\beta_2)2U\bar{t}u/v_F} e^{i(n_1+n_2-n_3)U|\bar{x}|/v_F} e^{in_3 2U\bar{t}u/v_F}$$

$$\times \left|\frac{\Lambda}{\pi v_F}\right|^{1+\gamma'_++V'_+} |\bar{x}|^{1+X'_+} \left(-2u\bar{t}+|\bar{x}|\right)^{D'_+} \left(2u\bar{t}+|\bar{x}|\right)^{S'_+} (2u\bar{t})^{T'_+} \left|\frac{\pi U}{\Lambda}\right|^{V'_+},$$

$$\tilde{\Delta}_- = \sum_{n_4,n_5,n_6} \tilde{\Gamma}'_-(n_4,n_5,n_6)\, e^{i(\beta_3+\beta_4)2U\bar{t}u/v_F} e^{i(n_4+n_5-n_6)U|\bar{x}|/v_F} e^{in_6 2U\bar{t}u/v_F}$$

$$\times \left|\frac{\Lambda}{\pi v_F}\right|^{\gamma'_-+V'_-} |\bar{x}|^{X'_-} \left(-2u\bar{t}+|\bar{x}|\right)^{D'_-} \left(2u\bar{t}+|\bar{x}|\right)^{S'_-} (2u\bar{t})^{T'_-} \left|\frac{\pi U}{\Lambda}\right|^{V'_-}$$

for $0 < 2u\bar{t} < \bar{x}$. Here, we left the n_j-dependence of the exponents $X_\pm, T_\pm, \ldots$ implicit. $\tilde{\Gamma}_\pm, \tilde{\Gamma}'_\pm$ are unknown numerical prefactors. The determinants for $\bar{x} < 0$ are obtained by complex conjugation.

The exponents differ in the two regimes $2u\bar{t} \gtrless |\bar{x}|$.

Regime $2u\bar{t} > |\bar{x}|$

Here the exponents are

$$X_+ = \left(-\beta_2+c^2-n_2\right)\left(\beta_2-c^2+n_2-n_3\right) + \left(-\beta_1-n_1+n_3\right)\left(\beta_1+n_1\right)$$
$$+ \left(-\beta_2-n_2+n_3\right)\left(\beta_2+n_2\right) + \left(-\beta_1-n_1-s^2\right)\left(\beta_1+n_1-n_3+s^2\right),$$

$$T_+ = \left(-n_1+n_3-s^2-\beta_1\right)\left(c^2-n_2-\beta_2\right) + \left(-n_1-s^2-\beta_1\right)\left(c^2-n_2+n_3-\beta_2\right)$$
$$+ \left(n_1-n_3+\beta_1\right)\left(n_2+\beta_2\right) + \left(n_1+\beta_1\right)\left(n_2-n_3+\beta_2\right),$$

$$D_+ = \left(n_1-n_3+\beta_1\right)\left(-n_2+n_3-\beta_2\right) + \left(-n_1+n_3-s^2-\beta_1\right)\left(-c^2+n_2-n_3+\beta_2\right),$$

$$S_+ = \left(\beta_1+n_1\right)\left(c^2-2\left(\beta_2+n_2\right)\right) - s^2\left(\beta_2-c^2+n_2\right),$$

$$\gamma_+ = -c^4-s^4,$$

$$X_- = \left(-n_4+n_6-\beta_3\right)\left(n_4+\beta_3\right) + \left(-n_4+cs-\beta_3\right)\left(n_4-n_6-cs+\beta_3\right)$$
$$+ \left(-n_5+n_6-\beta_4\right)\left(n_5+\beta_4\right) + \left(-n_5-cs-\beta_4\right)\left(n_5-n_6+cs+\beta_4\right),$$

$$T_- = \left(-n_4+n_6+cs-\beta_3\right)\left(-n_5-cs-\beta_4\right) + \left(-n_4+cs-\beta_3\right)\left(-n_5+n_6-cs-\beta_4\right)$$
$$+ \left(n_4-n_6+\beta_3\right)\left(n_5+\beta_4\right) + \left(n_4+\beta_3\right)\left(n_5-n_6+\beta_4\right),$$

$$D_- = \left(n_4-n_6+\beta_3\right)\left(-n_5+n_6-\beta_4\right) + \left(-n_4+n_6+cs-\beta_3\right)\left(n_5-n_6+cs+\beta_4\right),$$

$$S_- = cs\left(n_5+cs+\beta_4\right) + \left(n_4+\beta_3\right)\left(-cs-2\left(n_5+\beta_4\right)\right). \gamma_- = \qquad -2c^2s^2.$$

In the long-time limit $2u\bar{t} \gg |\bar{x}|$, the powers simplify to $\left(2u\bar{t}-|\bar{x}|\right)^{D_\pm} \left(2u\bar{t}+|\bar{x}|\right)^{S_\pm} (2u\bar{t})^{T_\pm} \to (2u\bar{t})^{\tilde{T}_\pm}$ with $\tilde{T}_+ = -2n_3^2 \leq 0$ and $\tilde{T}_- = -2n_6^2 \leq 0$. Thus the correlation function relaxes to a stationary solution

where solely terms with $n_3 = 0 = n_6$ contribute. The remaining powers simplify to

$$X_+ = -2\left(n_1 - \frac{-s^2 - 2\beta_1}{2}\right)^2 - 2\left(n_2 - \frac{c^2 - 2\beta_2}{2}\right)^2 - \frac{c^4 + s^4}{2},$$

$$V_+ = -2\left(n_1 - \frac{-s^2 - 2\beta_1}{2}\right)^2 - 2\left(n_2 - \frac{c^2 - 2\beta_2}{2}\right)^2 + \frac{c^4 + s^4}{2},$$

$$X_- = -2\left(n_4 - \frac{cs - 2\beta_3}{2}\right)^2 - 2\left(n_5 - \frac{-cs - 2\beta_4}{2}\right)^2 - c^2 s^2,$$

$$V_- = -2\left(n_4 - \frac{cs - 2\beta_3}{2}\right)^2 - 2\left(n_5 - \frac{-cs - 2\beta_4}{2}\right)^2 + c^2 s^2.$$

Since in the long-time limit the phases split into independent pulses, all Fredholm determinants factorize into Toeplitz determinants and the prefactors can be obtained with (A.14):

$$\tilde{\Gamma}_+(n_1, n_2, n_3 = 0) = \frac{G(1 - s^2 - \beta_1 - n_1)G(1 + s^2 + \beta_1 + n_1)G(1 + \beta_1 + n_1)G(1 - \beta_1 - n_1)}{G(1 - s^2)G(1 + s^2)}$$

$$\times \frac{G(1 + c^2 - \beta_2 - n_2)G(1 - c^2 + \beta_2 + n_2)G(1 + \beta_2 + n_2)G(1 - \beta_2 - n_2)}{G(1 + c^2)G(1 - c^2)},$$

$$\tilde{\Gamma}_-(n_4, n_5, n_6 = 0) = \frac{G(1 + cs - \beta_3 - n_4)G(1 - cs + \beta_3 + n_4)G(1 + \beta_3 + n_4)G(1 - \beta_3 - n_4)}{G(1 + cs)G(1 - cs)}$$

$$\times \frac{G(1 - cs - \beta_4 - n_5)G(1 + cs + \beta_4 + n_5)G(1 + \beta_4 + n_5)G(1 - \beta_4 - n_5)}{G(1 - cs)G(1 + cs)}.$$

For *moderate* repulsive interaction $\sqrt{2} - 1 \leq K \leq 1$, the dominant powers $\operatorname{Re} X_\pm$ are due to $(n_1, n_2) = (0,1), (0,0)$ and $(n_4, n_5) = (0,0)$. These contributions are taken into account in (7.7) with $\tilde{\Gamma}_1 \equiv \tilde{\Gamma}_+(0,0,0)\tilde{\Gamma}_-(0,0,0)$, $\tilde{\Gamma}_2 \equiv \tilde{\Gamma}_+(0,1,0)\tilde{\Gamma}_-(0,0,0)$.

In the equilibrium limit, $a \to 0$, prefactors vanish for all n_j but $n_1 = n_2 = n_4 = n_5 = 0$ for which one recovers the equilibrium exponents.

Regime $2u\bar{t} < |\bar{x}|$

Here the exponents are

$$X'_+ = \left(-c^2 + n_2 - n_3 - \beta_1\right)\left(c^2 - n_2 - \beta_2\right) + \left(-n_1 - s^2 - \beta_1\right)\left(n_1 - n_3 + s^2 - \beta_2\right)$$
$$+ \left(-n_2 + n_3 + \beta_1\right)\left(n_2 + \beta_2\right) + \left(n_1 + \beta_1\right)\left(-n_1 + n_3 + \beta_2\right),$$
$$T'_+ = \left(n_2 - n_3 - \beta_1\right)\left(n_1 + \beta_1\right) + \left(-n_1 - s^2 - \beta_1\right)\left(c^2 - n_2 + n_3 + \beta_1\right)$$
$$+ \left(n_1 - n_3 - \beta_2\right)\left(n_2 + \beta_2\right) + \left(c^2 - n_2 - \beta_2\right)\left(-n_1 + n_3 - s^2 + \beta_2\right),$$
$$D'_+ = \left(-n_2 + n_3 + \beta_1\right)\left(n_1 - n_3 - \beta_2\right) + \left(-c^2 + n_2 - n_3 - \beta_1\right)\left(-n_1 + n_3 - s^2 + \beta_2\right),$$
$$S'_+ = -s^2\left(-c^2 + n_2 + \beta_2\right) + \left(n_1 + \beta_1\right)\left(c^2 - 2\left(n_2 + \beta_2\right)\right),$$
$$X'_- = \left(n_5 - n_6 - cs - \beta_3\right)\left(-n_5 + cs - \beta_4\right) + \left(-n_4 - cs - \beta_3\right)\left(n_4 - n_6 + cs - \beta_4\right)$$
$$+ \left(-n_5 + n_6 + \beta_3\right)\left(n_5 + \beta_4\right) + \left(n_4 + \beta_3\right)\left(-n_4 + n_6 + \beta_4\right),$$
$$T'_- = \left(n_5 - n_6 - \beta_3\right)\left(n_4 + \beta_3\right) + \left(-n_4 - cs - \beta_3\right)\left(-n_5 + n_6 + cs + \beta_3\right)$$
$$+ \left(n_4 - n_6 - \beta_4\right)\left(n_5 + \beta_4\right) + \left(-n_5 + cs - \beta_4\right)\left(-n_4 + n_6 - cs + \beta_4\right),$$
$$D'_- = \left(-n_5 + n_6 + \beta_3\right)\left(n_4 - n_6 - \beta_4\right) + \left(n_5 - n_6 - cs - \beta_3\right)\left(-n_4 + n_6 - cs + \beta_4\right),$$
$$S'_- = -cs\left(n_5 - cs + \beta_4\right) + \left(n_4 + \beta_3\right)\left(cs - 2\left(n_5 + \beta_4\right)\right).$$

For long distances $|\bar{x}| \gg 2u\bar{t}$ the power-law dependence on distance simplifies to
$|\bar{x}|^{X'_\pm}\left(-2u\bar{t} + |\bar{x}|\right)^{D'_\pm}\left(2u\bar{t} + |\bar{x}|\right)^{S'_\pm} \to |\bar{x}|^{\tilde{X}_\pm}$ with the exponents

$$\tilde{X}_+ = -2(n_3 + 1/2 - n_1 - n_2)^2 - \frac{1}{2}, \quad \tilde{X}_- = -2(n_6 - n_4 - n_5)^2.$$

For $|\bar{x}| \to \infty$ all terms vanish except for $n_3 = n_1 + n_2$ or $n_3 = n_1 + n_2 - 1$, and $n_6 = n_4 + n_5$. Then $1 + \tilde{X}_+ = 0 = \tilde{X}_-$, i.e. the normalized determinants $\tilde{\Delta}_\pm$ are independent of $\bar{x}$, and correlations drop off like $G_+^<(\bar{t}; \bar{x}, 0) \sim G_{0+}^<(\bar{t}; \bar{x}, 0) \sim \bar{x}^{-1}$.

The remaining exponents are

$$T'_+(V'_+) = -2\left(n_1 - \frac{-1/2 - s^2 - 2\beta_1}{2}\right)^2 - 2\left(n_2 - \frac{-1/2 + c^2 - 2\beta_2}{2}\right)^2 + \frac{1}{4} \mp c^2 s^2 \qquad (7.8)$$

for $n_3 = n_1 + n_2$,

$$T'_+(V'_+) = -2\left(n_1 - \frac{1/2 - s^2 - 2\beta_1}{2}\right)^2 - 2\left(n_2 - \frac{1/2 + c^2 - 2\beta_2}{2}\right)^2 + \frac{1}{4} \mp c^2 s^2 \qquad (7.9)$$

for $n_3 = n_1 + n_2 - 1$ and

$$T'_-(V'_-) = -2\left(n_4 - \frac{-cs - 2\beta_3}{2}\right)^2 - 2\left(n_5 - \frac{cs - 2\beta_4}{2}\right)^2 \mp c^2 s^2 \qquad (7.10)$$

for $n_6 = n_4 + n_5$.

7.4 Conclusions

In this chapter we considered the time-evolution of the momentum distribution function of a nonequilibrium Luttinger liquid after an interaction quench. The initial state was chosen to be a double-step distribution function. Similarly to the equilibrium situation previously discussed by [115, 116] at finite times and long distances correlations are Fermi-liquid-like. The momentum distribution functions exhibit discontinuities with decaying quasiparticle weights, see Figs. 7.1 and 7.2. In both situations the system relaxes into a steady state with Luttinger-liquid-like power-law correlations, Fig. 7.3.

As expected the relaxation process does not lead to a complete loss of memory of the initial state: Neither when quenching out of equilibrium nor out of nonequilibrium does the steady state have the same powers as in the equilibrium state, see Fig. 7.3. In the nonequilibrium case the momentum distribution function never ceases to maintain a double-step structure. One of the main additional features arising from nonequilibrium is dephasing which leads to an expontial suppression of the quasiparticle weights.

To conclude, let us note that the applied formalism can deal with arbitrary initial states as well as interactions which are constrained to region with both spatial and temporal boundaries.
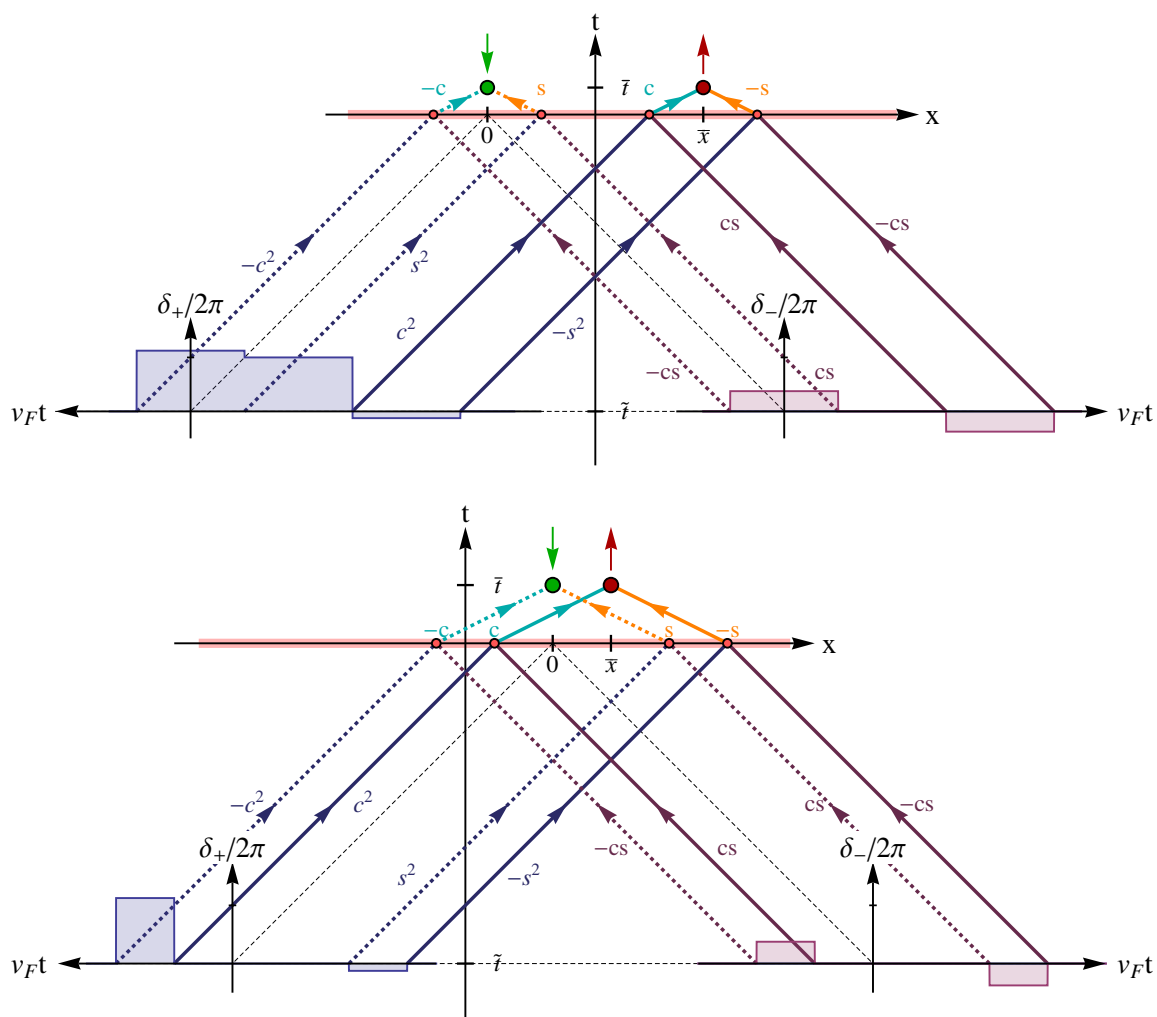
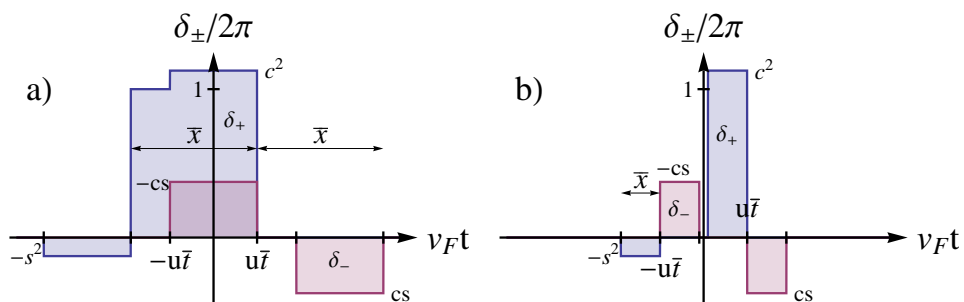**Figure 7.6:** *Trajectories of density peaks and the corresponding counting phases $\delta_\pm$ for short times $2u\bar{t} < \bar{x}$ (*upper plot*) and long times $2u\bar{t} > \bar{x}$ (*lower plot*).*

Figure 7.7: *Counting Phases δ_+ (*blue*) and δ_- (*magenta*) for a) $\bar{x} > 2u\bar{t}$ and b) $2u\bar{t} > \bar{x} > 0$.*

8 Chapter 8
Summary

In this thesis we developed a framework for nonequilibrium networks of interacting quantum wires which are coupled by tunneling or impurity scattering and gave some examples for its application. Examples for "quantum wires" may be right- and left-moving states in a nanowire and their tunnel-coupling may be provided by an backscattering impurity. The model is able to account for the physics in a large range of mesoscopic systems, and we discussed examples which are subject of ongoing theoretical and experimental research.

In Chapter 3, using the Keldysh formulation of functional bosonization, we derived the bosonic Keldysh action of the system, which takes the form of a Fredholm determinant and is highly reminiscent of the full counting statistics cumulant generating functional, though with interaction-induced time-dependent "counting fields". The dynamics of the electrons in the system enters via the time-dependent scattering matrix.

For the case of weak interchannel tunneling, we derived the lowest order expansion for the action which yields at every point of tunneling terms analogous to the Ambegaokar-Eckern-Schön action[29]. We further presented the corresponding saddle-point approximation scheme to evaluate physical observables, taking into account non-Gaussian correlations.

The main part of this work was devoted to applications of the framework. In Chapter 4, we considered the problem of tunneling into a Luttinger liquid with a single impurity biased by a voltage V. The tunneling rates we found have a double-edge structure with smeared power-law singularities. This indicates the presence of a plasmon bath which is populated through inelastic scattering of nonequilibrium electrons off the impurity. The bath "provides" energy and noise and thus has two effects: inelastic tunneling of electrons into/out of the wire and dephasing. We pointed out that the former is responsible for the double-edge structure while the latter leads to the smearing.

As a second application of our approximation scheme, in Chapter 5 we studied the quantum Hall Fabry-Pérot interferometer for arbitrary integer filling factor. Our results provide explanations for the large range of experimental findings: The visibility of Aharonov-Bohm (AB) oscillations is suppressed by renormalization of QPC transmissions and dephasing for high bias. The effective symmetrization of the chemical potentials of the two interferometer arms leads to the observed oscillatory features ("lobes") in the visibility, including the exact vanishing of visibility for certain values of bias.

Taking into account the electrostatic coupling of the current carrying edges with charge localized in the interferometer cell (in a "compressible island"), we can describe the motion of the interference loop upon varying the magnetic field. This may even lead to the somewhat counterintuitive result of a shrinking AB phase upon increasing magnetic field. Depending on experimental parameters such as

relative strengths of couplings between different edge states and the compressible island the system can fall into one of four different regimes with very distinct dependence of conductance on magnetic field and gate voltage.

The quantum Hall Mach-Zehnder interferometer is an example where the functional bosonization framework can be evaluated exactly, when assuming that interaction be absent outside the interferometer cell. For long-range intraarm interaction we found the visibility for arbitrary integer filling factors, and the evolution of the lobe structure as a function of QPC transmission.

Formally, the current could be expressed in terms of a Fredholm determinant, which in the strong coupling limit is of block Toeplitz form. Owing to its specific structure, by means of a Riemann-Hilbert problem it could be brought into conventional Toeplitz form, for which asymptotic expansions are known.

In addition we applied the nonequilibrium (full) bosonization approach presented in Sect. 2.3 to study the evolution of a Luttinger liquid, initially in a nonequilibrium state, after a sudden switch-on of the interaction. Similarly to an interaction quench from an initial equilibrium state, we observe a retardation in the build-up of power-law correlations typical for Luttinger liquids. At finite times $\bar{t}$ after the quench, correlations between long distances $|\bar{x}| \gg u\bar{t}$ (with plasmon velocity u) are Fermi-liquid-like and lead to discontinuities in the momentum distribution function at the Fermi edge. As an effect of nonequilibrium the quasiparticle weight corresponding to the discontinuity is not only algebraically suppressed for increasing times $\bar{t}$, but – due to dephasing – dominantly exponentially.

As $\bar{t} \to \infty$ the system relaxes to a steady state which differs both from the equilibrium and from the quenched equilibrium situation. Starting with a double-step distribution function, the steady-state momentum distribution function is still reminiscent of the initial two edges which no support power-law singularities (smeared by dephasing).

To conclude, let us discuss possible future research directions. Quantum wire network models cover a broad class of systems whose behavior under the influence of nonequilibrium and in the presence of interaction could be studied within the developed framework. Examples are edge states in spin quantum Hall topological insulators and two-dimensional electron gases at the (integer) quantum Hall transition. Further, of great interest is a generalization to fractional quantum Hall edge states, and in particular to systems with non-Abelian excitations which are promising candidates for the implementation of topological quantum computation.

While we developed an approximative approach for the limit of weak tunneling and discussed an exactly solvable example, it is important to understand under what general conditions and how we can proceed in a controllable way. For this purpose, and in general, the analysis of the asymptotic behavior of Fredholm determinants is relevant. While in this work in the specific situation of two coupled channels and zero temperature the arising block Toeplitz determinant could be reduced to conventional Toeplitz determinants, the general treatment of block Toeplitz determinants is still an interesting open question.

9

Chapter 9

List of Publications

1. S. Ngo Dinh, D. A. Bagrets, and A. D. Mirlin, "*Tunneling into a nonequilibrium Luttinger liquid with impurity*," Phys. Rev. B **81**, 081306(R) (2010).

2. S. Ngo Dinh and D. A. Bagrets, "*Influence of Coulomb interaction on the Aharonov-Bohm effect in an electronic Fabry-Pérot interferometer*," Phys. Rev. B **85**, 073403 (2012).

3. S. Ngo Dinh, D. A. Bagrets, and A. D. Mirlin, "*Nonequilibrium functional bosonization of quantum wire networks*," Ann. Phys. **327**, 2794 (2012).

4. S. Ngo Dinh, D. A. Bagrets, and A. D. Mirlin, "*Analytically solvable model of an electronic Mach-Zehnder interferometer*," Phys. Rev. B **87**, 195433 (2013).

5. S. Ngo Dinh, D. A. Bagrets, and A. D. Mirlin, "*Interaction quench in nonequilibrium Luttinger liquids*," arXiv:1310.0735 (*submitted to Phys. Rev. B*).

10 Chapter 10

Conference Contributions

10/2012	BMBF Workshop *Topological Materials for Nanoelectronics*, MPI Stuttgart, Germany (oral presentation)
06/2012	Advanced Research Workshop NanoPiter 2012 *Fundamentals of Electronic Nanosystems*, St. Petersburg, Russia (poster presentation)
04/2012	Workshop dedicated to P. Wölfle's 70th birthday *Electronic Correlations and Disorder in Quantum Matter*, Karlsruhe, Germany (poster presentation)
03/2012	Spring Meeting 2012 of the German Physical Society (DPG), Berlin, Germany (oral presentation)
12/2010	Winter School on *Topological States in Condensed Matter Systems*, IAS Jerusalem, Israel (poster presentation)
09/2011 & 09/2009	Center for Functional Nanostructures Summer Schools on Nano-Electronics, Bad Herrenalb, Germany (poster presentation)
07/2010	Workshop on *Interactions, Disorder, and Topology in Quantum Hall Systems*, MPIPKS Dresden, Germany (poster presentation)
05/2010	Workshop on *Localization Phenomena in Novel Phases of Condensed Matter*, ICTP Trieste, Italy (poster presentation)
03/2010	Spring Meeting 2010 of the German Physical Society (DPG), Regensburg, Germany (oral presentation)
09/2009	Workshop in memory of A. Schmid and A. Aronov, Karlsruhe, Germany (poster presentation)

A Appendix A
Asymptotics of Toeplitz determinants and Generalizations

In this chapter we summarize useful results on the asymptotic behavior of Toeplitz determinants $\Delta_N = \det(g_{j-k})_{1 \leq j,k \leq N}$ for large matrix sizes N. In what follows we assume the matrix elements drop off fast enough $\sum_{k=-\infty}^{\infty} |g_k| < \infty$, such that we can express them in terms of the "symbol" $g(e^{i\varphi}) \equiv \sum_{k=-\infty}^{\infty} g_k e^{ik\varphi}$, a complex-valued function on the unit circle with

$$g_{j-k} = \int_{-\pi}^{\pi} \frac{\mathrm{d}\varphi}{2\pi} \, g(e^{i\varphi}) e^{-i\varphi(j-k)}.$$

The strong Szegö limit theorem applies for sufficiently smooth symbols $g(z) = e^{V(z)}$. The logarithm $V(e^{i\varphi}) = \sum_{k=-\infty}^{\infty} V_k e^{ik\varphi}$ is assumed to be smooth with Fourier harmonics $V_k = \int_{-\pi}^{\pi} \frac{\mathrm{d}\varphi}{2\pi} V(e^{-ik\varphi})$ satisfying $\sum_{k=-\infty}^{\infty} |V_k|^2 |k| < \infty$. Then for large N the determinant behaves as

$$\Delta_N = e^{NV_0} \exp\left[\sum_{k=1}^{\infty} k V_k V_{-k} \right].$$

The Fisher-Hartwig (FH) formula (proven by [117]) allows to relax the smoothness conditions on $g(z)$. The symbols may have "FH singularities", i.e. be of the form

$$g(z) = e^{V(z)} \prod_{j=0}^{m} \left| z - z_j \right|^{2\alpha_j} \gamma_j(z) \left(z/z_j \right)^{\beta_j} \tag{A.1}$$

with integer $m \geq 0$, $z_j \equiv e^{i\varphi_j}$, $\mathrm{Re}\,\alpha_j > -\frac{1}{2}$, $\beta_j \in \mathbb{C}$,

$$\gamma_j(z) = \begin{cases} e^{i\pi\beta_j}, & -\pi < \arg z < \varphi_j, \\ e^{-i\pi\beta_j}, & \varphi_j < \arg z < \pi, \end{cases} \tag{A.2}$$

for $j = 0, \ldots, m$, and sufficiently smooth $V(z)$. The authors of [117] derived the leading asymptotic behavior of Δ_N for sufficiently close β_j, $\left| \beta_j - \beta_k \right| < 1$, $j, k = 0, \ldots, m$. In the context of our work and

of [21], we deal exclusively with $\alpha_j = 0$, hence, we will not bother about more general results here. The leading asymptotics according to [117] is

$$\Delta_N = e^{NV_0} N^{-\sum_{j=0}^m \beta_j^2} \prod_{0 \leq j < k \leq m} \left| z_j - z_k \right|^{2\beta_j \beta_k} \prod_{j=0}^m G(1 + \beta_j) G(1 - \beta_j) \tag{A.3}$$

where $V_0 = \int_{-\pi}^{\pi} \frac{\mathrm{d}\varphi}{2\pi} V(e^{i\varphi})$ and G is the Barnes G-function. The authors of [21] used a generalized result which is valid for arbitrary β_j and yields also subleading contributions:

$$\Delta_N = e^{NV_0} \sum_{n_0 + \ldots + n_m = 0} \prod_{j=0}^m z_j^{n_j N} \left[N^{-\sum_{j=0}^m \beta_j^2} \prod_{0 \leq j < k \leq m} \left| z_j - z_k \right|^{2\beta_j \beta_k} \prod_{j=0}^m G(1 + \beta_j) G(1 - \beta_j) \right]_{\beta_j \to \beta_j + n_j} . \tag{A.4}$$

We turn to an example which is ubiquitous throughout the main part of this thesis. Let $f(\epsilon)$ be some (stationary) distribution function and $\delta(t) = \bar{\delta} \mathbb{1}_{[0,\tau]}(t)$ some piecewise constant phase. The goal is to extract the large-τ asymptotic behavior of $\mathrm{Det}\left[\mathbb{1} + (e^{i\delta} - 1)f \right]$. By introducing the projector P_τ, which acts on functions $\phi(t)$ as $P_\tau \phi(t) = \phi(t) \mathbb{1}_{[0,\tau]}(t)$, we convince ourselves that the determinant in question,

$$\mathrm{Det}\left[\mathbb{1} + (e^{i\delta} - 1)f \right] = \mathrm{Det}\left[\mathbb{1} + P_\tau(e^{i\bar{\delta}} - 1)f \right] = \mathrm{Det}\left[\mathbb{1} + P_\tau(e^{i\bar{\delta}} - 1)f P_\tau \right],$$

is in fact effectively of Toeplitz form (cf. also the discussion in the beginning of Sect. 2.3). As high-energy regularization time is discretized, $t_j = j\Delta t = j\pi/\Lambda$ which amounts to restricting the energy range to $(-\Lambda, \Lambda]$. In energy representation the operator of interest reads

$$\tilde{g}(\epsilon) = 1 + (e^{i\bar{\delta}} - 1)f(\epsilon). \tag{A.5}$$

Being related to the time representation by Fourier transformation it corresponds to the symbol $g(z)$ provided energy $\epsilon \in (-\Lambda, \Lambda]$ and angle $\varphi \in (-\pi, \pi]$ are related by rescaling: $\varphi = \epsilon\pi/\Lambda$. The introduction of a hard cutoff $\pm\Lambda$ will give rise to unphysical effects at this energy scale. In order to avoid them and to make the above FH result applicable, we impose "periodic boundary conditions" in energy domain $\lim_{\epsilon \to -\Lambda} g(\epsilon) = \lim_{\epsilon \to \Lambda} g(\epsilon)$:

$$g(\epsilon) = e^{i\bar{\delta}\epsilon/(2\Lambda)} \left[1 + (e^{i\bar{\delta}} - 1)f(\epsilon) \right] \tag{A.6}$$

where we took into account $\lim_{\epsilon \to -\Lambda} f(\epsilon) = 1$, $\lim_{\epsilon \to \Lambda} f(\epsilon) = 0$. In discretized (dimensionless) time representation the Toeplitz matrix is

$$g_{j-k} = \int_{-\pi}^{\pi} \frac{\mathrm{d}\varphi}{2\pi} e^{-i\varphi(j-k)} g(e^{i\varphi}) = \int_{-\Lambda}^{\Lambda} \frac{\mathrm{d}\epsilon}{2\Lambda} e^{-i\epsilon\pi/\Lambda(j-k)} g(\epsilon). \tag{A.7}$$

To be specific we consider one of the examples of [21], the equilibrium distribution function $f_{\mathrm{single}}(\epsilon) = \theta(\mu - \epsilon)$. The symbol is

$$g(e^{i\varphi}) = \begin{cases} e^{i\bar{\delta}\varphi/(2\pi)} e^{i\bar{\delta}}, & -\pi < \varphi < \pi\mu/\Lambda, \\ e^{i\bar{\delta}\varphi/(2\pi)}, & \pi\mu/\Lambda < \varphi < \pi, \end{cases} \tag{A.8}$$

which is of the form (A.1) with $m = 0$, $\alpha_0 = 0$, $\beta_0 = \bar{\delta}/(2\pi)$, $z_0 = e^{i\pi\mu/\Lambda}$, and $V_0 = i\bar{\delta}(1 + \mu/\Lambda)/2$. According to Eq. (A.4) in the large-N limit the $\det(g_{j-k})$ asymptotically behaves as

$$\Delta[\bar{\delta}, f_{\text{single}}] = \exp\left[i\frac{\bar{\delta}}{2\pi}(\Lambda + \mu)\tau\right] \left(\frac{\Lambda\tau}{\pi}\right)^{-\left(\frac{\bar{\delta}}{2\pi}\right)^2} G\left(1 - \frac{\bar{\delta}}{2\pi}\right) G\left(1 + \frac{\bar{\delta}}{2\pi}\right) \tag{A.9}$$

Another example of [21] is the double-step distribution function $f_{\text{double}}(\epsilon) = (1 - a)\theta(\mu_0 - \epsilon) + a\theta(\mu_1 - \epsilon)$, $\mu_0 < \mu_1$. In this case the symbol reads

$$g(e^{i\varphi}) = \begin{cases} e^{i\bar{\delta}\varphi/(2\pi)}e^{i\bar{\delta}}, & -\Lambda < \varphi < \mu_0, \\ e^{i\bar{\delta}\varphi/(2\pi)}\left[1 + (e^{i\bar{\delta}} - 1)a\right], & \pi\mu_0/\Lambda < \varphi < \pi\mu_1/\Lambda, \\ e^{i\bar{\delta}\varphi/(2\pi)}, & \pi\mu_1/\Lambda < \varphi < \pi. \end{cases} \tag{A.10}$$

Hence, the symbol has two FH singularities $z_j = e^{i\pi\mu_j/\Lambda}$, $j = 0, 1$, with

$$e^{-2\pi i\beta_0} = \frac{1 + (e^{i\bar{\delta}} - 1)a}{e^{i\bar{\delta}}}, \quad e^{-2\pi i\beta_1} = \frac{1}{1 + (e^{i\bar{\delta}} - 1)a}. \tag{A.11}$$

We choose

$$\beta_1 = -\frac{i}{2\pi}\ln\left[1 + (e^{i\bar{\delta}} - 1)a\right], \quad \beta_0 = \frac{\bar{\delta}}{2\pi} - \beta_1. \tag{A.12}$$

It is then simple to show that the symbol has the form (A.1) with $m = 1$, $\alpha_j = 0$, and

$$V(z) = V_0 = i\bar{\delta}/2 + i\bar{\delta}\frac{\mu_0}{2\Lambda} + ieV\frac{\pi}{\Lambda}\beta_1 \tag{A.13}$$

where we introduced $eV = \mu_1 - \mu_0$. According to (A.4) the asymptotic behavior of the Toeplitz determinant $\det\left(g_{j-k}\right)$ is given by

$$\Delta[\bar{\delta}, f_{\text{double}}] = \exp\left[i\frac{\bar{\delta}}{2\pi}(\Lambda + \mu_0)\tau + \frac{eV\tau}{2\pi}\ln\left[1 + (e^{i\bar{\delta}} - 1)a\right]\right]$$
$$\times \sum_{n=-\infty}^{\infty} e^{-ieV\tau n} \left(\frac{\Lambda\tau}{\pi}\right)^{-(\beta_0+n)^2-(\beta_1-n)^2} \left(\frac{\pi eV}{\Lambda}\right)^{2(\beta_0+n)(\beta_1-n)}$$
$$\times G(1 + \beta_0 + n)G(1 - \beta_0 - n)G(1 + \beta_1 - n)G(1 - \beta_1 + n). \tag{A.14}$$

Identifying the asymptotically leading n-contributions requires maximizing the exponent

$$\text{Re}\left[-(\beta_0 + n)^2 - (\beta_1 - n)^2\right] = -2\left(n - n^*\right)^2 + \text{const.} \tag{A.15}$$

$$\text{with } n^* = \frac{1}{2}\text{Re}\left(\beta_1 - \beta_0\right) = -\frac{1}{2}\frac{\bar{\delta}}{2\pi}. \tag{A.16}$$

Note that $\left[-(\beta_0 + n)^2 - (\beta_1 - n)^2\right] - \left[2(\beta_0 + n)(\beta_1 - n)\right] = -(\beta_0 + \beta_1)^2$ is independent of n. Thus, terms dominant for $\Lambda\tau \gg 1$ are also leading for large voltages, $eV\tau \gg 1$. For the analysis of the

optimal value n^*, we make the decomposition $\bar{\delta} = 2\pi M + \bar{\delta}'$ with $M \in \mathbb{Z}$ and $|\bar{\delta}'| < \pi$. One can show that $\bar{\delta}'' \equiv \text{Im} \ln \left[(1-a) + ae^{i\bar{\delta}} \right]$ is a phase with the same sign as $\bar{\delta}'$ and which satisfies $|\bar{\delta}''| \leq |\bar{\delta}'|$. Then, $n^* = -\frac{M}{2} - \frac{\bar{\delta}' - 2\bar{\delta}''}{4\pi}$ and $|n^* + M/2| \leq 1/4$. Concluding, for even M, one single contribution, $n = -M/2$, for odd M, two comparable contributions, $n = -(M \pm 1)/2$, are significantly dominating. If in the latter case $a = 1/2$ and thus $\bar{\delta}'' = \bar{\delta}'/2$, both contributions come with equal exponents.

Numerical studies suggest that the above results (A.9) and (A.14) can be generalized to non-Toeplitz cases where the phase $\delta(t)$ may be a piecewise constant function of time[22]. Let us reiterate the idea. Consider the generalized Toeplitz matrix

$$g_{j,k} = \int_{-\Lambda}^{\Lambda} \frac{d\epsilon}{2\Lambda} e^{-i\epsilon\pi/\Lambda[j-k-\delta(t_j)/(2\pi)]} \tilde{g}(t_j, \epsilon), \quad \tilde{g}(t, \epsilon) \equiv 1 + \left(e^{i\delta(t)} - 1 \right) f(\epsilon) \tag{A.17}$$

where the notion of a symbol is generalized to a time- and energy dependent function. Phase $\delta(t)$ and distribution function $f(\epsilon)$ are assumed to be piecewise constant functions with jumps at times $\tau_1 < \tau_2 < \ldots < \tau_{N_\tau}$ and energies $\mu_1 < \mu_2 < \ldots < \mu_{N_\mu}$, respectively. They satisfy $\delta(t) = 0$ for $t \notin [\tau_1, \tau_{N_\tau}]$, $f(-\Lambda) = 1$ and $f(\epsilon) = 0$ for $\epsilon > \mu_{N_\mu}$ (periodic boundary conditions in energy domainare thus ensured as before). For $j \in \{1, \ldots, N_\tau - 1\}$, $k \in \{1, \ldots, N_\mu - 1\}$ and an arbitrary set of integers $\{n_{jk}\}$ we define

$$c_{jk} \equiv \frac{1}{2\pi i} \ln \tilde{g}(\tau_j + 0, \mu_k + 0) + n_{jk}, \tag{A.18}$$

$$c_{j0} \equiv \delta(t_j + 0)/(2\pi), \quad c_{0k} = c_{N_\tau, k} = c_{j, N_\mu} = 0. \tag{A.19}$$

Then we define for $j, l \in \{1, \ldots, N_t\}$, $k, m \in \{1, \ldots, N_\mu\}$:

$$\beta_{jk} \equiv c_{j,k-1} - c_{j,k} + c_{j-1,k} - c_{j-1,k-1}, \quad p_{jl} \equiv \sum_{m'=1}^{N_\mu} \beta_{jm'}\beta_{lm'}, \quad q_{km} \equiv \sum_{l'=1}^{N_t} \beta_{l'k}\beta_{l'm}. \tag{A.20}$$

Remember that c_{jk} and thus β_{jk}, p_{jl}, and q_{km} depend on the set of integers n_{jk}. In Eqn. (A.18) the logarithm $\ln \tilde{g}$ is to be evaluated at its principal branch, $\text{Im} \ln \tilde{g} \in (-\pi, \pi]$. Summation over different integers n_{jk} hence amounts to summing over different branches of the logarithms.

For large time and energy differences $|(\tau_j - \tau_l)(\mu_k - \mu_m)| \gg 1$ ($j \neq l$, $k \neq m$) the asymptotic behavior of $\det(g_{j,k})$ is given by the superposition

$$\Delta[\delta(t), f(\epsilon)] = \sum_{\{n_{jk}\}} \Gamma_{\{n_{jk}\}} \exp \left[i \sum_{1 \leq j < N_t} \left(c_{j0}(\Lambda + \mu_1) + \sum_{1 \leq k < N_\mu} c_{jk} \left(\mu_{k+1} - \mu_k \right) \right) (\tau_{j+1} - \tau_j) \right]$$

$$\times \prod_{1 \leq j < l < N_t} \prod_{1 \leq k < m < N_\mu} \left| \frac{\Lambda \left(\tau_j - \tau_l \right)}{\pi} \right|^{p_{jl}} \left| \frac{\pi \left(\mu_k - \mu_m \right)}{\Lambda} \right|^{q_{km}} \tag{A.21}$$

where $\Gamma_{\{n_{jk}\}}$ are constants which depend on c_{jk} (but not on τ_j and μ_k).

Bibliography

[1] Y. Imry, *Introduction to Mesoscopic Physics* (Oxford University Press, Oxford, 1997).

[2] S. D. Franceschi, R. Hanson, W. G. van der Wiel, J. M. Elzerman, J. J. Wijpkema, T. Fujisawa, S. Tarucha, and L. P. Kouwenhoven, "*Out-of-Equilibrium Kondo Effect in a Mesoscopic Device*," Phys. Rev. Lett. **89**, 156801 (2002).

[3] J. Paaske, A. Rosch, P. Wölfle, N. Mason, C. M. Marcus, and J. N. rd, "*Non-equilibrium singletŰtriplet Kondo effect in carbon nanotubes*," Nature Physics **2**, 460 (2006).

[4] M. Grobis, I. G. Rau, R. M. Potok, H. Shtrikman, and D. Goldhaber-Gordon, "*Universal Scaling in Nonequilibrium Transport through a Single Channel Kondo Dot*," Phys. Rev. Lett. **100**, 246601 (2008).

[5] T. Delattre, C. Feuillet-Palma, L. G. Herrmann, P. Morfin, J.-M. Berroir, G. Fève, B. Plaçais, D. C. Glattli, M.-S. Choi, C. Mora, and T. Kontos, "*Noisy Kondo impurities*," Nature Physics **5**, 208 (2009).

[6] D. A. Abanin and L. S. Levitov, "*Fermi-Edge Resonance and Tunneling in Nonequilibrium Electron Gas*," Phys. Rev. Lett. **94**, 186803 (2005).

[7] I. Snyman and Y. V. Nazarov, "*Polarization of a Charge Qubit Strongly Coupled to a Voltage-Driven Quantum Point Contact*," Phys. Rev. Lett. **99**, 096802 (2007).

[8] I. Neder, M. Heiblum, Y. Levinson, D. Mahalu, and V. Umansky, "*Unexpected Behavior in a Two-Path Electron Interferometer*," Phys. Rev. Lett. **96**, 016804 (2006).

[9] Y. Ji, Y. C. Chung, D. Sprinzak, M. Heiblum, D. Mahalu, and H. Shtrikman, "*An electronic Mach-Zehnder interferometer*," Nature (London) **422**, 415 (2003).

[10] Y. Aharonov and D. Bohm, "*Significance of Electromagnetic Potentials in the Quantum Theory*," Phys. Rev. **115**, 485 (1959).

[11] C. L. Kane and M. P. A. Fisher, "*Transport in a one-channel Luttinger liquid*," Phys. Rev. Lett. **68**, 1220 (1992).

[12] T. Giamarchi, *Quantum Physics in One Dimension* (Oxford University Press, Oxford, 2004).

[13] D. B. Gutman, Y. Gefen, and A. D. Mirlin, "*Bosonization of one-dimensional fermions out of equilibrium*," Phys. Rev. B **81**, 085436 (2010).

[14] D. B. Gutman, Y. Gefen, and A. D. Mirlin, "*Bosonization out of equilibrium*," EPL **90**, 37003 (2010).

[15] A. Grishin, I. V. Yurkevich, and I. V. Lerner, "*Functional integral bosonization for an impurity in a Luttinger liquid*," Phys. Rev. B **69**, 165108 (2004).

[16] I. V. Lerner and I. V. Yurkevich, "*Impurity in the Tomonaga-Luttinger model: a Functional Integral Approach*," in *Proceedings of LXXXI Les Houches School on 'Nanoscopic quantum transport'* (2005).

[17] A. Kamenev and A. Levchenko, "*Keldysh technique and non-linear sigma-model: basic principles and applications*," Advances in Physics **58**, 197 (2009).

[18] A. Kamenev, *Field Theory of Non-Equilibrium Systems* (Cambridge University Press, Cambridge, 2011).

[19] I. E. Dzyaloshinskii and K. B. Larkin, "*Correlation functions for a one-dimensional Fermi system with long-range interaction (Tomonaga model)*," JETP **38**, 202 (1973).

[20] I. Klich, "*Quantum Noise in Mesoscopic Physics*," (NATO Science Series, Kluwer, Dordrecht, 2003) Chap. "Full Counting Statistics: An elementary derivation of Levitov's formula".

[21] D. B. Gutman, Y. Gefen, and A. D. Mirlin, "*Non-equilibrium 1D many-body problems and asymptotic properties of Toeplitz determinants*," J. Phys. A: Math. Theor. **44**, 165003 (2011).

[22] I. V. Protopopov, D. B. Gutman, and A. D. Mirlin, "*Correlations in non-equilibrium Luttinger liquid and singular Fredholm determinants*," arXiv e-prints (2012), arXiv:1212.0708 [cond-mat.str-el] .

[23] L. S. Levitov and G. B. Lesovik, "*Charge distribution in quantum shot noise*," JETP Lett. **58**, 230 (1993).

[24] L. S. Levitov, H.-W. Lee, and G. B. Lesovik, "*Electron counting statistics and coherent states of electric current*," J. Math. Phys. **37**, 4845 (1996).

[25] D. A. Ivanov, H. Lee, and L. S. Levitov, "*Coherent states of alternating current*," Phys. Rev. B **56**, 6839 (1997).

[26] S. N. Dinh, D. A. Bagrets, and A. D. Mirlin, "*Nonequilibrium functional bosonization of quantum wire networks*," Ann. Phys. **327**, 2794 (2012).

[27] J. T. Chalker and P. D. Coddington, "*Percolation, quantum tunnelling and the integer Hall effect*," J. Phys. C **21**, 2665 (1988).

[28] I. Snyman and Y. V. Nazarov, "*Keldysh action of a multiterminal time-dependent scatterer*," Phys. Rev. B **77**, 165118 (2008).

[29] U. Eckern, G. Schön, and V. Ambegaokar, "*Superconductor-insulator transition in a single Josephson junction*," Phys. Rev. B **30**, 6419 (1984).

[30] L. S. Levitov and A. V. Shytov, "*Semiclassical theory of the Coulomb anomaly*," Sov. Phys. JETP **66**, 214 (1997).

[31] R. Landauer, "*Johnson-Nyquist noise derived from quantum mechanical transmission*," Physica D **38**, 226 (1987).

[32] T. Martin and R. Landauer, "*Wave-packet approach to noise in multichannel mesoscopic systems*," Phys. Rev. B **45**, 1742 (1992).

[33] B. Braunecker, "*Response of a Fermi gas to time-dependent perturbations: Riemann-Hilbert approach at nonzero temperatures*," Phys. Rev. B **73**, 075122 (2006).

[34] B. L. Altshuler and A. G. Aronov, *Electron-Electron Interaction In Disordered Systems* (Elsevier, Amsterdam, 1985).

[35] G.-L. Ingold and Y. V. Nazarov, "*Single Charge Tunneling: Coulomb Blockade Phenomena in Nanostructures*," (Plenum Press, New York, 1992) Chap. "Charge Tunneling Rates in Ultrasmall Junctions".

[36] J. M. Valles, R. C. Dynes, and J. P. Garno, "*Temperature dependence of the two-dimensional electronic density of states in disordered metal films*," Phys. Rev. B **40**, 7590 (1989).

[37] J. M. Valles, R. C. Dynes, and J. P. Garno, "*Superconductivity and the electronic density of states in disordered two-dimensional metals*," Phys. Rev. B **40**, 6680 (1989).

[38] J. P. Eisenstein, T. J. Gramila, L. N. Pfeiffer, and K. W. West, "*Probing a two-dimensional Fermi surface by tunneling*," Phys. Rev. B **44**, 6511 (1991).

[39] A. M. Chang, L. N. Pfeiffer, and K. W. West, "*Observation of Chiral Luttinger Behavior in Electron Tunneling into Fractional Quantum Hall Edges*," Phys. Rev. Lett. **77**, 2538 (1996).

[40] Y. Jompol, C. J. B. Ford, J. P. Griffiths, I. Farrer, G. A. C. Jones, D. Anderson, D. A. Ritchie, T. W. Silk, and A. J. Schofield, "*Probing Spin-Charge Separation in a Tomonaga-Luttinger Liquid*," Science **325**, 597 (2009).

[41] H. Pothier, S. Guéron, N. O. Birge, D. Esteve, and M. H. Devoret, "*Energy Distribution Function of Quasiparticles in Mesoscopic Wires*," Phys. Rev. Lett. **79**, 3490 (1997).

[42] Y.-F. Chen, T. Dirks, G. Al-Zoubi, N. O. Birge, and N. Mason, "*Nonequilibrium Tunneling Spectroscopy in Carbon Nanotubes*," Phys. Rev. Lett. **102**, 036804 (2009).

[43] T. Dirks, Y.-F. Chen, N. O. Birge, and N. Mason, "*Superconducting Tunneling Spectroscopy of a Carbon Nanotube Quantum Dot*," Appl. Phys. Lett. **95**, 192103 (2009).

[44] M. Bockrath, D. H. Cobden, A. G. Rinzler, R. E. Smalley, L. Balents, and P. L. McEuen, "*Luttinger-liquid behavior in carbon nanotubes*," Nature **397**, 598 (1999).

[45] Z. Yao, H. W. C. Postma, L. Balents, and C. Dekker, "*Carbon nanotube intramolecular junctions*," Nature **402**, 273 (1999).

[46] H. W. C. Postma, M. de Jonge, Z. Yao, and C. Dekker, "*Electrical transport through carbon nanotube junctions created by mechanical manipulation*," Phys. Rev. B **62**, R10653 (2000).

[47] S. G. Jakobs, V. Meden, and H. Schoeller, "*Nonequilibrium Functional Renormalization Group for Interacting Quantum Systems*," Phys. Rev. Lett. **99**, 150603 (2007).

[48] M. Trushin and A. L. Chudnovskiy, "*Tunneling into strongly biased Tomonaga-Luttinger liquid*," Europhys. Lett. **82**, 17008 (2008).

[49] C. Bena, "*The tunneling conductance between a superconducting STM tip and an out-of-equilibrium carbon nanotube*," arXiv e-prints (2009), arXiv:0909.0867 [cond-mat.str-el] .

[50] D. B. Gutman, Y. Gefen, and A. D. Mirlin, "*Nonequilibrium Luttinger Liquid: Zero-Bias Anomaly and Dephasing*," Phys. Rev. Lett. **101**, 126802 (2008).

[51] D. B. Gutman, Y. Gefen, and A. D. Mirlin, "*Tunneling spectroscopy of Luttinger-liquid structures far from equilibrium*," Phys. Rev. B **80**, 045106 (2009).

[52] Y. Oreg and A. M. Finkelstein, "*Interedge Interaction in the Quantum Hall Effect*," Phys. Rev. Lett. **74**, 3668 (1995).

[53] Y. Oreg and A. M. Finkel'stein, "*Enhancement of the Tunneling Density of States in Tomonaga-Luttinger Liquids*," Phys. Rev. Lett. **76**, 4230 (1996).

[54] Y. Oreg and A. M. Finkel'stein, "*Oreg and Finkel'stein Reply*," Phys. Rev. Lett. **78**, 4528 (1997).

[55] M. Fabrizio and A. O. Gogolin, "*Comment on 'Enhancement of the Tunneling Density of States in Tomonaga-Luttinger Liquids'*," Phys. Rev. Lett. **78**, 4527 (1997).

[56] S. Eggert, H. Johannesson, and A. Mattsson, "*Boundary Effects on Spectral Properties of Interacting Electrons in One Dimension*," Phys. Rev. Lett. **76**, 1505 (1996).

[57] A. V. Lebedev, A. Crépieux, and T. Martin, "*Electron injection in a nanotube with leads: Finite-frequency noise correlations and anomalous charges*," Phys. Rev. B **71**, 075416 (2005).

[58] D. A. Bagrets, I. V. Gornyi, A. D. Mirlin, and D. G. Polyakov, "*Relaxation processes in a disordered Luttinger liquid*," Semiconductors **42**, 994 (2008).

[59] D. A. Bagrets, I. V. Gornyi, and D. G. Polyakov, "*Nonequilibrium kinetics of a disordered Luttinger liquid*," Phys. Rev. B **80**, 113403 (2009).

[60] P. Fendley, A. W. W. Ludwig, and H. Saleur, "*Exact nonequilibrium transport through point contacts in quantum wires and fractional quantum Hall devices*," Phys. Rev. B **52**, 8934 (1995).

[61] U. Weiss, "*Low-temperature conduction and DC current noise in a quantum wire with impurity*," Solid State Commun. **100**, 281 (1996).

[62] R. Egger and H. Grabert, "*Applying voltage sources to a Luttinger liquid with arbitrary transmission*," Phys. Rev. B **58**, 10761 (1998).

[63] B. Trauzettel, I. Safi, F. Dolcini, and H. Grabert, "*Appearance of Fractional Charge in the Noise of Nonchiral Luttinger Liquids*," Phys. Rev. Lett. **92**, 226405 (2004).

[64] S. N. Dinh, D. A. Bagrets, and A. D. Mirlin, "*Tunneling into a nonequilibrium Luttinger liquid with impurity*," Phys. Rev. B **81**, 081306(R) (2010).

[65] I. S. Gradshtein and I. M. Ryzhik, *Table of Integrals, Series, and Products* (Academic Press, 1980).

[66] D. T. McClure, Y. Zhang, B. Rosenow, E. M. Levenson-Falk, C. M. Marcus, L. N. Pfeiffer, and K. W. West, "*Edge-State Velocity and Coherence in a Quantum Hall Fabry-Pérot Interferometer*," Phys. Rev. Lett. **103**, 206806 (2009).

[67] Y. Zhang, D. T. McClure, E. M. Levenson-Falk, and C. M. Marcus, "*Distinct signatures for Coulomb blockade and Aharonov-Bohm interference in electronic Fabry-Perot interferometers,*" Phys. Rev. B **79**, 241304(R) (2009).

[68] Y. Yamauchi, M. Hashisaka, S. Nakamura, K. Chida, S. Kasai, T. Ono, R. Leturcq, K. Ensslin, D. C. Driscoll, A. C. Gossard, and K. Kobayashi1, "*Universality of bias- and temperature-induced dephasing in ballistic electronic interferometers,*" Phys. Rev. B **79**, 161306(R) (2009).

[69] N. Ofek, A. Bid, M. Heiblum, A. Stern, V. Umansky, and D. Mahalu, "*The Role of Interactions in an Electronic Fabry-Perot Interferometer Operating in the Quantum all Effect Regime,*" Proc. Natl. Acad. Sci. USA **107**, 5276 (2010).

[70] I. Neder, M. Heiblum, D. Mahalu, and V. Umansky, "*Entanglement, Dephasing, and Phase Recovery via Cross-Correlation Measurements of Electrons,*" Phys. Rev. Lett. **98**, 036803 (2007).

[71] I. Neder, F. Marquardt, M. Heiblum, D. Mahalu, and V. Umansky, "*Controlled Dephasing of Electrons by Non-Gaussian Shot Noise,*" Nat. Phys. **3**, 534 (2007).

[72] P. Roulleau, F. Portier, D. C. Glattli, P. Roche, A. Cavanna, G. Faini, U. Gennser, and D. Mailly, "*Finite bias visibility of the electronic Mach-Zehnder interferometer,*" Phys. Rev. B **76**, 161309(R) (2007).

[73] P. Roulleau, F. Portier, P. Roche, A. Cavanna, G. Faini, U. Gennser, and D. Mailly, "*Direct Measurement of the Coherence Length of Edge States in the Integer Quantum Hall Regime,*" Phys. Rev. Lett. **100**, 126802 (2008).

[74] P. Roulleau, F. Portier, P. Roche, A. Cavanna, G. Faini, U. Gennser, and D. Mailly, "*Noise Dephasing in Edge States of the Integer Quantum Hall Regime,*" Phys. Rev. Lett. **101**, 186803 (2008).

[75] P. Roulleau, F. Portier, P. Roche, A. Cavanna, G. Faini, U. Gennser, and D. Mailly, "*Tuning Decoherence with a Voltage Probe,*" Phys. Rev. Lett. **102**, 236802 (2009).

[76] L. V. Litvin, H.-P. Tranitz, W. Wegscheider, and C. Strunk, "*Decoherence and single electron charging in an electronic Mach-Zehnder interferometer,*" Phys. Rev. B **75**, 033315 (2007).

[77] L. V. Litvin, A. Helzel, H.-P. Tranitz, W. Wegscheider, and C. Strunk, "*Edge-channel interference controlled by Landau level filling,*" Phys. Rev. B **78**, 075303 (2008).

[78] L. V. Litvin, A. Helzel, H.-P. Tranitz, W. Wegscheider, and C. Strunk, "*Phase of the transmission amplitude for a quantum dot embedded in the arm of an electronic Mach-Zehnder interferometer,*" Phys. Rev. B **81**, 205425 (2010).

[79] E. Bieri, M. Weiss, O. Göktas, M. Hauser, C. Schönenberger, S. Oberholzer, and C. Strunk, "*Finite-bias visibility dependence in an electronic Mach-Zehnder interferometer,*" Phys. Rev. B **79**, 245324 (2009).

[80] P.-A. Huynh, F. Portier, H. le Sueur, G. Faini, U. Gennser, D. Mailly, F. Pierre, W. Wegscheider, and P. Roche, "*Quantum Coherence Engineering in the Integer Quantum Hall Regime,*" Phys. Rev. Lett. **108**, 256802 (2012).

[81] A. Helzel, L. V. Litvin, I. P. Levkivskyi, E. V. Sukhorukov, W. Wegscheider, and C. Strunk, "*Noise-induced Phase Transition in an Electronic Mach-Zehnder Interferometer: a Manifestation of Non-Gaussian Noise,*" arXiv:1211.5951 (2012).

[82] C. Nayak, S. H. Simon, A. Stern, M. Freedman, and S. D. Sarma, "*Non-Abelian Anyons and Topological Quantum Computation,*" Rev. Mod. Phys. **80**, 1083 (2008).

[83] E. V. Sukhorukov and V. V. Cheianov, "*Resonant dephasing in the electronic Mach-Zehnder interferometer,*" Phys. Rev. Lett. **99**, 156801 (2007).

[84] J. T. Chalker, Y. Gefen, and M. Y. Veillette, "*Decoherence and interactions in an electronic Mach-Zehnder interferometer,*" Phys. Rev. B **76**, 085320 (2007).

[85] I. P. Levkivskyi and E. V. Sukhorukov, "*Dephasing in the electronic Mach-Zehnder interferometer at filling factor $\nu = 2$,*" Phys. Rev. B **78**, 045322 (2008).

[86] I. Neder and E. Ginossar, "*Behavior of electronic interferometers in the nonlinear regime,*" Phys. Rev. Lett. **100**, 196806 (2008).

[87] S.-C. Youn, H.-W. Lee, and H.-S. Sim, "*Nonequilibrium Dephasing in an Electronic Mach-Zehnder Interferometer,*" Phys. Rev. Lett. **100**, 196807 (2008).

[88] D. L. Kovrizhin and J. T. Chalker, "*Exactly solved model for an electronic Mach-Zehnder interferometer,*" Phys. Rev. B **80**, 161306 (2009).

[89] M. Schneider, D. A. Bagrets, and A. D. Mirlin, "*Theory of the nonequilibrium electronic Mach-Zehnder interferometer,*" Phys. Rev. B **84**, 075401 (2011).

[90] C. de C. Chamon, D. E. Freed, S. A. Kivelson, S. L. Sondhi, and X. G. Wen, "*Two point-contact interferometer for quantum Hall systems,*" Phys. Rev. B **55**, 2331 (1997).

[91] B. Rosenow and B. I. Halperin, "*Influence of Interactions on Flux and Back-Gate Period of Quantum Hall Interferometers,*" Phys. Rev. Lett. **98**, 106801 (2007).

[92] B. I. Halperin, A. Stern, I. Neder, and B. Rosenow, "*Theory of the Fabry-Pérot quantum Hall interferometer,*" Phys. Rev. B **83**, 155440 (2011).

[93] S. N. Dinh and D. A. Bagrets, "*Influence of Coulomb interaction on the Aharonov-Bohm effect in an electronic Fabry-Pérot interferometer,*" Phys. Rev. B **85**, 073403 (2012).

[94] D. B. Chklovskii, K. A. Matveev, and B. I. Shklovskii, "*Ballistic conductance of interacting electrons in the quantum Hall regime,*" Phys. Rev. B **47**, 12605 (1993).

[95] D. B. Chklovskii, B. I. Shklovskii, and L. I. Glazman, "*Electrostatics of edge channels,*" Phys. Rev. B **46**, 4026 (1992).

[96] N. R. Cooper and J. T. Chalker, "*Coulomb Interactions and the Integer Quantum Hall Effect: Screening and Transport,*" Phys. Rev. B **48**, 4530 (1993).

[97] Y. V. Nazarov and Y. M. Blanter, *Quantum transport: introduction to nanoscience* (Cambridge University Press, Cambridge, 2009).

[98] A. K. Evans, L. I. Glazman, and B. I. Shklovskii, "*Coulomb blockade in the quantum-Hall-effect state*," Phys. Rev. B **48**, 11120 (1993).

[99] A. Furusaki and K. A. Matveev, "*Theory of strong inelastic cotunneling*," Phys. Rev. B **52**, 16676 (1995).

[100] D. A. Bagrets and Y. V. Nazarov, "*Full Current Statistics in the Regime of Weak Coulomb Interaction*," Phys. Rev. Lett. **94**, 056801 (2005).

[101] I. P. Levkivskyi and E. V. Sukhorukov, "*Noise-Induced Phase Transition in the Electronic Mach-Zehnder Interferometer*," Phys. Rev. Lett. **103**, 036801 (2009).

[102] D. L. Kovrizhin and J. T. Chalker, "*Multiparticle interference in electronic Mach-Zehnder interferometers*," Phys. Rev. B **81**, 155318 (2010).

[103] M. J. Rufino, D. L. Kovrizhin, and J. T. Chalker, "*Solution of a model for the two-channel electronic Mach-Zehnder interferometer*," arXiv:1209.1127 (2012).

[104] C. Altimiras, H. le Sueur, U. Gennser, A. Cavanna, D. Mailly, and F. Pierre, "*Non-equilibrium edge-channel spectroscopy in the integer quantum Hall regime*," Nature Physics **6**, 34 (2010).

[105] H. le Sueur, C. Altimiras, U. Gennser, A. Cavanna, D. Mailly, and F. Pierre, "*Energy Relaxation in the Integer Quantum Hall Regime*," Phys. Rev. Lett. **105**, 056803 (2010).

[106] H. le Sueur, C. Altimiras, U. Gennser, A. Cavanna, D. Mailly, and F. Pierre, "*Tuning Energy Relaxation along Quantum Hall Channels*," Phys. Rev. Lett. **105**, 226804 (2010).

[107] D. L. Kovrizhin and J. T. Chalker, "*Relaxation in Driven Integer Quantum Hall Edge States*," Phys. Rev. Lett. **109**, 106403 (2012).

[108] I. P. Levkivskyi and E. V. Sukhorukov, "*Energy relaxation at quantum Hall edge*," Phys. Rev. B **85**, 075309 (2012).

[109] X.-G. Wen, *Quantum Field Theory of Many-body Systems* (Oxford University Press, Oxford, 2004).

[110] V. V. Ponomarenko and D. V. Averin, "*Charge transfer statistics in symmetric fractional edge-state Mach-Zehnder interferometer*," Phys. Rev. B **80**, 201313 (2009).

[111] V. V. Ponomarenko and D. V. Averin, "*Braiding of anyonic quasiparticles in charge transfer statistics of a symmetric fractional edge-state Mach-Zehnder interferometer*," Phys. Rev. B **82**, 205411 (2010).

[112] B. A. Muzykantskii and Y. Adamov, "*Scattering Approach to Counting Statistics in Quantum Pumps*," Phys. Rev. B **68**, 155304 (2003).

[113] M. Rigol, V. Dunjko, V. Yurovsky, and M. Olshanii, "*Relaxation in a Completely Integrable Many-Body Quantum System: An Ab Initio Study of the Dynamics of the Highly Excited States of 1D Lattice Hard-Core Bosons*," Phys. Rev. Lett. **98**, 050405 (2007).

[114] T. Kinoshita, T. Wenger, and D. S. Weiss, "*Luttinger liquid universality in the time evolution after an interaction quench*," Nature **440**, 900 (2006).

[115] M. A. Cazalilla, "*The Luttinger model following a sudden interaction switch-on,*" Phys. Rev. Lett. **97**, 156403 (2006).

[116] A. Iucci and M. A. Cazalilla, "*Quantum quench dynamics of the Luttinger model,*" Phys. Rev. A **80**, 063619 (2009).

[117] P. Deift, A. Its, and I. Krasovsky, "*Asymptotics of Toeplitz, Hankel, and Toeplitz+Hankel determinants with Fisher-Hartwig singularities,*" Ann. Math. **174**, 1243 (2011).

Acknowledgments